Investigation of metal nanomaterials as a sensing element in LSPR-based optical fibre sensor development

A thesis submitted

by

MINH HIEU TU

for the degree of

Doctor of Philosophy

at

City University London

School of Engineering and Mathematical Sciences

January 2014

Table of Contents

List of Figures

List of Tables

Acknowledgements

First and foremost, I would like to send my dearest gratitude to the two supervisors, Professor Tong Sun and Professor K.T.V Grattan, for their immense helpfulness during my Ph.D. Without their patience and kind, their knowledge and insight, their encouragement and support, this thesis would not be made possible.

I would also want to thank Dr. Hien Nguyen, who introduced me to this opportunity to work in the Optical Fibre Sensor group in City University London as a Ph.D research student, and also for her support during my time here.

To all fellows and colleagues in our group, Jie Cao, Nahid Raoufi, Lourdes Shanika Alwis, Shuying Chen, Bochao Zhou, Shuo Yang, Miodrag Vidakovic, Mohammad Karimi, Colum McCague, Jacques Oliver, Dr. Fredderic Surre, Dr. Matthias Fabian, Dr Martin Ams and Dr Stephen Wren, thank you all for our precious moments together. Hope that we could meet again in the near future.

*To my dearest family, my grandmother, **Vu Thi Son**, my father **Tu Trong Hieu**, my mother **Cao Thi Thu Ha** and my lovely sister **Tu Boi Hoan**, I dedicate this thesis for you. Your endless love, encouragement and support are the best source of energy for me. I love you all.*

*To my dear wife, **My Anh Trinh**, I am really lucky to have you in my life. Your support and your care make me stronger each and every day. Thank you for being with me. I hope we could go together as far as possible in our life journey.*

To other friends and colleagues whose names I could not remember to put into this thesis at this very moment, thank you for being there and sharing with me some moment of my life. I wish all the best for you.

London, 06 January 2014

Copyright Declaration

Abstract

This thesis aims to explore and demonstrate the potential of using optical fibres both as a waveguide material and a transducer for wide sensing applications, based on a comprehensive review of the localised surface plasmon resonance (LSPR) phenomenon, which occurs at a nanoscale level when light interacts with metallic nanoparticles at a resonance wavelength.

The LSPR effect of metallic nanomaterials has shown a strong dependence on the local surrounding environment. A small change for example in the refractive index or in the solution concentration can result in a variation in the LSPR spectrum. Based on this underpinning sensing mechanism, a portable system using an optical fibre coated with gold nanoparticles (AuNPs) as a sensing probe has been developed and tested for the refractive index measurement. Coupled with this, a systematic approach has been developed and applied in this work to optimize the performance of the developed system by considering several key factors, such as the size of nanoparticles produced, pH, coating time and coating temperature.

The above optimised probes coated with gold-nanoparticles are further cross-compared with those optimized but coated with gold nanorods with a high aspect ratio. Both types of probes are also prepared for a specific biosensing application based on the antibody-antigen interaction to create wavelength-based sensors for the detection of anti-human IgG. Both probes have exhibited excellent refractive index (RI) sensitivity, showing ~914 nm/RIU (refractive index unit) for the probe coated with gold nanoparticles and ~601 nm/RIU for the one coated with gold nanorods. When using the modified probes for the detection of anti-human IgG, both probes are able to achieve a good LOD (limit of detection) at 1.6 nM.

Based on the above cross-comparison, further research has been undertaken to explore the potential of nanoparticles of the alloy of gold and silver, with an aim to combine the robustness of gold and the excellent LSPR effect of silver. To do so, various alloy particles with varied gold/silver ratio and sizes have been prepared and tested for their respective refractive index sensitivities. The probe coated with alloy particles with bigger size and higher silver content has shown better performance in RI sensing. The work has shown a clear relationship between the size of alloys, the content ratio of alloys and RI sensitivity.

Research has also been undertaken in this thesis to explore the excellent LSPR effect of hollow nanoparticles resulting from the enhanced coupling between the interior and exterior of the hollow particles. Gold hollow nanocages have been successfully synthesised and tested with different hollowness and a LSPR sensor coated with gold nanocages has shown an excellent sensitivity as high as ~1933 nm/RIU, which is more than 3 times higher than that coated with AuNPs. This result has confirmed that a significant improvement in sensitivity can be made possible for further biosensing as well as chemical sensing applications.

Abbreviations and Symbols

AgNP	Silver nanoparticle
AuNP	Gold Nanoparticle
AuNR	Gold Nanorod
BEM	Boundary Element Method
CFU	Colony-forming Unit
ConA	Concanavalin A
DDA	Discrete Dipole Approximation
ssDNA	Single-stranded DNA
EBL	Electron Beam Lithography
FBG	Fibre Bragg Grating
FDTD	Finite Difference Time Domain
FEM	Finite Element Method
FOM	Figure of merit
FPIA	Fluorescence Polarization Immunoassay
FWHM	Full Width at Half Maximum
GMT	Generalised Multipole Technique
HRTEM	High Resolution Transmission Electron Microscope
LbL	Layer-By-Layer
LC-MS/MS	Liquid Chromatography – Mass Spectroscopy
LED	Light-emitting Diode
LOD	Limit of Detection
LPG	Long Period Fibre Grating
LPW	Longitudinal Plasmon Wavelength
LSPR	Localised Surface Plasmon Resonance
MDL	Method detection limit
NIR	Near-Infrared
NSL	Nano-sphere Lithography
PCF	Photonic Crystal Fibre
PECVD	Plasma-enhanced chemical vapour Deposition
PVD	Physical Vapour Deposition
QCM	Quartz Micro Balance
RI	Refractive Index
RIU	Refractive Index Unit
SAM	Self-Assembled Monolayer
SERS	Surface-Enhanced Raman Scattering
S/N	Signal to Noise Ratio
SPR	Surface Plasmon Resonance
TEM	Transmission Electron Microscope
TLM	Transmission Line Matrix
TPW	Transverse Plasmon Wavelength
UV	Ultraviolet
VIE	Volume Integral Equation
XPS	X-ray Photoelectron Spectroscopy

XRD	X-ray diffraction
AAO	Anodic Aluminium Oxide
AChE	Acetylcholinesterase
APTMS	3-Aminopropyltrimethoxysilane
APTES	3-Aminopropyltriethoxysilane
BSA	Bovine serum albumin
CTAB	Cetyl-trimethyl ammonium bromide
DI	De-ionized
DNA	Deoxyribonucleic acid
EDC	N-(3-Dimethylaminopropyl)-N'-ethylcarbodiimide hydrochloride
FA	Folic acid
FTO	Fluorine-doped Tin Oxide
hCG	Pregnancyshuman Chorionic Gonadotropin
hDHFR	Human dihydrofolate reductase enzyme
ITO	Indium Tin Oxide
M3G	Morphine-3-Glucuronide
MG	N-(2-mercaptopropionyl)glycine
MPTMS	3-Mercaptopropyl trimethoxysilane
MPTES	3-Mercaptopropyl triethoxysilane
MTX	methotrexate
MUA	11-Mercaptoundecaonic Acid
NHS	N-hydroxysuccinimide
PAA	Porous Anodic Alumina
PBS	Phosphate Buffer Solution
PDMS	Poly(dimethylsiloxane)
PEG	Polyethyleneglycol
PMMA	poly(methyl methacrylate)
PVP	Polyvinylpyrrolindone
RNA	Ribonucleic Acid
Sulfo-NHS	*N-hydroxysulfosuccinimide*
TEOS	Tetraethoxysilane
THF	Tetrahydrofuran
TMSPED	N-[3-(trimethoxysilyl)propyl]ethylenediamine
TNT	2,4,6-trinitrotoluene
TSNP	Triangular Silver Nanoplate
VOCs	Volatile Organic Compounds
β_{SP}	Propagation constant
c	Speed of light in vacuum
ω	Frequency of light
λ	Wavelength of light
ε_d	Dielectric constant of dielectric medium
ε_m	Dielectric constant of metal
ε_1	Real part of the dielectric function of the metal nanoparticle
ε_2	Imaginary part of the dielectric function of the metal nanoparticle
m	Sensitivity factor

N_A	Electron density
n_D	Refractive index of the dielectric
P_j	Depolarisation factor
R, a	Radius of spherical nanoparticle
V	Volume of the particle
σ_{abs}	Absorbance at cross-section
σ_{ext}	Extinction at cross-section
σ_{sca}	Scattering at cross-section
Δn	Change of refractive index
Δλ	LSPR wavelength shift

Au	Gold
Ag	Silver
Br	Bromine
S	Sulphur
Si	Silicon
Pt	Platinum

Introduction

1.1. Introduction

A sensor is a device which converts physical, chemical and biological parameters which could not be directly measureable into electrical signals that can be directly processed and perceived [1]. In addition to that, the converted signals should be correlated to the amount of input parameters for quantitative purposes.

A sensor is usually considered to be an extension of human perception, providing information both quantitatively and qualitatively. In addition, a range of artificial sensors has been developed to assist human being in capturing non-human perceptive signals, such as seismic vibrations or signals beyond visible range in order to interpret, analyse and visualise the information thus to help with the detection, anticipation and prevention purposes . Sensors can also provide factual, numerical and calculated data to minimise misinterpretation and misperception which might be caused by human brain activity. From another point of view, sensors are exceptionally beneficial to the society in being able to better manage human disabilities, providing timely information for health care, alarming and rescue purposes, navigating and tracking disabled people, etc. [2].

In this thesis, an optical fibre sensor system using a metallic nanostructure based on plasmonic effect is explored and detailed. A typical optical fibre sensor uses light as a transducing signal which is propagating through an optical fibre. Optical interactions of incoming light and the measurands, either direct or non-direct, would cause differences in the outgoing light via various modulation mechanisms and the equipped detectors would convert those differences into electrical signals. Nanomaterials, in particular those with metallic nanostructures, are normally defined to have at least one dimension being smaller than 100nm, yet possess unique

physical properties which are different from their bulk metallic structures [3]. Among those, the plasmonic effect, which is based on "**interaction processes between electromagnetic radiation and conduction electrons at metallic interfaces or in small metallic nanostructures, leading to an enhanced optical near field of sub-wavelength dimension**" [4], is considered one of the most fascinating phenomena. As a result, extensive research has been undertaken to develop a wide range of sensor systems, based on the plasmonic effect, which have shown a huge potential for applications in chemical and biosensing.

The original research in this field did not draw much attention when the work was first published, but was fully acknowledged several decades later [5]. One of the reasons is that the potential of a research could not be easily assessed, especially through theoretical research. Colloidal gold and other metals were created early in 15th – 16th century and one of their first applications was to stain glass for churches, cathedrals or minsters due to their fascinating colours. It was M. Faraday [6] who first conducted an experiment synthesising gold colloid in the laboratory with intense reddish colour in 1857. But the real advancement in nanotechnology did not occur until in the past few decades, supported strongly by both theoretical understanding and the availability of advanced fabrication technologies. Similarly, theoretical studies of surface plasmons were reported as early as 1900s with the most notable by G. Mie [7] in his original paper in 1908, but it was not until 1950s that the paper was fully acknowledged. The first surface plasmon sensing application was reported later in 1983 by Liedberg *et al.* [8]. A similar progress path for optical fibres with the theoretical framework being set up early in 1910 by D. Hondros and P. Debye [9], but first experimental attempt was conducted much later in 1950s by H. H. Hopkins and N. S. Kapany [10], and high attenuation glass fibre optics were fabricated by K.C. Kao and G. A. Hockham [11] in 1966.

S. Mayer [4] summarised four major elements needed for rapid development of plasmonic materials and they were:

- Advanced technologies, including both advanced fabrication techniques, such as electron beam lithography (EBL), nanosphere-lithography (NSL) and

characterisation techniques, such as high-resolution transmission electron microscopy (HRTEM), X-ray diffraction (XRD) system, etc.)

- The availability of high resolution optical detectors, such as dark field microscopy, high resolution photo-detector and photo multiplier.
- Advanced computing, data analysis and numerical modelling, such as multivariable data analysis techniques, artificial neutral network, etc.
- Widespread needs in real life.

A typical example is the development of an advanced optical fibre plasmonic sensor which requires the advancement in fibre optics, plasmonic effects and nanomaterials; and their integration enables widened sensory applications. Fibre optics provides miniaturisation and compactness, along with non-evasiveness, high power transmittance and instant response due to the optical properties of light. The plasmonic effect, especially in nanomaterials, brings ultrasensitive sensing mechanism down to single molecule level. When they are integrated together, plasmonic optical fibre sensors offer a powerful yet simple solution for nanoscale sensing and detection.

In this thesis, refractive index is specifically chosen as a sensing parameter because of its generic nature. Refractive index, as a ratio of light speed in vacuum and in a particular medium, represents the uniqueness of a medium, which is closely related to the concentration of the solution, temperature, viscosity, etc. Therefore, the sensitivity in refractive index sensing provides a generic indication of the performance of a sensor system which could thus be further modified to satisfy the need for specificity and selectivity. The refractive index sensitivity also provides some important insights into the concept of sensor design, allowing for the careful consideration of issues, such as limitation, the elimination of impurity, minimisation or enhancement of the interference effect and proper control of dynamic sensing range.

It was in 1993 that the first paper published applying plasmonic effect on a decladded optical fibre by deposition of a thin layer of gold film onto it, conducted by R. C. Jorgerson and S. S. Yee [12]. In 2000, localised surface plasmon resonance (LSPR) was reported to be incorporated experimentally within the glass substrate via colloidal nanogold suspended on the glass slide by Okamoto *et al.* [13]. L-K. Chau *et al.* [14] were the first that proposed novel LSPR based optical fibre using gold nanoparticles and applied in biosensing via demonstration of biotin-streptavidin interaction. Since then, various configurations and sensing strategies have been developed and the research in this area is still growing exponentially, which has benefited tremendously from the rapid expansion in the development of nanomaterials and nanotechnology. In light of the above, the aims and objectives of this thesis are determined and presented below.

1.2. Objectives and structure of the thesis

This thesis aims to explore in detail the sensing capacity of an optical sensor system, using nanomaterials fabricated with various morphologies and structures incorporating gold and/or silver particles and optical fibre as a generic sensor substrate with the transducing mechanism being based on localised surface plasmon resonance. Thus the detailed aims and objectives of this thesis can be summarised as follows:

- To establish a thorough understanding of plasmonic nanomaterials and their wide applications in optical fibre sensing, through a series of carefully designed experiments.
- To evaluate sensing capacity of different metal nanomaterials when they are incorporated with optical fibres, particularly in RI sensing.
- To demonstrate the bio-sensing ability of the plasmonic sensors through antigen-antibody detection.
- To estimate and predict the huge potential of advanced nanostructures in sensing applications.

The thesis is divided by 8 chapters, each of which represents different topic and the content of each chapter is summarised as follow:

Chapter 1 provides an overview of the topic, aims, objectives and the structure of the thesis.

Chapter 2 introduces some theoretical background related to the work in this thesis.

Chapter 3 presents a comprehensive literature review on the subject of LSPR sensors, in particular those using gold and/or silver nanomaterials.

Chapter 4 shows the detailed research undertaken by the author to produce optical fibre sensors using gold nanoparticles. This chapter shows the details including the synthesis of gold nanoparticles and their immobilisation onto optical fibres, followed by extensive evaluation of the sensors created in terms of their sensitivity, repeatability and stability. The work also considered various parameters which could affect the sensor performance, such as temperature, pH and coating time.

Chapter 5 shows the performance cross-comparison between the LSPR sensors coated with gold nanoparticles and those coated with gold nanorods, and their applications in biosensing area.

Chapter 6 details the development of optical fibre LSPR sensors coated with gold-silver alloys, highlighting detailed synthesis of various alloys with varying content and size, and their impact on the sensitivity of the sensors created, in particular in RI sensing.

Chapter 7 details the development of optical fibre LSPR sensors coated with hollow nanomaterials and their application in RI sensing. This chapter also summarises and compares all the LSPR sensors reported by literature and created by the author and their sensitivities in RI sensing.

Chapter 8 concludes all the results obtained and discussed in the thesis and highlights some important future work, covering the areas of nanomaterials design and selection, sensing capacity and applications.

A list of journal and conference publications by the author is included at the end of the thesis.

1.3. References

1. Hauptmann, P., *Sensors : principles and applications*. 1993, Munich: Carl Hanser ; Hemel Hempstead : Prentice Hall.
2. Wolbring, G. and V. Leopatra, *Sensors: Views of Staff of a Disability Service Organization.* Journal of Personalized Medicine, 2013. **3**(1): p. 23-39.
3. Arregui, F.J., *Introduction*, in *Sensors Based On Nanostructure Materials*, F.J. Arregui, Editor. 2009, Springer: New York.
4. Maier, S.A., *Plasmonics : fundamentals and applications*. 2006, Bath ; New York: Springer.
5. Wriedt, T., *Mie Theory: A Review*, in *The Mie Theory - Basic and Applications*, W. Hergert and T. Wriedt, Editors. 2012, Springer: Heidelberg.
6. Faraday, M., *Experimental Relations of Gold (and Other Metals) to Light.* Philosophy Trans. Royal Society London, 1857. **147**(145).
7. Mie, G., *Articles on the optical characteristics of turbid tubes, especially colloidal metal solutions.* Annalen Der Physik, 1908. **25**(3): p. 377-445.
8. Liedberg, B., C. Nylander, and I. Lunström, *Surface plasmon resonance for gas detection and biosensing.* Sensors and Actuators, 1983. **4**(0): p. 299-304.
9. Hondros, D. and P. Debye, *Electromagnetic waves in dielectrical wires.* Annalen Der Physik, 1910. **32**(8): p. 465-476.
10. Hopkins, H.H. and N.S. Kapany, *A Flexible Fibrescope, Using Static Scanning.* Nature, 1954. **173**(4392): p. 39-41.
11. Kao, K.C. and G.A. Hockham, *Dielectric-fibre Surface Waveguides For Optical Frequencies.* Proceedings of the Institution of Electrical Engineers-London, 1966. **113**(7): p. 1151-&.
12. Jorgenson, R.C. and S.S. Yee, *A fiber-optic chemical sensor based on surface plasmon resonance.* Sensors and Actuators B: Chemical, 1993. **12**(3): p. 213-220.
13. Okamoto, T., I. Yamaguchi, and T. Kobayashi, *Local plasmon sensor with gold colloid monolayers deposited upon glass substrates.* Opt. Lett., 2000. **25**(6): p. 372-374.
14. Cheng, S.F. and L.K. Chau, *Colloidal Gold-Modified Optical Fiber for Chemical and Biochemical Sensing.* Analytical Chemistry, 2003. **75**(1): p. 16-21.

Background and Theory

Theoretical studies set a solid background for better understanding, modelling and applying advanced techniques to address challenges arising from the real world. In this chapter, the theoretical background for optical fibre-based sensing based on surface plasmon resonance (SPR) and localised surface plasmon resonance (LSPR) is given prior to the detailed discussions on the manipulation of the LSPR effect through the variation of the morphologies of the gold and/or silver nanomaterials.

2.1. Optical fibres for wave-guiding and sensing

Since the first discovery of a light transmitted medium in 1841 by D. Colladen and J. Babinet, and shortly afterward by J. Tyndall in 1870 [1], fibre optic has increasingly been considered as one of the fastest developed fields, in particular, for telecommunications and for sensing. The simplicity, durability and affordability of optical fibres greatly accelerate their commercial adaptability.

Optical fibres are of compact size and light weight and along with their exceptional light transmittance, electromagnetic interference-free and inexpensive cost; they have found niche markets for sensing, showing advantages over their electrical counterparts. To create an optical fibre sensor, a section of an optical fibre can be functionalised as an active part, for example, through coating a thin layer of gold film/particles to form SPR/ LSPR-based sensors as discussed in detail in this work. If a section of fibre with its refractive index is being periodically modulated, fibre Bragg grating (FBG) or long period grating (LPG)–based sensors can thus be created for strain/temperature measurements [2-4]. Using the above sensor designs, optical fibre is acting as a waveguide, guiding the excitation light to the sensing part and delivering the modulated optical signal to a photo-detector or a spectrometer for

further signal analysis. The sensor, i.e. the functionalised fibre section, is able to modulate the optical signal when the sensor interacts with the target measurands.

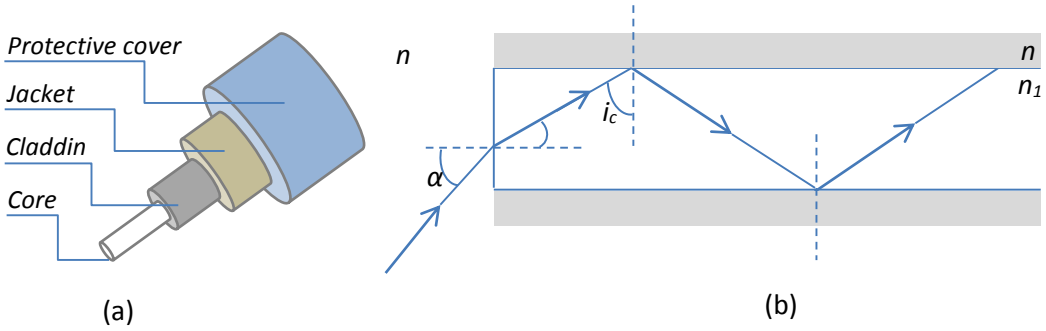

Figure 2.1: a) Typical fibre structure and b) Total internal reflection inside a fibre core. n_0, n_1, n_2 is respectively the refractive index of the outside medium, the fibre core and the cladding.

As illustrated in Fig. 2.1 (a), a basic optical fibre consists of two key parts: the fibre core and the cladding. The outer layers such as jacket and protective cover are primarily used for the fibre's protection. Light transmission inside the fibre is governed by total internal reflection phenomenon, as illustrated in Fig. 2.1 (b).

Optical fibre sensors are usually classified into two major types: intrinsic and extrinsic optical fibre sensors [5]. In an extrinsic sensor, optical fibre acts merely as a waveguide and the actual sensing activity in the sensor occurs outside of optical fibre itself. In an intrinsic sensor, the sensor action is taken place inside the fibre, i.e. the fibre itself acts both as a sensor and a waveguide. Various configurations and sensing mechanisms have been reported to meet various sensing targets, for example, for monitoring physical parameters (temperature, strain, pressure, vibration, refractive index, etc.), chemical analytes (gas, vapours, alcohols, metal ions, etc.) and biological reagents (antibody, enzyme, protein, DNA, etc.) [6, 7].

As the variation of the target parameter(s) is encoded in the optical signals transmitted by the fibre, an optical fibre sensor system is usually sensitive to the optical interference induced by the surrounding environment, such as light, temperature, humidity, etc. This type of interference, however, can be limited through a careful design and configuration of the sensor. The performance of an optical fibre sensor system can also be limited by the availability and specifications

of the system components available, for example, the bandwidth of a light source or the response time of a photo-detector. The selection of these components, however, is not just be determined by their specifications but also by their associated costs and the overall system performance required.

2.2. Surface Plasmon Resonance (SPR)

Both SPR and Localised Surface Plasmon Resonance (LSPR) are based on the plasmonic effect, but their underpinning sensing mechanisms are different. Surface plasmon resonance, which was firstly discovered by Wood in 1902 **[8]**, is the collective oscillation of electrons propagating along the metal-dielectric interface. When light from a light source interacts with a metal-dielectric interface, photons from this light source are transferred to a packet of electrons, which are called surface plamons **[9]**. Resonance only occurs when specific conditions were satisfied, i.e. when the frequency of the photons matches exactly the oscillation of free electrons generated. Two most common SPR configurations, as shown in Fig. 2.2, are Krestchmann and Otto configurations. In Krestchmann configuration as shown in Fig. 2.2(a), a metal layer, normally gold, is deposited on the glass surface of a prism and the coupling between the excitation and plasmon occurs at the outer surface of the gold layer. This is the most used configuration in practical applications, where the gold surface could be modified to be a local specific binding site for chemical or biological reagents. In the Otto configuration as shown in Fig. 2.2(b), the metal layer is positioned not directly on but close to the prism surface, allowing the evanescent electromagnetic wave to interact with the metal layer and excite the surface plasmons.

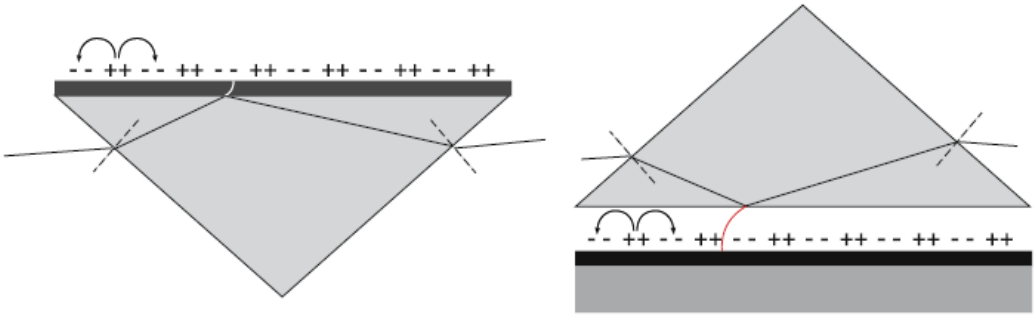

(a) (b)

Figure 2.2: (a) Krestchmann and (b) Otto configurations for SPR effect. Reproduced from Ref. [10] © Springer 2007.

Surface plasmons are usually characterised by the propagation constant β_{SP} which is given by equation (2.1) below [11]:

$$\beta_{SP} = \frac{\omega}{c} n_{ef} = \frac{\omega}{c} \sqrt{\frac{\varepsilon_M {n_D}^2}{\varepsilon_M + {n_D}^2}} \qquad \text{(Eq. 2.1)}$$

In Equation (2.1), ω is the angular frequency, c is the speed of light in vacuum, ε_M is permittivity of the metal and n_D is the refractive index of the dielectric. Therefore, surface plasmons depend largely on the angular frequency, refractive index of dielectric medium and the permittivity of the metal. Because the evanescent field is highly local (from 150 – 400 nm from the excitation surface) [11], a small change in the local surface of the metal layer could induce a large change in plasmonic effect, making SPR a highly sensitive technique for sensing, especially in biological interactions.

Based on the characteristics of the SPR effect, three main strategies, i.e. modulations of wavelength, angle or intensity [11] as illustrated in Fig. 2.3, are usually used to meet various sensing needs. In a sensor design based on the modulation of wavelength as shown in Fig. 2.3.a, a polychromatic light source with fixed incident angle can be used to excite the evanescent field, and a spectrometer is equipped to collect reflective beam. The surrounding refractive index change can induce the shift in plasmonic wavelengths and this shift would be used as a sensor output. An angle based technique is illustrated in Fig. 2.3.b, where a monochromatic light source with a fixed wavelength is used and the angle of incident beam is seen to vary as a function

of the surrounding refractive index. In the intensity-based sensing layout shown in Fig. 2.3.c, with the incident angle and wavelength of the incident light being both fixed, the change in refractive index is represented by the change in the intensity of the output signal.

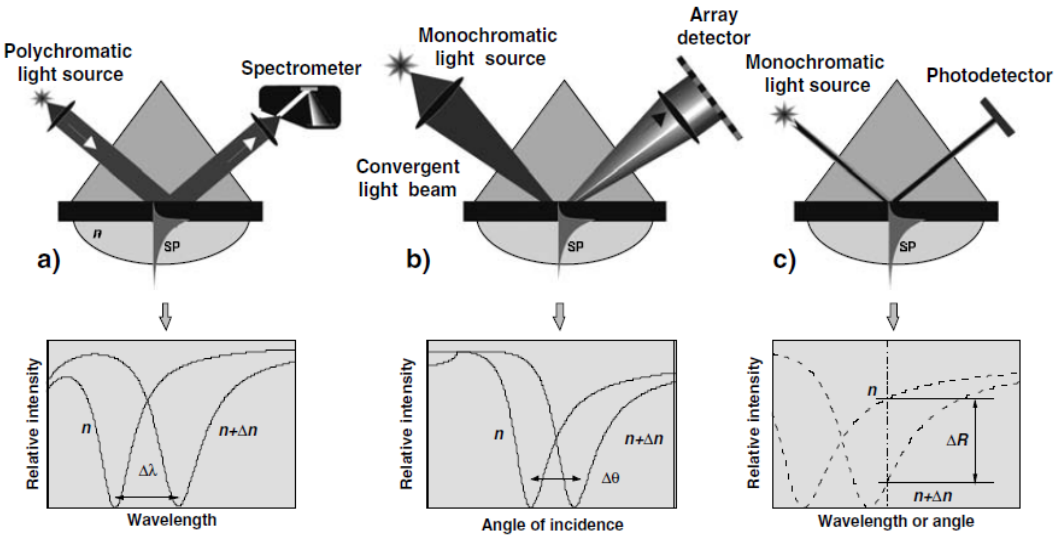

Figure 2.3: SPR sensing strategies based on modulation of a) wavelength, b) angle of incidence and c) light intensity. Reprinted from Ref. [11]. © Springer 2008

2.3. Localised Surface Plasmon Resonance (LSPR)

Localised surface plasmon (LSP) is a phenomenon where the electrons of metallic structure coupled with electromagnetic field from excitation light **[10]**. It arises from the scattering properties of small, conductive particles in an oscillating electromagnetic field. As illustrated graphically in Fig. 2.4, the electronic and ionic clusters are formed on the curved surfaces of the particles when they are excited by light. These clusters create an effective restoring force which subsequently induces the resonance and enhancement of electromagnetic field both inside and outside of the metallic particles and this effect is termed localised surface plasmon resonance (LSPR).

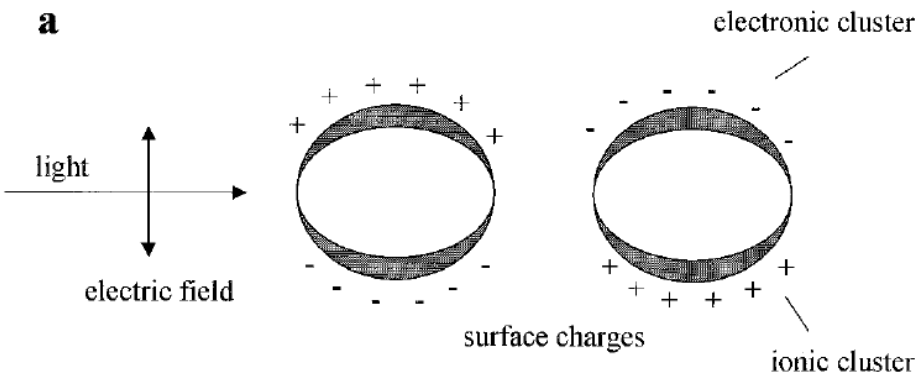

Figure 2.4: Schematic illustration of localised surface plasmon. Reproduced from Ref. [12] © Taylor & Francis 2000

LSPR could occur with normal or direct light interaction. Therefore, there is a range of light sources which can be used to create a LSPR sensing system. For noble metal like gold and silver, the resonance wavelengths are within visible range, for example, colloidal solutions of those metals are brightly colourful [13]. This phenomenon is related to the scattering and absorbance properties of small metal particles which has been explained in theory by Gustav Mie (1869-1957) using Maxwell's equation of electromagnetic field documented in his well-known paper published in 1908 [14]. This ground-breaking study has laid a solid foundation for characterising, modelling and anticipating properties of other nanostructures than spherical small particles. Below include some fundamental theories behind.

2.3.1. Mie theory

As mentioned above, Mie extensively computed light scattering by small spherical particles using Maxwell's equations in electromagnetic theory. Using this approach, he successfully explained the distinct ruby-red colour of gold colloidal solution by absorbance and scattering theory. It was not until 1950s that this research on colloids became the centre of attention. Since then, a lot of efforts have been made towards modifications, applications and corrections of Mie's original theory with particles other than gold and with different size and morphology. These include non-spherical particles, sphere particles in an absorbing medium and coated, distorted, magnetic, chiral and anisotropic spheres, from few nm up to 10 µm in diameter.

To explore Maxwell's equation for spherical particles in non-absorbing medium, Mie established several important equations for scattering, absorbance and extinction at the cross-section. Detailed mathematical calculations could be found in textbooks, especially in the ones by Bohren and Huffman (1983) or by Kreibig and Vollmer (1995). In this thesis, only some final equations are presented as follows:

$$\sigma_{sca} = \frac{2\pi}{|k|^2}\sum_{L=1}^{\infty}(2L+1)(|a_L|^2 + |b_L|^2) \qquad \text{(Eq. 2.2)}$$

$$\sigma_{ext} = \frac{2\pi}{|k|^2}\sum_{L=1}^{\infty}(2L+1)[Re(a_L + b_L)] \qquad \text{(Eq. 2.3)}$$

$$\sigma_{abs} = \sigma_{sca} - \sigma_{ext} \qquad \text{(Eq. 2.4)}$$

where k is the wavevector of incoming light and L are integers representing the dipole, quadrupole, and higher multipoles of scattering. a_L and b_L are the following parameters, composed of Ricatti – Bessel function Ψ_L and χ_L

$$a_L = \frac{m\Psi_L(mx)\Psi_L'(x) - \Psi_L'(mx)\Psi_L(x)}{m\Psi_L(mx)\chi_L'(x) - \Psi_L'(mx)\chi_L(x)} \qquad \text{(Eq. 2.5)}$$

$$b_L = \frac{\Psi_L(mx)\Psi_L'(x) - m\Psi_L'(mx)\Psi_L(x)}{\Psi_L(mx)\chi_L'(x) - m\Psi_L'(mx)\chi_L(x)} \qquad \text{(Eq. 2.6)}$$

Where $m = \tilde{n}/n_m$ and $\tilde{n} = n_R + in_I$ is the complex refractive index of the metal material, n_m is the refractive index of the surrounding medium. So that

$$m = \frac{\tilde{n}}{n_m} = \frac{n_R + i n_I}{n_m} \quad \text{(Eq. 2.7)}$$

$$x = k_m r = \frac{2\pi}{\lambda_m} r \quad \text{(Eq. 2.8)}$$

With k_m is the wavenumber in the medium.

Equations 2.1-2.7 are general and could be applied for numerous particles with different size and shape. Under some special circumstances, these equations can be simplified to help understanding the effect. For example, when spherical particles with diameters much smaller than that of the wavelength of the excitation light, i.e. $2\pi r \ll \lambda \; or \; x \ll 1$, equations (2.5) and (2.6) used to calculate a_L and b_L can be simplified as given in equations (2.9) and (2.10), assuming higher order of a_L and b_L are zero.

$$a_1 \approx -\frac{i2x^3}{3}\frac{m^2-1}{m^2+2} \quad \text{(Eq. 2.9)}$$

$$b_1 \approx 0 \quad \text{(Eq. 2.10)}$$

Substitute m in Eq. (2.7) into Eq. (2.9), we have:

$$a_1 \approx -i\frac{2x^3}{3}\frac{{n_R}^2-{n_I}^2+2in_Rn_I-{n_m}^2}{{n_R}^2-{n_I}^2+2in_Rn_I+2{n_m}^2} \quad \text{(Eq. 2.11)}$$

Next, with complex metal dielectric function, we have

$$\tilde{\varepsilon} = \varepsilon_1 + i\varepsilon_2$$

$$\varepsilon_1 = {n_R}^2 - {n_I}^2$$

$$\varepsilon_2 = 2n_Rn_I$$

And with medium dielectric function $\varepsilon_m = {n_m}^2$, equation (2.11) can be modified to be

$$a_1 \approx \frac{2x^3}{3}\frac{-i{\varepsilon_1}^2-i\varepsilon_1\varepsilon_m+3\varepsilon_2\varepsilon_m-i{\varepsilon_2}^2+2i{\varepsilon_m}^2}{(\varepsilon_1+2\varepsilon_m)^2+(\varepsilon_2)^2} \quad \text{(Eq. 2.12)}$$

Substitute this value into Eq. (2.2) and (2.3), the scattering and extinction coefficients can thus be expressed by equations (2.13) and (2.14):

$$\sigma_{sca} = \frac{32\pi^4 {\varepsilon_m}^2 V^2}{\lambda^4} \frac{(\varepsilon_1 - \varepsilon_m)^2 + (\varepsilon_2)^2}{(\varepsilon_1 + 2\varepsilon_m)^2 + (\varepsilon_2)^2} \quad \text{(Eq. 2.13)}$$

$$\sigma_{ext} = \frac{18\pi {\varepsilon_m}^{3/2} V}{\lambda} \frac{\varepsilon_2(\lambda)}{[\varepsilon_1(\lambda) + 2\varepsilon_m]^2 + \varepsilon_2(\lambda)^2} \quad \text{(Eq. 2.14)}$$

Equation (2.14) could be used for establishing extinction spectra of small nanoparticles when excited by light. It can be seen clearly that σ_{ext} depends on particle's size (V – volume of the particle, related to r – its radius), particle's characteristics (ε_1 and ε_2) and surrounding medium (ε_m). Extinction can be maximised when $[\varepsilon_1(\lambda) + 2\varepsilon_m]^2 + \varepsilon_2(\lambda)^2$ is a minimum and this can be achieved when $\varepsilon_1 = -2\varepsilon_m$. When this specific condition is considered for Gold and Silver, σ_{ext} can be calculated precisely [15, 16]. It has been reported that the theoretical data obtained matched well with the experimental data obtained from small gold and silver particle [17-19].

In the case of real life, where the particle is not spherical, equation (2.15) below can be derived, with χ representing the aspect ratio, i.e. the ratio between in-plane diameter and out-of-plane height of the nanoparticle (in case of a sphere, χ = 2); N_A is the areal density of the nanoparticle and a is the radius of the particle [20]:

$$\sigma_{ext} = \frac{24\pi N_A a^3 {\varepsilon_m}^{3/2}}{\lambda \ln(10)} \left[\frac{\varepsilon_2}{[\varepsilon_1 + \chi\varepsilon_m]^2 + {\varepsilon_2}^2} \right] \quad \text{(Eq. 2.15)}$$

Therefore, by varying χ value, this approximation could be used for anticipating the extinction spectra of elongated particles rather than spheres. With χ being ranged from 2 (spheres) to 17 (rod with 5:1 aspect ratio), the extinction spectra of nanorod particles with varying aspect ratio can thus be obtained using Eq. 2.15 [18, 20].

Table 2.1: Values of dielectric constants of different metals. Adapted from Ref. [21] © Springer 2010

Metal	Dielectric constant ($\varepsilon_1 + i\varepsilon_2$)	$\varepsilon_1/\varepsilon_2$
Gold (Au)	-10.92 + 1.49i	7.33
Copper (Cu)	-14.67 + 0.72i	20.4
Silver (Ag)	-18.22 + 0.48i	38.0
Aluminium (Al)	-42.00 + 16.40i	2.56

Table 2.1 lists some dielectric constant values of several common metals and based on the equations listed above, their corresponding extinction spectra can be calculated and cross-compared. Figure 2.5 shows the results obtained for gold and silver. Figure 2.5 (a) illustrates the real part of extinction spectra of gold (yellow line) and silver (grey line), in which $\varepsilon_{1(Au)} > \varepsilon_{1(Ag)}$. Figure 2.5 (b) demonstrates the imaginary part of the complex dielectric functions of gold and silver, which has played an important role in plasmon resonance and is related to peak broadening. Loss is lower in Ag lower than that in gold, therefore, theoretically, the resonance peak of Ag appears to be sharper than that of Au [15].

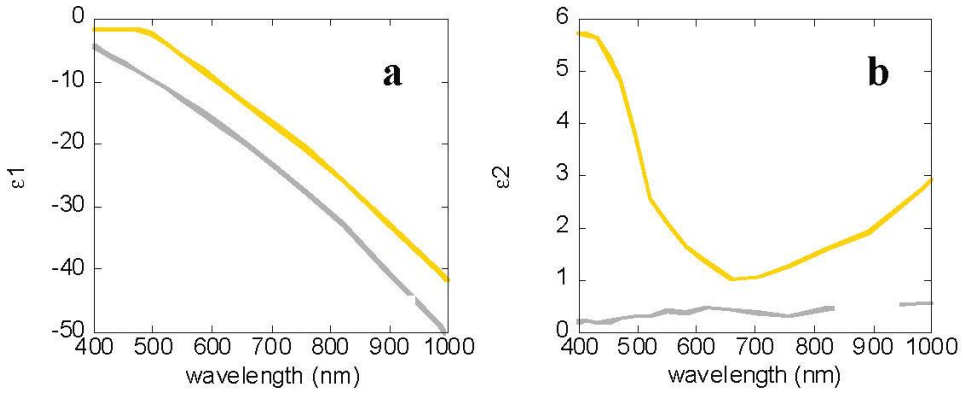

Figure 2.5: (a) Real and (b) Imaginary part of extinction spectra from gold (yellow line) and silver (grey line). Reproduced from Ref. [15] © ACS Publications 2011

The fact that σ_{ext} depends on ε_m is particularly important for sensing applications and this underpins the sensing mechanism for refractive index measurement using LSPR approach. Also, in from Eq. 2.15, σ_{ext} shows to be dependent of particles' size (a – radius of the particle) and particle's characteristic (χ – the aspect ratio of the particle). It is important to note that equations (2.9) to (2.15) are only valid when particles are small (i.e. diameter <10 nm).

The induced wavelength shift can also be predicted using the above equations as described below [22]:

$$\Delta\lambda_{max} = m\Delta n\left(1 - e^{-2d/l_d}\right) \quad \text{(Eq. 2.16)}$$

where Δn is the change in refractive index, m is the bulk refractive index response of the particles, d is the thickness of absorbate layer and l_d is electromagnetic field decay length.

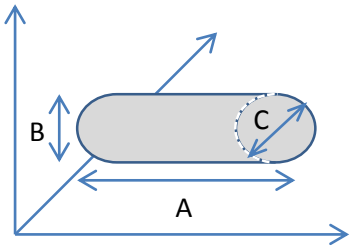

Figure 2.6: Illustration of elongated particle with three axes, A,B and C with A > B = C.

For elongated particles like nanorods, R. Gans [23, 24] adapted and extended Mie theory, and obtained the result shown below [12]:

$$\sigma_{ext} = \frac{\omega}{3c}\varepsilon_m{}^{3/2}V\sum_j \frac{\left(1/P_j^2\right)\varepsilon_2}{\{\varepsilon_1+[(1-P_j)/P_j]\varepsilon_m\}^2+{\varepsilon_2}^2} \quad \text{(Eq. 2.17)}$$

where P_j are the depolarisation factors along three axes A, B, C of the nanorod, and A > B = C (illustrated in Fig. 2.6), which are predetermined as:

$$P_A = \frac{1-e^2}{e^2}\left[\frac{1}{2e}\ln\left(\frac{1+e}{1-e}\right) - 1\right] \quad \text{(Eq. 2.18)}$$

$$P_B = P_C = \frac{1-P_A}{2} \quad \text{(Eq. 2.19)}$$

The relationship between value e and aspect ratio R is given below:

$$e = \sqrt{\left[1 - \left(\frac{B}{A}\right)^2\right]} = \sqrt{1 - \frac{1}{R^2}} \quad \text{(Eq. 2.20)}$$

Based upon the above calculations, extensive research has been undertaken to model extinction spectra of particles with different sizes, shapes and compositions. Haiss *et al.* [17] developed a corrected calculation method which enables the theoretical data to fit well with experimental data of nanogold particles with diameters varying from 4 to 100nm. Several theoretical models have also been

established for non-spherical particles [25]. Mie theory has already been modified for an absorbing medium, rather than non-absorbing medium in its original theory [25]. Other types of spherical particles have also been extensively explored, such as coated particles, distorted particles, magnetic particles or chiral and anisotropic particles.

2.3.2. Discrete Dipole Approximation (DDA) calculation

The original Mie theory can only be applied for small spherical particles, which has shown some limitations. In reality, the as-prepared nanomaterials always show a certain level of deviation from the ideal spherical shape, therefore it is important to modify the calculation method(s) to fit for the 'real' shapes of particles. A numerical method was proposed by E.M. Purcell and C.R. Pennypacker [26] to 'fill in the gap' of Mie theory for nonspherical particles. The complicated and lengthy calculations can be found in a book chapter by Enguehard [27], or in many other important papers [22, 28-32]. Zhao *et al.* [16] gave an concise and straightforward summary of common methods used in modelling and describing nanoparticles' properties, including scattering and absorbance spectra and DDA was first introduced in the paper.

In general, in DDA calculation, a nonspherical particle is described using three dimensional arrays of dipole elements confined in a cubic grid. Each of these elements has its polarisability α_i (i: 1 →N) determined by a nanoparticle dielectric function. The dipole P_i in each element is defined as $P_i = \alpha_i E_{loc,i}$, in which $E_{loc,i}$ is the sum of incident and retarded fields of the other N – 1 elements, as given in Eq. 2.21:

$$E_{loc,i} = E_{inc,i} + E_{dipole,i} = E^0 e^{ik\cdot r_i} - \sum_{\substack{j=1 \\ j\neq i}}^{N} A_{ij} \cdot P_j \qquad \text{(Eq. 2.21)}$$

where E^0 is the amplitude of incident wavelength, and $k = {}^{2\pi}/_{\lambda}$ is the wave vector.

A_{ij} is the matrix of dipole interaction and is given by:

$$A_{ij} = k^2 e^{ikr_{ij}} \frac{r_{ij}\times(r_{ij}\times P_j)}{{r_{ij}}^3} + e^{ikr_{ij}}(1 - ikr_{ij}) \frac{[{r_{ij}}^2 P_j - 3r_{ij}(r_{ij}\cdot P_j)]}{{r_{ij}}^5} \qquad \text{(Eq. 2.22)}$$

With r_{ij} is the vector from element i to element j.

After having solved these equations, the final conclusion for extinction cross-section is given by

$$C_{ext} = \frac{4\pi k}{|\vec{E}^{inc}|^2} \sum_{j=1}^{N} Im\left[\vec{E}_j^{inc,*} \cdot \vec{P}_j\right] \quad \text{(Eq. 2.23)}$$

DDA method has been well recognised and widely applied in simulation of extensive structures, such as nanotriangle, nanodisk, nanocube, core-shell particles, hollow particles and many others, with diameter ranged from few nanometre to hundreds nanometre. For example, the El-Sayed group has used DDA calculation for various type of nanostructures, ranging from gold to silver, such as gold-silver alloy of different content ratio and size [33], gold nanorod [34], gold nanocages [35] as well as for coupling effect of nanoparticles [36]. The calculation has shown a good fit with experimental results and has provided a powerful tool for applications in sensing area, for example, for enhancement of RI sensitivity by using gold nanoframes [37].

In addition to Mie theory and DDA method, several other numerical methods have been widely reported. In 1998, Thomas Wriedt [30] reviewed different calculation methods, including point matching method, T-matrix method, generalised multipole technique (GMT) and other volume-based methods such as Finite Difference Time Domain (FDTD), Transmission Line Matrix (TLM), Volume Integral Equation (VIE) and Finite Element Method (FEM). Myroshnychenko *et al.* [38] summarised several popular methods with their own advantages and disadvantages, including DDA, FDTD and boundary element method (BEM). A comprehensive review of characterisation of light scattering by particles was given by A.R. Jones [39]. With the advancement of computational technology both in terms of capacity and of computational speed, numerical methods offer extremely powerful tools to help discover and characterise more and more diverse nanostructures for various applications.

2.4. Conclusions

This chapter has focused on the background and fundamental theory in relation to fibre optics, SPR and LSPR. With technological advancement both in the optical fibre manufacturing and in materials science driven by the telecommunications industry, optical fibre proves to be an excellent material not only for light transmission, information and data transfer but also in sensing area. Optical fibres can be a suitable sensor substrate, serving both as a waveguide and as a sensor/transducer when a section of fibre is functionalised, for example, as a SPR or LSPR sensor.

The chapter has also reviewed the underpinning theory for SPR and LSPR, which includes Mie scattering theory and DDA calculations together with some numerical models created for a wide variety of nanostructures, with different sizes, shapes, materials, etc.

2.5. References

1. Al-Azzawi, A., *Fibre optics : principles and practices*. 2007, Boca Raton, Fla.: CRC ; London : Taylor & Francis [distributor].
2. Mokhtar, M.R., K. Owens, J. Kwasny, S.E. Taylor, P.A.M. Basheer, D. Cleland, Y. Bai, M. Sonebi, G. Davis, A. Gupta, I. Hogg, B. Bell, W. Doherty, S. McKeague, D. Moore, K. Greeves, T. Sun, and K.T.V. Grattan, *Fiber-Optic Strain Sensor System With Temperature Compensation for Arch Bridge Condition Monitoring.* Ieee Sensors Journal, 2012. **12**(5): p. 1470-1476.
3. Alwis, L., T. Sun, and K.T.V. Grattan, *Design and performance evaluation of polyvinyl alcohol/polyimide coated optical fibre grating-based humidity sensors.* Review of Scientific Instruments, 2013. **84**(2).
4. Alwis, L., T. Sun, and K.T.V. Grattan, *Fibre optic long period grating-based humidity sensor probe using a Michelson interferometric arrangement.* Sensors and Actuators B-Chemical, 2013. **178**: p. 694-699.
5. Grattan, K.T.V. and Y.N. Ning, *Classification of optical fiber sensors*, in *Optical Fiber Sensor Technology*, K.T.V. Grattan, Editor. 1998, Chapman & Hall: London, UK.
6. Udd, E.E., *Fiber optic sensors*. 1993, Bellingham, Washington, DC: SPIE Optical Engineering Press.
7. Grattan, K.T.V. and B.T. Meggitt, *Optical fiber sensor technology*. Vol. 2. 1998, London: Chapman & Hall.
8. Wood, R.W., *On a remarkable case of uneven distribution of light in a diffraction grating spectrum.* Philosophical Magazine, 1902. **4**(19-24): p. 396-402.
9. Mol, N.J. and M.J. Fischer, *Surface Plasmon Resonance: A General Introduction*, in *Surface Plasmon Resonance: Methods and Protocols*, N.J. Mol and M.J.E. Fische, Editors. 2010. p. 1-14.
10. Maier, S.A., *Plasmonics : fundamentals and applications*. 2006, Bath ; New York: Springer.
11. Piliarik, M., H. Vaisocherová, and J. Homola, *Surface Plasmon Resonance Biosensing*, in *Biosensors and Biodetection*, A. Rasooly and K.E. Herold, Editors. 2008. p. 65-88.
12. Link, S. and M.A. El-Sayed, *Shape and size dependence of radiative, non-radiative and photothermal properties of gold nanocrystals.* International Reviews in Physical Chemistry, 2000. **19**(3): p. 409-453.
13. Steinbrück, A., A. Csaki, and W. Fritzsche, *Metal Nanoparticles for Molecular Plasmonics*, in *Reviews in Plasmonics*, C.D. Geddes, Editor. 2010, Springer: New York, USA.
14. Mie, G., *Articles on the optical characteristics of turbid tubes, especially colloidal metal solutions.* Annalen Der Physik, 1908. **25**(3): p. 377-445.
15. Mayer, K.M. and J.H. Hafner, *Localized Surface Plasmon Resonance Sensors.* Chemical Reviews, 2011. **111**(6): p. 3828-3857.
16. Zhao, J., A.O. Pinchuk, J.M. McMahon, S. Li, L.K. Ausman, A.L. Atkinson, and G.C. Schatz, *Methods for Describing the Electromagnetic Properties of Silver and Gold Nanoparticles.* Accounts of Chemical Research, 2008. **41**(12): p. 1710-1720.
17. Haiss, W., N.T.K. Thanh, J. Aveyard, and D.G. Fernig, *Determination of Size and Concentration of Gold Nanoparticles from UV−Vis Spectra.* Analytical Chemistry, 2007. **79**(11): p. 4215-4221.
18. Kelly, K.L., E. Coronado, L.L. Zhao, and G.C. Schatz, *The Optical Properties of Metal Nanoparticles: The Influence of Size, Shape, and Dielectric Environment.* The Journal of Physical Chemistry B, 2002. **107**(3): p. 668-677.

19. Mock, J.J., M. Barbic, D.R. Smith, D.A. Schultz, and S. Schultz, *Shape effects in plasmon resonance of individual colloidal silver nanoparticles.* Journal of Chemical Physics, 2002. **116**(15): p. 6755-6759.
20. Haes, A.J. and R.P. Van Duyne, *A unified view of propagating and localized surface plasmon resonance biosensors.* Analytical and Bioanalytical Chemistry, 2004. **379**(7-8): p. 920-930.
21. Gupta, B.D., *Surface Plasmon Resonance Based Fiber Optic Sensors*, in *Review in Plasmonics*, C.D. Geddes, Editor. 2010, Springer: New York, USA. p. 105-138.
22. Willets, K.A. and R.P. Van Duyne, *Localized Surface Plasmon Resonance Spectroscopy and Sensing.* Annual Review of Physical Chemistry, 2007. **58**(1): p. 267-297.
23. Gans, R., *The shape of ultra microscopic gold particles.* Annalen Der Physik, 1912. **37**(5): p. 881-900.
24. Gans, R., *The state of ultramicroscopic silver particles.* Annalen Der Physik, 1915. **47**(10): p. 270-U14.
25. Wriedt, T., *Mie Theory: A Review*, in *The Mie Theory - Basic and Applications*, W. Hergert and T. Wriedt, Editors. 2012, Springer: Heidelberg.
26. Purcell, E.M. and Pennypac.Cr, *Scattering And Absorption Of Light By Nonspherical Dielectric Grains.* Astrophysical Journal, 1973. **186**(2): p. 705-714.
27. Enguehard, F., *Mie Theory and the Discrete Dipole Approximation. Calculating Radiative Properties of Particulate Media, with Application to Nanostructured Materials*, in *Thermal Nanosystems and Nanomaterials*, S. Volz, Editor. 2009, Springer-Verlag Berlin: Berlin. p. 151-212.
28. Draine, B.T. and P.J. Flatau, *Discrete-dipole Approximation For Scattering Calculations.* Journal of the Optical Society of America a-Optics Image Science and Vision, 1994. **11**(4): p. 1491-1499.
29. Ghosh, S.K. and T. Pal, *Interparticle Coupling Effect on the Surface Plasmon Resonance of Gold Nanoparticles: From Theory to Applications.* Chemical Reviews, 2007. **107**(11): p. 4797-4862.
30. Wriedt, T., *A Review of Elastic Light Scattering Theories.* Particle & Particle Systems Characterization, 1998. **15**(2): p. 67-74.
31. Hartland, G.V., *Optical Studies of Dynamics in Noble Metal Nanostructures.* Chemical Reviews, 2011. **111**(6): p. 3858-3887.
32. Noguez, C., *Surface Plasmons on Metal Nanoparticles: The Influence of Shape and Physical Environment.* The Journal of Physical Chemistry C, 2007. **111**(10): p. 3806-3819.
33. Lee, K.-S. and M.A. El-Sayed, *Gold and silver nanoparticles in sensing and imaging: Sensitivity of plasmon response to size, shape, and metal composition.* Journal of Physical Chemistry B, 2006. **110**(39): p. 19220-19225.
34. Lee, K.-S. and M.A. El-Sayed, *Dependence of the Enhanced Optical Scattering Efficiency Relative to That of Absorption for Gold Metal Nanorods on Aspect Ratio, Size, End-Cap Shape, and Medium Refractive Index.* The Journal of Physical Chemistry B, 2005. **109**(43): p. 20331-20338.
35. Mahmoud, M.A., B. Snyder, and M.A. El-Sayed, *Surface Plasmon Fields and Coupling in the Hollow Gold Nanoparticles and Surface-Enhanced Raman Spectroscopy. Theory and Experiment†.* The Journal of Physical Chemistry C, 2010. **114**(16): p. 7436-7443.
36. Jain, P.K. and M.A. El-Sayed, *Plasmonic coupling in noble metal nanostructures.* Chemical Physics Letters, 2010. **487**(4-6): p. 153-164.
37. Mahmoud, M.A. and M.A. El-Sayed, *Gold Nanoframes: Very High Surface Plasmon Fields and Excellent Near-Infrared Sensors.* Journal of American Chemical Society, 2010. **132**(36): p. 12704-12710.

38. Myroshnychenko, V., J. Rodriguez-Fernandez, I. Pastoriza-Santos, A.M. Funston, C. Novo, P. Mulvaney, L.M. Liz-Marzan, and F.J. Garcia de Abajo, *Modelling the optical response of gold nanoparticles.* Chemical Society Reviews, 2008. **37**(9): p. 1792-1805.
39. Jones, A.R., *Light scattering for particle characterization.* Progress in Energy and Combustion Science, 1999. **25**(1): p. 1-53.

Review of advanced sensing technologies based on LSPR effect

Localised Surface Plasmon Resonance (LSPR), as theoretically introduced in Chapter 2, is the phenomenon that occurs when the evanescent field interacts with the metallic noble nanomaterials. The charge density oscillations inside nanomaterials resonate with the excitation light at a certain incident wavelength, resulting in the appearance of strong absorption and scattering peak and the enhancement of the electromagnetic field [1-4]. LSPR effect has gained much of interest, due to its huge potential in various application areas, including clinical and medical bio-sensing and chemical sensing, imaging and therapy, etc. LSPR also shows the potential for miniaturisation, which can be exemplified by a lab-on-a-chip design, integrating a range of microfluidic devices, being coupled with the multiplexing capability to create, for example, electric noses for medical and security applications. Many comprehensive reviews have been published in the last decade, providing rich information and deep understanding of different aspects in relation to LSPR, ranging from synthesis [5-7], fabrication techniques [2, 8, 9], theoretical calculations [10] to applications [5, 6, 8, 11]. This chapter aims to review the state-of-the-art technologies reported and thus provides collective information, in particular, in the field of LSPR-based sensing. This chapter starts with the introduction of a generic LSPR sensor configuration, which includes the key components required to create a LSPR-based sensor. This is followed by discussions on the sensing mechanisms and the strategies which have been widely deployed for sensing. Detailed discussions in terms of the impact made by the variation of the size, shape and type of nanomaterials have also been made in this chapter, providing a comprehensive review of the materials and morphology reported in literature. The chapter also covers the applications reported in chemical sensing and biosensing area and

concludes with the discussions on the technological advancement in the field and potential for future exploitation.

3.1. Generic layout of a LSPR sensor

LSPR has early been applied for sensing, due to its spectral enhancement and dependence on the medium surrounding the nanomaterial. Different sensing strategies have been derived from this phenomenon and Fig. 3.1 shows a generic configuration of a LSPR sensor system, in which the sensing area is usually coated with plasmonic materials. Light from a light source (**L**) is guided to interact with the sensing area and the resulting spectral signal variation is collected by a detector (**D**).

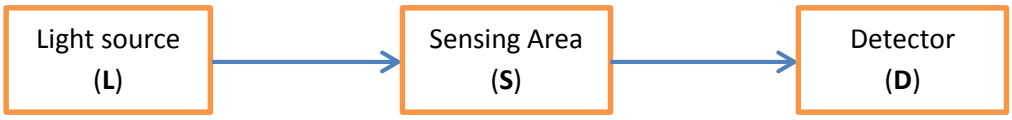

Figure 3.1: A generic LSPR sensor layout

Various light sources can be used for this purpose, ranging from white light sources (typically with a wavelength range of 200-2500nm), light-emitting diodes (LEDs) to normal laser sources. Spectroscopic techniques are usually used for the detection of LSPR induced spectral variations, ranging from UV-Visible to near infrared (NIR), which is dependent on the corresponding LSPR absorbance characteristics. Dark field spectroscopy has been used extensively for single nanoparticle sensing [12]. Other techniques such as surface-enhanced Raman spectroscopy (SERS) or quartz micro balance (QCM) have also been reported to be used as detectors.

A glass slide was first chosen as the main platform for the deposition of nanomaterials [13-17]. Several other materials, such as indium tin oxide (ITO) glass [18-22], fluorine-doped tin oxide (FTO) polymer [23] or anodic aluminium oxide (AAO) platform [24, 25], have also been chosen, either for the enhancement of stability, transparency or for the ease of fabrication. Nanomaterials have also been coated onto optical fibres, either on the end-surface or on the decladded portion of the fibre to create a highly sensitive, versatile and compact sensing probe [26-39]. The interaction between the propagated light along the fibre and the sensing surface

results in the change in LSPR peak when the surrounding medium varies. Single mode fibres, multimode fibres with different core and cladding, photonic crystal fibres (PCF) [39] and other metal-doped fibres have also been reported in literature.

Extensive research has been undertaken and reported for the preparation and synthesis of various nanomaterials and for their corresponding immobilisation on various types of sensor substrates. A detailed discussion on nanomaterials is included in Section 3.3 of this chapter, with a primary focus on the noble metallic nanomaterials such as gold or silver. A number of preparation and deposition techniques have been explored, which includes both chemical techniques, such as seed-growth method, metal ion reduction, co-polymer reduction and physical methods, such as nanosphere lithography (NSL), electron beam lithography (EBL), laser ablation and electro-deposition. Other less popular preparation schemes, such as “green chemistry”, have also been proposed. In conjunction with the synthesis methods, various immobilisation techniques have been proposed to coat the nanomaterials onto a substrate surface, which include the application of silanisation agents, sol-gel techniques, bi-functional compounds, electrostatic force or other physical interactions, in situ chemical oxidation, hydrothermal growth, liquid-phase deposition, etc. [8].

In term of sensing, as illustrated in Fig. 3.2, two main streams, i.e. bulk sensing, commonly referring to refractive index (RI) sensing and molecular sensing or single particle sensing, have been recognised [11]. Different types of spectroscopic techniques have been used in different sensing streams. Bulk refractive index sensing is normally related to ensemble spectroscopy while molecular sensing to scattering spectroscopy (i.e. dark field microscopy). Ensemble spectroscopy covers a broader spectrum than that of single particle scattering spectroscopy and offers a higher magnitude. Therefore, bulk sensing offers larger dynamic range and multiplexing capacity. The single nanoparticle scattering spectroscopy, however, can achieve a much lower limit of detection (LOD) and better signal to noise ratio (S/N).

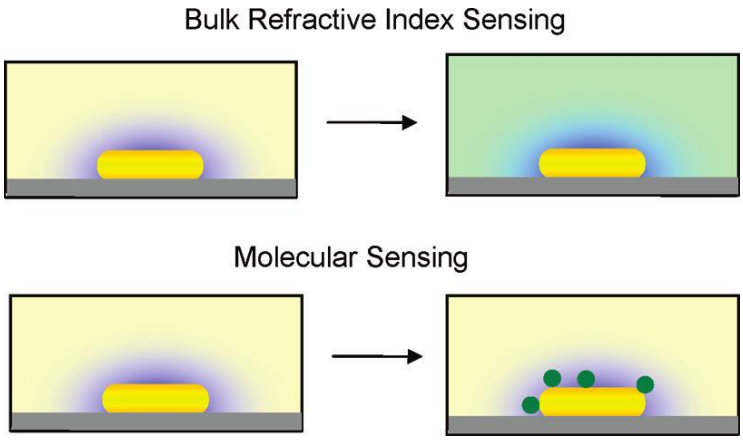

Figure 3.2: Bulk sensing vs. molecular sensing. Reprinted from ref [11]. Copyright 2011 ©American Chemical Society

In general, the evaluation of sensing capacity involves several parameters, including sensitivity, limit of detection (LOD), method detection limit (MDL), etc. In terms of RI sensing, the RI of a surrounding medium would affect the sensing layer and thus modulate the LSPR spectra. The sensitivity can be calculated using Eq. (3.1):

$$S = \frac{d\lambda_{peak}}{dn} \quad \text{(Eq. 3.1)}$$

$$FOM = \frac{S}{FWHM} \quad \text{(Eq. 3.2)}$$

Another parameter which is widely used to characterise the sensing ability of a nanoparticle is the figure of merit (FOM) as described in Eq. (3.2), where FWHM stands for full width at half maximum value. Larger particles demonstrate a higher peak shift and a broader peak width compared to smaller particles when they are in different RI solutions.

Overall, there are 3 main sensing strategies and they are summarised as follows [2]:

- ***LSPR absorbance-based technique.*** The change in the surrounding medium of the sensing surface triggers the change in LSPR absorbance spectra. This change could be exhibited and quantified as the difference in the absorbance intensity or the shift in the peak wavelength.

- ***Colorimetric technique***. This technique can be implemented when there is a colour change as a result of the aggregation of metallic nanoparticles in solution.

- ***Direct LSPR spectral monitoring technique***. The change in LSPR spectrum, induced by the morphology change as a result of the direct interaction between analyte and nanoparticles, is monitored directly using a spectrometer.

3.1.1. LSPR absorbance-based technique

This sensing approach is the most widely used strategy reported in literature. The change in the immediate medium surrounding the active sensing layer affects the LSPR absorbance or scattering peak of the nanomaterials, thus resulting in a shift in the peak wavelength and/or a change in the intensity of the absorbance. This approach is widely used for monitoring RI of the surrounding medium/environment through monitoring the wavelength shift or intensity change in the absorbance spectrum of the solution, with its RI being varied by the change in the concentrations of analyte, such as glucose [6]. Using the single particle approach, a specific antibody which has been immobilised onto the sensing surface can capture the free antigen in solution, hence inflicting the shift in wavelength or the change in signal intensity.

3.1.2. Colorimetric technique

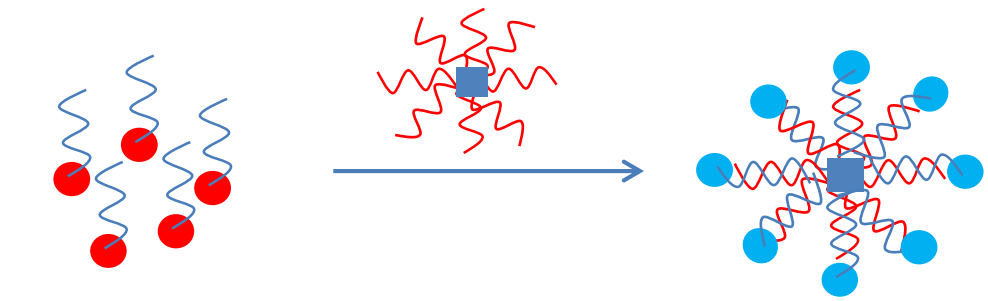

Figure 3.3: Illustration of colour change due to the aggregation of metallic NPs

The colorimetric technique has been used for the detection of DNA using oligonucleotide-coated gold nanoparticles dispersed in solution [40]. These metallic nanoparticles are coated with a single DNA strand (ssDNA) and are dispersed freely in solution. Upon binding with the complimentary strand, the aggregation occurs, resulting in a significant change in colour (Fig. 3.3). The aggregation creates a huge intermolecular interaction between metallic nanoparticles and the inter-particle coupling results in a shift in the peak wavelength, leading to an obvious colour change which can be observed by naked eyes [41].

Based on this aggregation phenomenon, a similar approach has been applied based on biotin-streptavidin, antibody-antigen or glucose-Concanavalin A (conA) interactions. Direct applications have included the detection of DNA , metal ions in solution such as Ag^{+} [42], Hg^{2+} [43, 44], Fe^{3+} [45] , thiol-containing amino acids, enzyme [46, 47], bacteria [48-51], protein, TNT [52], etc. Their advantages including the ease of fabrication and implementation and low cost have enabled this strategy to be more applicable for disposable and low-cost applications.

3.1.3. Direct LSPR spectral monitoring technique

This type of technique is based on the effect caused directly by the analyte, which has an ability for directly affect the morphology of the nanometallic layer, and as a result inducing the change in the LSPR absorbance or scattering spectra. Bi *et al.* [53] proposed a method for detection of Mecury ion (Hg^{2+}) by using silver nanoparticles of different morphology. Silver nanorods, nanospheres and nanoplates were self-prepared by different seed-growth methods. With the presence of Hg^{2+} ion, replacement reaction would occur, resulting in the etching of the morphology of those particles. The change in morphology would introduce the change in LSPR absorbance spectra of the solution. The linearity between the concentration of Hg^{2+} and the wavelength shift was recorded over the range from 10 – 1500 nM with AgNR. Similarly, Shan *et al.* [54] proposed an approach to detect H_2O_2, based on its etching effect on gold nanorods. H_2O_2 would induce a shape-change of AuNR in solution, leading to a change in aspect ratio of AuNR, hence affecting directly the LSPR spectra of the solution. The limit of detection was reported to be 0.046 µM. The

disadvantage, however, is the interference with the other molecules present in the sample solutions. For example, for Hg^{2+} detection, other metal ions could create a similar effect, making this approach being non-specific.

However, the main disadvantage of this approach is the non-reversibility of reaction between the analyte and the metallic layer. In this case, the metallic layer would be permanently damaged, making it unsuitable for reusable purpose. Therefore, this method could be very costly.

To sum up, metallic nanoparticles, especially gold and silver, with the profound LSPR effect have demonstrated their powerful capability to be used in various sensing schemes. In the following sections, discussions are made on their corresponding preparations, properties and applications.

3.2. Preparation, fabrication and immobilisation techniques

Two of the most popular materials in LSPR study are gold and silver because of their strong absorbance bands in nanostructure. This section is dedicated for an introduction of the preparation techniques, coating methods and the rationale behind various choices.

Chemical approach is considered to be traditional for preparing nanoparticles, since it begins with famous Faraday's experiment on gold colloidal solution in 1857 [55]. Since then, chemical approach has evolved to achieve different morphology with controllability over nanostructure's parameters. Basically, this approach is a two-step synthesis, based on reduction of metal ion to metal in nanostructure. First step is to create nuclei – it is also called seed-formation step. Second step is to grow the seed into different particle-structures of choice, allowing for an appropriate control over the growth period using different surfactants. The choice for the reduction agent, protecting agent, surfactant, temperature, reaction rates, molar ratio, etc. can be varied to achieve desirable morphology. The formation process is also coupled with the other techniques, such as micelle formation, microwave ultrasonic, hydrothermal evaporation, etc. To date, a number of particles with different shapes have been successfully synthesised using this approach, ranging from nanospheres, nanorods,

nanotriangles, nanocubes, nanorice to more complex structures such as hollow nanocubes, nanobranches, nanostars, nanowires, etc. The composition of those particles can be varied, from single metals such as gold, silver, copper and platinum to an alloy of these, or from the core-shell structure to a structure with two or more multilayers.

Using a physical approach, lithography has demonstrated to be a powerful tool to create a monodispersed, highly ordered film of metallic particles with desired size, shape, inter-particle distance. Among these, electro-beam lithography (EBL) is able to provide an accurate control of gold nanoislands in a substrate. The disadvantage is that it requires expensive equipment and long-time sample preparation. Nanosphere lithography (NSL) is an inexpensive alternative, which is simple and inexpensive to create a highly ordered film of gold or silver nanotriangles array. Modifications of these methods have also been reported in order to further enhance the uniformity and the desirable morphology of the particles, such as creating gold nanodisks on glass by hollow-mask colloidal lithography [56], making Au-Ag triangle array on glass by NSL [57], or using the advantage of EBL to create gold nanostar, nanoellipse and nanoring [58]. The strength of using a physics method lies in the creation of highly ordered array of metal materials and the control of the size, shape and interparticle distance required, in addition to the fabrication of a wide variety of plasmonic structure, such as gold nanohole [59], nanogap [60] or nanowell [61] for biosensing applications. However, costly equipment, extended fabrication time and less flexibility are the main disadvantages that inhibit the potential of those methods in commercialisation.

Different from the physical technique, which is able to deposit the nanomaterials directly onto the surface of a substrate, the chemical approach requires a suitable method for immobilising nanoparticles onto the substrate. For gold and silver, because of their high affinity with sulphide and amine, the most commonly used method is silanisation. Using this method, the surface of a substrate (normally glass) is first modified with a silanised agent. Different organo-silane compounds, e.g. 3-mercaptopropyltrimethoxysilane (MPTMS), 3-mercaptopropyltrimethoxysilane (MPTES), 3-aminopropyltrimethoxysilane (APTMS), 3-aminopropyltriethoxysilane

(APTES), N-[3-(trimethoxysilyl)propyl]ethylenediamine (TMSPED), are widely used. Normally, thio-terminated compound has a higher adhesiveness towards gold or silver nanoparticles than amine-terminated compound [62]. A common strategy for immobilisation of AuNPs on a glass surface is illustrated in Fig. 3.4. Electrostatic interactions between compounds are the main driving force to adhere these together.

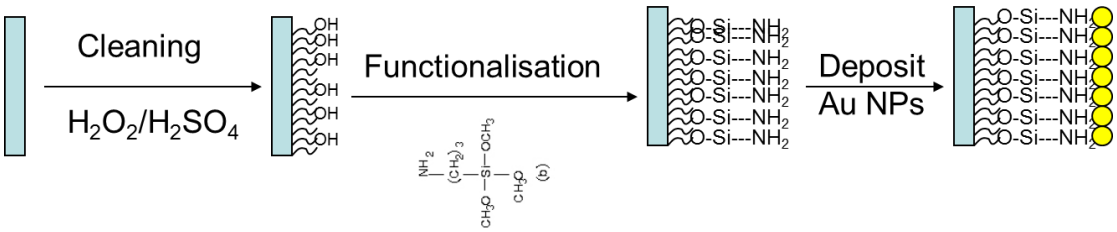

Figure 3.4: Illustration of immobilisation of AuNPs onto a glass slide

Sol-gel process is also used as one of the immobilisation techniques. It involves two main steps: the first is hydrolysis of a precursor under acidic or alkaline conditions and the second is to condense the hydrolysed products. This process is able to create a highly stable substrate with high surface density.

Another efficient immobilisation method is to use layer-by-layer (LbL) technique via electrostatic interactions as illustrated in Fig 3.5. Using this approach, a number of bilayers of different charge can be laid alternately on the substrate through dip coating. AuNPs or AgNPs can be immobilised by electrostatic interactions between their charge layer and the charge layer of their protective agents, such as citrate (negative charge) or cetyl trimethylammonium bromide – known as CTAB (positive charge) [8].

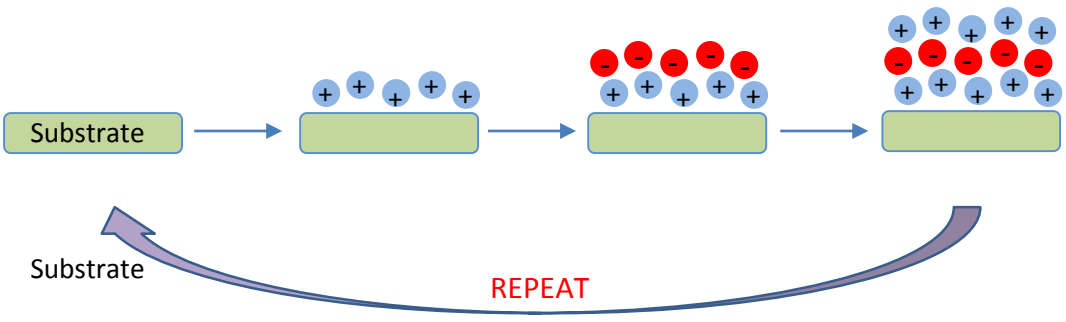

Figure 3.5: Schematic illustration of LbL technique by the deposition of layers of opposite charge.

3.3. Effect of size, shape and materials

Both the theoretical and practical studies of plasmonic properties of nanomaterials conclude the importance of their morphology.

3.3.1. Theoretical studies

Gold colloidal solutions were practically synthesised in the laboratory as early as in 1857 by Michael Faraday[55]. But the theoretical model by solving Maxwell's classical electromagnetic theory to explain the phenomenon exhibited by spherical particles in nanoscale was not reported until in 1908 by Mie [63]. Given the fact that the classical calculation reported by G. Mie is very limited to spherical particles with certain diameters, there have been several advanced numerical methods proposed to fill in the gaps. The most widely used methods include discrete dipole approximation (DDA) [64, 65], finite difference time domain (FDTD) [66, 67], and finite element method (FEM) [68]. Each of these theoretical models and calculations can only be applied for specific scenarios with limitations in the particle diameters, shapes and/or materials.

Based on the above, several attempts have been made to assess the RI sensing capacity of nanomaterials in relation to the size, shape and aspect ratio of the particles used. For example, Nusz *et al.* developed a model for rational choice of gold nanorod with different aspect ratio in label-free biosening [69]. In this research, the sensitivity was simulated, showing its dependence on the aspect ratio of the nanorods and a higher aspect ratio leads to a higher sensitivity in terms of RI sensing. Sharma *et al.* also demonstrated the effect of size and type of materials on the sensitivity through several publications in theoretical calculations [37, 70-73]. Gold, silver, copper and Indium Tin Oxide (ITO) have been considered in the model, using optical fibres as a sensor substrate, and it was concluded that the highest sensitivity can be achieved by using ITO.

The trend for the sensitivity enhancement for gold and silver nanospherical particles was demonstrated in a study by Lee *et al.* [74]. In their work, 3 different sizes of

20nm, 40nm and 60nm have been investigated, confirming that a bigger size leading to a higher sensitivity. In another study Miller and Lazarides [75] reported that the sensitivity of LSPR sensors based on nanoparticles varied linearly with their corresponding plasmonic resonant wavelength.

It is important to note that, because of the complexity in sensor design and fabrication, it is difficult to predict accurately the RI sensitivity of a LSPR sensor using models or calculations. In fact, most of the research has been based on experimental results, followed by simulations made in a confined situation. For example, Mahmoud *et al.* experimentally analysed the sensitivity of a LSPR sensor made of gold nanoframes and the experimental results obtained were supported by DDA calculation, which was subsequently used to simulate and predict the sensitivity of other types of nanoframes with different wall size and thickness [76].

3.3.2. Experimental studies

A large amount of experimental data has been reported in literature regarding RI sensitivity. In this section, a summary, rather than a comprehensive list of these reports will be presented. It focuses primarily on two materials, gold and silver.

A series of experiments has been undertaken on LSPR sensors based on gold and silver nanoparticles to evaluate their RI sensing capacity and the impact made by the shape of nanoparticles used. Mock *et al.* demonstrated the sensitivity of LSPR sensors based on silver nanoparticles in the forms of spherical, cubic and triangular with a similar volumetric structure [77]. It was reported that that silver nanotriangle provided a much higher sensitivity than that of nanosphere [78].

Gold nanosphere has been used early in RI sensing, but the sensitivity is not very high. It was reported that 80 nm/RIU could be achieved with gold island in a glass substrate using thermal evaporation [79]. Similar results were obtained by using gold nanoparticles in a different sensing configuration [80-82]. A higher sensitivity could be achieved by increasing the diameter of gold nanoparticles, such as 137 nm/RIU and 187 nm/RIU could be achieved by 90nm and 130nm of AuNPs coated on ITO surfaces, respectively [18]. Another important sensing strategy is to improve the

sensitivity of AuNPs to 245 nm/RIU, based on interparticles interactions, as proposed by Di *et al.* [19, 20]. Live *et al.* [83] reported the highest sensitivity of AuNPs in glass substrate to be achieved, at 579 nm/RIU, using nanosphere lithography (NSL) to create particles at near micron sizes.

And silver has been at the centre of attention due to its higher sensitivity compared to gold. For example, in the same experimental setup, AgNPs-based sensors have shown a sensitivity of 71.7 nm/RIU compared to 32.7 nm/RIU of gold-based sensors [81]. In a setup using dark field microscopy, single spherical AgNPs with diameters ranging from 40 nm to 90 nm have been reported with the highest RI sensitivity of 160 nm/RIU in oil with RI change from 1.44 to 1.56 having been demonstrated [78]. However, due to the chemical instability of silver, AgNP-based sensors are not as widely used as AuNP-based sensors. When they are exposed to air, AgNPs could easily react with sulphur compounds in the air to create Ag_2S, hence the nanomaterials could be completely destroyed over a short period of time. To overcome this limitation, Ag-Au core-shell particles can be used as they can both enhance the stability and increase the sensitivity of the sensors produced. Xia *et al.* reported the sensitivity of up to 409 nm/RIU for core-shell nanostructures [84]. Other reports also confirmed the enhancement of sensitivity when using core-shell nanoparticles including gold shell – silica core [85] or vice versa [86], silver shell – gold core [87] or gold shell – silver core [88, 89], Ag core – Au shell nanorods [90], etc. The sensitivity of the sensors has shown to be increased significantly through various modifications of the sensor configurations and the research in the field is still on-going.

It is important to point out that sharp-tipped particles, such as nanotriangle [91] or bipyramid [92], seem to be able to offer a very high sensitivity. Various strategies have been devised to achieve desirable shapes, including nanotriangle [15, 57, 93], nanobipyramid [94, 95], nanostar [58], nanorice [96, 97], etc. Among these, triangular silver nanoplate (TSNP)-based LSPR sensor has demonstrated the highest sensitivity of up to 1096 nm/RIU [98-100]. This exceptional high sensitivity might be related to a combined effect which includes the configuration using sharp-tipped nanomaterials, highly ordered assembly and big particle size (200nm in length).

Chung *et al.* [101] have summarised these sensing characteristics in relation to various plasmonic nanostructures and the details are shown in Table 3.1. In addition to varying the size and shape of particles, several attempts have also been made to create different structures based on the array of nanomaterials on substrate, such as nanogaps [60], nanopillars or hollow nanotubes [102, 103]. The outcomes of the experiments have shown a promise in achieving a high sensitivity through an appropriate use of a sensing strategy and innovation in fabrication techniques, thus achieving wide applications in biosensing.

Table 3.1: Sensing characteristics of plasmonic nanostructures. Adapted from Ref. [101] © MDPI 2011

Nanostructure	Structure Dimensions	Sensitivity	Ref.
Silver spherical nanoparticles	Diameter: 35 nm	161 nm/RIU	[12]
Silver triangular nanoparticles	Diameter: 35 nm	197 nm/RIU	[12]
Silver rodlike nanoparticles	Aspect ratio 5:1 Diameter: 35nm	235 nm/RIU	[12]
Gold nano rods	Aspect ratio 3.5:1 Radius: 40 nm	650 nm/RIU	[74]
Gold colloidal nanoparticles	Diameter: 30 nm	70.9 nm/RIU	[104]
Hollow gold nano shell	Diameter: 50 nm Wall thickness: 4.5 nm	408 nm/RIU	[104]
Arrays of gold nanodisk	Pitch of nanodisk: 162 nm, 340 nm	167 nm/RIU 327 nm/RIU	[105]
Gold nanodisk trimers	Small disk diameter: 96 nm Larger disk diameter: 127 nm Pitch between trimers: 400 nm	170 nm/RIU 373.9nm/RIU	[106]
Gold nanorings	Diameter: 150 nm Thickness: 20 nm	880 nm/RIU	[107]
Gold nanoring trimers	Outer diameter:120 nm Wall thickness: 33 nm Ring height: 24 nm	345 nm/RIU	[106]
Nanocubes	Size : 100 nm	165 nm/RIU	[108]
Nanocrescents	Diameter: 410 nm Deposition angle:10° Aspect ratio: 4	879 nm/RIU	[109]
Nanostars	Core size: 30–50 nm Conical tips: 10–60 nm	218 nm/RIU	[110]
Nanocross and nanobar	Length: 380nm Width: 76 nm $\alpha = 60°$	710 nm/RIU 1,000 nm/RIU	[111]
Double nanopillars with nanogap	Diameter: 425 nm	642 nm/RIU 1,056 nm/RIU	[112]

	Height: 288 nm Nanogap: 33 nm		
Planar metamaterials analogue of EIT	Length: 400 nm, 340 nm Width: 80 nm, 90 nm Gap: 45 nm	725 nm/RIU	[113]
Plasmonic nanorod metamaterials	Length: 20–700 nm Diameter: 10–50 nm Pitch: 40–70 nm	30,000 nm/RIU	[114]
Arrays of plasmonic nanotubes	Length: 120 nm Inner diameter: 22 nm Outer diameter: 44 nm Pitch: 55 nm	250 nm/RIU	[102]
Nanopillar arrays	Radius: 100 nm Height: 400 nm Pitch: 600 nm	675 nm/RIU	[115]

As shown in Table 3.1, an exceptionally high sensitivity, over 1000 nm/RIU, can be achieved using TSNP [98-100] or using gold nanocross [111]. Further sensitivity enhancement can be achieved by using gold nanostar particles on tapered fibre to increase the sensitivity to 1190 nm/RIU [35] or by coating a thin layer of gold film reported by Cao *et al.* [116] to achieve the sensitivity of 2977 nm/RIU. Zhou et al [117] reported the potential of achieving 3770nm/RIU through theoretical analysis by incorporating silver nanocubes into a photonic crystal fibre (PCF). The use of metamaterial has been reported to be able to increase the sensitivity by 2 to 3 order of magnitude compared to normal gold nanoparticles. Gu *et al.* reported in 2011 a powerful tool to grow gold nanorods tightly on the glass substrate, create a layer of metamaterial and achieve 30000 nm/RIU [118]. Although only a theoretical calculation based on a short range of RI change has been made, the exceptionally high sensitivity which is expected to be achievable gives a clear indication that this might be a useful approach to explore. The disadvantage, however, lies in the use of highly expensive equipment and complicated technique which could prevent it from being commercialised and mass-produced.

3.4. Sensing applications

Tailoring morphology and increasing RI sensitivity lead to a wide spectrum of applications for sensing through surface modification using metal nanoparticles in order to form a selective layer.

3.4.1. Biosensing

Similar to SPR, LSPR provides a similar (or sometimes even higher) sensitivity showing the advantage of miniaturisation. Nanotechnology enables the sensing device to be compact, portable and much cheaper compared to SPR sensors. Cross-comparison between LSPR and SPR sensors has been made and reported and detailed in Table 3.2.

Table 3.2: Comparison between SPR and LSPR. Adapted from ref. [1] ©Springer 2004

Feature/Characteristic	SPR	LSPR
Label-free detection	Yes	Yes
Distance dependence	~1000nm	~30nm
Refractive Index Sensitivity	$2x10^6$ nm/RIU	$2x10^2$ nm/RIU
Modes	Angle shift, wavelength shift, imaging	Extinction, scattering, imaging
Temperature control	Yes	No
Chemical identification	SPR-Raman	LSPR-SERS
Field Portability	No	Yes
Commercially available	Yes	No
Cost	US $150.000 – 300.000	US $5000 (multiple particles) US $50.000 (single particle)
Spatial resolution	~10x10 µm	1 nanoparticle
Non-specific binding	Minimal	Minimal
Real-time detection	Time scale = 10^{-1} – 10^3 s Planar diffusion	Time scale = 10^{-1} – 10^3 s Radical diffusion
Multiplexed capacity	Yes	Yes
Small molecule sensitivity	Good	Better
Microfluidic compatibility	Yes	Yes

Similar to SPR sensors, LSPR for biosensing is label-free. Using the LSPR technique, it is possible to achieve single particle sensing, which can incredibly limit the amount of analyte needed for analysis and this is usually very important for the analysis of

biological samples, such as human or anthropology sample. This technique, however, usually requires signal amplification due to the weak signals generated from particle sensors.

The selectivity of a LSPR sensor to bioanalyte is usually realised through various selective interactions, such as enzyme, biotin-avidin, antibody-antigen, aptamer-protein, DNA based technique, or Concanavalin A (ConA) – monosaccharide, as detailed below. The standard procedure for the fabrication of LSPR sensors is to immobilise one of the pair on the surface of nanoparticles, and upon binding with the other, LSPR spectra would change, leading to detection of the specific bioreagent.

3.4.1.1. Enzyme interaction based technique

An enzyme is a class of large proteins that is responsible for life-sustaining in almost every living matter in the universe. It is regarded as a biocatalyst to greatly increase metabolic processes. The simple reaction is described below:

$$\mathbf{E + S} \quad \rightleftarrows \quad \mathbf{E\text{-}S} \quad \rightleftarrows \quad \mathbf{E\text{-}P} \quad \rightleftarrows \quad \mathbf{E + P} \qquad \text{(Eq. 3.3)}$$

where enzyme (**E**) binds with substrate (**S**) to create an intermediate (**E-S**) which has lower activation energy than normal reaction condition. Subsequently, the **E-S** would be converted into a complex E-P and then decomposed to the precursor enzyme and the product (**P**). This process is illustrated clearly in Fig. 3.6.

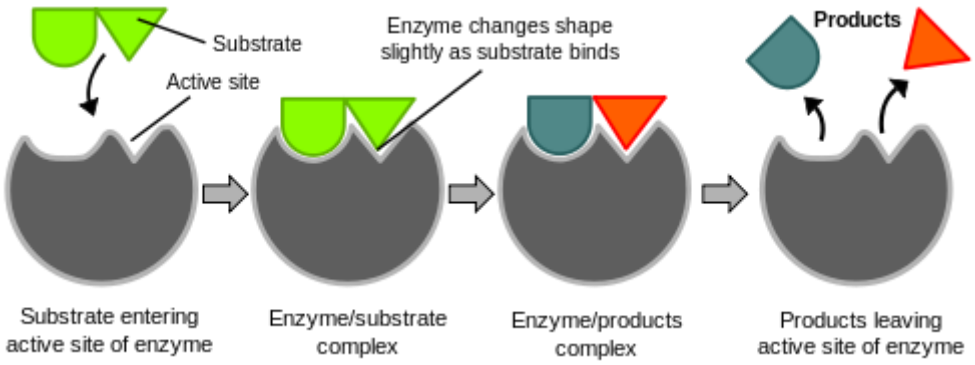

Figure 3.6: "Lock and Key" mechanism of Enzyme catalyst. Reproduced from Ref. [119]

The simple mechanism behind the enzymatic catalyst effect for the reaction in Eq. 3.3 is described in Fig. 3.7. Without an enzyme acting as a catalyst, the reaction must

undergo the transition state TS_u in order to convert the substrate (S) into the product (P) and this requires a higher standard free energy of activation ΔG_u^*. In the presence of an appropriate enzyme (E), however, the reaction requires a much lower activation energy that can be recoursed through three transition steps, TS_{c1}, TS_{c2} and TS_{c3}, respectively. Although the total energy needed for the reaction could not be different ($\Delta G_u^* = \Delta G_{C1}^* + \Delta G_{C2}^* + \Delta G_{C3}^*$), the required activation energy in case of enzyme reaction is lower ($\Delta G_C^* \ll \Delta G_u^*$), hence it is easier to make the reaction happen with less requirements for conditions, such as at lower temperature or pressure [120].

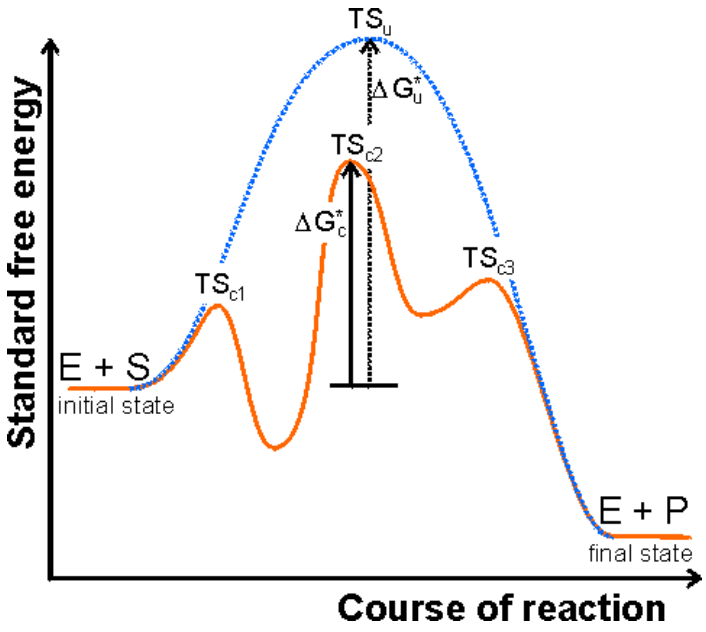

Figure 3.7: Enzyme catalyst mechanism. Yellow line is the course of reaction with the enzymatic catalyst and the blue line is the reaction without catalyst. Reproduced from Ref. [120]

Enzyme biocatalyst is specific and each enzyme recognises only its specific target, based on the predefined size, shape, charge and hydrophobic/hydrophilic properties of the substrate. This type of sensing mechanism is frequently referred to as "lock and key" mechanism.

Based on this mechanism, a number of studies have been undertaken to create a number of biosensors, using different types of enzymes [29, 46, 48, 105, 121-125]. Lin *et al.* (2006) created a novel gold nanoparticle-based biosensor using Acetylcholinesterase (AChE) as an enzyme for the detection of organophosphorus pesticides [126]. AChE acted as a biocatalyst in the reaction to convert

Butyrylthiocholine into Thiocholine, which was subsequently characterised by UV-Vis spectra at 405nm. The sensor enables the detection of paraoxon in range of 1-100ppb with a LOD of 0.234ppb and it is highly reproducible. Zhao *et al.* reported the creation of a competitive binding assay in order to detect methotrexate (MTX), an anticancer drug via gold nanoparticles coated with folic acid (FA-AuNPs) and human dihydrofolate reductase enzyme (hDHFR). The method achieved excellent reproducibility and sensitivity with a LOD of 155 nM. This method has also been tested with real clinical samples with high accuracy in comparison to other reference methods such as fluorescence polarization immunoassay (FPIA) and liquid chromatography – mass spectroscopy (LC-MS/MS) [125].

3.4.1.2. Biotin – Avidin interaction based technique

This interaction is a common binding technique used in LSPR biosensing because of its strong conjunction, specificity and commercial availability. Avidin is a class of large protein (M_w ~ 50 kDa) molecules with four specific binding sites for biotin, commonly known as tetrameric glycoprotein [127]. The affinity between biotin – avidin is exceptionally high, with a dissociation constant (K_d) ~ 10^{14} M^{-1} [11]. This high affinity enables the sensors created with a LOD level in the range of few femtomolar. The small size of biotin molecules also makes the fabrication process much easier as they can be easily immobilised onto the sensor substrates. In addition, the four binding sites help biotin-avidin interaction to be adapted, for example in a sandwich type assay, to enhance the sensing capacity.

Even using the same interaction, different LODs, ranging from few pM to micro molar, have been reported. This huge difference is due to the variation in sensor configurations, types of metals used, morphology and the experimental conditions. In 2004, Haes *et al.* [1] reported less than pM in LOD, equal to less than 100 streptavidin compound per nanoparticle with NSL-based silver nanotriangles. Arai *et al.* reported that a biosensor made through the deposition of a thin nanostructured silver film on a glass substrate is able to detect streptavidin in range of 16 nM – 8µM [128]. Barbillon *et al.* created a highly sensitive biosensor of gold nanocylinder with 100nm diameter and 200nm inter-particle distance in glass substrate fabricated by

EBL. This sensor could lower the LOD to 1.25 x10^{-18} mol for Streptavidin, equal to 75 molecules per nanoparticles. Also later in 2009, this group used EBL to create gold nanodisks on glass substrate, by then lowered detection limit to 7pM for Streptavidin [129]. Marinakos *et al.* proposed the use of AuNRs on a glass slide to create an effective biosensor with a low LOD of 19 nM in serum and 94 pM in phosphate buffer solution (PBS) [80]. Based on the advantage demonstrated by nanoshells over their solid spherical counterparts, Wang *et al.* proposed a biosensor for detection of Streptavidin in blood sample in 2008, with a LOD of 3 µg/mL and a wide dynamic range from 3 to 50 µg/mL [130]. In general, biotin-avidin has become one of the popular interaction techniques used for the design of LSPR biosensors.

3.4.1.3. Antibody – antigen

Antibody – antigen interaction is one of the most widely used techniques for biosensing due to the high selectivity, strong binding affinity and easy production of this type of sensors. Antibody, or known as immunoglobin (Ig), is a large Y-shaped protein produced by an immune system to "identify and neutralise extruded objects like bacteria or virus" [131]. Each tip of the Y shape has a specific binding site for a certain antigen, allowing antibody-antigen interaction to be selective, similar to a key-lock mechanism as illustrated in Fig. 3.6. The association constant K_a, defined below (Ab: antibody, Ag: antigen), varies from 10^5 to 10^{12} M^{-1} in the case of antibody-antigen interaction, which makes the latter an ideal technique for the creation of sensors with a detection limit in range of nM to pM.

$$Ab + Ag \rightleftarrows Ab{:}Ag$$

$$K_a = \frac{[Ab{:}Ag]}{[Ab][Ag]}$$

To configure a biosensor, antibody is usually immobilised on the surface of a metallic nanomaterial. When the interaction between the antibody and the target antigen occurs, there is a change in LSPR spectra as a result of the surrounding refractive index change due to the binding. This change would be recorded and the real-time kinetic of binding event could also be displayed and analysed.

A large number of studies based on this interaction have been reported in literature [19, 20, 24, 25, 27, 28, 36, 99, 132-138]. Because antibody could be produced biologically in response to almost every antigen, the applicability of this method is enormous. Detection of pathogens by this method draws the most attention because of its direct sensing mechanism. Several examples include the detection of *Salmonella* [134], biomarker for Alzheimer's disease [139], heptatitis B virus [140] or influenza virus [141]. Antibody, extracted from human, goat or rabbit, has occasionally been used to verify the sensing capacity of a system [99, 132, 136]. The LOD of such a sensor system could be down to few CFU/mL [142].

3.4.1.4. Aptamer interactions

Compared to antibody-antigen interaction, aptamer interaction is a relatively new discovery since 1990, following the independent reports by two groups, Gold's [143] and Szostak's [144] . It is a specific nucleic acid sequence that binds non-nucleic acid targets with high affinity and specificity, and could be used to target a number of molecules, ranging from metal ions, amino acids, short peptides to proteins and even some pathogenic microorganisms. In general, an aptamer is immobilised onto the surface of an optical device either through affinity interactions (including ionic, hydrophobic and Van der Waal's force), covalent binding or chemisorption methods [145]. Subsequently, the folding activity upon specific targets is able to induce a change in LSPR spectra, similar to the other interactions (Fig. 3.8).

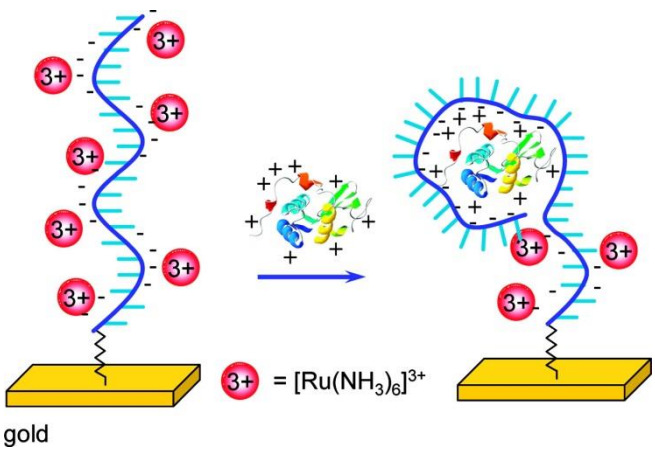

Figure 3.8: Illustration of aptamer folding mechanism. Adapted from Ref. [146] ©ACS 2007.

Aptamer-based immunoassays have been developed in conjunction with the SPR technique. Kim Do-Kyun *et al.* in 2008 [147] fabricated a chip with gold deposition onto a porous anodic alumina (PAA) layer. An aptamer specified for thrombin detection was then immobilised on the chip, creating an LSPR-based optical sensor with a very low LOD at 1 nM for thrombin. Zheng *et al.* developed an in-solution based method using AuNR and aptamer-folding ability to detect thrombin [148]. Using this technique, the AuNR is coated with a specific aptamer for thrombin, and then be mixed in a solution of tosyl-activated magnetic beads. With the presence of thrombin, aptamers are folded and subsequently AuNRs are aggregated on the beads due to the magnetic force to form a pellet. This, as a result, lowers the concentration of AuNR in the solution and decreases the intensity of the absorbance spectra of the solution.

Even though there are currently limited reports on this particular sensing application, aptamer folding could be a promising route for biosensor as well as chemical sensor development when it is coupled with LSPR, especially in case of single nanoparticle sensing. In this scheme, the sensitivity of the system could be further enhanced and the LOD could also be lowered to the molecular level. The flexibility in designing an aptamer for a specific target can also be employed to secure the specificity and reduce the non-specific binding, compared to other interactions such as enzyme interaction or antibody-antigen interaction.

3.4.1.5. Nucleic Acids Hybridization

Nucleic acids, most commonly known as DNA (Deoxyribonucleic acid) and RNA (Ribonucleic acid), are the basic materials that create all life on earth. While DNA is responsible for storage of genetic information, RNA is mainly responsible for the transfer of information within cells [131]. DNA mostly is made of double-stranded helices, composed by 4 different nucleobases, Adenine (A), cytosine (C), guanine (G) and thymine (T). In RNA, nucleobases are of a similar structure expect thymine (T), which is replaced by Uracil (U).

Hydrogen bonds can only be formed between two different pairs, such as G-C and A-T. This permits two complementary nucleic acids to form a double-strand association

complex, called hybridization. Nucleic acid based biosensing applications typically require immobilisation of a single-stranded sequence (ssDNA) to the surface of the substrate. This sequence is traditionally allowed to bind with a target sequence of interest. The optimization of the immobilization procedure can provide an increase in signal intensity, selectivity, and sensitivity.

Researchers have explored this application extensively and numerous studies have been reported [23, 26, 86, 149-152]. However, due to the small molecular weight of short strain, the direct approach of monitoring change in signal upon hybridization is often less practical. Huang *et al.* reported the fabrication of a gold nanoring-coated chip for short sequence DNA application, with high sensitivity and selectivity [153]. The most commonly used approach based on DNA hybridization is colorimetric method, where the gold nanoparticles are capped with ssDNA in solution. Upon the presence of the complementary DNA, gold nanoparticles will aggregate and cause visible colour change. A number of applications based on this are discussed in this section.

To amplify the signal, a sandwich based assay is normally implemented. For example, in the report by Spadavecchia *et al.*, gold nanorods and nanostars are employed to create a sandwich assay for DNA hybridization, which is illustrated in Fig. 3.9 [152]. Using this method, firstly, the glass substrate was cleaned and deposited with gold nanoisland by thermal evaporation; and then the substrate was subsequently covered by the deposition of SiO_x overlayer for later linking with the pre-selected DNA sequence. Gold nanorod and gold nanostar solutions were prepared and the metallic particles were conjugated with the complementary DNA. Simple UV-Vis spectra were recorded for measurement upon the binding of the conjugated particles onto the glass substrate. The plasmon coupling between the gold nanoisland on the substrate and the metallic particles (gold nanorods and gold nanostars) when specific binding between two complementary DNAs occurred enabled the larger peak-shift in the absorbance spectrum of the probe (Fig.3.9B and Fig. 3.9C), compared to that without the gold nanoparticles (Fig. 3.9A). Using this method, the LOD of a complementary DNA has been dramatically reduced, from 40 nM to 0.2 nM when gold nanostars are used.

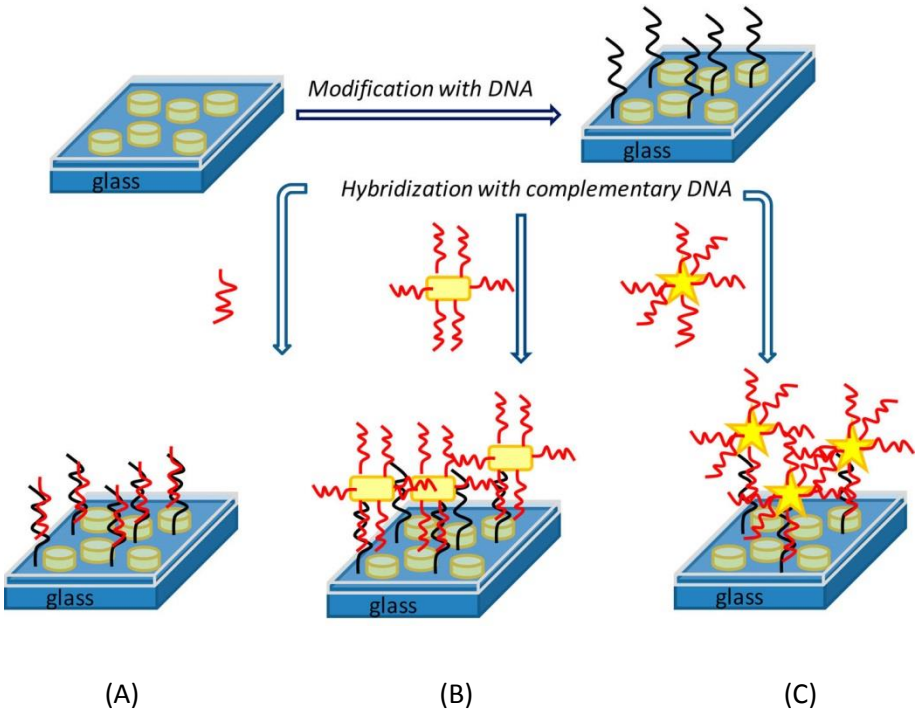

Figure 3.9: Sandwich assay for signal amplification.

A: Binding without gold nanoparticles. B: Binding with Gold nanorods, C: Binding with Gold nanostars.

Reproduced from Ref. [152] © ACS Publications 2013

An alternative approach based on DNA interaction is a colorimetric solution-based technique. In this case, metal nanoparticles exhibit a strong coupling effect when being aggregated, due to the inter-particle interactions. Based on this phenomenon, plenty of sensory strategies have been proposed in literature for qualitative purposes.

Bakthavathsalam *et al.* reported a method for detection of E. Coli by gold capped DNA sequence [50]. The group used a solution of gold nanoparticles functionalised with single stranded DNA as a probe for the detection of E. Coli. In the presence of E. Coli complementary DNA, the solution remained red with the addition of HCl, whereas the sample without complementary DNA would turn blue due to the aggregation induced by the acid. With this method, the LOD could reach the low level of 54 ng of the DNA and possibly being reduced to 11.4 ng with pre-treatment. Recently, Majdinasab *et al.* developed an assay for Salmonella detection using a similar approach, and reported a good sensitivity with LOD of 21.78 ng/mL which was more sensitive than that of the traditional PCR technique (47.4 ng/mL) used in this

test [51]. Mycobacterial could also be directly detected by this method with a low LOD of 18.75ng in 10 mL sample volume [49]. Using a more complex approach, a multi-spot array of gold nanoparticles on a chip has been fabricated to detect BIGH3 gene, which has been associated with common corneal dystrophies; and the achieved LOD was very low at 1 nM [150].

Further to the success demonstrated in bioassay, a report by Wu *et al.* in 2010 provided a route to create a colorimetric assay for the detection of silver ion, which is illustrated in Fig 3.10 [42]. This approach is based on the specific recognition property of Ag+ ion with a Cytosine-Cytosine mismatched base pair. Firstly, 13 nm AuNP (in diameter) were prepared and coated with specific nucleotides. With the presence of Ag^{+}, those nucleotides desorbed resulted in aggregation of AuNP and induced a colour change visible to naked eye. The amount of change could be quantified for example by using a light-scattering method such as surface enhanced Raman scattering (SERS). The calculated LOD was 62 nM.

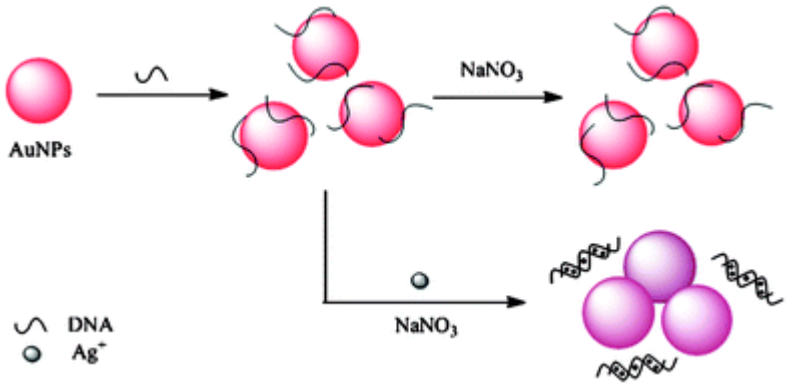

Figure 3.10: Colorimetric assay for Ag+ ion detection. Adapted from Ref. [42] ©RSC Publising 2010

3.4.1.6. Concanavalin A - saccharide interaction

Concanavalin A (ConA), first isolated from jack-bean meal in 1936, is a lectin compound with molecular weight of 104 kDa [68]. It has four binding sites with specificity for branched polysaccharide with *α-D-glucopyranosyl* or *α-D-mannopyranosyl* units, e.g. glucose or mannose [154]. The kinetics of the reaction between ConA and p-nitrophenyl-α-D-mannopyranoside sugar was studied in 1973 by R.D. Gray and R.H. Glew and the disassociate constant was found to be 4.09 ± 0.62

x 10^{-5} M [155]. Therefore, with the associate constant in the range of 10^{7} M^{-1}, ConA is an excellent candidate for the quantitation of sugar-like compounds.

Based on this interaction, there were several reports in literature using ConA as a receptor for the determination of glucose based on LSPR effect [68, 156, 157]. Yonzon et al fabricated a LSPR chip for the study of the binding event between ConA and monosaccaride [68]. The technique involved was using a nanosphere lithography technique to fabricate silver nanoislands on a glass substrate, and subsequently coating this surface with mannose-thiol compounds via the sulphur-terminated linker tri(ethylene glycol) disulfide. Upon the binding of ConA in solution to the mannose coated on the chip, the LSPR spectrum of the system was shown to be red-shifted and the peak shift was reported to be at 17.8 nm when 19.8 µM solution of ConA was injected. Based on this result, the authors also proposed a procedure for a chip fabrication for the simultaneous analysis of mannose and galactose.

In another attempt, Guiliano et al reported an excellent transducer for the study of the kinetics of ConA – mannose reaction [157]. The group prepared a glass substrate with a gold nanoisland and a thin gold film using the thermal evaporation technique. Subsequently, ConA was immobilised onto the surface via PEG-silane linkage. In parallel, mannose-coated gold nanoparticles (Man-NPs) were prepared. Similar to the other sensing techniques, the absorbance spectra of the probe was red-shifted, upon the binding event between ConA and Man-NPs, and the quantification was done by monitoring the peak shift (Fig. 3.11).

Bellapadrona *et al.* also proposed a similar approach, but using multiplayer gold nanoparticles coated on glass slide [156]. The prepared substrate was coated with a layer of D-glucose by dip-coating technique. The measurement was then taken in ConA solutions of different concentration. LOD of this technique has been reported to be at 20 µg/mL or 180 nM.

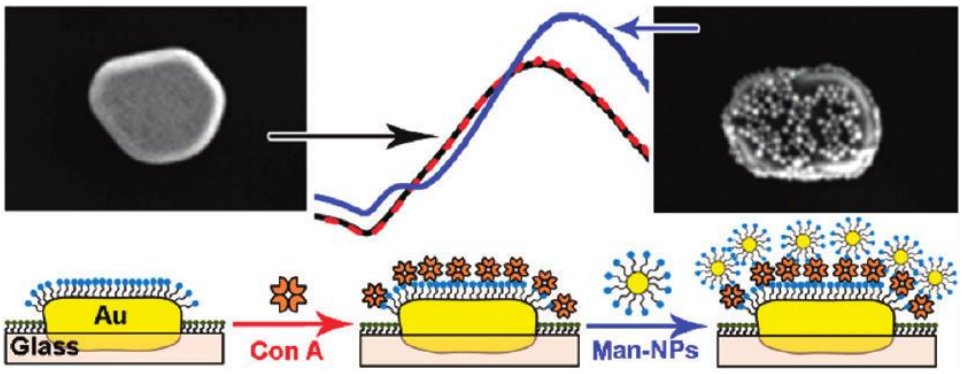

Figure 3.11: Illustration of the fabrication and recognition scheme of the sensor by Guiliano *et al.* Reprinted from ref. [157] © 2011 ACS.

3.4.2. Chemical sensing

In addition to biosensing, LSPR has also been used for chemical sensing, for example, for the detection of heavy metal ions or other small compounds like VOCs, H_2, CO, ethanol or aldehyde. Most of the chemical interactions, however, are not specific; therefore the selectivity is required to be improved.

3.4.2.1. Heavy metal detection

Several attempts have been made and reported in applying the LSPR based technique to detect heavy metal ions. Lin *et al.* [158] presented a LSPR-based reflective optical fibre sensor for detection of Ni^{2+} in high pressure condition. The sensor was constructed by coating gold nanospheres onto an unclad portion of an optical fibre, which was subsequently modified with N-(2-mercaptopropionyl)glycine (MG). MG has been known for being an excellent terdendate ligand with a deprotonated and coordinated amide nitrogen and could form a polynuclear complex through sulfhydryl bridge with a transition metal ion, e.g. Ni^{2+} [159]. In this test, the constructed probe was used for detection of Ni^{2+} in a system using a laser diode with 635 nm wavelength as a light source. Both MG and the forming complex of MG and Ni^{2+} are transparent at the detection wavelength at 635nm, therefore the ratio of the intensity at 635 nm of incoming light and reflective light was used as an output as the concentration of Ni^{2+} was varied from 0 to 9 x 10^{-4} M. With this strategy, the sensitivity and LOD reported for Ni^{2+} sensing was 35.9 M^{-1} and 1.72 x 10^{-5} M at ambient conditions and at 308 K respectively.

Pb^{2+} detection has been demonstrated by Lin *et al.* [27] by using a LSPR fibre optic based sensor coated with monoclonal antibody. The binding event occurred between a Pb^{2+}- EDTA complex and the monoclonal antibody coated on AuNPs which have been immobilised on the surface of an optical fibre core. The LOD of Pb^{2+} reported was 0.27 ppb, and this highly reproducible result could be maintained over a period of 35 days. On a similar study, this group also reported an optical fibre sensor for Cd (II) detection [160], based on the immobilisation of phytochelatins, (*γ*Glc-Cys)8-Gly onto the gold nanoparticle-modified optical fibre. The LOD could reach 0.16 ppb of Cd^{2+} concentration and the sensor could also retain high stability over a long period of time. However, the question of selectivity still remains unanswered.

Hg^{2+} has drawn a significant amount of attention and several strategies based on LSPR have been devised. Huang *et al.* [161] reported a method for Hg^{2+} detection based on high affinity of Hg^{2+} toward AuNRs. The presence of Hg^{2+} in a Na_3PO_4-AuNR solution would create amalgamation between Hg^{2+} and Au, thus change the LSPR properties of the particles and induce a wavelength shift. This method provided an excellent sensitivity and could detect as low as 10^{-13} M of Hg^{2+} with a very good selectivity. Bi *et al.* [53] presented a similar approach by monitoring the etching effect of Hg^{2+} onto silver nanoparticles of different shapes, including nanospheres, nanorods and nanoplates. Another approach has been proposed recently by Xiong *et al.* [43] based on aggregation of AuNPs. Basically, two short sequences of oligonucleotide Thymine-Thymine mismatch pair, oligo-1 and oligo-2 were absorbed onto AuNPs. With the presence of Hg^{2+}, desorption occurred and triggered the aggregation of AuNPs and increased light scattering intensity. The dynamic range of detection was reported to be from 53 to 530 nM with a detection limit of 29.4 nM. Even though these approaches have shown to be able to offer a very high sensitivity, their sensing activities are irreversible, therefore not suitable for scaling-up or for reusable applications.

3.4.2.2. Volatile Organic Compounds (VOCs), gas and other small chemical compounds sensing

Applications for chemical vapour detection in gaseous form were also reported by using the LSPR technique. Dharmalingam *et al.* [162] created a gold-yttria stabilised zirconia (Au-YSZ) film by physical vapour deposition technique (PVD) to detect H_2 and CO. Ghodselahi *et al.* [163] presented a Cu@CuO core-shell nanoparticle film for CO gas sensing with a high sensitivity. Chen *et al.* [164] proposed an approach for developing partially selective VOCs sensor with AgNPs. Even though the sensitivity and selectivity of the sensor was still not desirable (the LOD was ranged from 18 to 300ppm), this sensor has shown a highly linear performance within a certain sensing range and could be used for industrial leakage and spill detection. Another strategy was proposed by Dalfovo *et al.* [165] in 2012. In this study, AuNPs coated with surfactant and immobilised on a gold film deposited on a glass slide, acted as a sensor for detection of several different VOCs including toluene, hexane, acetone, ethanol, isopropanol and 1-butanol. In another attempt, Ma *et al.* [166] reported a fabricated silver nanotriangle array on a chip for ethanol vapour sensing. This sensor could achieve excellent detection limit of 10 mg/L with fast response, high stability and reversibility. The selectivity, however, is still an issue because other VOCs, such as propanol, benzene, acetone or hexane, could induce similar effects.

The LSPR technique has also been reported for detection of small chemical compounds. For example, formaldehyde in water could be detected by using gold nanorod film [167], uric acid estimation by using PVP coated AgNPs [168] or hydroxide sensing by using Ag nanoplates [54].

Another interesting application is the detection of trinitrotoluene (TNT) by gold capped with ethylenediamine (EDA) [52]. EDA could be strongly absorbed onto the surface of AuNPs via its protonated amino group. On the other hand, EDA, which is an electron-rich ligand, could have a strong donor-acceptor interaction with TNT, which has an electron-deficient aromatic ring. Therefore, the presence of the trace amount of TNT in a solution of EDA-capped AuNPs could lead to the aggregation of the gold nanoparticles, causing the colour change from red to blue, as illustrated in Fig. 3.12. This technique is able to detect 400 pM level of TNT with an excellent selectivity. The limit of detection could be lowered to 40 pM when combined with UV-Vis spectroscopy, or even to 0.4 pM using the dynamic light scattering method.

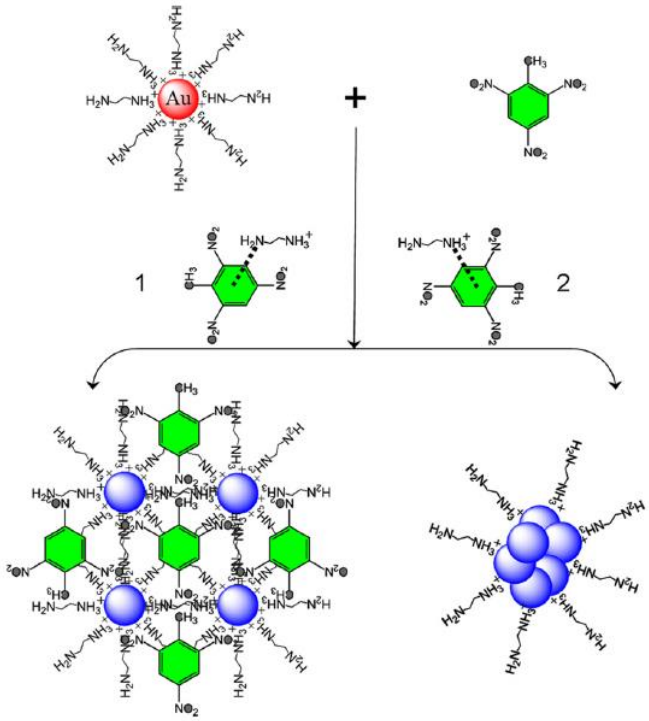

Figure 3.12: Sensing mechanism for TNT by methylethylene capped AuNPs. Reproduced from Ref [52] © Elsevier 2012

3.4.2.3. pH sensing

Plasmonic nanoparticles can be used in designing a pH sensor with a required sensing range by being incorporated with a pH-sensitive material. Nuopponen *et al.* [169] created a pH sensor by the preparation AuNPs using block co-polymer PMAA-b-PNIPAM, and the working range of the reported sensor was from pH 5 to 8. The co-polymer was prepared with dithiobenzoate chain end, therefore would be bound to the AuNPs surface. pH was found to be able to affect the binding event; hence the optical properties of the system were pH-dependant. However, the probe was found to be highly temperature dependent and the particle agglomeration was irreversible.

Later, Mack *et al.* [170] reported a pH sensor based on plasmonic crystal. The plasmonic crystal used was the gold coated nanowells array prepared by thermal evaporation of gold film onto the predefined substrate. The substrate was then coated with a thin film of hydrogel to form a pH sensing layer. As a result, pH was determined in the range from 1.44 to 7.86 with a precision of 0.1 pH unit. The advantage of this method is the reversible sensing mechanism used.

A highly sensitive pH sensor has been reported by Jiang *et al.* [171] by using a gold nanocrescents system covered with poly-HEMA hydrogel. Within the sensing range from pH 4.5 to 6.4, a high precision was achieved to be at 0.045 pH unit. The sensor was also reported to be stable and repeatable even after 1 month of storage.

3.5. Technological advancement

More advantageous sensing features can be created when the LSPR effect by metallic nanoparticles is combined with other advanced techniques, such as multiplexing, being in conjunction with microfluidic devices and integration with fibre optics.

3.5.1. Multiplexing

Materials with different shape and size and composition possess their own unique LSPR peak in either absorbance spectra or scattering spectra. Thus, the combination of several materials could lead to a possibility of multiplexing in order to target multiple agents, compounds or analytes. For example, Huang *et al.* [135] created a multiplexed sensor by fabricating 4 different types of AuNRs with different aspect ratio and coated them onto 4 glass slides and aligned 4 different AuNRs together to make a multi throughput sensing system. For detection, goat antibody, human antibody and rabbit antibody were immobilised on each type of AuNR to simultaneously determine corresponding antigens by independently monitoring different LSPR peak. Based on this principle, this group also presented an immunoassay for simultaneous detection of S. japonicum and tuberculosis in human serum specimen [123]. In another study, Chen *et al.* [172] built their own multiplexing system for chemical vapour sensing by combining the using of AuNP, AgNP and Au/Ag core-shell nanoparticles. Notably, a multispot gold capped nanoparticle array chip was developed by Yoo *et al.* [150], for detection of BIGH3 gene. These examples demonstrate a strong advantage of multiplexing that those plasmonic nanoparticles could offer. This offers the potential for commercialisation of an integrated system with high throughput.

3.5.2. Combination with microfluidics

The birth of microfluidic devices in 1990s gives rise to the exponential development of miniaturisation, especially in the field of gene chip, lab-on-a-chip, chromatography, chemical microreactors, etc. [173]. Combined with microfluidic device, LSPR technique shows the possibility of miniaturisation and decreases the sample amount yet with highly sensitive, fast and reliable response. A typical example is the work done by Huang *et al.* in 2009 [174], to create a LSPR based system combining with microfluidic device using gold nanoparticles. In this test, their system could reach a resolution of 10^{-4} RIU and the LOD of anti-biotin using this setup was 270 ng/mL. The significant advantage of this system is their ability in precisely controlling the amount of sample transported to the sensing area, therefore enhancing the sensitivity, selectivity as well as reducing the quantity of the sample and the reagent required. Guo *et al.* [175] proposed a similar system with an effective volume of 0.75 µL using gold nanorods to detect RS-melagatran. This sensor system exhibited excellent enantioselectivity for RS-melagatran and the LOD is 0.9 nM. Recently, SadAbadi *et al.* [176] directly synthesised AuNPs in a poly(dimethylsiloxane) (PDMS) microfluidic chip to create a highly sensitive device for detection of bovine growth hormones, with an excellent LOD of 3.7 ng/mL (or 185 pM).

3.5.3. LSPR coupling with optical fibres

Optical fibres are an excellent wave guide for light propagation. By combining optical fibres with plasmonic nanomaterial, a compact system with a high sensitivity, reliability and inexpensive cost can be produced. Numerous attempts have been made in this field in order to meet the demand from the commercial market.

Normally, a multimode fibre is preferred in this approach due to its large surface area for immobilisation of the metallic nanoparticles. Several configurations have been explored and employed to date, including decladded fibre, tapered fibre [35, 177], U-bent fibre [28, 178] and tapered tip [31, 32] as illustrated in Fig. 3.13.

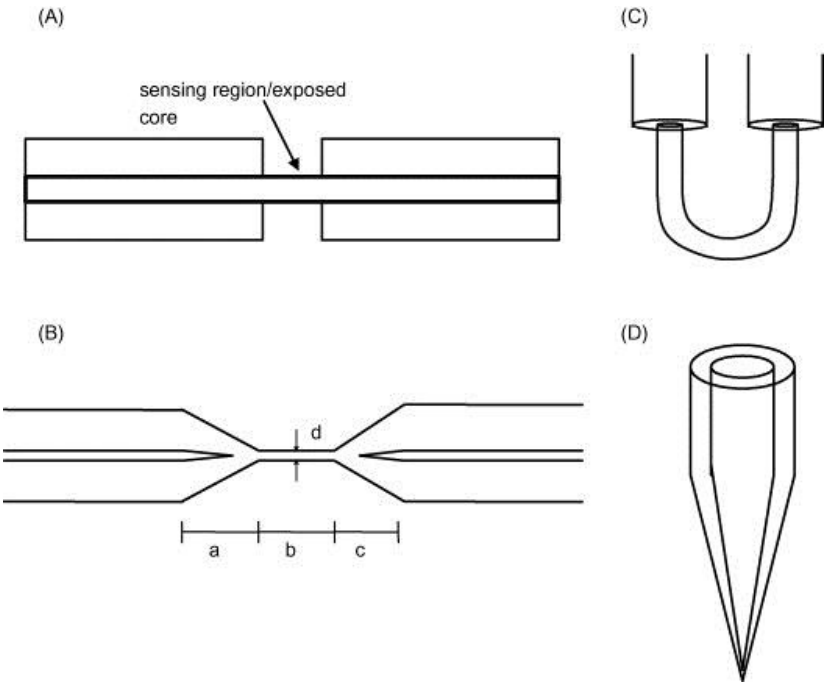

Figure 3.13: Common fibre configurations used in sensing. Reproduced from Ref. [179] © Elsevier 2007
A) Decladded fibre B) Tapered fibre C) U-bent fibre D) Tapered tip

Single mode fibres can also be used as a LSPR sensor substrate. Because of its very narrow core, the penetration depth of the evanescent field is normally very small, around 100nm [179]. Therefore, in case of single mode fibre sensor, the cladding is often removed uniformly on a portion of the fibre and the sensing layer.

To date, plasma-enhanced chemical vapor deposition (PECVD) or chemical vapour deposition (sputter coating) has been employed as one of the immobilisation techniques, but it usually requires expensive equipment. Chemistry-wise, i.e. immobilisations via electrostatic force by Layer-by-Layer (LbL) technique or by strong interaction of gold and amine or sulphide linker can provide a much simpler and cheaper alternative. The main drawback is that it is difficult to control the surface density of deposition, inter-particle distance and the coating thickness.

Through the modification of the fibre structure, it is possible to increase the sensitivity of the system. For example, side-polished fibre [180, 181], tapered fibre or sharp fibre tip [38] have all been reported to be able to enhance the performance of a sensor probe, due to the enhancement of the evanescent field. In a tapered fibre, the evanescent field has been exposed and the magnitude and the penetration depth have also been increased [179]. In a report, Mignani *et al.* [182] expressed that the

sensitivity of a tapered fibre could be 10 times higher than that of normal fibre. The power in the evanescent field has also been reported to be 100 times higher than that of normal polished fibre [183]. Using other configurations like U-bent, sharp tip or side-polished fibres, the resulting enhanced evanescent field encourages more light interactions with the surface material/coating, thus improving significantly the sensor performance.

The combination of LSPR effect and optical fibres as a sensor substrate has shown a great promise as summarised by Lee *et al.* [184]. It was predicted by Homola *et al.* [185], both by theoretical and experimental studies on D-shaped single mode fibre coated with a thin layer of gold film, that a high RI sensitivity up to 5000 nm/RIU could be achieved. Gupta *et al.* theoretically calculated the sensitivity of 3000 nm/RIU using Au-Ag nanoparticles film coated on a de-cladded multimode fibre [70] and 2700 – 15000 nm/RIU with gold coated on off-cladding tapered fibre [186, 187]. Based on experiments, Zhang *et al.* [35] reported a sensitivity of 1190 nm/RIU using gold nanostar on a tapered single mode optical fibre.

Various applications using LSPR based optical fibre sensors have been widely reported. In 2006, Lin *et al.* [126] proposed the use of 10 nm gold nanoparticles and the enzyme technique to create a sensor for pesticide with a LOD of 0.234 ppb. In 2007, this group also developed similar sensors for the detection of Ni^{2+} and proposed the demonstration for biotin and antibody sensing [158]. The LOD for Ni^{2+}, biotin and antibody is 1.72×10^{-5} M, $7.82\ 10^{-10}$ M and 0.1 ng/mL, respectively. In 2008, a sensor for Pb^{2+} detection using a similar strategy was also reported, with a LOD of 0.27 ppb [27]. Sai *et al.* [28] studied gold nanoparticles with a U-bent fibre to fabricate an intensity-based biosensor for antibody-antigen interaction and the reported LOD was 0.8 nM. Huang *et al.* [29] applied gold nanoparticle coated optical fibre in developing label-free biosensor for Guanosine 3',5'-cyclic monophosphate (cGMP), which was an intracellular second messenger and the developed sensor had a working range over 0.1 – 100 pmol/mL for cGMP with a high stability over 4 weeks. Shao *et al.* [181] proposed a similar sensing strategy with different gold nanoparticle sizes for detection of rabbit antibody with a LOD of 11.1 nmol/mL. Chen *et al.* [30] devised a sensor for HF with a detectable range from 1% to 5% of HF in solution.

Jeong *et al.* [32, 34, 36] assembled gold nanoparticles on the end-face of an optical fibre to create a highly sensitive sensor for Interferon-gamma (IFN-γ), with a LOD of 12.6 pg/mL. Choosing the end-face of an optical fibre as a sensing platform, Lin *et al.* [33] performed EBL to strictly control the fabrication of gold island on the tip of an optical fibre to create a highly sensitive sensor and demonstrate the sensing feasibility with biotin-streptavidin interaction. Recently, Rivero *et al.* [188] successfully developed a silver nanoparticles based optical fibre sensor for humidity measurement, combining LSPR and Lossy-mode Resonance with a high sensitivity (0.943 nm/RH%), large dynamic range and nearly instant response time (less than 500ms).

With various sensing strategies and techniques, research in the field of LSPR coupled with optical fibres is expanding rapidly. Benefited from the small size and electromagnetic interference-free property of optical fibre, this combination provides an effective route for developing highly sensitive, reliable and inexpensive sensors for both chemical and biological applications.

3.6. Summary

LSPR has become a powerful tool in sensing area based on its unique properties. This chapter gives a comprehensive overview of the research in LSPR through its properties, strategies and applications in relation to sensing. The purpose of this is to establish a solid foundation for the work and discussions given in the following chapters.

In summary, main discoveries and reports in the field related to LSPR as a powerful sensing tool have been explored. The generic layout of a sensor based on the LSPR effect has been sketched with each element of the setup being discussed. Three main sensing mechanisms, i.e. LSPR absorbance-based technique, colorimetric technique and direct LSPR spectral monitoring technique, have been widely employed for different applications, from bioanalysis, chemical detection to clinical testing and health and safety security enhancement. The properties and characteristics of the metallic nanomarterials, in particular gold and silver, were analysed, showing their influence on LSPR phenomenon, both theoretically and experimentally. The realisation, preparation and immobilisation of various morphologies of nanostructures were also presented. The applications of LSPR in sensing area, especially in biosensing and chemical sensing were discussed, with a particular attention to the interactions which determine the sensor selectivity. Integration of LSPR with the other advanced techniques/materials, for example, with optical fibres, has also been discussed in this chapter in order to optimise and promote the versatility, convenience and enhancement in sensing.

The research and development in the field is still on-going and with the ease in controlling and modifying LSPR spectra by customising the structure and arrangement of the nanomaterials, LSPR-based sensor can be readily suitable for applications ranging from simple colorimetric identification to highly sensitive lab-based experiments.

3.7. References

1. Haes, A.J. and R.P. Van Duyne, *A unified view of propagating and localized surface plasmon resonance biosensors.* Analytical and Bioanalytical Chemistry, 2004. **379**(7-8): p. 920-930.
2. Hutter, E. and J.H. Fendler, *Exploitation of localized surface plasmon resonance.* Advanced Materials, 2004. **16**(19): p. 1685-1706.
3. Zhao, J., X. Zhang, C.R. Yonzon, A.J. Haes, and R.P. Van Duyne, *Localized surface plasmon resonance biosensors.* Nanomedicine, 2006. **1**(2): p. 219-228.
4. Anker, J.N., W.P. Hall, O. Lyandres, N.C. Shah, J. Zhao, and R.P. Van Duyne, *Biosensing with plasmonic nanosensors.* Nature Materials, 2008. **7**(6): p. 442-453.
5. Haes, A.J., C.L. Haynes, A.D. McFarland, G.C. Schatz, R.R. Van Duyne, and S.L. Zou, *Plasmonic materials for surface-enhanced sensing and spectroscopy.* Mrs Bulletin, 2005. **30**(5): p. 368-375.
6. Yonzon, C.R., D.A. Stuart, X.Y. Zhang, A.D. McFarland, C.L. Haynes, and R.P. Van Duyne, *Towards advanced chemical and biological nanosensors - An overview.* Talanta, 2005. **67**(3): p. 438-448.
7. Sepulveda, B., P.C. Angelome, L.M. Lechuga, and L.M. Liz-Marzan, *LSPR-based nanobiosensors.* Nano Today, 2009. **4**(3): p. 244-251.
8. Pena-Pereira, F., R.M.B.O. Duarte, and A.C. Duarte, *Immobilization strategies and analytical applications for metallic and metal-oxide nanomaterials on surfaces.* Trac-Trends in Analytical Chemistry, 2012. **40**: p. 90-105.
9. Bolduc, O.R. and J.-F. Masson, *Advances in Surface Plasmon Resonance Sensing with Nanoparticles and Thin Films: Nanomaterials, Surface Chemistry, and Hybrid Plasmonic Techniques.* Analytical Chemistry, 2011. **83**(21): p. 8057-8062.
10. Hong, Y., Y.-M. Huh, D.S. Yoon, and J. Yang, *Nanobiosensors Based on Localized Surface Plasmon Resonance for Biomarker Detection.* Journal of Nanomaterials, 2012.
11. Mayer, K.M. and J.H. Hafner, *Localized Surface Plasmon Resonance Sensors.* Chemical Reviews, 2011. **111**(6): p. 3828-3857.
12. McFarland, A.D. and R.P. Van Duyne, *Single silver nanoparticles as real-time optical sensors with zeptomole sensitivity.* Nano Letters, 2003. **3**(8): p. 1057-1062.
13. Yonzon, C.R., E. Jeoungf, S.L. Zou, G.C. Schatz, M. Mrksich, and R.P. Van Duyne, *A comparative analysis of localized and propagating surface plasmon resonance sensors: The binding of concanavalin a to a monosaccharide functionalized self-assembled monolayer.* Journal of the American Chemical Society, 2004. **126**(39): p. 12669-12676.
14. Haes, A.J., S.L. Zou, G.C. Schatz, and R.P. Van Duyne, *A nanoscale optical biosensor: The long range distance dependence of the localized surface plasmon resonance of noble metal nanoparticles.* Journal of Physical Chemistry B, 2004. **108**(1): p. 109-116.
15. Dahlin, A.B., J.O. Tegenfeldt, and F. Hook, *Improving the instrumental resolution of sensors based on localized surface plasmon resonance.* Analytical Chemistry, 2006. **78**(13): p. 4416-4423.
16. Haes, A.J., S. Zou, J. Zhao, G.C. Schatz, and R.P. Van Duyne, *Localized surface plasmon resonance spectroscopy near molecular resonances.* Journal of the American Chemical Society, 2006. **128**(33): p. 10905-10914.
17. Kitano, H., Y. Anraku, and H. Shinohara, *Sensing capabilities of colloidal gold monolayer modified with a phenylboronic acid-carrying polymer brush.* Biomacromolecules, 2006. **7**(4): p. 1065-1071.

18. Wang, Y., J. Deng, J. Di, and Y. Tu, *Electrodeposition of large size gold nanoparticles on indium tin oxide glass and application as refractive index sensor.* Electrochemistry Communications, 2009. **11**(5): p. 1034-1037.
19. Deng, J., Y. Song, Y. Wang, and J. Di, *Label-free optical biosensor based on localized surface plasmon resonance of twin-linked gold nanoparticles electrodeposited on ITO glass.* Biosensors & Bioelectronics, 2010. **26**(2): p. 615-619.
20. Hu, Y., Y. Song, Y. Wang, and J. Di, *Electrochemical synthesis of gold nanoparticles onto indium tin oxide glass and application in biosensors.* Thin Solid Films, 2011. **519**(19): p. 6605-6609.
21. Praig, V.G., G. Piret, M. Manesse, X. Castel, R. Boukherroub, and S. Szunerits, *Seed-mediated electrochemical growth of gold nanostructures on indium tin oxide thin films.* Electrochimica Acta, 2008. **53**(27): p. 7838-7844.
22. Sannomiya, T., H. Dermutz, C. Hafner, J. Voeroes, and A.B. Dahlin, *Electrochemistry on a Localized Surface Plasmon Resonance Sensor.* Langmuir, 2010. **26**(10): p. 7619-7626.
23. Cantale, V., F.C. Simeone, R. Gambari, and M.A. Rampi, *Gold nano-islands on FTO as plasmonic nanostructures for biosensors.* Sensors and Actuators B-Chemical, 2011. **152**(2): p. 206-213.
24. Yeom, S.-H., M.-E. Han, B.-H. Kang, K.-J. Kim, H. Yuan, N.-S. Eum, and S.-W. Kang, *Enhancement of the sensitivity of LSPR-based CRP immunosensors by Au nanoparticle antibody conjugation.* Sensors and Actuators B-Chemical, 2013. **177**: p. 376-383.
25. Yeom, S.-H., O.-G. Kim, B.-H. Kang, K.-J. Kim, H. Yuan, D.-H. Kwon, H.-R. Kim, and S.-W. Kang, *Highly sensitive nano-porous lattice biosensor based on localized surface plasmon resonance and interference.* Optics Express, 2011. **19**(23): p. 22882-22891.
26. Endo, T., K. Kerman, N. Nagatani, Y. Takamura, and E. Tamiya, *Label-free detection of peptide nucleic acid-DNA hybridization using localized surface plasmon resonance based optical biosensor.* Analytical Chemistry, 2005. **77**(21): p. 6976-6984.
27. Lin, T.-J. and M.-F. Chung, *Using monoclonal antibody to determine lead ions with a localized surface plasmon resonance fiber-optic biosensor.* Sensors, 2008. **8**(1): p. 582-593.
28. Sai, V.V.R., T. Kundu, and S. Mukherji, *Novel U-bent fiber optic probe for localized surface plasmon resonance based biosensor.* Biosensors & Bioelectronics, 2009. **24**(9): p. 2804-2809.
29. Huang, K.-T., T.-J. Lin, and M.-H. Hsu, *Determination of cyclic GMP concentration using a gold nanoparticle-modified optical fiber.* Biosensors & Bioelectronics, 2010. **26**(1): p. 11-15.
30. Chen, I.C., S.-S. Lin, T.-J. Lin, and J.-K. Du, *Detection of Hydrofluoric Acid by a SiO2 Sol-Gel Coating Fiber-Optic Probe Based on Reflection-Based Localized Surface Plasmon Resonance.* Sensors, 2011. **11**(2): p. 1907-1923.
31. Gouvea, P.M.P., H. Jang, I.C.S. Carvalho, M. Cremona, A.M.B. Braga, and M. Fokine, *Internal specular reflection from nanoparticle layers on the end face of optical fibers.* Journal of Applied Physics, 2011. **109**(10).
32. Jeong, H.-H., N. Erdene, S.-K. Lee, D.-H. Jeong, and J.-H. Park, *Fabrication of fiber-optic localized surface plasmon resonance sensor and its application to detect antibody-antigen reaction of interferon-gamma.* Optical Engineering, 2011. **50**(12).
33. Lin, Y., Y. Zou, and R.G. Lindquist, *A reflection-based localized surface plasmon resonance fiber-optic probe for biochemical sensing.* Biomedical Optics Express, 2011. **2**(3): p. 478-484.
34. Jeong, H.-H., N. Erdene, J.-H. Park, D.-H. Jeong, and S.-K. Lee, *Analysis of Fiber-Optic Localized Surface Plasmon Resonance Sensor by Controlling Formation of Gold*

Nanoparticles and its Bio-Application. Journal of Nanoscience and Nanotechnology, 2012. **12**(10): p. 7815-7821.

35. Zhang, Q., C. Xue, Y. Yuan, J. Lee, D. Sun, and J. Xiong, *Fiber Surface Modification Technology for Fiber-Optic Localized Surface Plasmon Resonance Biosensors.* Sensors, 2012. **12**(3): p. 2729-2741.
36. Jeong, H.-H., N. Erdene, J.-H. Park, D.-H. Jeong, H.-Y. Lee, and S.-K. Lee, *Real-time label-free immunoassay of interferon-gamma and prostate-specific antigen using a Fiber-Optic Localized Surface Plasmon Resonance sensor.* Biosensors & Bioelectronics, 2013. **39**(1): p. 346-351.
37. Rani, M., N.K. Sharma, and V. Sajal, *Localized surface plasmon resonance based fiber optic sensor with nanoparticles.* Optics Communications, 2013. **292**: p. 92-100.
38. Jeong, H.-H., Y.-J. Son, S.-K. Kang, H.-J. Kim, H.-J. Roh, N. Erdene, J.-H. Park, D.-H. Jeong, H.-Y. Lee, and S.-K. Lee, *Fiber-Optic Refractive Index Sensor Based on the Cone-Based Round Structure.* Ieee Sensors Journal, 2013. **13**(1): p. 351-358.
39. Tou, Z.Q., C.C. Chan, W.C. Wong, and L.H. Chen, *Fiber Optic Refractometer Based on Cladding Excitation of Localized Surface Plasmon Resonance.* Ieee Photonics Technology Letters, 2013. **25**(6): p. 556-559.
40. Mirkin, C.A., R.L. Letsinger, R.C. Mucic, and J.J. Storhoff, *A DNA-based method for rationally assembling nanoparticles into macroscopic materials.* Nature, 1996. **382**(6592): p. 607-609.
41. Ghosh, S.K. and T. Pal, *Interparticle Coupling Effect on the Surface Plasmon Resonance of Gold Nanoparticles: From Theory to Applications.* Chemical Reviews, 2007. **107**(11): p. 4797-4862.
42. Wu, C., C. Xiong, L. Wang, C. Lan, and L. Ling, *Sensitive and selective localized surface plasmon resonance light-scattering sensor for Ag+ with unmodified gold nanoparticles.* Analyst, 2010. **135**(10): p. 2682-2687.
43. Xiong, C. and L. Ling, *Localized Surface Plasmon Resonance Light-Scattering Sensor for Mercury(II) Ion with Label-Free Gold Nanoparticles.* Journal of Nanoscience and Nanotechnology, 2013. **13**(2): p. 1406-1410.
44. You, J., H. Hu, J. Zhou, L. Zhang, Y. Zhang, and T. Kondo, *Novel Cellulose Polyampholyte-Gold Nanoparticle-Based Colorimetric Competition Assay for the Detection of Cysteine and Mercury(II).* Langmuir, 2013. **29**(16): p. 5085-5092.
45. Tripathy, S.K., J.Y. Woo, and C.-S. Han, *Colorimetric detection of Fe(III) ions using label-free gold nanoparticles and acidic thiourea mixture.* Sensors and Actuators B-Chemical, 2013. **181**: p. 114-118.
46. Wang, S., M. Wu, G. Wen, A. Liang, and Z. Jiang, *Label-Free Aptamer Nanogold Resonance Scattering Method for Trace Alkaline Phosphatase Coupling the Adenosine Triphosphate Reaction.* Analytical Letters, 2013. **46**(3): p. 461-472.
47. Li, C.M., S.J. Zhen, J. Wang, Y.F. Li, and C.Z. Huang, *A gold nanoparticles-based colorimetric assay for alkaline phosphatase detection with tunable dynamic range.* Biosensors & Bioelectronics, 2013. **43**: p. 366-371.
48. Jiang, T., R. Liu, X. Huang, H. Feng, W. Teo, and B. Xing, *Colorimetric screening of bacterial enzyme activity and inhibition based on the aggregation of gold nanoparticles.* Chemical Communications, 2009(15): p. 1972-1974.
49. Liandris, E., M. Gazouli, M. Andreadou, M. Comor, N. Abazovic, L.A. Sechi, and J. Ikonomopoulos, *Direct detection of unamplified DNA from pathogenic mycobacteria using DNA-derivatized gold nanoparticles.* Journal of Microbiological Methods, 2009. **78**(3): p. 260-264.
50. Bakthavathsalam, P., V.K. Rajendran, and J.A.B. Mohammed, *A direct detection of Escherichia coli genomic DNA using gold nanoprobes.* Journal of Nanobiotechnology, 2012. **10**.

51. Majdinasab, M., M. Aminlari, M.H. Sheikhi, M. Niakousari, and S. Shekarforoosh, *Detection of inv A gene of Salmonella by DNA-gold nanoparticles biosensor and its comparison with PCR.* Journal of Experimental Nanoscience, 2013. **8**(2): p. 223-239.
52. Lin, D., H. Liu, K. Qian, X. Zhou, L. Yang, and J. Liu, *Ultrasensitive optical detection of trinitrotoluene by ethylenediamine-capped gold nanoparticles.* Analytica Chimica Acta, 2012. **744**: p. 92-98.
53. Bi, N., Y. Chen, H. Qi, X. Zheng, Y. Chen, X. Liao, H. Zhang, and Y. Tian, *A sensitive localized surface plasmon resonance sensor for determining mercury(II) ion using noble metal nanoparticles as probe.* Spectrochimica Acta Part a-Molecular and Biomolecular Spectroscopy, 2012. **95**: p. 276-281.
54. Shan, G., S. Zheng, S. Chen, Y. Chen, and Y. Liu, *Detection of label-free H2O2 based on sensitive Au nanorods as sensor.* Colloids and Surfaces B-Biointerfaces, 2013. **102**: p. 327-330.
55. Faraday, M., *Experimental Relations of Gold (and Other Metals) to Light.* Philosophy Trans. Royal Society London, 1857. **147**(145).
56. Otte, M.A., M.C. Estevez, D. Regatos, L.M. Lechuga, and B. Sepulveda, *Guiding Light in Monolayers of Sparse and Random Plasmonic Meta-atoms.* Acs Nano, 2011. **5**(11): p. 9179-9186.
57. Zhu, S. and Y. Fu, *Hybridization of localized surface plasmon resonance-based Au-Ag nanoparticles.* Biomedical Microdevices, 2009. **11**(3): p. 579-583.
58. Shen, H., N. Guillot, J. Rouxel, M.L. de la Chapelle, and T. Toury, *Optimized plasmonic nanostructures for improved sensing activities.* Optics Express, 2012. **20**(19): p. 21278-21290.
59. Feuz, L., P. Jonsson, M.P. Jonsson, and F. Hook, *Improving the Limit of Detection of Nanoscale Sensors by Directed Binding to High-Sensitivity Areas.* Acs Nano, 2010. **4**(4): p. 2167-2177.
60. Awang, R.A., S.H. El-Gohary, N.-H. Kim, and K.M. Byun, *Enhancement of field-analyte interaction at metallic nanogap arrays for sensitive localized surface plasmon resonance detection.* Applied Optics, 2012. **51**(31): p. 7437-7442.
61. Lee, S.Y., S.-H. Kim, S.G. Jang, C.-J. Heo, J.W. Shim, and S.-M. Yang, *High-Fidelity Optofluidic On-Chip Sensors Using Well-Defined Gold Nanowell Crystals.* Analytical Chemistry, 2011. **83**(23): p. 9174-9180.
62. Benjamin, S.F., R.N. Matthew, S.Q. Jamie, and G.S. Joseph, *Adhesion of chemically and electrostatically bound gold nanoparticles to a self-assembled silane monolayer investigated by atomic force volume spectroscopy.* Journal of Nanoparticle Research, 2008.
63. Mie, G., *Articles on the optical characteristics of turbid tubes, especially colloidal metal solutions.* Annalen Der Physik, 1908. **25**(3): p. 377-445.
64. Jradi, S., J. Plain, and P. Royer, *Method for manufacturing metallic nano-objects on metallic nano-structure that is utilized in e.g. surface-enhanced Raman scattering spectroscopy, involves transforming precursor solution into film such that nano-objects are placed in pores*. Univ Troyes Technologie; Royer P.
65. Barchiesi, D., S. Kessentini, N. Guillot, M.L. de la Chapelle, and T. Grosges, *Localized surface plasmon resonance in arrays of nano-gold cylinders: inverse problem and propagation of uncertainties.* Optics Express, 2013. **21**(2): p. 2245-2262.
66. Ringe, E., J.M. McMahon, K. Sohn, C. Cobley, Y. Xia, J. Huang, G.C. Schatz, L.D. Marks, and R.P. Van Duyne, *Unraveling the Effects of Size, Composition, and Substrate on the Localized Surface Plasmon Resonance Frequencies of Gold and Silver Nanocubes: A Systematic Single-Particle Approach.* Journal of Physical Chemistry C, 2010. **114**(29): p. 12511-12516.

67. Potara, M., A.-M. Gabudean, and S. Astilean, *Solution-phase, dual LSPR-SERS plasmonic sensors of high sensitivity and stability based on chitosan-coated anisotropic silver nanoparticles.* Journal of Materials Chemistry, 2011. **21**(11): p. 3625-3633.
68. Yonzon, C.R., E. Jeoung, S. Zou, G.C. Schatz, M. Mrksich, and R.P. Van Duyne, *A Comparative Analysis of Localized and Propagating Surface Plasmon Resonance Sensors: The Binding of Concanavalin A to a Monosaccharide Functionalized Self-Assembled Monolayer.* Journal of the American Chemical Society, 2004. **126**(39): p. 12669-12676.
69. Nusz, G.J., A.C. Curry, S.M. Marinakos, A. Wax, and A. Chilkoti, *Rational Selection of Gold Nanorod Geometry for Label-Free Plasmonic Biosensors.* Acs Nano, 2009. **3**(4): p. 795-806.
70. Sharma, A.K. and B.D. Gupta, *Fibre-optic sensor based on surface plasmon resonance with Ag–Au alloy nanoparticle films.* Nanotechnology, 2006. **17**(1): p. 124-131.
71. Sharma, A.K. and G.J. Mohr, *On the performance of surface plasmon resonance based fibre optic sensor with different bimetallic nanoparticle alloy combinations.* Journal of Physics D: Applied Physics, 2008. **41**(5): p. 055106.
72. Sharma, A.K., H.S. Pattanaik, and G.J. Mohr, *On the temperature sensing capability of a fibre optic SPR mechanism based on bimetallic alloy nanoparticles.* Journal of Physics D: Applied Physics, 2009. **42**(4): p. 045104.
73. Sharma, A.K. and G.J. Mohr, *On the Application of Different Bimetallic Alloy Nanoparticle Combinations in Fiber Optic Surface Plasmon Resonance Salinity Sensor and Its Performance Optimization Against Thermal Effects.* Journal of Nanoscience and Nanotechnology, 2010. **10**(5): p. 3145-3154.
74. Lee, K.-S. and M.A. El-Sayed, *Gold and silver nanoparticles in sensing and imaging: Sensitivity of plasmon response to size, shape, and metal composition.* Journal of Physical Chemistry B, 2006. **110**(39): p. 19220-19225.
75. Miller, M.M. and A.A. Lazarides, *Sensitivity of metal nanoparticle surface plasmon resonance to the dielectric environment.* Journal of Physical Chemistry B, 2005. **109**(46): p. 21556-21565.
76. Mahmoud, M.A. and M.A. El-Sayed, *Gold Nanoframes: Very High Surface Plasmon Fields and Excellent Near-Infrared Sensors.* Journal of American Chemical Society, 2010. **132**(36): p. 12704-12710.
77. Mock, J.J., M. Barbic, D.R. Smith, D.A. Schultz, and S. Schultz, *Shape effects in plasmon resonance of individual colloidal silver nanoparticles.* Journal of Chemical Physics, 2002. **116**(15): p. 6755-6759.
78. Mock, J.J., D.R. Smith, and S. Schultz, *Local Refractive Index Dependence of Plasmon Resonance Spectra from Individual Nanoparticles.* Nano Letters, 2003. **3**(4): p. 485-491.
79. Karakouz, T., A. Vaskevich, and I. Rubinstein, *Polymer-Coated Gold Island Films as Localized Plasmon Transducers for Gas Sensing.* Journal of Physical Chemistry B, 2008. **112**(46): p. 14530-14538.
80. Marinakos, S.M., S. Chen, and A. Chilkoti, *Plasmonic detection of a model analyte in serum by a gold nanorod sensor.* Analytical Chemistry, 2007. **79**(14): p. 5278-5283.
81. Cheng, C.-S., Y.-Q. Chen, and C.-J. Lu, *Organic vapour sensing using localized surface plasmon resonance spectrum of metallic nanoparticles self assemble monolayer.* Talanta, 2007. **73**(2): p. 358-365.
82. Nguyen Ba, T., H. Yoshikawa, E. Tamiya, V. Pham Hung, Y. Takamura, and T. Ashahi, *Propitious Immobilization of Gold Nanoparticles on Poly(dimethylsiloxane) Substrate for Local Surface Plasmon Resonance Based Biosensor.* Japanese Journal of Applied Physics, 2012. **51**(3).

83. Live, L.S., M.-P. Murray-Methot, and J.-F. Masson, *Localized and Propagating Surface Plasmons in Gold Particles of Near-Micron Size.* Journal of Physical Chemistry C, 2009. **113**(1): p. 40-44.
84. Sun, Y. and Y. Xia, *Increased Sensitivity of Surface Plasmon Resonance of Gold Nanoshells Compared to That of Gold Solid Colloids in Response to Environmental Changes.* Analytical Chemistry, 2002. **74**(20): p. 5297-5305.
85. Khlebtsov, B.N. and N.G. Khlebtsov, *Plasmon resonance of gold nanoshells: Sensitivity to the local dielectric enviromment - art. no. 616402*, in *Saratov Fall Meeting 2005: Coherent Optics of Ordered and Random Media VI*, D.A.K.N.G. Zimnyakov, Editor. 2006. p. 16402-16402.
86. Endo, T., D. Ikeda, Y. Kawakami, Y. Yanagida, and T. Hatsuzawa, *Fabrication of core-shell Structured nanoparticle layer substrate for excitation of localized surface plasmon resonance and its optical response for DNA in aqueous conditions.* Analytica Chimica Acta, 2010. **661**(2): p. 200-205.
87. Dong, P., Y. Lin, J. Deng, and J. Di, *Ultrathin Gold-Shell Coated Silver Nanoparticles onto a Glass Platform for Improvement of Plasmonic Sensors.* Acs Applied Materials & Interfaces, 2013. **5**(7): p. 2392-2399.
88. Steinbrueck, A., O. Stranik, A. Csaki, and W. Fritzsche, *Sensoric potential of gold-silver core-shell nanoparticles.* Analytical and Bioanalytical Chemistry, 2011. **401**(4): p. 1241-1249.
89. Deng, J., J. Du, Y. Wang, Y. Tu, and J. Di, *Synthesis of ultrathin silver shell on gold core for reducing substrate effect of LSPR sensor.* Electrochemistry Communications, 2011. **13**(12): p. 1517-1520.
90. Wu, C. and Q.-H. Xu, *Stable and Functionable Mesoporous Silica-Coated Gold Nanorods as Sensitive Localized Surface Plasmon Resonance (LSPR) Nanosensors.* Langmuir, 2009. **25**(16): p. 9441-9446.
91. Banholzer, M.J., N. Harris, J.E. Millstone, G.C. Schatz, and C.A. Mirkin, *Abnormally Large Plasmonic Shifts in Silica-Protected Gold Triangular Nanoprisms†.* The Journal of Physical Chemistry C, 2010. **114**(16): p. 7521-7526.
92. Burgin, J., M. Liu, and P. Guyot-Sionnest, *Dielectric Sensing with Deposited Gold Bipyramids.* The Journal of Physical Chemistry C, 2008. **112**(49): p. 19279-19282.
93. Whitney, A.V., J.W. Elam, S.L. Zou, A.V. Zinovev, P.C. Stair, G.C. Schatz, and R.P. Van Duyne, *Localized surface plasmon resonance nanosensor: A high-resolution distance-dependence study using atomic layer deposition.* Journal of Physical Chemistry B, 2005. **109**(43): p. 20522-20528.
94. Lee, S., K.M. Mayer, and J.H. Hafner, *Improved Localized Surface Plasmon Resonance Immunoassay with Gold Bipyramid Substrates.* Analytical Chemistry, 2009. **81**(11): p. 4450-4455.
95. Mayer, K.M., F. Hao, S. Lee, P. Nordlander, and J.H. Hafner, *A single molecule immunoassay by localized surface plasmon resonance.* Nanotechnology, 2010. **21**(25).
96. Wang, H., D.W. Brandl, P. Nordlander, and N.J. Halas, *Plasmonic Nanostructures: Artificial Molecules.* Accounts of Chemical Research, 2006. **40**(1): p. 53-62.
97. Wang, H., D.W. Brandl, F. Le, P. Nordlander, and N.J. Halas, *Nanorice: A hybrid plasmonic nanostructure.* Nano Letters, 2006. **6**(4): p. 827-832.
98. Charles, D.E., M. Gara, D. Aherne, D.M. Ledwith, J.M. Kelly, W.J. Blau, and M.E. Brennan-Fournet, *Scaling of Surface Plasmon Resonances in Triangular Silver Nanoplate Sols for Enhanced Refractive Index Sensing.* Plasmonics, 2011. **6**(2): p. 351-362.

99. Beeram, S.R. and F.P. Zamborini, *Selective Attachment of Antibodies to the Edges of Gold Nanostructures for Enhanced Localized Surface Plasmon Resonance Biosensing.* Journal of the American Chemical Society, 2009. **131**(33): p. 11689-+.
100. Charles, D.E., D. Aherne, M. Gara, D.M. Ledwith, Y.K. Gun'ko, J.M. Kelly, W.J. Blau, and M.E. Brennan-Fournet, *Versatile Solution Phase Triangular Silver Nanoplates for Highly Sensitive Plasmon Resonance Sensing.* Acs Nano, 2010. **4**(1): p. 55-64.
101. Chung, T., S.-Y. Lee, E.Y. Song, H. Chun, and B. Lee, *Plasmonic Nanostructures for Nano-Scale Bio-Sensing.* Sensors, 2011. **11**(11): p. 10907-10929.
102. McPhillips, J., A. Murphy, M.P. Jonsson, W.R. Hendren, R. Atkinson, F. Hook, A.V. Zayats, and R.J. Pollard, *High-Performance Biosensing Using Arrays of Plasmonic Nanotubes.* Acs Nano, 2010. **4**(4): p. 2210-2216.
103. Zhu, J. and X.-c. Deng, *Improve the refractive index sensitivity of gold nanotube by reducing the restoring force of localized surface plasmon resonance.* Sensors and Actuators B-Chemical, 2011. **155**(2): p. 843-847.
104. Sun, Y.G. and Y.N. Xia, *Increased sensitivity of surface plasmon resonance of gold nanoshells compared to that of gold solid colloids in response to environmental changes.* Analytical Chemistry, 2002. **74**(20): p. 5297-5305.
105. Lee, S.-W., K.-S. Lee, J. Ahn, J.-J. Lee, M.-G. Kim, and Y.-B. Shin, *Highly Sensitive Biosensing Using Arrays of Plasmonic Au Nanodisks Realized by Nanoimprint Lithography.* ACS Nano, 2011. **5**(2): p. 897-904.
106. Lin, V.K., S.L. Teo, R. Marty, A. Arbouet, C. Girard, E. Alarcon-Llado, S.H. Liu, M.Y. Han, S. Tripathy, and A. Mlayah, *Dual wavelength sensing based on interacting gold nanodisk trimers.* Nanotechnology, 2010. **21**(30).
107. Larsson, E.M., J. Alegret, M. Kall, and D.S. Sutherland, *Sensing characteristics of NIR localized surface plasmon resonances in gold nanorings for application as ultrasensitive biosensors.* Nano Letters, 2007. **7**(5): p. 1256-1263.
108. Galush, W.J., S.A. Shelby, M.J. Mulvihill, A. Tao, P. Yang, and J.T. Groves, *A Nanocube Plasmonic Sensor for Molecular Binding on Membrane Surfaces.* Nano Letters, 2009. **9**(5): p. 2077-2082.
109. Bukasov, R., T.A. Ali, P. Nordlander, and J.S. Shumaker-Parry, *Probing the Plasmonic Near-Field of Gold Nanocrescent Antennas.* ACS Nano, 2010. **4**(11): p. 6639-6650.
110. Dondapati, S.K., T.K. Sau, C. Hrelescu, T.A. Klar, F.D. Stefani, and J. Feldmann, *Label-free Biosensing Based on Single Gold Nanostars as Plasmonic Transducers.* ACS Nano, 2010. **4**(11): p. 6318-6322.
111. Verellen, N., P. Van Dorpe, C. Huang, K. Lodewijks, G.A.E. Vandenbosch, L. Lagae, and V.V. Moshchalkov, *Plasmon Line Shaping Using Nanocrosses for High Sensitivity Localized Surface Plasmon Resonance Sensing.* Nano Letters, 2011. **11**(2): p. 391-397.
112. Kubo, W. and S. Fujikawa, *Au Double Nanopillars with Nanogap for Plasmonic Sensor.* Nano Letters, 2011. **11**(1): p. 8-15.
113. Liu, N., T. Weiss, M. Mesch, L. Langguth, U. Eigenthaler, M. Hirscher, C. Soennichsen, and H. Giessen, *Planar Metamaterial Analogue of Electromagnetically Induced Transparency for Plasmonic Sensing.* Nano Letters, 2010. **10**(4): p. 1103-1107.
114. Kabashin, A.V., P. Evans, S. Pastkovsky, W. Hendren, G.A. Wurtz, R. Atkinson, R. Pollard, V.A. Podolskiy, and A.V. Zayats, *Plasmonic nanorod metamaterials for biosensing.* Nature Materials, 2009. **8**(11): p. 867-871.
115. Cetin, A.E., A.A. Yanik, C. Yilmaz, S. Somu, A. Busnaina, and H. Altug, *Monopole antenna arrays for optical trapping, spectroscopy, and sensing.* Applied Physics Letters, 2011. **98**(11).
116. Cao, J., E.K. Galbraith, T. Sun, and K.T.V. Grattan, *Cross-Comparison of Surface Plasmon Resonance-Based Optical Fiber Sensors With Different Coating Structures.* IEEE Sensors Journal, 2012. **12**(7): p. 2355-2361.

117. Zhou, C., *Localized surface plasmonic resonance study of silver nanocubes for photonic crystal fiber sensor.* Optics and Lasers in Engineering, 2012. **50**(11): p. 1592-1595.
118. Gu, Y., Q. Li, J. Xiao, K. Wu, and G.P. Wang, *Plasmonic metamaterials for ultrasensitive refractive index sensing at near infrared.* Journal of Applied Physics, 2011. **109**(2).
119. [cited 2013 03/07]; Available from: https://en.wikipedia.org/wiki/Enzyme.
120. Chaplin, M. [cited 2013 03/07]; Available from: http://www.lsbu.ac.uk/water/enztech/mechan.html.
121. Endo, T., R. Ikeda, Y. Yanagida, and T. Hatsuzawa, *Stimuli-responsive hydrogel-silver nanoparticles composite for development of localized surface plasmon resonance-based optical biosensor.* Analytica Chimica Acta, 2008. **611**(2): p. 205-211.
122. Lee, T.-H., S.-W. Lee, J.-A. Jung, J. Ahn, M.-G. Kim, and Y.-B. Shin, *Signal Amplification by Enzymatic Reaction in an Immunosensor Based on Localized Surface Plasmon Resonance (LSPR).* Sensors, 2010. **10**(3): p. 2045-2053.
123. Huang, H., F. Liu, S. Huang, S. Yuan, B. Liao, S. Yi, Y. Zeng, and P.K. Chu, *Sensitive and simultaneous detection of different disease markers using multiplexed gold nanorods.* Analytica Chimica Acta, 2012. **755**: p. 108-114.
124. Wang, J., *Electrochemical biosensing based on noble metal nanoparticles.* Microchimica Acta, 2012. **177**(3-4): p. 245-270.
125. Zhao, S.S., M.A. Bichelberger, D.Y. Colin, R. Robitaille, J.N. Pelletier, and J.-F. Masson, *Monitoring methotrexate in clinical samples from cancer patients during chemotherapy with a LSPR-based competitive sensor.* Analyst, 2012. **137**(20): p. 4742-4750.
126. Lin, T.-J., K.-T. Huang, and C.-Y. Liu, *Determination of organophosphorous pesticides by a novel biosensor based on localized surface plasmon resonance.* Biosensors & Bioelectronics, 2006. **22**(4): p. 513-518.
127. McMahon, R.J., *Avidin-biotin interactions : methods and applications*. 2008, Totowa, N.J.: Humana ; [London : Springer, distributor].
128. Arai, T., P.K.R. Kumar, C. Rockstuhl, K. Awazu, and J. Tominaga, *An optical biosensor based on localized surface plasmon resonance of silver nanostructured films.* Journal of Optics a-Pure and Applied Optics, 2007. **9**(7): p. 699-703.
129. Barbillon, G., J.L. Bijeon, J. Plain, and P. Royer, *Sensitive detection of biological species through localized surface-plasmon resonance on gold nanodisks.* Thin Solid Films, 2009. **517**(9): p. 2997-3000.
130. Wang, Y., W. Qian, Y. Tan, and S. Ding, *A label-free biosensor based on gold nanoshell monolayers for monitoring biomolecular interactions in diluted whole blood.* Biosensors & Bioelectronics, 2008. **23**(7): p. 1166-1170.
131. Banica, F.-G., *Chemical sensors and biosensors : fundamentals and applications*. 2012, UK: John Wiley & Sons.
132. Mayer, K.M., S. Lee, H. Liao, B.C. Rostro, A. Fuentes, P.T. Scully, C.L. Nehl, and J.H. Hafner, *A label-free immunoassay based upon localized surface plasmon resonance of gold nanorods.* Acs Nano, 2008. **2**(4): p. 687-692.
133. Fida, F., L. Varin, S. Badilescu, M. Kahrizi, and V.-V. Truong, *Gold Nanoparticle Ring and Hole Structures for Sensing Proteins and Antigen-Antibody Interactions.* Plasmonics, 2009. **4**(3): p. 201-207.
134. Fu, J., B. Park, and Y. Zhao, *Limitation of a localized surface plasmon resonance sensor for Salmonella detection.* Sensors and Actuators B-Chemical, 2009. **141**(1): p. 276-283.

135. Huang, H., C. He, Y. Zeng, X. Xia, X. Yu, P. Yi, and Z. Chen, *A novel label-free multi-throughput optical biosensor based on localized surface plasmon resonance.* Biosensors & Bioelectronics, 2009. **24**(7): p. 2255-2259.
136. Huang, H., C. Tang, Y. Zeng, X. Yu, B. Liao, X. Xia, P. Yi, and P.K. Chu, *Label-free optical biosensor based on localized surface plasmon resonance of immobilized gold nanorods.* Colloids and Surfaces B-Biointerfaces, 2009. **71**(1): p. 96-101.
137. Bi, N., Y. Sun, Y. Tian, D. Song, L. Wang, J. Wang, and H. Zhang, *Analysis of immunoreaction with localized surface plasmon resonance biosensor.* Spectrochimica Acta Part a-Molecular and Biomolecular Spectroscopy, 2010. **75**(3): p. 1163-1167.
138. Kim, D.-K., T.J. Park, E. Tamiya, and S.Y. Lee, *Label-Free Detection of Leptin Antibody-Antigen Interaction by Using LSPR-Based Optical Biosensor.* Journal of Nanoscience and Nanotechnology, 2011. **11**(5): p. 4188-4193.
139. Haes, A.J., L. Chang, W.L. Klein, and R.P. Van Duyne, *Detection of a biomarker for Alzheimer's disease from synthetic and clinical samples using a nanoscale optical biosensor.* Journal of the American Chemical Society, 2005. **127**(7): p. 2264-2271.
140. Zheng, S., D.-K. Kim, T.J. Park, S.J. Lee, and S.Y. Lee, *Label-free optical diagnosis of hepatitis B virus with genetically engineered fusion proteins.* Talanta, 2010. **82**(2): p. 803-809.
141. Park, T.J., S.J. Lee, D.-K. Kim, N.S. Heo, J.Y. Park, and S.Y. Lee, *Development of label-free optical diagnosis for sensitive detection of influenza virus with genetically engineered fusion protein.* Talanta, 2012. **89**: p. 246-252.
142. Torun, Ö., İ. Hakkı Boyacı, E. Temür, and U. Tamer, *Comparison of sensing strategies in SPR biosensor for rapid and sensitive enumeration of bacteria.* Biosensors and Bioelectronics, 2012. **37**(1): p. 53-60.
143. Tuerk, C. and L. Gold, *SYSTEMATIC EVOLUTION OF LIGANDS BY EXPONENTIAL ENRICHMENT - RNA LIGANDS TO BACTERIOPHAGE-T4 DNA-POLYMERASE.* Science, 1990. **249**(4968): p. 505-510.
144. Ellington, A.D. and J.W. Szostak, *INVITRO SELECTION OF RNA MOLECULES THAT BIND SPECIFIC LIGANDS.* Nature, 1990. **346**(6287): p. 818-822.
145. Sassolas, A., L.J. Blum, and B.D. Leca-Bouvier, *Optical detection systems using immobilized aptamers.* Biosens Bioelectron, 2011.
146. Cheng, A.K.H., B. Ge, and H.-Z. Yu, *Aptamer-Based Biosensors for Label-Free Voltammetric Detection of Lysozyme.* Analytical Chemistry, 2007. **79**(14): p. 5158-5164.
147. Kim, D.-K., K. Kerman, H.M. Hiep, M. Saito, S. Yamamura, Y. Takamura, Y.-S. Kwon, and E. Tamiya, *Label-free optical detection of aptamer-protein interactions using gold-capped.* Analytical Biochemistry, 2008. **379**(1): p. 1-7.
148. Zheng, R. and B.D. Cameron, *Aptamer-based localized surface plasmon resonance sensor for monitoring glycated proteins*, in *Plasmonics in Biology and Medicine Viii*, T. VoDinh and J.R. Lakowicz, Editors. 2011.
149. Galopin, E., L. Touahir, J. Niedziolka-Joensson, R. Boukherroub, A.C. Gouget-Laemmel, J.-N. Chazalviel, F. Ozanam, and S. Szunerits, *Amorphous silicon-carbon alloys for efficient localized surface plasmon resonance sensing.* Biosensors & Bioelectronics, 2010. **25**(5): p. 1199-1203.
150. Yoo, S.Y., D.-K. Kim, T.J. Park, E.K. Kim, E. Tamiya, and S.Y. Lee, *Detection of the Most Common Corneal Dystrophies Caused by BIGH3 Gene Point Mutations Using a Multispot Gold-Capped Nanoparticle Array Chip.* Analytical Chemistry, 2010. **82**(4): p. 1349-1357.
151. Touahir, L., E. Galopin, R. Boukherroub, A.C. Gouget-Laemmel, J.-N. Chazalviel, F. Ozanam, O. Saison, A. Akjouj, Y. Pennec, B. Djafari-Rouhani, and S. Szunerits,

Plasmonic properties of silver nanostructures coated with an amorphous silicon-carbon alloy and their applications for sensitive sensing of DNA hybridization. Analyst, 2011. **136**(9): p. 1859-1866.

152. Spadavecchia, J., A. Burras, J. Lyskawa, P. Woisel, W. Laure, C.-M. Pradier, R. Boukherroub, and S. Szunerits, *Approach for Plasmonic Based DNA Sensing: Amplification of the Wavelength Shift and Simultaneous Detection of the Plasmon Modes of Gold Nanostructures.* Analytical Chemistry, 2013. **85**(6): p. 3288-3296.
153. Huang, C., J. Ye, S. Wang, T. Stakenborg, and L. Lagae, *Gold nanoring as a sensitive plasmonic biosensor for on-chip DNA detection.* Applied Physics Letters, 2012. **100**(17).
154. Goldstein, I.J., C.E. Hollerman, and J.M. Merrick, *Protein-carbohydrate interaction I. The interaction of polysaccharides with concanavalin A.* Biochimica et Biophysica Acta (BBA) - General Subjects, 1965. **97**(1): p. 68-76.
155. Gray, R.D. and R.H. Glew, *KINETICS OF CARBOHYDRATE BINDING TO CONCANAVALIN-A.* Journal of Biological Chemistry, 1973. **248**(21): p. 7547-7551.
156. Vaccarello, P., L. Tran, J. Meinen, C. Kwon, Y. Abate, and Y.-S. Shon, *Characterization of localized surface plasmon resonance transducers produced from Au-25 nanoparticle multilayers.* Colloids and Surfaces a-Physicochemical and Engineering Aspects, 2012. **402**: p. 146-151.
157. Bellapadrona, G., A.B. Tesler, D. Gruenstein, L.H. Hossain, R. Kikkeri, P.H. Seeberger, A. Vaskevich, and I. Rubinstein, *Optimization of Localized Surface Plasmon Resonance Transducers for Studying Carbohydrate-Protein Interactions.* Analytical Chemistry, 2012. **84**(1): p. 232-240.
158. Lin, T.-J. and C.-T. Lou, *Reflection-based localized surface plasmon resonance fiber-optic probe for chemical and biochemical sensing at high-pressure conditions.* Journal of Supercritical Fluids, 2007. **41**(2): p. 317-325.
159. Sovago, I. and R.B. Martin, *Transition metal ion induced deprotonation of amide hydrogens in sulfhydryl containing compounds.* Journal of Inorganic and Nuclear Chemistry, 1981. **43**(2): p. 425-429.
160. Lin, T.-J. and M.-F. Chung, *Detection of cadmium by a fiber-optic biosensor based on localized surface plasmon resonance.* Biosensors & Bioelectronics, 2009. **24**(5): p. 1213-1218.
161. Huang, H., C. Qu, X. Liu, S. Huang, Z. Xu, Y. Zhu, and P.K. Chu, *Amplification of localized surface plasmon resonance signals by a gold nanorod assembly and ultra-sensitive detection of mercury.* Chemical Communications, 2011. **47**(24): p. 6897-6899.
162. Dharmalingam, G., N.A. Joy, B. Grisafe, and M.A. Carpenter, *Plasmonics-based detection of H-2 and CO: discrimination between reducing gases facilitated by material control.* Beilstein Journal of Nanotechnology, 2012. **3**: p. 712-721.
163. Ghodselahi, T., H. Zahrabi, M.H. Saani, and M.A. Vesaghi, *CO Gas Sensor Properties of Cu@CuO Core-Shell Nanoparticles Based on Localized Surface Plasmon Resonance.* Journal of Physical Chemistry C, 2011. **115**(45): p. 22126-22130.
164. Chen, Y.-Q. and C.-J. Lu, *Surface modification on silver nanoparticles for enhancing vapor selectivity of localized surface plasmon resonance sensors.* Sensors and Actuators B-Chemical, 2009. **135**(2): p. 492-498.
165. Dalfovo, M.C., R.C. Salvarezza, and F.J. Ibanez, *Improved Vapor Selectivity and Stability of Localized Surface Plasmon Resonance with a Surfactant-Coated Au Nanoparticles Film.* Analytical Chemistry, 2012. **84**(11): p. 4886-4892.
166. Ma, W., H. Yang, W. Wang, P. Gao, and J. Yao, *Ethanol Vapor Sensing Properties of Triangular Silver Nanostructures Based on Localized Surface Plasmon Resonance.* Sensors, 2011. **11**(9): p. 8643-8653.

167. Nengsih, S., A.A. Umar, M.M. Salleh, and M. Oyama, *Detection of Formaldehyde in Water: A Shape-Effect on the Plasmonic Sensing Properties of the Gold Nanoparticles.* Sensors, 2012. **12**(8): p. 10309-10325.
168. Misra, N., V. Kumar, L. Borde, and L. Varshney, *Localized surface plasmon resonance-optical sensors based on radiolytically synthesized silver nanoparticles for estimation of uric acid.* Sensors and Actuators B-Chemical, 2013. **178**: p. 371-378.
169. Nuopponen, M. and H. Tenhu, *Gold Nanoparticles Protected with pH and Temperature-Sensitive Diblock Copolymers.* Langmuir, 2007. **23**(10): p. 5352-5357.
170. Mack, N.H., J.W. Wackerly, V. Malyarchuk, J.A. Rogers, J.S. Moore, and R.G. Nuzzo, *Optical Transduction of Chemical Forces.* Nano Letters, 2007. **7**(3): p. 733-737.
171. Jiang, H., J. Markowski, and J. Sabarinathan, *Near-infrared optical response of thin film pH-sensitive hydrogel coated on a gold nanocrescent array.* Optics Express, 2009. **17**(24): p. 21802-21807.
172. Chen, K.-J. and C.-J. Lu, *A vapor sensor array using multiple localized surface plasmon resonance bands in a single UV-vis spectrum.* Talanta, 2010. **81**(4-5): p. 1670-1675.
173. Tabeling, P., *Introduction to microfluidics*. 2005, Oxford: Oxford University Press.
174. Huang, C., K. Bonroy, G. Reekmans, W. Laureyn, K. Verhaegen, I. De Vlaminck, L. Lagae, and G. Borghs, *Localized surface plasmon resonance biosensor integrated with microfluidic chip.* Biomedical Microdevices, 2009. **11**(4): p. 893-901.
175. Guo, L., Y. Yin, R. Huang, B. Qiu, Z. Lin, H.-H. Yang, J. Li, and G. Chen, *Enantioselective analysis of melagatran via an LSPR biosensor integrated with a microfluidic chip.* Lab on a Chip, 2012. **12**(20): p. 3901-3906.
176. SadAbadi, H., S. Badilescu, M. Packirisamy, and R. Wuethrich, *Integration of gold nanoparticles in PDMS microfluidics for lab-on-a-chip plasmonic biosensing of growth hormones.* Biosensors & Bioelectronics, 2013. **44**: p. 77-84.
177. Lin, H.-Y., C.-H. Huang, G.-L. Cheng, N.-K. Chen, and H.-C. Chui, *Tapered optical fiber sensor based on localized surface plasmon resonance.* Optics Express, 2012. **20**(19): p. 21693-21701.
178. Dutta, R., R. Bharadwaj, S. Mukherji, and T. Kundu, *Study of localized surface-plasmon-resonance-based optical fiber sensor.* Applied Optics, 2011. **50**(25): p. E138-E144.
179. Leung, A., P.M. Shankar, and R. Mutharasan, *A review of fiber-optic biosensors.* Sensors and Actuators B: Chemical, 2007. **125**(2): p. 688-703.
180. Lee, H., H.-J. Kim, J.-H. Park, D.H. Jeong, and S.-K. Lee, *Effects of surface density and size of gold nanoparticles in a fiber-optic localized surface plasmon resonance sensor and its application to peptide detection.* Measurement Science & Technology, 2010. **21**(8).
181. Shao, Y., S. Xu, X. Zheng, Y. Wang, and W. Xu, *Optical Fiber LSPR Biosensor Prepared by Gold Nanoparticle Assembly on Polyelectrolyte Multilayer.* Sensors, 2010. **10**(4): p. 3585-3596.
182. Mignani, A.G., R. Falciai, and L. Ciaccheri, *Evanescent wave absorption spectroscopy by means of bi-tapered multimode optical fibers.* Applied Spectroscopy, 1998. **52**(4): p. 546-551.
183. Mackenzie, H.S. and F.P. Payne, *Evanescent Field Amplification In A Tapered Single-mode Optical Fiber.* Electronics Letters, 1990. **26**(2): p. 130-132.
184. Lee, B., S. Roh, and J. Park, *Current status of micro- and nano-structured optical fiber sensors.* Optical Fiber Technology, 2009. **15**(3): p. 209-221.
185. Homola, J.í., R. Slavík, and J.í. tyroký, *Interaction between fiber modes and surface plasmon waves: spectral properties.* Optics Letters, 1997. **22**(18): p. 1403-1405.

186. Verma, R.K., A.K. Sharma, and B.D. Gupta, *Surface plasmon resonance based tapered fiber optic sensor with different taper profiles.* Optics Communications, 2008. **281**(6): p. 1486-1491.
187. Verma, R.K., A.K. Sharma, and B.D. Gupta, *Modeling of Tapered Fiber-Optic Surface Plasmon Resonance Sensor With Enhanced Sensitivity.* Photonics Technology Letters, IEEE, 2007. **19**(22): p. 1786-1788.
188. Rivero, P.J., A. Urrutia, J. Goicoechea, and F.J. Arregui, *Optical fiber humidity sensors based on Localized Surface Plasmon Resonance (LSPR) and Lossy-mode resonance (LMR) in overlays loaded with silver nanoparticles.* Sensors and Actuators B-Chemical, 2012. **173**: p. 244-249.

Optimisation of gold-nanoparticle-based optical fibre localised surface plasmon resonance (LSPR)-based sensors

4.1. Introduction

As discussed in Chapter 3, gold and silver are the most extensively explored metals based on their strong LSPR properties. Gold nanoparticles (AuNPs) have been of particular interest over a wide range of fields because of the breadth of their potential applications.

There have been two major approaches considered – both chemical and physical [1] – to prepare gold colloids solutions. The chemical approach includes the conventional reduction process using different agents like citrates [2] or sodium bohydrate [3, 4], or the two-phase synthesis method [5] and other complex methods such as ligand reduction by phosphines, amines or carboxylates or by using micro-emulsions, reversed micelles, surfactants, membranes and polyelectrolytes [1]. The physical method, however, relies on creating the AuNPs through a physical chemistry process such as photochemistry, sonochemistry, radiolysis or thermolysis [1, 6]. Recently, more attempts have been made towards implementing 'green chemistry' by using bio-reducing agents in order to create AuNPs [7-9]. Table 4.1 shows a summary of the methods used for the preparation of gold colloidal solutions. Each method has its own advantages and disadvantages, but the common goal of all of techniques considered is to optimise the fabrication process and thus to achieve the uniformity of the AuNPs created.

Table 4.1: Several approaches for AuNPs synthesis

Technique	Reagents/Surfactant	AuNP size (in diameter)	Ref.
Chemical reduction	**Sodium citrate**	14 -24 nm	[2]
	$LiBH_4$/THF	4 nm	[4]
	$NaBH_4$/Polymer PMPP	5.1 – 7.4 nm	[10, 11]
	Hydrazin/CTAB	10 – 60 nm	[12]
	Amino acids	15-40 nm	[13, 14]
	Sodium napthalenide	1.9 – 5.2 nm	[15]
	Peptides	11-14 nm	[16]
	Sodium diphenylamine/PVP	10 – 66 nm	[17]
Thiol-reduction	**Thiol derivatives**	1 – 4 nm	[3, 5, 18]
Sonochemistry		9 nm	[19, 20]
Seed-growth	TX100/Sodium Citrate	20 – 110 nm	[21]
Physics method	EBI technique with polymer	2 – 3 nm	[22]
UV irradiation	PMMA nanocomposites	50 – 120 nm	[23]
Green chemistry	Various*		[7-9, 24]

Among the different types of metal nanoparticles, gold colloids have shown both a unique stability and highly desirable properties such as size-related electronic, magnetic and optical effects. One of the most important characteristics of the gold colloids is their surfactant properties which are suitable, for example, for the creation of a surface plasmon band to enable their potential applications in sensors, in a wide range of bio-recognition actions as well as in catalysis and biosynthesis [25-28]. Through the modification and/or functionalization of the surface of the AuNPs layer on a certain substrate, many different types of sensors can thus be created. A typical example is the creation of a LSPR sensor by immobilising an AuNP layer onto the surface of an optical fibre glass substrate as discussed in detail in Chapter 3. The sensors fabricated have demonstrated a rapid response to environmental changes thus shown potential for real-time monitoring. As a result, extensive research has been undertaken and reported in this area, discussing methods to enhance the sensitivity, reproducibility and robustness of sensors of this type [6, 25-35].

Both the sizes and shapes of gold nanoparticles have long been considered as major factors in characterising the optical properties of the coated surface [36] as different sizes and shapes can result in different LSPR properties. As a result, extensive work has been undertaken to explore and manipulate the sizes and shapes of gold particles, ranging from gold nanospheres to gold nanorods, nanotube, nanobipyramids, etc., in order to achieve different optical properties and characteristics [36-39]. However, limited systematic discussions have been made so

far to correlate these key contributing factors, such as gold-nanoparticle sizes and their related parameters including coating time, pH condition and coating temperature, to the sensor performance, and this forms the core of the work discussed in this Chapter.

Building upon the previous research discussed in Chapter 3, this Chapter focused on the establishment of a new systematic approach used for the performance optimization of LSPR-based optical fibre sensors through the exploration of various key parameters that are related closely to the sensor fabrication process. In this chapter, a systematic research is undertaken to evaluate the sensor performance as a function of the size of the AuNPs, the pH condition of AuNPs solutions used, the AuNPs coating time and the coating temperature and thus to optimise the sensitivity of various LSPR sensors created and calibrated using solutions with known refractive index (RI) values. In order to do so, the most common and easiest method for size controlling and adjustment of AuNPs has been selected, chemical reduction of $HAuCl_4$ by sodium citrate [2]. At first, a solution of Chloroauric acid was prepared and brought into boiling under vigorous stirring. Subsequently, a freshly prepared solution of sodium citrate was put into the boiling solution and the reaction started immediately. The reaction has undergone two key stages: nucleation and growth. At the very beginning of the reaction, sodium citrate reduced $HAuCl_4$ into very small nucleic particles, called seeds, typically with diameter less than 5nm. As the reaction went on with strong stirring, more seeds were being formed and the nucleation rate was decreasing. As more gold atoms were formed from the reduction, these would be deposited onto the preformed seeds, creating a next step called growth step. In growth period, depends on the ratio between gold precursor and the reduction agent, size of the particles could be controlled. Sodium citrate also acted as a surfactant to halt the growth period to finalise the particles' diameter. Therefore, by controlling the amount of sodium citrate and the ratio between $HAuCl_4$ and $Na_3C_5H_7O_6$, it is possible to achieve the desirable size of the AuNPs. By this method, AuNPs could be synthesised with high monodispersity, which is the key point for later characterisations.

4.2. Experimental Setup

The details of the experimental procedures undertaken in the preparation and evaluation of the performance of the AuNPs are given below.

4.2.1. Chemical and Apparatus

The following were purchased from Sigma-Alrich: gold chloride hydrates ($HAuCl_4.3H_2O$), sodium citrate tribasic dehydrate ($Na_3C_6H_5O_7$), 3-aminopropyl trimethoxysilane 97%. In addition, CH_3OH (Analytical Reagent Grade) and H_2SO_4 95% (Laboratory Reagent Grade) were purchased from Fisher Scientific. H_2O_2 37% solution was purchased from ACROS.

The optical fibre was purchased from Thorlab: type BFH37-600, the fibre coupler type SPLIT400-UV-VIS from OceanOptics, the light source was a halogen light source, type HL-2000-FHSA obtained from Mikropack and the Spectrometer used was Maya type 2000PRO, obtained from Ocean Optics.

4.2.2. Synthesis of gold colloids

A common method [40] for the fabrication of Au-NPs has been slightly modified and used here for synthesising gold nanoparticles of 4 different sizes, i.e. 13nm, 20nm, 40nm, 60nm respectively, chosen specifically in this work to evaluate the particle size effect on the LSPR sensor performance. Based on the basic reduction reaction between $HAuCl_4$ and sodium citrate ($Na_3C_6H_5O_7$), gold nanoparticles solutions with different sizes have been made using the following procedure.

First of all, 5 mg of $HAuCl_4$ was dissolved in 50 mL distilled water and then the solution was heated until boiling. Following this, a known amount of sodium citrate was added quickly to the boiled solution, resulting in a colour change from slight yellow colour to dark-green after few seconds. The solution colour was then seen to change slowly to red/purple. The solution was kept being heated for a further 10 minutes before the heat source was removed, following which the solution was kept stirred for another 15 minutes before being ready for the sensor preparation discussed

below. The remaining solution prepared was kept in a refrigerator (at 4^{o}C) to ensure the sample being stable over the experimental period for one or two months.

4.2.3. Optical fibre sensor preparation

Figure 4.1 illustrates in diagrammatic form the procedure for the creation of the optical fibre sensors used in this work. Initially, both ends of the optical fibre used (of 600 μm diameter) were carefully and sequentially polished with polishing papers from Thorlabs with four different grit sizes of 5 μm, 3 μm, 1 μm and 0.3 μm, respectively, keeping one end with 20mm unclad section as a sensing area.

The fibre was then washed and hydroxylised with Piranha solution (with a ratio of 7:3 of H_2SO_4: H_2O_2) for 30 minutes. Subsequently it was washed and sonicated with distilled water before being placed in an oven for 1 hour at 120^{o}C. After the above pre-treatment, the unclad fibre section was functionalised with APTMS solution in methanol (5% v/v) for 4 hours, after which it was washed several times with methanol followed by water. After the above treatment, the fibre was then placed in an oven (overnight at 100 ^{o}C) to dry. The fibre was then ready for being coated with AuNPs through a dip coating process, undertaken over a period of several hours.

After the coating process, the coated fibre was washed carefully several times with distilled water, dried under a nitrogen gas flow and then coated with silver mirror at the distal end of the fibre to make the fibre sensor thus created to be of a reflective sensor design when connected to a light source, as shown in Fig 4.2, for ease of the spectral recording. The coating of silver mirror was done by using Tollen's reagent. To prepare Tollen's reagent solution, the first step taken was to prepare fresh 10 mL solutions of $AgNO_3$ 0.1 M, sodium hydroxide NaOH 1 M and dextrose 0.25 M. Ammoniac solution was then added dropwise to 2 mL of as-prepared $AgNO_3$, until the colour of the solution was changed from transparent to yellowish brown and to transparent again. By adding 1.4 mL of NaOH solution, the colour of the solution was changed to brown. Some more drops of ammoniac solution are added until the mixture is changed to be transparent again. The fibre was then dipped into the reagent solution and in the meantime 0.4 mL dextrose was added. After 2 min, a

silver mirror was completely formed at the end surface of the fibre. The fibre was then taken out, washed with distilled water and dried under a gentle stream of nitrogen.

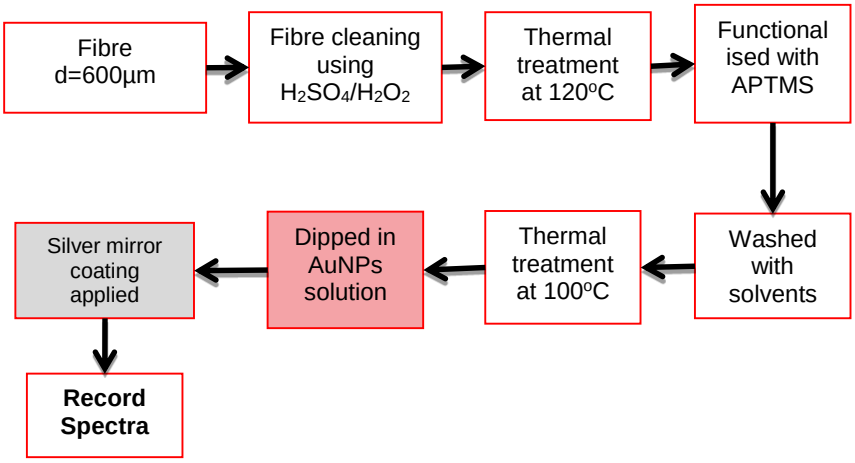

Figure 4.1: Schematic procedure for the coating process

4.2.4. Optical fibre sensor system

Figure 4.2 shows a schematic diagram of a typical LSPR sensor system used in this work, where the sensor probe was connected to a broadband light source, a halogen lamp, via a 1x2 fibre coupler and thus to allow the sensor area to be fully illuminated by the light. The silver mirror coated at the end surface of the fibre enables the light to be reflected back via the 1x2 coupler and captured by a mini-spectrometer. That spectrometer was connected to a computer so that the reflected absorbance spectra can be recorded in real-time when the probe was submerged in solutions with known and different refractive indices.

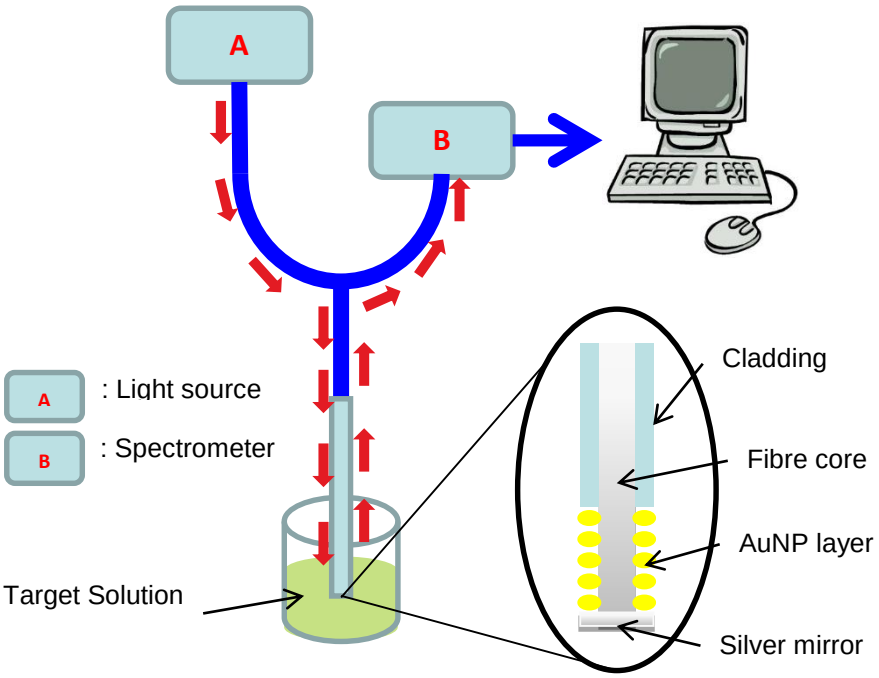

Figure 4.2: Schematic diagram of the sensor system setup used in this work

Table 4.2 lists a number of solvents used to create solutions with different yet known refractive index, allowing for the sensor calibration over the refractive index (RI) range from 1.333 (water) to 1.424 (dichloromethane).

Table 4.2: Refractive Index (RI) values of different solvents used to provide RI calibrations

Solvent	RI
Water	**1.333**
Acetonitrile	**1.344**
Acetone	**1.359**
Petroleum Ether	**1.365**
Hexane	**1.375**
n-Propyl Alcohol	**1.386**
Methanol:Toluol 1:3	**1.393**
Tetrahydrofuran	**1.407**
Dicholoromethane	**1.424**

4.3. Experimental results and discussions

4.3.1. Characteristics of a gold nanoparticle coated surface

Surface density of a gold nanoparticle-coated optical fibre plays an important role in determining the characteristic of the sensor. The properties of the sensor are dependent on two major factors, i.e. the characteristics of the metal itself and the

surface density [41]. The surface density of different sensors is closely related to the coating method and can be calculated using the simple equation below:

$$\boldsymbol{Surface\ Density}\ (\%) = \frac{\boldsymbol{S_{Au-NP}}}{\boldsymbol{S_{total}}} \times \mathbf{100}\% \qquad \text{(Eq. 4.1)}$$

where the surface density is calculated as a ratio between the surface area covered by gold nanoparticles ($\boldsymbol{S_{Au-NP}}$) and the overall surface area ($\boldsymbol{S_{total}}$). Based on equation (4.1) and the SEM (Scanning Electron Microscope) images of Au-NP coated coverslips taken and shown in Fig. 4.3, the surface density can thus be calculated to be 43.5%, 37.1%, 23.7% and 17.9%, respectively when the surface is coated with Au-NPs with sizes of 13nm, 20nm, 40nm and 60nm. The obtained surface density as a function of Au-NP size is illustrated in Fig 4.4.

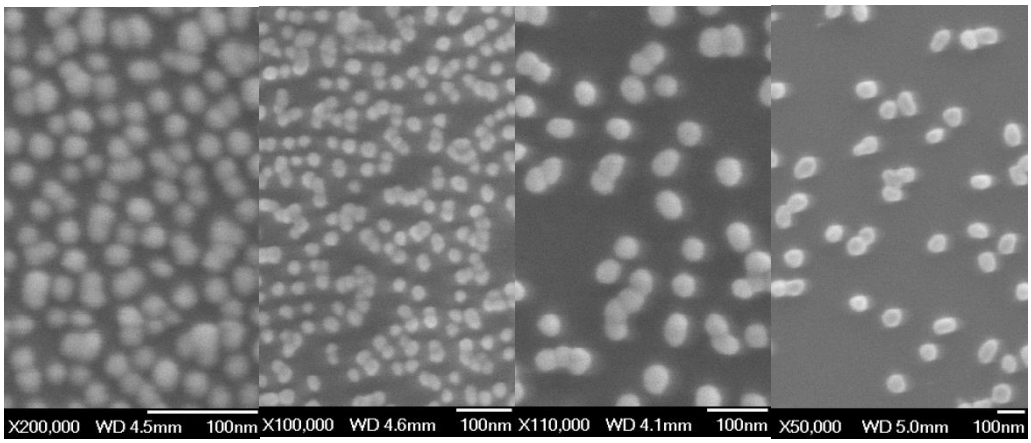

Figure 4.3: SEM of different sizes of AuNPs coated. From left to right: 13nm, 20nm, 40nm and 60nm. Scale bar is included in each image.

The results obtained have confirmed that a higher density can be achieved when the surface is coated with Au-NPs with smaller sizes. The reason for this is that a AuNP is normally covered by negative ions of citrate when synthesized. When the AuNP is bigger in size, a larger number of negative citrate ions would surround a single particle; therefore there is a stronger electrostatic force around the particle. When they are immobilised on the surface of a coverslip, it would be harder for a bigger particle to achieve high surface density than for a smaller one. Lee *et al.* [27] has reported a similar effect and noted that, achieving highest surface density might not be necessarily for the sensor design in order to achieve a high sensitivity.

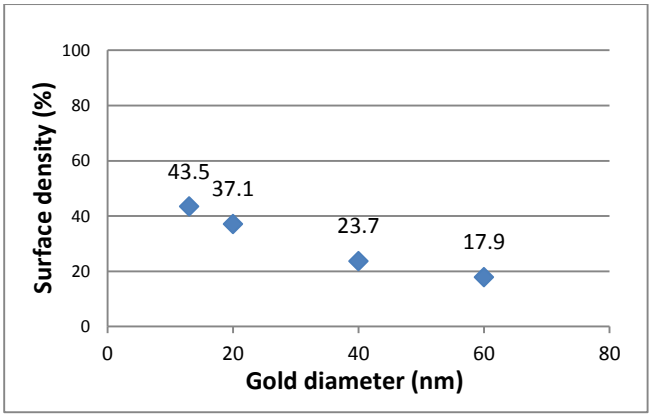

Figure 4.4: Surface density of coverslips coated with AuNPs with different sizes

4.3.2. AuNPs size – effect on the LSPR sensor sensitivity

In this work, 4 different gold solutions with different AuNPs sizes of 13nm, 20nm, 40nm and 60nm were synthesised and used to investigate the impact of the AuNPs size on the sensitivity of the LSPR sensor using the experimental setup shown in Fig 4.2 to record their respective absorbance spectra as a function of the known refractive index of the solution used. The sizes of gold nanoparticles were determined based on the absorption spectra of their corresponding synthesised solutions.

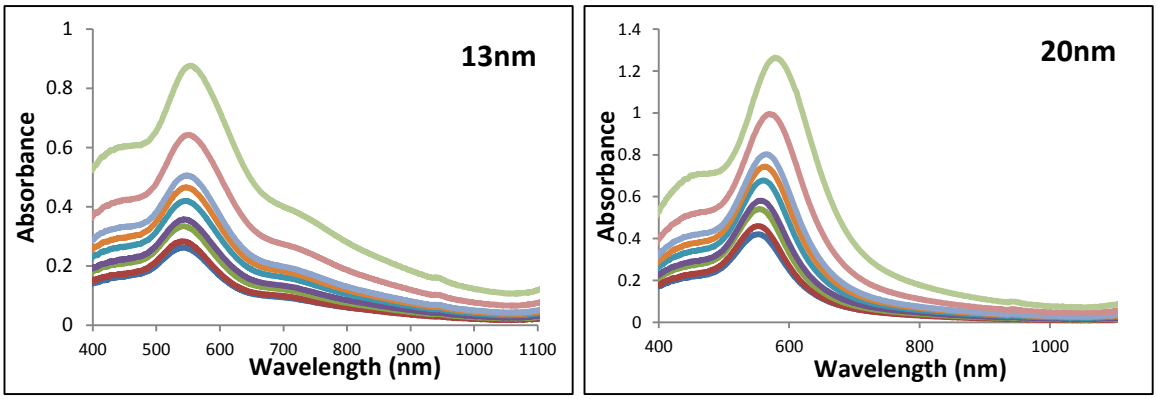

a) 13nm AuNPs coated fibre

b) 20nm AuNPs coated fibre

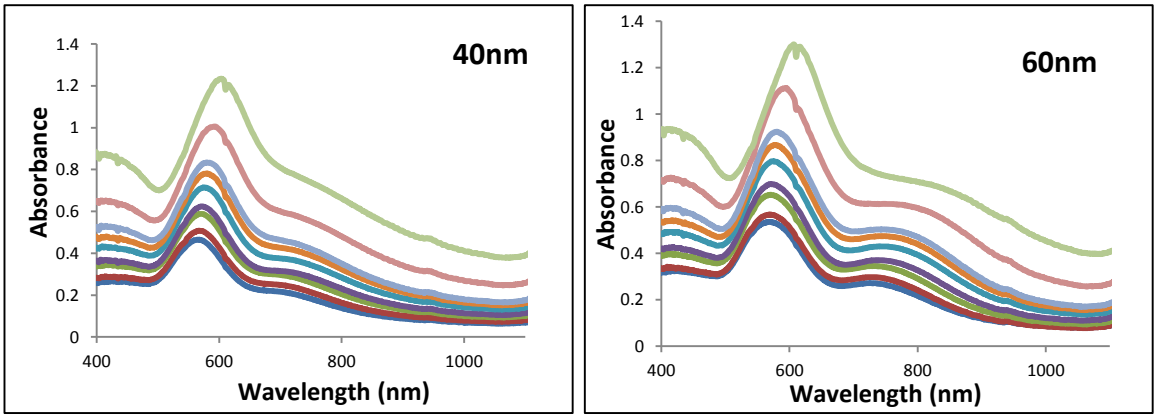

c) 40nm AuNPs coated fibre

d) 60nm AuNPs coated fibre

Figure 4.5: Absorbance spectra of LSPR sensors with AuNP sizes of (a) 13nm, (b) 20nm, (c) 40nm and (d) 60nm respectively. Different spectra in one graph are recorded in different solvents with different RI values over the range from 1.333 to 1.424.

Colour indices for various solvents with different RI values as follows

1.333 1.344 1.359 1.365 1.375 1.385 1.393 1.407 1.424

Figure 4.5 shows a set of absorbance spectra obtained when the AuNPs size is changed and within each diagram, the absorbance spectrum varies as a function of the refractive index, indicating the potential specific sensitivity of each sensor design. Fig. 4.6 summarises the peak wavelength change as a function of the refractive index variation, when the AuNPs size is varied. The sensitivity of the LSPR sensor, however, can be expressed theoretically and is given by the slope of their respective linear correlation, as given below.

$$S = \frac{d\lambda_{max}}{dn} \qquad \text{(Eq. 4.2)}$$

In Eq. 4.2, λ_{max} is peak value in the absorbance spectrum, and n is the refractive index value of the solvent.

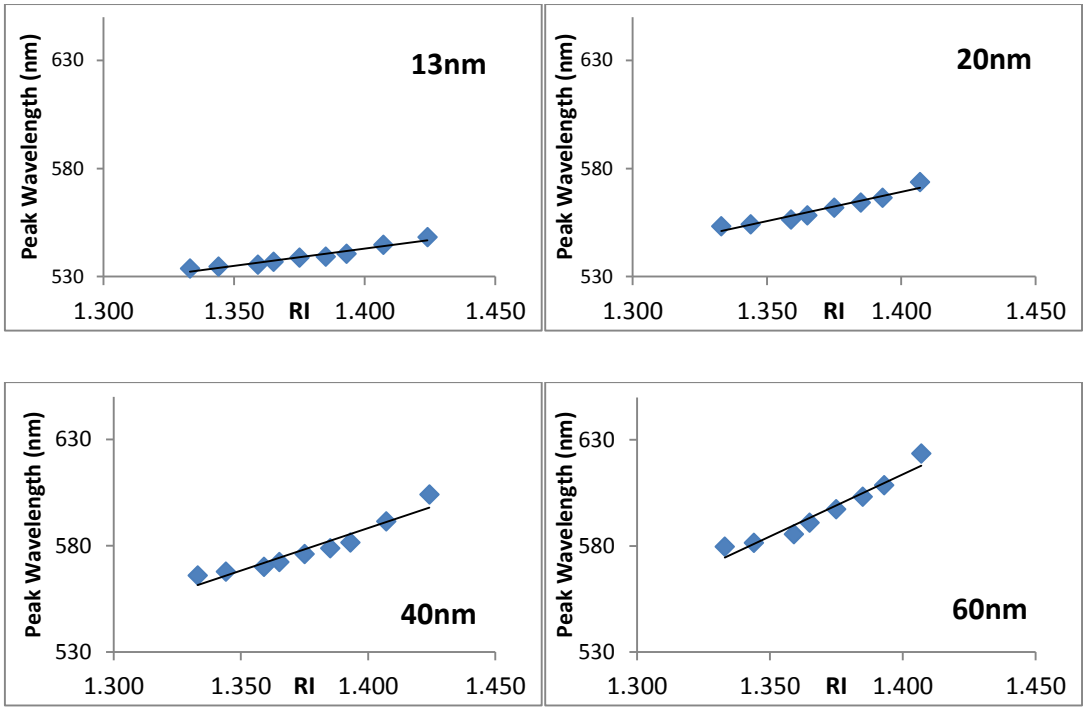

Figure 4.6: Plot of peak wavelength vs. RI value for 4 sensor probes coated with different sizes of AuNPs, i.e. 13nm, 20nm, 40nm and 60nm respectively.

To verify the repeatability of the results obtained, for each of the AuNP sizes chosen, three sensor probes were fabricated and tested. The sensitivity of each sensor was calculated with the results obtained being compared. In this work the sensitivity showing a standard deviation was calculated using Origin® software.

As shown in Fig 4.7, the calculated sensitivities of the sensors coated with AuNPs with the same size are consistent and it is noticeable that the sensitivity increases with the particle size. For the 13nm AuNP-coated sensors, the sensitivity is determined to be 154 ± 14 (nm/RIU); for 20nm, it is 266 ± 27 (nm/RIU); for 40nm, it is 418 ± 44 and for 60nm, it is 571 ± 68. This provides clear evidence that increasing the gold nanoparticles size leads to a higher sensitivity for the sensor in response to the surrounding environmental RI change. This agrees well with the findings reported by several authors in the literature [30, 42, 43] and as shown in Fig. 4.8, and it can be seen that the sensitivity of the sensors tested in this work is very close to that reported by Shao *et al.* [31], who have investigated two different sizes of gold nanoparticles (using the same technique demonstrated in this work), i.e. 23nm and 48nm respectively. A similar research has been undertaken by Wang *et al.* [42], who have made a comparison in sensitivity for 3 different sizes of gold nanoparticles, i.e.

36nm, 90nm and 136nm respectively. However, they investigated the change in absorbance at a fixed wavelength, instead of the resonance wavelength shift as shown in this work, as a function of the change in RI.

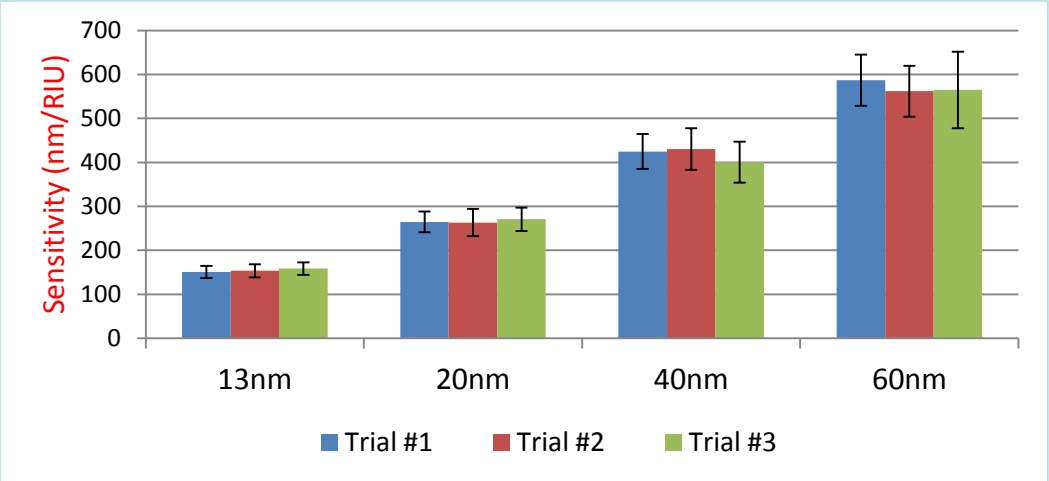

Figure 4.7: Sensitivity comparison of 4 groups of sensors coated with different sizes of AuNPs

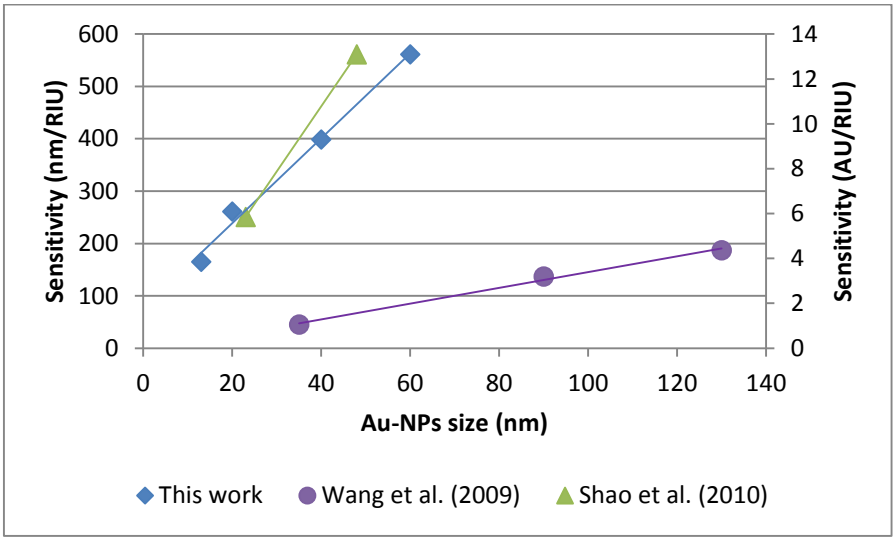

Figure 4.8: Sensitivity comparison of the results from this work with those reported from several examples in the literature. This work and the one of Shao *et al.* 's sensitivities were presented in nm/RIU, while the work from Wang *et al.* was recorded in AU/RIU.

4.3.3. Effects of the pH of gold nanoparticle solutions on LSPR sensor sensitivity

Lee *et al.* [41] previously reported that the pH of the gold solution significantly affects the immobilization of the AuNPs on the surface of an optical fibre. They stated that, over the range from pH 5.9 to pH 11.4, increasing the pH will result in a decreasing of the surface density of the gold nanoparticles on the fibre. In their synthesis, the pH values of the original gold nanoparticle solutions used are quite different and are of values 5.7, 4.9, 3.9 and 3.5 respectively for 13 nm, 20 nm, 40 nm and 60 nm AuNPs solutions. Thus in order to investigate in more detail the impact of the change in the pH, the pH value for all the gold solutions used in this work was adjusted to be 5.7. Fig. 4.9 shows the results obtained when the pH of all the gold solutions with different AuNPs sizes are set to be the same. Again for each size, three samples (denoted as Trials #1, 2 and 3) were used to evaluate the repeatability of the performance of the sensors.

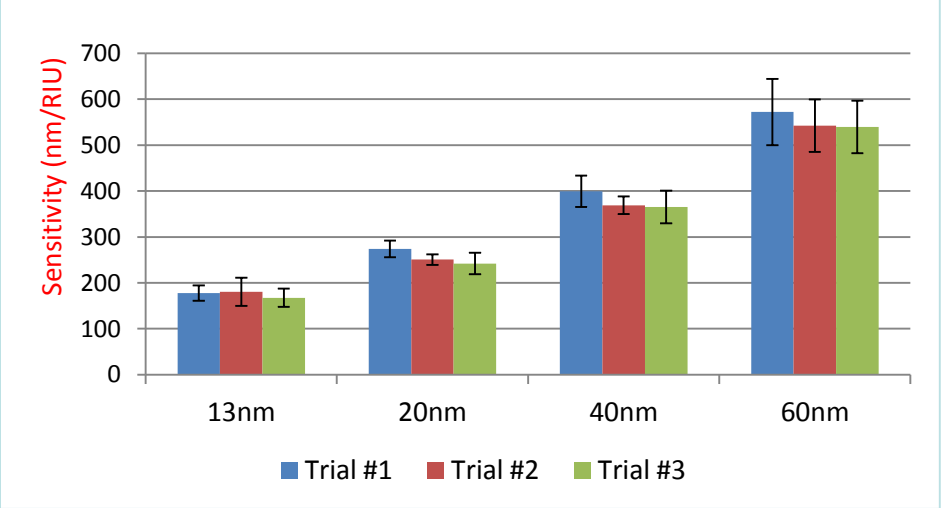

Figure 4.9: Sensitivity comparison of the sensors when the pH of the gold solutions is the same (pH 5.7)

The sensitivity of the above sensors made under the same pH conditions, i.e. pH = 5.7, is cross-compared with that of those created using the original pH solutions, i.e pH = 5.7 for 13nm AuNP solution; pH = 4.9 for 20nm AuNP solution; pH = 3.9 for 40nm AuNP solution and pH = 3.5 for 60nm AuNP solution. The results obtained are shown in Fig. 4.10.

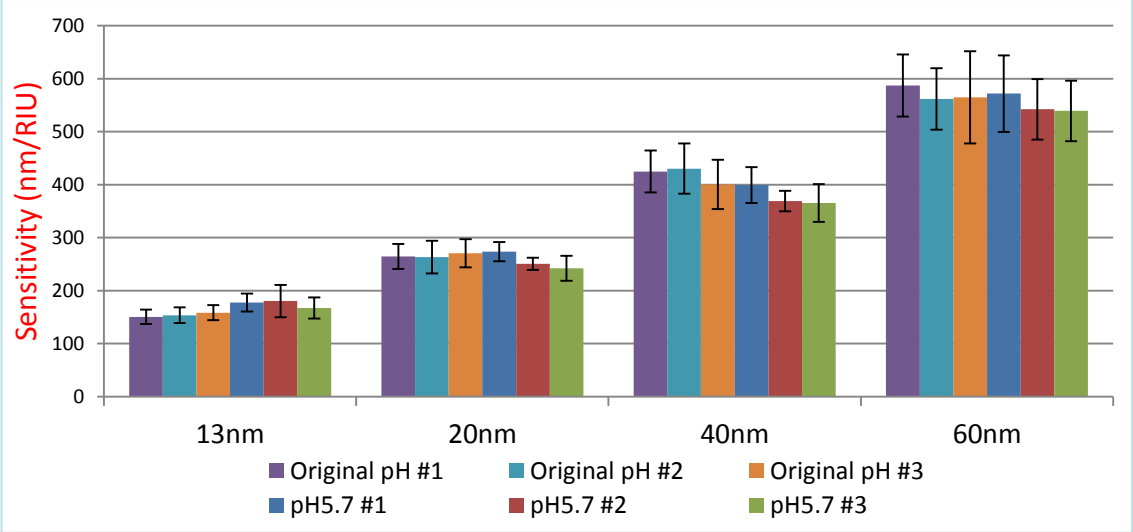

Figure 4.10: Sensitivity comparison before and after the pH adjustment. Original pH values were 5.7 (for 13nm AuNP solution), 4.9 (for 20nm AuNP solution), 3.9 (for 40nm AuNP solution) and 3.5 (for 60nm AuNP solution)

It is noticeable that the change of the pH of the gold solutions from the values originally used, ranging from 3.5 to the standardised value of pH of 5.7, seems not to have a significant effect on the sensitivities of the different sensors made. This may be due to the fact that the pH change in this work is not significant, i.e. the biggest change was from 3.5 to 5.7, and the smallest was from 4.9 to 5.7. However, it should be noted that all solutions are required to be acidic.

4.3.4. Effects of coating time

Electrostatic interaction between gold nanoparticles and the amino group of the silanised layer would lead to the formation of the sensing layer. Normally, a longer coating time induces a higher surface density of the coating – therefore a higher surface plasmon resonance (SPR) effect occurs, resulting in a higher sensitivity of the sensor. This work is aimed to investigate relationship between the sensitivity of the sensors made and their respective coating time by varying the coating time and in the meantime monitoring the sensor performance.

In order to do this, two different experimental arrangements were created. In the first experiment (which was repeated for consistency), five different coating time ranging from 1 hour to 5 hours was used for each gold nanoparticle size: the coating time was controlled manually. The results obtained are shown in Fig. 4.11.

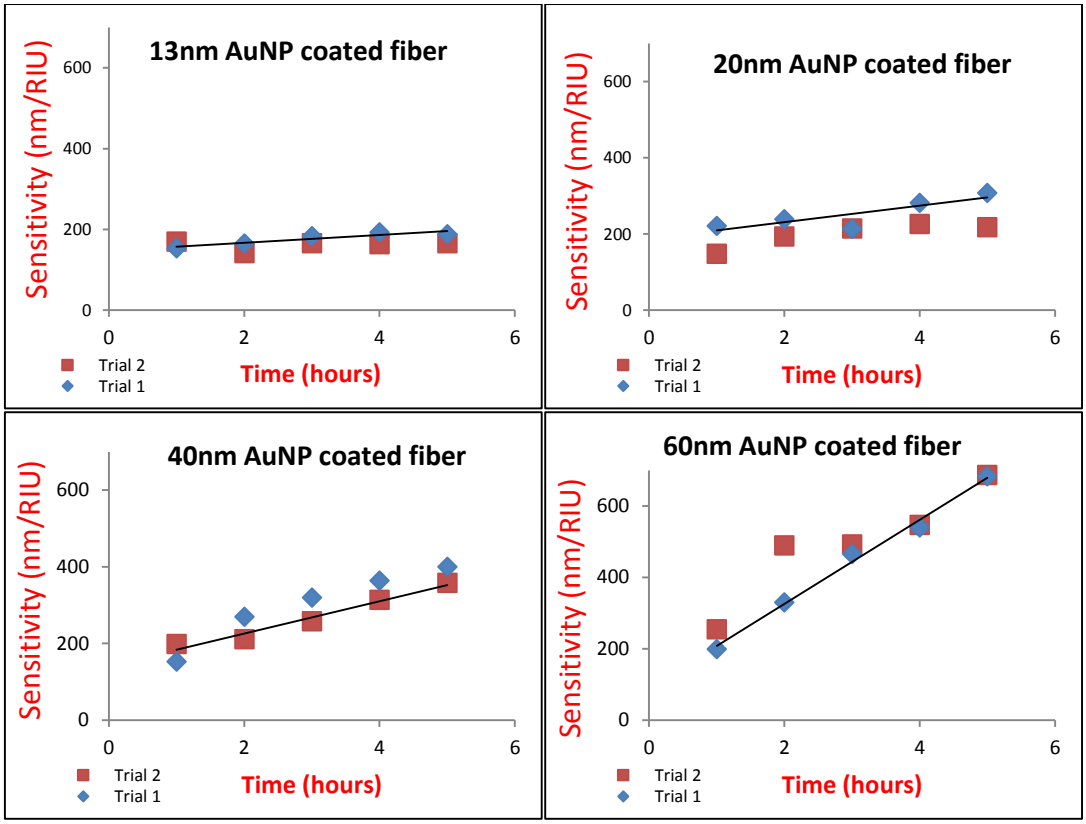

Figure 4.11: Effect of coating time on sensitivity for 4 different AuNP coated fibres with two trials each

It was observed that the longer coating time does, as would be expected, make the sensor more sensitive. When the AuNPs size is small, e.g. 13nm, the increase in sensitivity caused by the increased coating time is not very evident. However, with the increase of AuNP size, the coating time effect becomes more significant. This arises because when the AuNP particle size is small, the interaction will be greater and smaller gold nanoparticles are more easily immobilised. Given the fact that all the gold particles are negatively charged, the larger sized particles experience a greater mutual interaction prior to being attached to the fibre surface.

In order to monitor more accurately the effects of the coating time, a second experimental arrangement was made, allowing for a continuous monitoring through a small modification in the coating procedure. This is to be realised by coating the silver mirror on the distal end of the fibre *before* the AuNPs are attached rather than *after,* as was done in the first experiment discussed above. This modification enables the computer to record in real time the absorbance features from the sensor probe during the entire coating process.

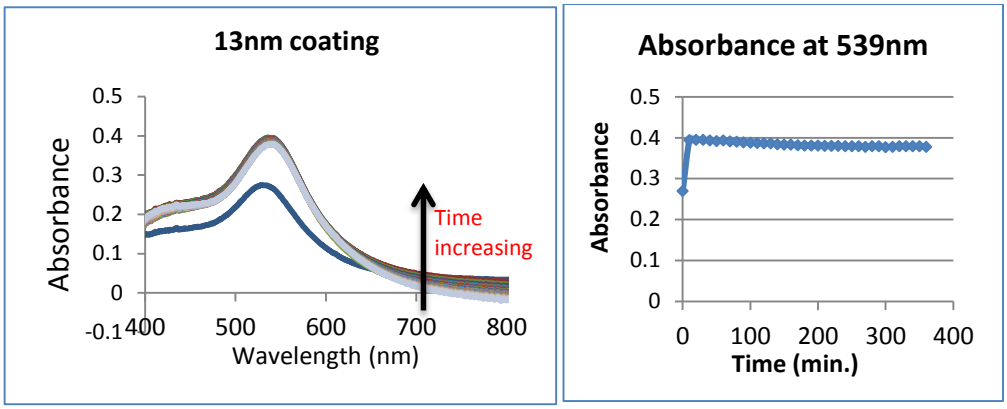

a) Absorbance spectra observed during the coating process

b) Absorbance of 13nm AuNP-coated fibre at 539nm as funtion of time

Figure 4.12: Absorbance spectra obtained during the 13nm AuNPs coating process

Fig. 4.12 shows a typical set of experimental results obtained. For 13nm AuNPs, a period of 20 to 30 minutes is required for the point of saturation to be reached and thus a total time of 30 minutes will be sufficient for a complete coating of 13nm gold nanoparticles.

For larger size AuNPs, the optimum coating time was seen to vary. The work done has shown that it takes about 100 minutes for the 20nm AuNPs coating to reach saturation. Similarly, for 40nm and 60nm AuNP particle sizes, the optimum time is longer, typically in the range of 200 minutes and 240 minutes respectively. Fig. 4.13 shows the recorded data for the 60nm LSPR sensor. It is noticable that the absorbance reaches saturation after a particular time period and therefore there is no need to leave the fibre in the coating solution longer than the saturation time. In addition, the longer coating time gives more opportunity for the gold particles to become aggregated onto the surface of the fibre, making different sizes and shapes, and hence making it more difficult to produce a sensor in a reproducible and controllable way. Therefore, the optimum coating time indicated in Figures 4.12 and 4.13 should be used to avoid the problems indicated.

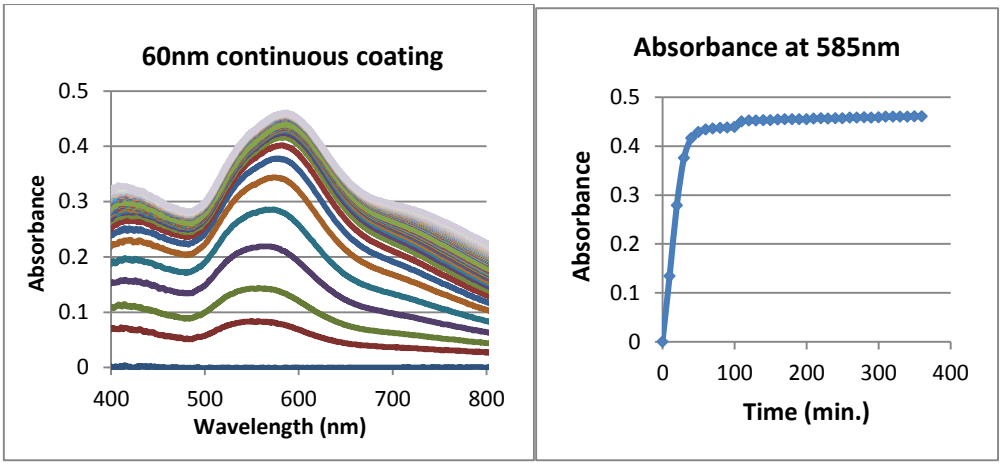

a) Absorbance spectra recorded during the coating process

b) Absorbance change for 60nm AuNPs-coated fibre at 585nm as a funtion of time

Figure 4.13: Absorbance spectra obtained during the 60nm AuNP coating process

4.3.5. Effects of temperature on the coating

Temperature is crucial to almost every process in chemistry. Normally, the thermal effect increases the rate of a reaction or indeed it could completely change the nature of the process. Thus in this work, the entire coating process for the 60nm AuNPs has been carried out again in a temperature and humidity controlled chamber, where the temperature can be controlled and set to be 25, 30, 35, 40 and 45^{o}C respectively (room temperature was 19 ^{o}C). After each sensor was coated at the specific temperature, the sensor performance was recorded: the sensors were submerged in different solvents of different refractive indices, where the results obtained are shown in Fig. 4.14:

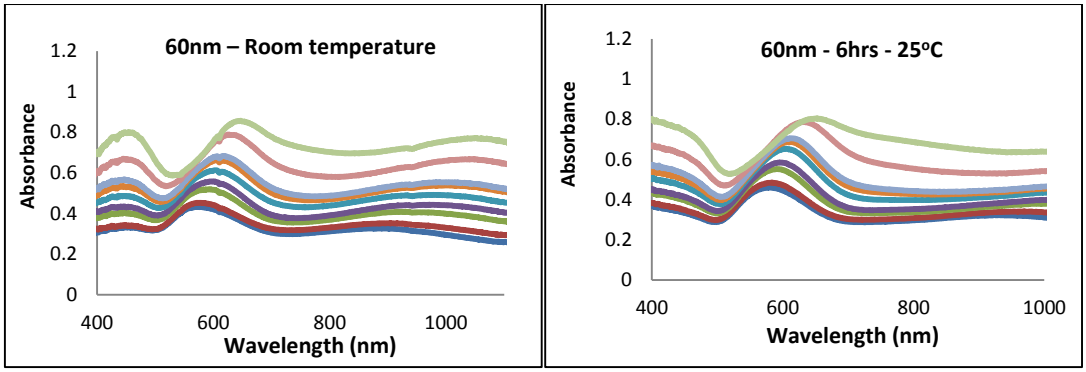

a) 4 hours coating, 60nm AuNP, Room temperature

b) 6 hours coating, 60nm AuNP, 25°C coating temp.

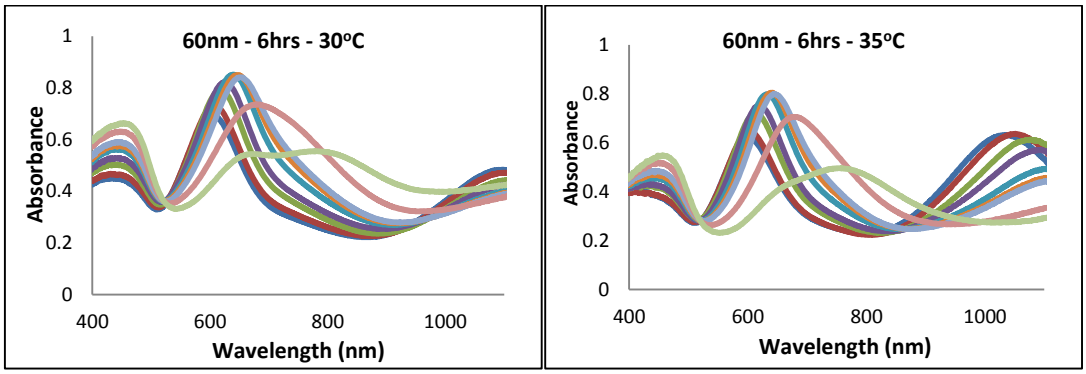

c) 6 hours coating, 60nm AuNP, 30°C coating temp.

d) 6 hours coating, 60nm AuNP, 35°C coating temp.

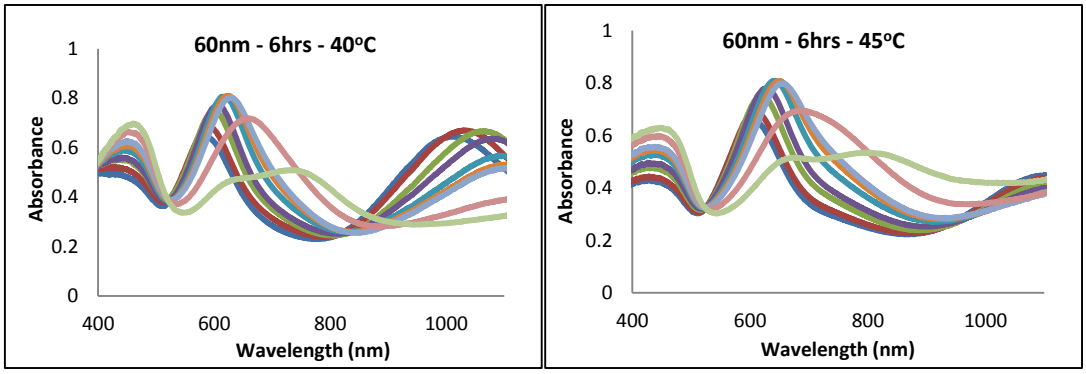

e) 6 hours coating, 60nm AuNP, 40°C coating temp.

f) 6 hours coating, 60nm AuNP, 45°C coating temp.

Figure 4.14: Absorbance spectra of 60nm AuNP coated fibres with different coating temperatures. Colour indices for various solvents with different RI values as follows

1.333 1.344 1.359 1.365 1.375 1.385 1.393 1.407 1.424

It can be seen clearly that the performance of the sensors coated both at 25°C and at room temperature (~19°C) is quite similar. However, a difference in the sensor performance has been observed from the sensors coated at higher temperatures and when the sensors are submerged in solutions with RI values higher than 1.4. Based

on the results summarised in Fig. 4.15, 25°C is considered to be the optimised coating temperature for ensuring both high sensitivity and wide sensing range.

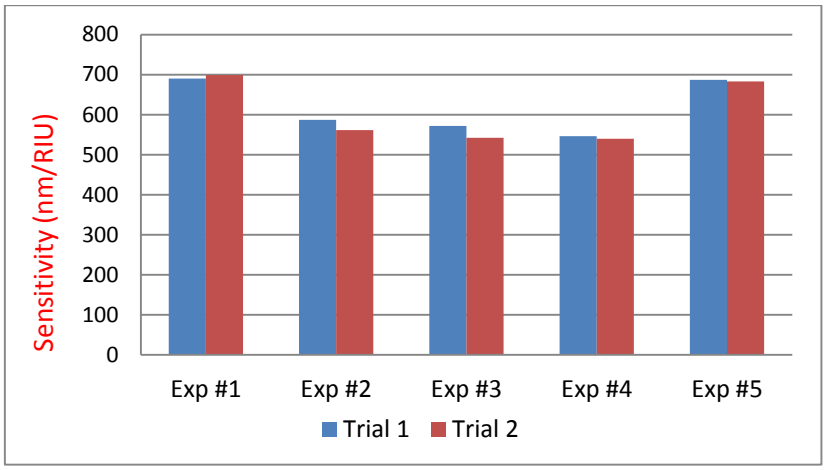

Experiment	Exp #1	Exp #2	Exp #3	Exp #4	Exp #5
Temperature	25°C	RT* (~19°C)	RT (~19°C)	RT (~19°C)	RT (~19°C)
Coating time	6 hours	4 hours	4 hours	4 hours	5 hours
Coating pH	pH 5.7	pH 3.5	pH 5.7	pH 5.7	pH 5.7

**RT: Room temperature*

Figure 4.15: Comparison of sensitivities of several 60 nm AuNP-coated sensors produced under different coating conditions

4.3.6. Stability and Reusability

In order to verify the stability of SPR-based sensors, one fibre coated with 60 nm AuNPs was monitored for 10 days when it was subjected to a solution with a constant RI of 1.333 (water), followed by a RI of 1.375 (n-hexane) for another 10 days. The peak wavelength recorded from the sensor over each of the 10-day periods is shown in Fig. 4.16.

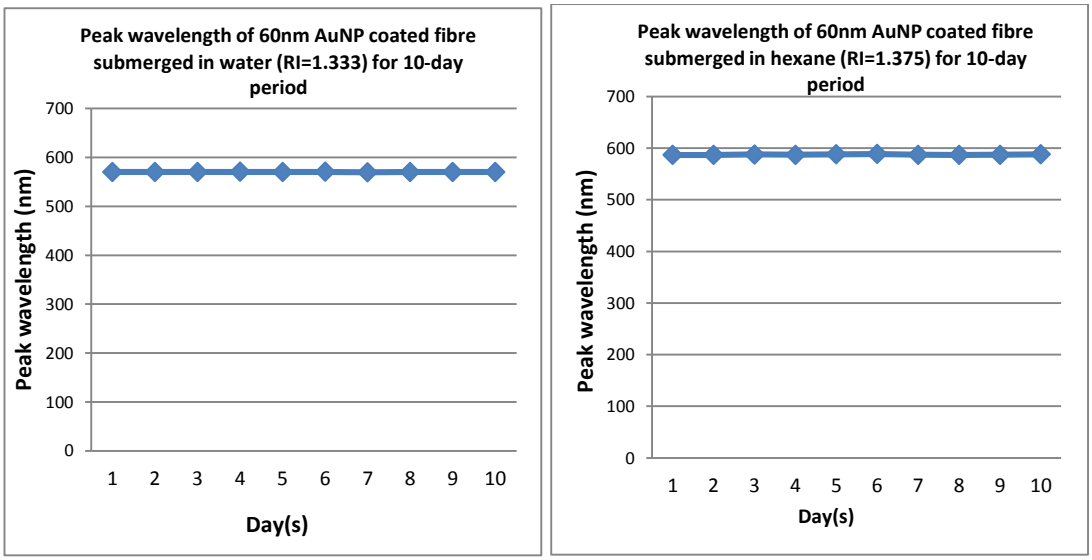

a) in water (RI = 1.333) *b) in n-hexane (RI = 1.375)*

Figure 4.16: Peak wavelength monitoring of a 60nm AuNP coated fibre for a period of 10 days.

a) in water (RI = 1.333) b) in n-hexane (RI = 1.375)

As illustrated in Fig. 4.16, the stability of the sensor has been verified in the tests carried out over a fixed period of time (10 days). The peak wavelength of the sensor has shown to be constant over that test period, showing very little variation (less than 0.1%) when the sensor was exposed to solutions of different RI values.

Reusability of the sensor was also evaluated by subjecting the same sensor to multiple test cycles of tests (cycled over 10 times) when the RI of the test solution was varied from 1.333 to 1.424 where the results obtained are shown in Fig. 4.17, where a good repeatability (and thus reusability) of the sensor has been demonstrated. The largest deviation was observed when the probe was submerged in the solution with a refractive index value of 1.424, with an average peak wavelength of 628.96 nm and a standard deviation of 1.49 nm being observed.

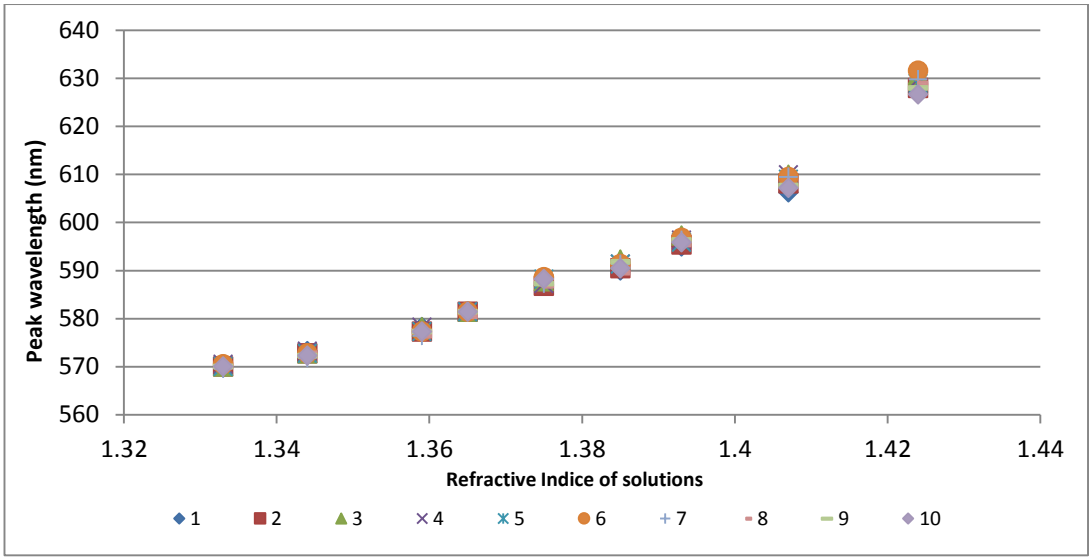

Figure 4.17: Reusability test of the sensor

4.4. Conclusions

This work has presented a systematic approach by giving a careful consideration to key factors affecting their coating process onto optical fibres, in order to optimise the sensitivity of a series of LSPR-based sensors based on AuNPs. As a result the following conclusions can be drawn:

- The increase of the diameter of gold nanospheres leads to a higher sensitivity of the LSPR sensor when it is subjected to refractive index changes in the surrounding environment.

- Changes of pH in the coating AuNPs solution, in the range from 3 to 5, did not significantly affect the coating process and thus the LSPR sensor performance.

- Prior to the absorption saturation being reached, the use of a longer coating time makes the sensor more sensitive to the surrounding environment. This saturation point is different for different AuNP sizes, where the smaller size requires a shorter time for coating on the fibre.

- Temperature can significantly affect the coating process. The systematic research underaken in this work confirms that 25°C is considered to be the optimised coating temperature ensuring both high sensitivity and a wide sensing range. Higher temperatures (30°C and over) were seen to cause

abnormalities in the sensor performance and thus to create a shortened sensing range.

- The sensor has been tested and proven to be repeatible and thus reusable. This has been verified through extensive tests disucssed in this chapter.

This work establishes a solid background for fabricating and characterising an optical fibre sensor coated with metal nanoparticles. Based on this work, a wider exploration is to be undertaken by considering different morphology and metal composition, with an aim to enhance further the sensitivity of LSPR sensors and widen their potential applications and the details will be discussed in the following chapters.

4.5. References

1. Daniel, M.C. and D. Astruc, *Gold Nanoparticles: Assembly, supramolecular chemistry, quantum-size-related properties, and applications toward Biology, Catalysis, and Nanotechnology.* Chemical Reviews 2004. **104**(1): p. 293-346.
2. Turkevich, J., P.C. Stevenson, and J. Hillier, *A study of the nucleation and growth processes in the synthesis of colloidal gold.* Discussions of the Faraday Society, 1951. **11**: p. 55.
3. Hussain, I., S. Graham, Z. Wang, B. Tan, D.C. Sherrington, S.P. Rannard, A.I. Cooper, and M. Brust, *Size-Controlled Synthesis of Near-Monodisperse Gold Nanoparticles in the 1–4 nm Range Using Polymeric Stabilizers.* Journal of The American Chemical Society, 2005. **127**(47): p. 16398-16399.
4. Yee, C.K., R. Jordan, A. Ulman, H. White, A. King, M. Rafailovich, and J. Sokolov, *Novel one-phase synthesis of thiol-fuctionalized gold, palladium, and iridium nanoparticles using superhydride.* Langmuir, 1999. **15**(10): p. 3486-3491.
5. Brust, M., M. Walker, D. Bethell, D.J. Schiffrin, and R. Whyman, *Synthesis Of Thiol-derivatized Gold Nanoparticles In A 2-phase Liquid-Liquid System.* Journal of the Chemical Society-Chemical Communications, 1994(7): p. 801-802.
6. Sakai, T., H. Enomoto, K. Torigoe, H. Sakai, and M. Abe, *Surfactant- and reducer-free synthesis of gold nanoparticles in aqueous solutions.* Colloids and Surfaces A: Physicochemical and Engineering Aspects, 2009. **347**(1-3): p. 18-26.
7. Shervani, Z. and Y. Yamamoto, *Size and morphology controlled synthesis of gold nanoparticles in green solvent: Effect of reducing agents.* Materials Letters, 2011. **65**(1): p. 92-95.
8. Philip, D., *Green synthesis of gold and silver nanoparticles using Hibiscus rosa sinensis.* Physica E: Low-dimensional Systems and Nanostructures, 2010. **42**(5): p. 1417-1424.
9. Huang, X., H. Wu, X. Liao, and B. Shi, *One-step, size-controlled synthesis of gold nanoparticles at room temperature using plant tannin.* Green Chemistry, 2010. **12**(3): p. 395.
10. Walker, C.H., J.V. St John, and P. Wisian-Neilson, *Synthesis and Size Control of Gold Nanoparticles Stabilized by Poly(methylphenylphosphazene).* Journal of The American Chemical Society, 2001. **123**(16): p. 3846-3847.
11. Esparza, R., G. Rosas, M. Lopezfuentes, J. Sanchezramirez, U. Pal, J. Ascencio, and R. Perez, *Synthesis of gold nanoparticles with different atomistic structural characteristics.* Materials Characterization, 2007. **58**(8-9): p. 694-700.
12. Mandal, S., S.K. Arumugam, S.D. Adyanthaya, R. Pasricha, and M. Sastry, *Use of aqueous foams for the synthesis of gold nanoparticles of variable morphology.* Journal of Materials Chemistry, 2004. **14**(1): p. 43.
13. Bhargava, S.K., J.M. Booth, S. Agrawal, P. Coloe, and G. Kar, *Gold nanoparticle formation during bromoaurate reduction by amino acids.* Langmuir, 2005. **21**(13): p. 5949-5956.
14. Zhu, H., Z. Pan, E. Hagaman, C. Liang, S. Overbury, and S. Dai, *Facile one-pot synthesis of gold nanoparticles stabilized with bifunctional amino/siloxy ligands.* Journal of Colloid and Interface Science, 2005. **287**(1): p. 360-365.
15. Schulz-Dobrick, M., K.V. Sarathy, and M. Jansen, *Surfactant-Free Synthesis and Functionalization of Gold Nanoparticles.* Journal of The American Chemical Society, 2005. **127**(37): p. 12816-12817.

16. Slocik, J.M., M.O. Stone, and R.R. Naik, *Synthesis of Gold Nanoparticles Using Multifunctional Peptides.* Small, 2005. **1**(11): p. 1048-1052.
17. Liu, Q., H. Liu, Q. Zhou, Y. Liang, G. Yin, and Z. Xu, *Synthesis of nearly monodispersive gold nanoparticles by a sodium diphenylamine sulfonate reduction process.* Journal of Materials Science, 2006. **41**(12): p. 3657-3662.
18. Frenkel, A.I., S. Nemzer, I. Pister, L. Soussan, T. Harris, Y. Sun, and M.H. Rafailovich, *Size-controlled synthesis and characterization of thiol-stabilized gold nanoparticles.* The Journal of Chemical Physics, 2005. **123**(18): p. 184701.
19. Chen, W., W.P. Cai, C.H. Liang, and L.D. Zhang, *Synthesis of gold nanoparticles dispersed within pores of mesoporous silica induced by ultrasonic irradiation and its characterization.* Materials Research Bulletin, 2001. **36**(1-2): p. 335-342
20. Okitsu, K., M. Ashokkumar, and F. Grieser, *Sonochemical Synthesis of Gold Nanoparticles: Effects of Ultrasound Frequency.* Journal of Physical Chemistry B 2005. **109**(44): p. 20673-20675.
21. Sau, T.K., A. Pal, N.R. Jana, Z.L. Wang, and T. Pal, *Size controlled synthesis of gold nanoparticles using photochemically prepared seed particles.* Journal of Nanoparticle Research 2001. **3**(4): p. 257-261
22. Kim, J.U., S.H. Cha, K. Shin, J. J.Y., and J.C. Lee, *Synthesis of Gold Nanoparticles from Gold(I)–Alkanethiolate Complexes with Supramolecular Structures through Electron Beam Irradiation in TEM.* Journal of The American Chemical Society, 2005. **127**(28): p. 9962-9963.
23. Abyaneh, M.K., D. Paramanik, S. Varma, S.W. Gosavi, and S.K. Kulkarni, *Formation of gold nanoparticles in polymethylmethacrylate by UV irradiation.* Journal of Physics D: Applied Physics, 2007. **40**(12): p. 3771-3779.
24. Yu, C.-C., Y.-C. Liu, K.-H. Yang, C.-C. Li, and C.-C. Wang, *A new and clean method on synthesis of gold nanoparticles from bulk gold substrates.* Materials Chemistry and Physics, 2011. **125**(1-2): p. 109-112.
25. Wang, L., T. Li, Y. Du, C. Chen, B. Li, M. Zhou, and S. Dong, *Au NPs-enhanced surface plasmon resonance for sensitive detection of mercury(II) ions.* Biosensors and Bioelectronics, 2010. **25**(12): p. 2622-2626.
26. Hall, W.P., S.N. Ngatia, and R.P. Van Duyne, *LSPR Biosensor Signal Enhancement Using Nanoparticle–Antibody Conjugates.* The Journal of Physical Chemistry C, 2011: p. 110110114445084.
27. Velasco-Garcia, M.N., *Optical biosensors for probing at the cellular level: A review of recent progress and future prospects.* Seminars in Cell & Developmental Biology, 2009. **20**(1): p. 27-33.
28. Silva, L.I.B., F.D.P. Ferreira, A.C. Freitas, T.A.P. Rocha-Santos, and A.C. Duarte, *Optical fiber biosensor coupled to chromatographic separation for screening of dopamine, norepinephrine and epinephrine in human urine and plasma.* Talanta, 2009. **80**(2): p. 853-857.
29. Vogel, N., M. Jung, N.L. Bocchio, M. Retsch, M. Kreiter, and I. KÃ¶per, *Reusable Localized Surface Plasmon Sensors Based on Ultrastable Nanostructures.* Small, 2010. **6**(1): p. 104-109.
30. Shao, Y., S. Xu, X. Zheng, Y. Wang, and W. Xu, *Optical Fiber LSPR Biosensor Prepared by Gold Nanoparticle Assembly on Polyelectrolyte Multilayer.* Sensors, 2010. **10**(4): p. 3585-3596.
31. Mustafa, D.E., T. Yang, Z. Xuan, S. Chen, H. Tu, and A. Zhang, *Surface Plasmon Coupling Effect of Gold Nanoparticles with Different Shape and Size on Conventional Surface Plasmon Resonance Signal.* Plasmonics, 2010. **5**(3): p. 221-231.

32. Fu, J. and Y. Zhao, *Au nanoparticle based localized surface plasmon resonance substrates fabricated by dynamic shadowing growth.* Nanotechnology, 2010. **21**(17): p. 175303.
33. Valadez, A.M., C.A. Lana, S.-I. Tu, M.T. Morgan, and A.K. Bhunia, *Evanescent Wave Fiber Optic Biosensor for Salmonella Detection in Food.* Sensors, 2009. **9**(7): p. 5810-5824.
34. Premachandran, C.S., A. Khairyanto, K.C.W. Sheng, J. Singh, J. Teo, Y.S. Xu, N.G. Chen, C. Sheppard, and M. Olivo, *Design, Fabrication, and Assembly of an Optical Biosensor Probe Package for OCT (Optical Coherence Tomography) Application.* Ieee Transactions on Advanced Packaging, 2009. **32**(2): p. 417-422.
35. Liu, F.-K., *Analysis and applications of nanoparticles in the separation sciences: A case of gold nanoparticles.* Journal of Chromatography A, 2009. **1216**(52): p. 9034-9047.
36. Chen, H., X. Kou, Z. Yang, W. Ni, and J. Wang, *Shape- and Size-Dependent Refractive Index Sensitivity of Gold Nanoparticles.* Langmuir, 2008. **24**(10): p. 5233-5237.
37. Sharma, V., K. Park, and M. Srinivasarao, *Colloidal dispersion of gold nanorods: Historical background, optical properties, seed-mediated synthesis, shape separation and self-assembly.* Materials Science and Engineering: R: Reports, 2009. **65**(1–3): p. 1-38.
38. Afshar, R., *Gold nanorods: synthesis and self-assembly*. 2007.
39. Hu, X.G., W.L. Cheng, T. Wang, E.K. Wang, and S.J. Dong, *Well-ordered end-to-end linkage of gold nanorods.* Nanotechnology, 2005. **16**(10): p. 2164-2169.
40. Cheng, S.F. and L.K. Chau, *Colloidal Gold-Modified Optical Fiber for Chemical and Biochemical Sensing.* Analytical Chemistry, 2003. **75**(1): p. 16-21.
41. Lee, H., H.-J. Kim, J.-H. Park, D.H. Jeong, and S.-K. Lee, *Effects of surface density and size of gold nanoparticles in a fiber-optic localized surface plasmon resonance sensor and its application to peptide detection.* Measurement Science and Technology, 2010. **21**(8): p. 085805.
42. Wang, Y., J. Deng, J. Di, and Y. Tu, *Electrodeposition of large size gold nanoparticles on indium tin oxide glass and application as refractive index sensor.* Electrochemistry Communications, 2009. **11**(5): p. 1034-1037.
43. Sharma, A. and B. Gupta, *On the sensitivity and signal to noise ratio of a step-index fiber optic surface plasmon resonance sensor with bimetallic layers.* Optics Communications, 2005. **245**(1-6): p. 159-169.

Gold nanoparticle- and gold nanorod-based optical fibre probes: Evaluation, Comparison and Applications

5.1. Introduction

Localised surface plasmon resonance (LSPR) has been explored as an effective tool for sensory applications with details having been discussed and analysed extensively, both theoretically and experimentally in previous chapters. In Chapter 4, key factors and conditions for the enhancement of sensitivities of the LSPR-based optical fibre sensors were investigated and optimal settings were proposed based on the experimental data obtained. The conclusion was made based on the performance of LSPR sensors coated with gold nanoparticles with spherical shapes (AuNPs). It was also indicated in Chapter 3, based on the theoretical calculations and simulation results, that there is a possibility to achieve a higher sensitivity using other shapes, such as nanorod (AuNR), nanorice [1], nanocube [2] or nanostar [3]. The shape, size and composition of the nanoparticles contribute mostly towards their LSPR absorbance and scattering spectra [4], thus could also affect their sensory performance.

Compared to the other metal, gold is one of the most desirable metals for the preparation of label-free biosensors as gold demonstrates better affinity with biomolecules and resistance to oxidisation [5]. Gold nanorods could be seen as an elongated nanosphere, where the length and the width of the particle could be varied (Fig. 5.1). The ratio between the length and the width is called aspect ratio R. In the theoretical calculation (as shown in Chapter 2), the value R would be critical in the determination of the LSPR absorbance spectrum of the particle [6, 7]. When an AuNR interacts with polarised light, it would exhibit two possible oscillations thus create two bands in its LSPR absorbance spectrum due to its shape, which are named

transverse and longitudinal plasmon wavelength (TPW and LPW, respectively). The transverse oscillation occurs perpendicularly to the length of the particle while the longitudinal one appears along the particle's length. Therefore, in particles with different aspect ratio but with similar width, the transverse plasmon peaks were positioned at the same place in the absorbance spectra, while the longitudinal peaks' positions were different with different aspect ratio [8]. Particles with higher aspect ratio would have their absorbance spectra more shifted to the red [9]. As suggested by Miller *et al.* [10], the higher position of the absorbance's peak would presumably lead to a higher sensitivity in RI sensing. Hence, gold nanorod should provide better performance in term of sensing than that of gold nanoparticle.

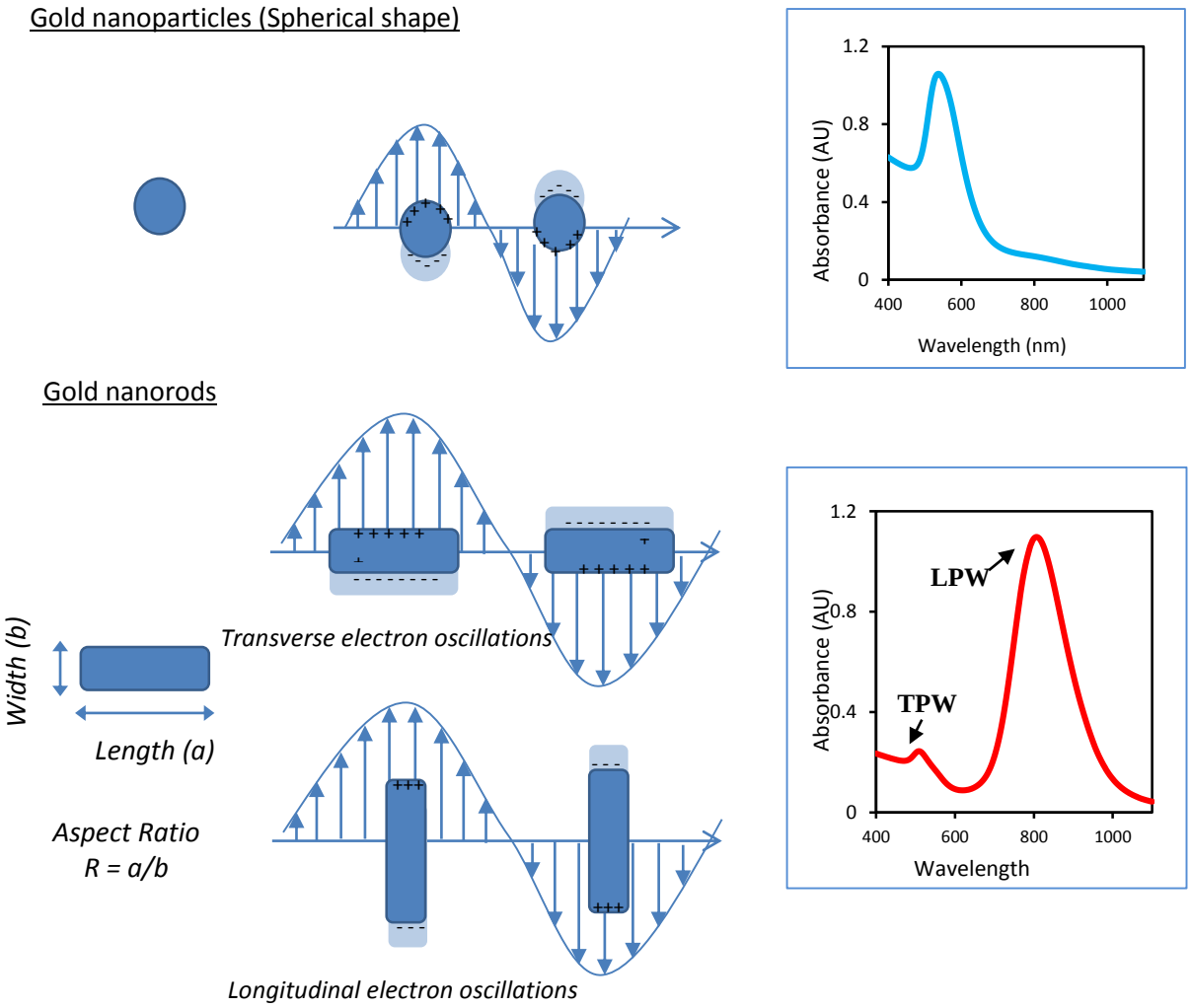

Figure 5.1: Excitation in AuNP and AuNR.
From left to right: Illustration of the particles, their excitation states and their corresponding exhibit absorption.

The previously reported Refractive Index (RI) sensing using LSPR sensors was often carried by measuring the change in absorbance at a peak wavelength when the probe was submerged in different RI solutions. In bio-applications, intensity measurement is widely considered rather than the peak wavelength shift [11-16]. This is because the change in peak wavelength induced by the bio-interaction at the surface of the reported sensors was too small to be detected by the probe. In other words, the resolution of the probe in term of wavelength shift was not high enough for bio-detection, compared to that based on the intensity measurement. The intensity-based technique, however, suffers from the interference from the surrounding environment, such as light conditions or varying temperatures. Therefore, improving the sensitivity of the wavelength-based technique could offer the bio-sensors better performance due to their intrinsic insensitivity to the surrounding environment.

In previous chapters discussions were made to improve the sensor performance by considering optimised conditions, including pH condition, coating time, coating temperature and the size of the particles with an aim to achieve a higher sensitivity in RI sensing with GNPs-based optical fibre sensors. Cao *et al.* [8] in the same research group at City University London reported that LSPR sensors coated with gold nanorods (AuNRs) with a higher aspect ratio offer higher sensitivity. Therefore, this Chapter focused on the cross-comparison of two types of LSPR sensor systems using two different nanomaterials, AuNP and AuNR, with each being in its respective optimised conditions discussed respectively in Chapter 4 and in [8]. To do so, a set of LSPR sensors is fabricated using a common technique [17-19] and in order to facilitate antibody-antigen interaction, surface modification of the AuNP and AuNR coated optical fibres has been implemented in order to obtain label-free sensors. The prepared fibres would be first coated with AuNP and AuNR via silanised linkers, and subsequently be coated with human antibody IgG via NHS/EDC linker. Upon the binding with free antigen anti-IgG, the change in absorbance spectrum of the probe would indicate the concentration of the target solution.

5.2. Experimental Setup

5.2.1. Materials

Gold (III) chloride trihydrate ($HAuCl_4 \cdot 3H_2O$), sodium citrate, ascorbic acid, silver nitrate ($AgNO_3$), cetyltrimethylammonium bromide (CTAB), sodium borohydride ($NaBH_4$), sodium citrate tribasic dehydrate ($Na_3C_6H_5O_7$), 3-aminopropyl trimethoxysilane 97% (APTMS), 3-Mercaptopropyltrimethoxysilane (MPTMS), potassium hydroxide (KOH), tin (II) chloride dehydrate, dextrose, human IgG (purified immunoglobulin, reagent grade), anti-human IgG (whole molecule, produced in goat), 11-Mercaptoundecanoic acid (MUA), bovine serum albumin (BSA), N-(3-Dimethylaminopropyl)-N'-ethylcarbodiimide hydrochloride (EDC) and *N*-hydroxysulfosuccinimide (Sulfo-NHS) were purchased from Sigma Aldrich.

Ultrapure de-ionized (DI) water (18 MΩ) was used to prepare all solutions. All chemicals and reagents were of analytical grade and used as received. All procedures were conducted at room temperature unless specified otherwise. Multimode optical fibres of diameter 600 µm and NA=0.37 were purchased from Thorlabs.

5.2.2. Synthesis of AuNPs and AuNRs and their characterisation

AuNPs with a mean diameter of 60 nm and AuNRs with a mean aspect ratio about 4.1 were chosen based on the optimisation results obtained by the author and discussed in Chapter 4 and by Cao et al [8]. This forms the basis of this work for cross-comparison of their refractive index sensitivities using the methods reported previously [20, 21]. In brief, 60 nm AuNPs solution was prepared by citrate reduction method [22], and the ratio between precursor $HAuCl_4$ and sodium citrate has been pre-calculated to achieve the desirable size. In a typical synthesis, 5 mg of $HAuCl_4 \cdot 3H_2O$ was dissolved in 50 mL DI water and heated until boiling. 300 µL of 1% sodium citrate tribasic dehydrate solution was then rapidly added, resulting in an immediate colour change from nearly colourless to dark-green. The colour was then slowly changed to red/purple, and the mixture was heated for a further 10 minutes before the heat source was removed. This was followed by stirring the solution for a further 15 minutes in order to stabilise the particle size distribution.

In order to achieve AuNR, a common seed-mediated technique has been employed to reach high yield and monodispersity, reported by Nikoobakht *et al.* [23], with a slight modification. The technique involves two steps: firstly, to create a seed solution of gold spherical nanoparticles with a very small size (less than 4nm in diameter) and secondly, to grow the as-prepared seeds into nanorods with desirable aspect ratio. The seeds were prepared by reducing 5 mL of $HAuCl_4$ 0.5 mM using a strong reduction agent $NaBH_4$ (600 µL of $NaBH_4$ 0.01M) in the presence of protective agent CTAB (5 mL of CTAB 0.2 M). Afterwards, the solution was aged for 3 hours in room temperature and then 100 µL of this seed solution was added into the growing solution, containing surfactant (30 mL of CTAB 0.2 M), growing material (30 mL of $HAuCl_4$ 1 mM), catalyst (310 µL of $AgNO_3$ 0.02 M) and a mild reducing agent (420 µL of ascorbic acid 0.0788 M). The growing period lasted for 24 hours at a constant 30 ^oC and then the mixture was subjected to a series of centrifugation and washing in order to remove the excess CTAB.

An accurate measurement of the mean diameter and the aspect ratio of the AuNPs and AuNRs synthesised was undertaken by using a JEOL 1010 transmission electron microscope (TEM). The TEM samples were prepared by placing 2 µL of diluted AuNPs or AuNRs solutions on a 3 mm 400-mesh Formvar coated copper grid (purchased from Agar Scientific) and evaporating the solution at room temperature. Fig. 5.2 (a) and (b) show the TEM images of the as-synthesised AuNPs and AuNRs respectively.

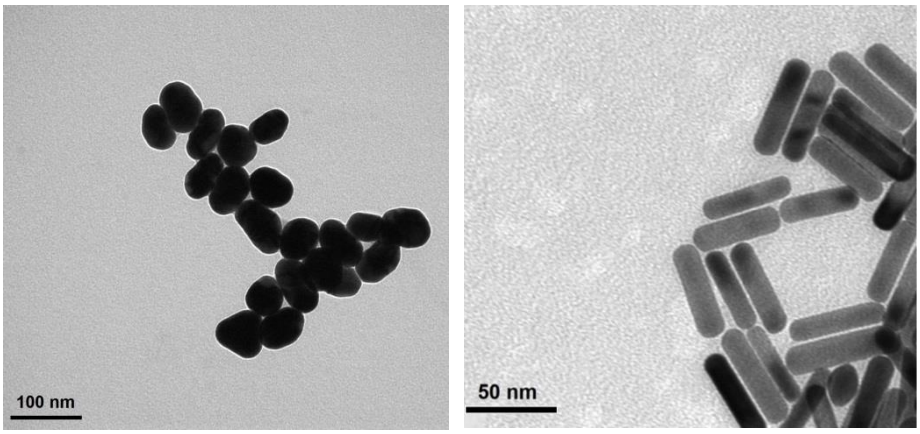

(a) (b)

Figure 5.2: TEM images of (a) 60nm AuNPs and (b) AuNRs with aspect ratio 4.1.

5.2.3. Preparation of LSPR sensor probes

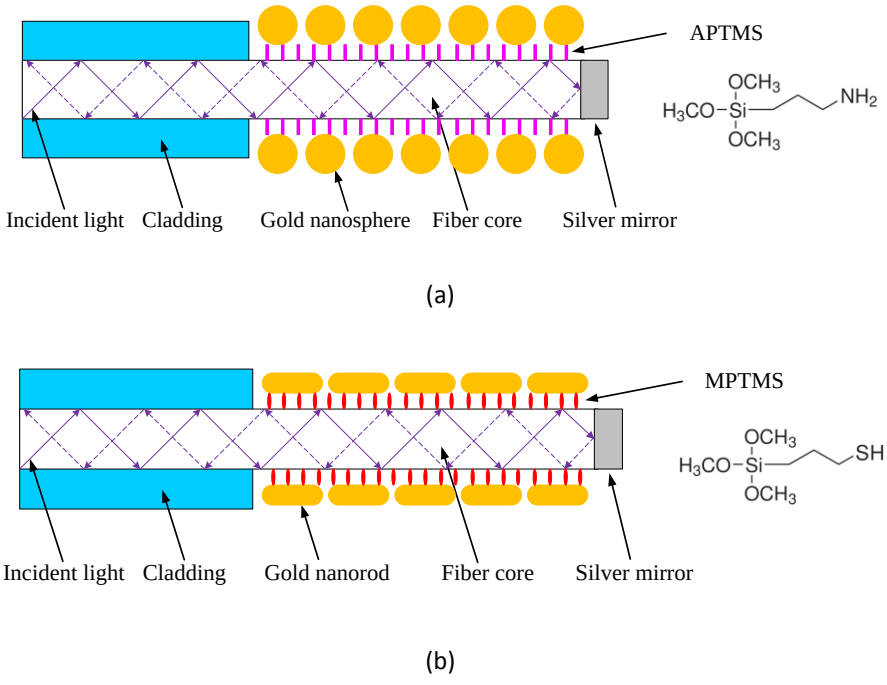

Figure 5.3: Schematic diagrams of the structure of (a) AuNPs-coated and (b) AuNRs-coated optical fibre sensor probes.

Fig. 5.3 (a) and (b) demonstrate the schematic diagrams of the AuNPs- and AuNRs-based LSPR sensor probes prepared in this work respectively. The preparation of the fibres for coating was described earlier in previous chapters, with only a slight modification for different materials.

AuNPs were immobilised on the surface of the fibre core via electrostatic interaction. As-synthesised AuNPs were gold spherical nanoparticles covered with negatively charged citrate ion. The surface of the fibre core, after being exposed with H_2SO_4/H_2O_2 mixture, had free hydroxyl (-OH) groups. Afterwards, this probe was coated with an organosilanised agent (APTMS), which has been chosen as a linker for the coating of AuNPs, using a dip-coating technique. APTMS has amino groups which were positive charged and could act as a suitable platform for the formation of a uniform self-assembled monolayer (SAM) of the negatively charged AuNPs.

On the other hand, as-prepared AuNRs were coated with a layer of CTAB molecules, which was also positively charged. Therefore, the repulsive force between the same charged molecules prevents the formation of a successful coating if using APTMS for

AuNRs. Instead of that, 3-mercaptopropyltrimethoxysilan (MPTMS), another organosilanised agent with sulfhydryl (-SH) terminate was used. The thiol group in MPTMS was negatively charged, therefore more suitable for AuNRs coating. In addition, the formation of strong Au-S covalent bonds helped to create a stable and uniform monolayer [24-27].

Finally, in order to create a reflective sensor, the above-prepared probes (both with AuNPs and AuNRs) were coated with a silver mirror at the end surface of the fibre. The process involves the use of Tollen's reagent to initiate a reaction, i.e. reducing a silver complex created by mixing a solution of $AgNO_3$ with NH_3, to form a thin layer of silver mirror (Ag atoms) at the end surface of the probe by a mild reducing agent, dextrose. The fabricated probes were photographed and shown in Fig. 5.4.

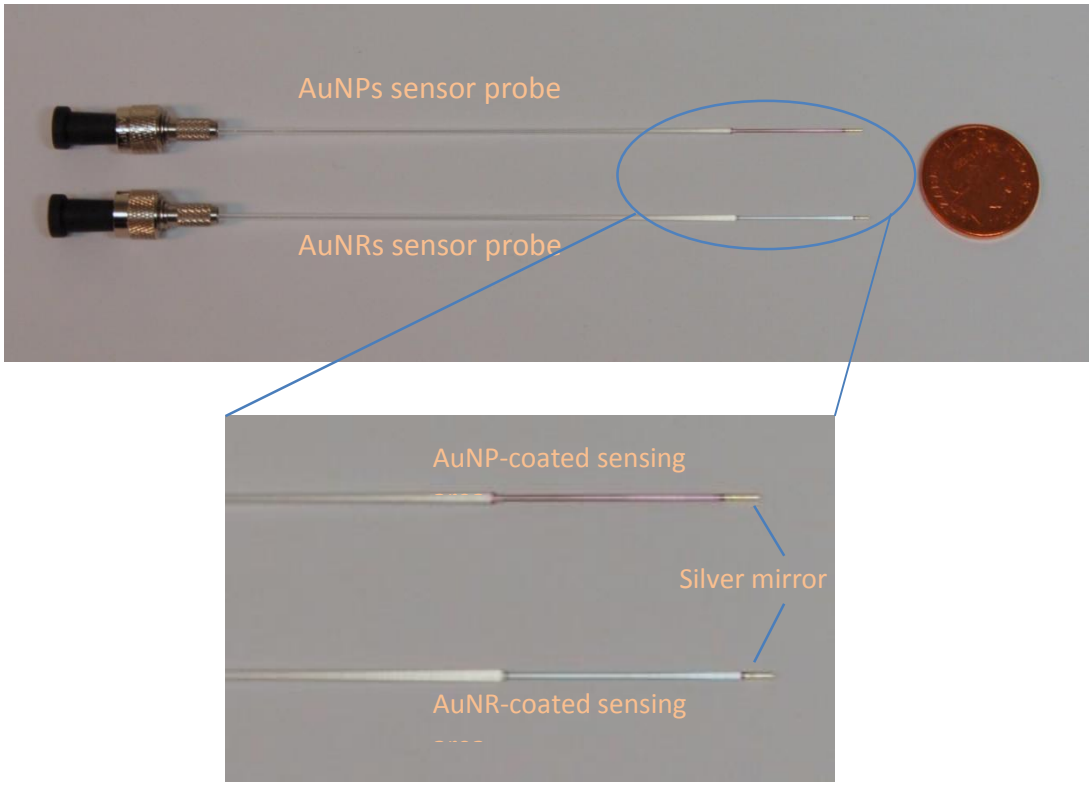

Figure 5.4: Photographs showing the AuNP- and AuNR- coated sensor probes developed in this work.

5.2.4. Functionalisation of LSPR sensor probes

In order to demonstrate the capacity of the prepared probes in biosensing area, AuNP- and AuNR-coated fibres were further functionalised for antigen detection and in this particular case, the detection of anti-human IgG. The functionalisation process

was illustrated in Fig. 5.5 and described as follows. Firstly, the gold nanomaterial coated probes were immersed in a solution of MUA in ethanol to form carboxyl groups on the surface of gold nanomaterials. This carboxyl groups acted as the anchors for the immobilisation of the human antibody IgG via Carbodiimide crosslinker reaction between carboxyl group and EDC and NHS [28, 29]. Furthermore, the probe was treated with bovine serum albumin (BSA) to block the sensing surface from nonspecific absorption. More details of the preparation process could be found in the published work by Cao *et al.* [20].

Upon binding, the interaction between antigen (the anti-human IgG in the solution) and antibody (the human IgG immobilised on the probe) thus created a local refractive index change, from which the modulated signal could be detected via LSPR effect.

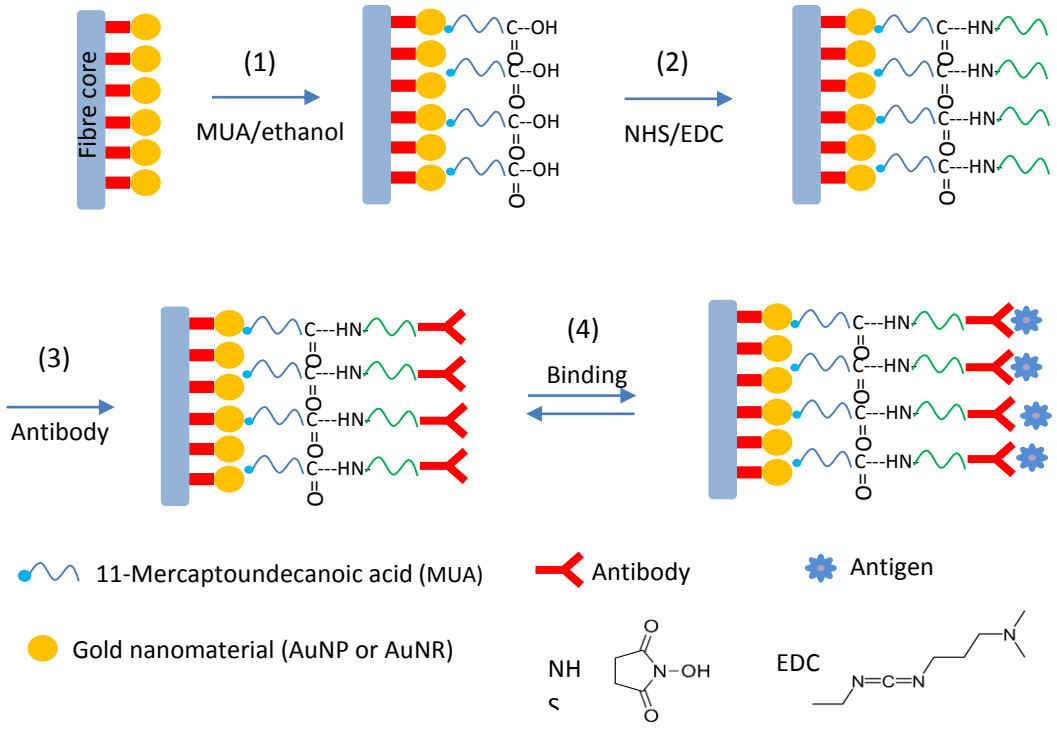

Figure 5.5: Schematics of bio-sensing approaches using AuNP- or AuNR- based LSPR sensors.

5.2.5. Experimental setup

The experimental set-up used for the evaluation of LSPR sensor performance in this work is similar to that described in Chapter 4 and is shown in Fig. 5.6. As illustrated, the sensor probe was connected to one end of a 1x2 fibre coupler, in which the incident light is launched from a white light source. The interaction between the sensor probe and the test solution is able to modulate the incident light, which is then reflected and captured by a mini-spectrometer (Ocean Optics Maya 2000pro), connected to the other end of the coupler. Thus the signals obtained could be displayed and monitored by a computer connected to the mini-spectrometer.

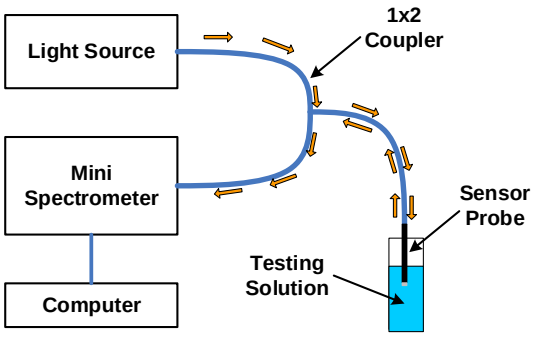

Figure 5.6: Schematic diagram of a typical LSPR sensor system.

5.3. Results and discussions

5.3.1. Preparation of the LSPR sensor probes

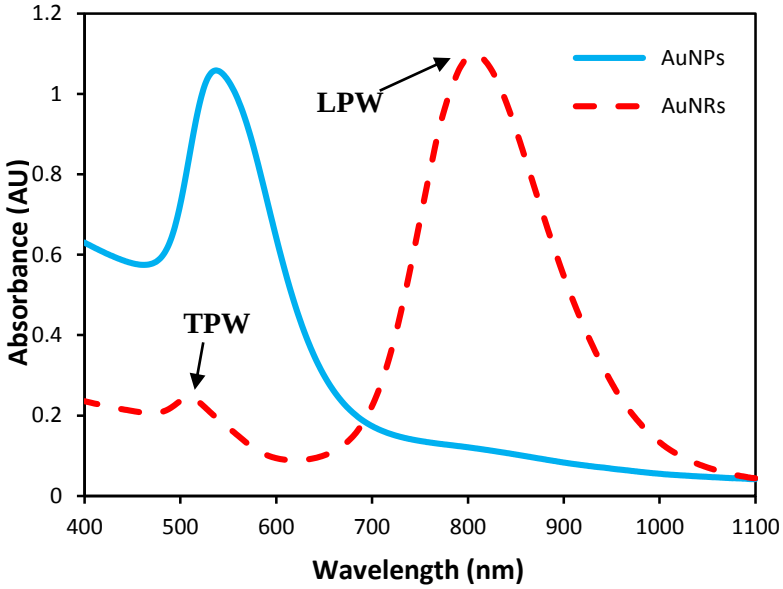

Figure 5.7: Absorption spectra of a 60 nm AuNPs solution and a AuNRs solution with an aspect ratio of 4.1.

The absorption spectra of AuNP and AuNR solutions in this work were illustrated in Fig. 5.7. In the spectrum of AuNPs, only one peak appeared at ~560nm and this confirmed the successful preparation. On the other hand, the spectrum of AuNRs shows two plasmon bands, one was at 510nm and the other was at 810nm. These bands appeared due to the resonance between the incoming light and the transverse and longitudinal electron oscillation, respectively (called transverse plasmon wavelength and longitudinal plasmon wavelength, TPW and LPW, as seen in Fig. 5.7). It was also noted that, while the synthesis of AuNP was simple and straightforward, the preparation of AuNR required more effort and precise control of the synthesis conditions, such as temperature [30-32], aging period, pH condition [33] or seed amount to achieve consistent results [34-36].

5.3.2. Sensitivity to surrounding refractive index change

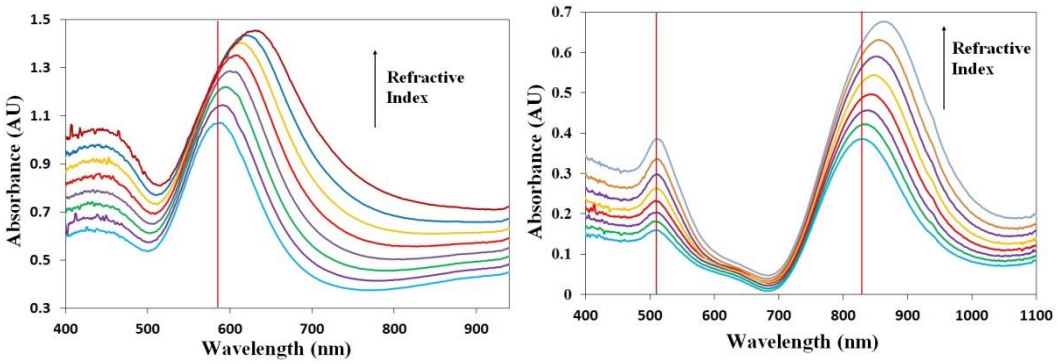

(a) (b)

Figure 5.8: Absorbance spectra of (a) 60 nm AuNP-based LSPR sensor, (b) AuNR-based LSPR sensor with an aspect ratio of 4.1, both showing an increase with the increase of the refractive index of the testing solutions.

Different refractive index solutions, from 1.330 to 1.400, with an increment step of 0.010 have been prepared by mixing methanol, ethanol, toluene in different ratios, and their refractive indices were further confirmed by a refractometer. RI sensitivity test was carried out using both probes, and the sensitivities were calculated using Eq. 5.1 as shown below, where S is the calculated sensitivity, λ_{max} is the peak wavelength and n is the refractive index of the solution.

$$S = \frac{d\lambda_{max}}{dn} \qquad \text{(Eq. 5.1)}$$

As illustrated in Fig. 5.8, the absorption peaks of both AuNP- and AuNR-coated probes were shifted to red in the spectrum with the increase of the refractive index of the surrounding medium. In the particular spectra of AuNR, both its two peaks, TPW and LPW, had increased in intensity, but only LPW peak has shown a noticeable and quantifiable peak shift (Fig. 5.8b). Therefore, the peak shift of the resonance wavelength of AuNP and the LPW of AuNR in different RI solutions could be chosen for quantitative calculations.

In addition to the above test, different probes with different sensing length were prepared in order to investigate an optimised length for sensing. Three lengths have been chosen, 0.5 cm, 1 cm and 2 cm, and for each length and each material (AuNP and AuNR), 7 probes were prepared to ensure the repetition of the data. The sensitivities were calculated using Eq. 5.1 and plotted in Fig. 5.9. The highest

sensitivity AuNP-coated probe achieved was the one with 2 cm sensing length, and it was 914 nm/RIU. Similar trend was observed with AuNR, and a 2 cm sensing length probe of AuNR (with aspect ratio 4.1) has a sensitivity of 601 nm/RIU. In this test, the RI sensitivity of both AuNP- and AuNR- based sensors increases with the increase of sensing length. It could be explained by the fact that, the sensor with a longer length promotes more interactions between light and the nanoparticles coated on the surface of the fibre core. This was also confirmed in a report by Chau *et al.* [37]. Although a longer length could lead to a higher sensitivity of the probe, longer than 2 cm could lead to the difficulty in probe handling and preparation. Moreover, a longer sensing length could introduce more light loss, thus resulting in poor signal-to-noise ratio. In this work, a sensing length of 2 was chosen for the preparation of both AuNP- and AuNR- based bio-sensors.

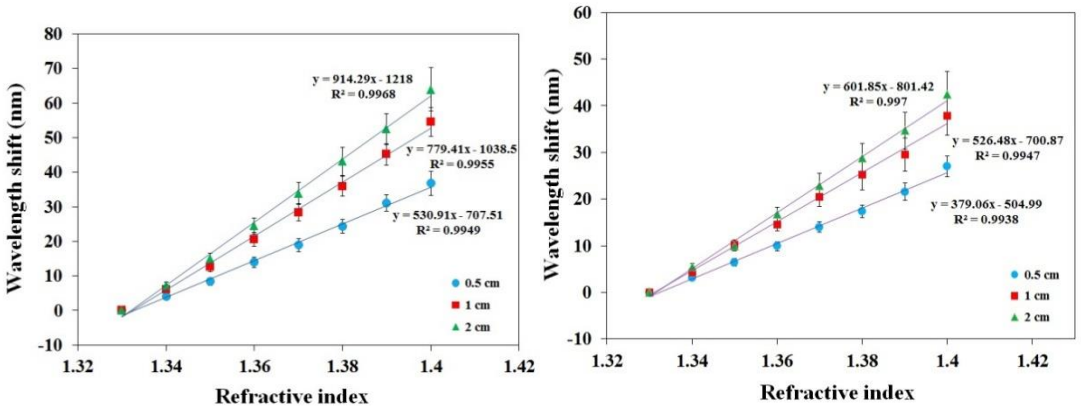

(a) (b)

Figure 5.9: RI sensitivities of (a) AuNP-based sensors and (b) AuNR-based sensors with different sensing length.

5.3.3. Stability of the sensor probe

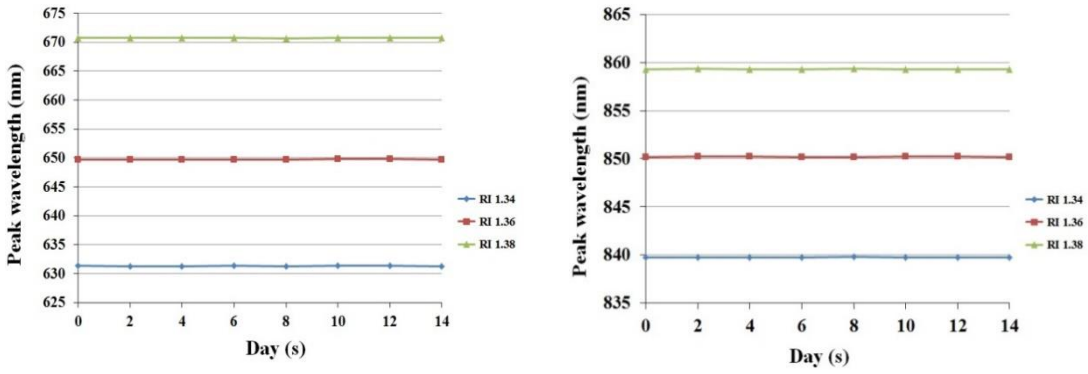

Figure 5.10: Peak wavelength monitoring of (a) AuNP-based sensor and (b) AuNR-based sensor subjected in solutions with different refractive indexes for a period of two weeks.

The stability of the LSPR sensors has been verified by testing repetitively the prepared probes in different RI solutions for a period of two weeks. Each measurement was taken every two days and in the solutions with refractive index of 1.340, 1.360 and 1.380 respectively. In between, the probes were kept in a DI water solution at room temperature. As shown in Fig. 5.10, both types of LSPR sensors (AuNP-coated and AuNR-coated) were found to be stable for at least two week time. Only very small variations (less than 0.05 nm) in the peak wavelengths have been observed and this proved the stability of the fabricated sensors over the testing period.

5.3.4. Biosensor applications

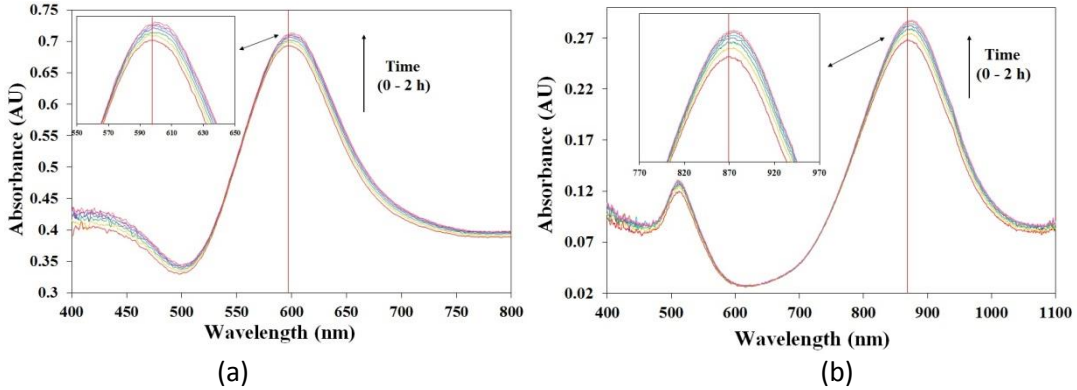

Figure 5.11: Monitoring the process of anti-human IgG binding to human IgG immobilised on (a) AuNPs-based and (b) AuNRs-based LSPR biosensors over a period of 2 hours.

Antibody-antigen interaction was chosen in this experiment for the demonstration of biosensing application due to its ease in fabrication, high stability and strong

interaction. EDC/NHS technique [17] has been used for the immobilisation of the antibody (human IgG) onto the metallic coated probes (for both AuNP and AuNR), as described earlier in Fig. 5.5.

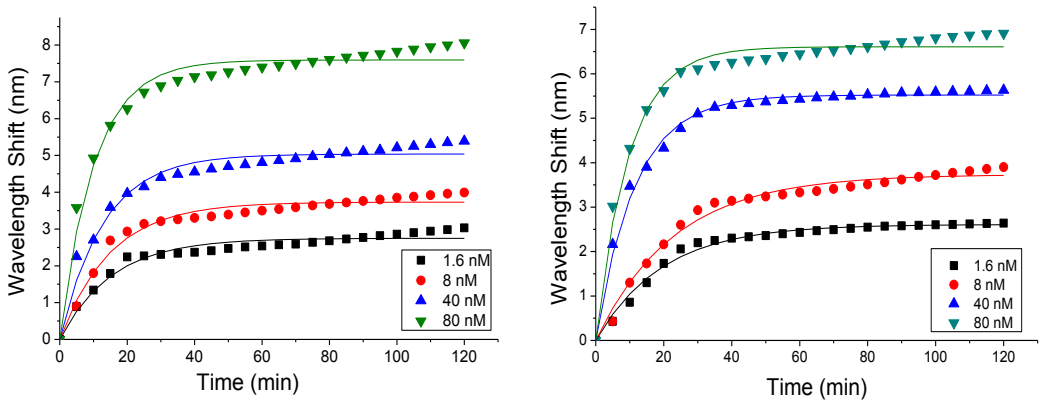

Figure 5.12: (a) Peak wavelength shift of AuNP-based LSPR biosensor and (b) LPW peak wavelength shift of AuNR-based LSPR biosensor as a function of the incubation time at different concentrations of anti-human IgG. The corresponding coloured lines are the mathematically fitted curves with each data set.

The kinetics of the binding between antigen and antibody has been studied in this work, based on the experimental data obtained and shown in Fig. 5.11 and Fig. 5.12. Before the binding, a final probe (a probe which has been functionalised with antibody) was immersed in PBS solution with pH 7.4 until a stable spectrum was recognised and recorded. Subsequently, this probe was immersed in solutions with different concentrations of the corresponding antigen. The spectrum was recorded every 5 min within a period of 2 hours. As seen in Fig. 5.11, as soon as the binding took place, the spectrum of the probe has shown a slow increase of the peak absorbance and a peak wavelength shift to the red, in both AuNP-based and AuNR-based probes. The data of the peak resonance wavelengths (in case of AuNP-based probe) and the LPW peaks (in case of AuNR-based probe) were presented in Fig. 5.12. When free antigens in the solution bound to the surface via antibody-antigen interaction, they would induce a change in the local refractive index at a very close distance to the probe. Thus, this change in refractive index could be picked up by LSPR effect via gold nanoparticles and represented by the red shift in the peak wavelength or the LPW peak. In the first 30 min in both AuNP and AuNR cases, the shift of the wavelength was approximately linearly proportional to the reaction time.

After that, the rate of the binding was seen to gradually slow down, as the binding sites on the sensing region were gradually filled up. After 2 hours, saturation was reached. In this test, different sensor probes were incubated in the anti-human IgG solution at concentrations of 1.6 nM, 8 nM, 40 nM and 80 nM for 2 hours.

Antibody-antigen interaction could be represented by equation Eq. 5.2, with *Ab* stands for antibody (the human IgG) and *Ag* stands for antigen (the anti-human IgG).

$$Ab + Ag \rightleftarrows Ab{:}Ag \qquad \text{(Eq. 5.2)}$$

While the antibody was immobilised on the fibre, the rate of binding would be entirely dependent on the concentration of the antigen, therefore, a first order kinetics of the reaction could be applied and descried in Eq. 5.2 and Eq. 5.3, where R is the rate of the binding interaction, k is the rate constant, [Ag] is the concentration of the antigen at the time t, $[Ag]_0$ is the initial concentration of the antigen [38, 39]:

$$R = -\frac{d[Ag]}{dt} = k\,[Ag] \qquad \text{(Eq. 5.3)}$$

Therefore, we could have

$$[Ag] = [Ag]_o\, e^{-kt} \qquad \text{(Eq. 5.4)}$$

In the previous refractive index sensitivity test, it was assumed that, the refractive index of the surrounding medium and the shift of the resonance wavelength were linearly related, and, that the refractive index of the surrounding medium was governed by the amount of antigen attached to the antibody coated on the fibre surface.

Therefore,

$$WShift = \gamma = C \cdot ([Ag]_0 - [Ag]) \qquad \text{(Eq. 5.5)}$$

Wshift or γ is the wavelength shift value, and C is a constant which represents the linear relationship between the wavelength shift and the concentration of the antigen.

And γ can also be expressed as

$$\gamma = C \cdot ([Ag]_0 - [Ag]_0 e^{-kt}) = C \cdot [Ag]_0 (1 - e^{-kt}) \quad \text{(Eq. 5.6)}$$

Equation 5.6 describes the kinetics of the reaction which depends on the initial concentration of the antigen, and the experimental data obtained could also confirm this theory. Combining equations (5.5) and (5.6), the wavelength shift of the resonance peak is expressed against the reaction time and this can be used to visualise the kinetics of the binding. As the binding has occurred, the concentration of the antigen in the solution gradually decreased.

Based on the above, the experimental data shown in Fig. 5.12 can thus be fitted using Eq. 5.6 and shown in solid lines in Fig. 5.12a and 5.12b. The fitted curves and equations have been derived using Origin Software, based on Equation 5.6. The fitted curve was describe generally as below

$$y = A\,(1 - e^{-Bx}) \quad \text{(Eq. 5.7)}$$

In this case, $A = C \cdot [Ag]_0$ and $B = k$. The calculation of B would indicate the associate rate constant of the binding event, one of the important parameters in kinetic study.

A very good agreement between the experimental data and the fitted curves has been observed, confirming both the success of the sensor fabrication and suggesting the capacity of using this type of probes as a tool for establishing and studying the kinetics of bio-reactions. Using the fitted equation, the following data were extracted, leading to the calculation of A and B in equation 5.7. A set of B values obtained, representing the associate constant values, k, as expressed in equation 5.7, was presented in Fig. 5.13.

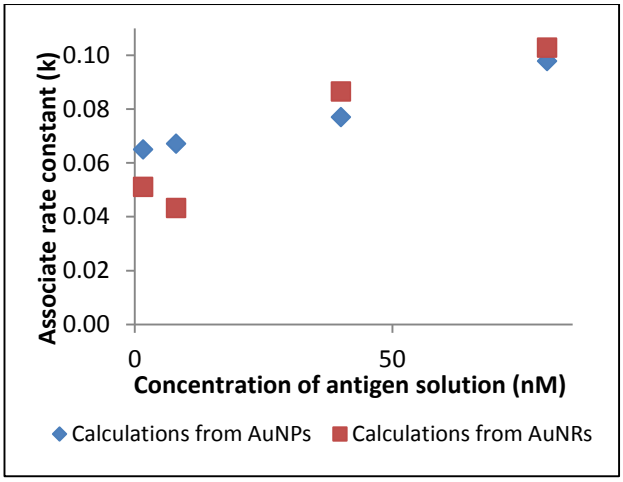

Solution concentration	B value (from AuNPs)	B value (from AuNRs
1.6 nM	0.06505	0.05110
8 nM	0.06717	0.04327
40 nM	0.07701	0.08650
80 nM	0.09782	0.10282
Mean	**0.07676**	**0.07092**

Figure 5.13: The calculated associate rate constant of the binding event.

The calculated associate rate constants were close to each other despite the fact that there was a big difference in the solution concentrations. The mean value calculated from a set of experimental data obtained from the AuNPs based sensor probe was 7.676 x 10^{-2} s^{-1}, while the one from AuNR-based sensor probe was 7.092 x 10^{-2} s^{-1}.

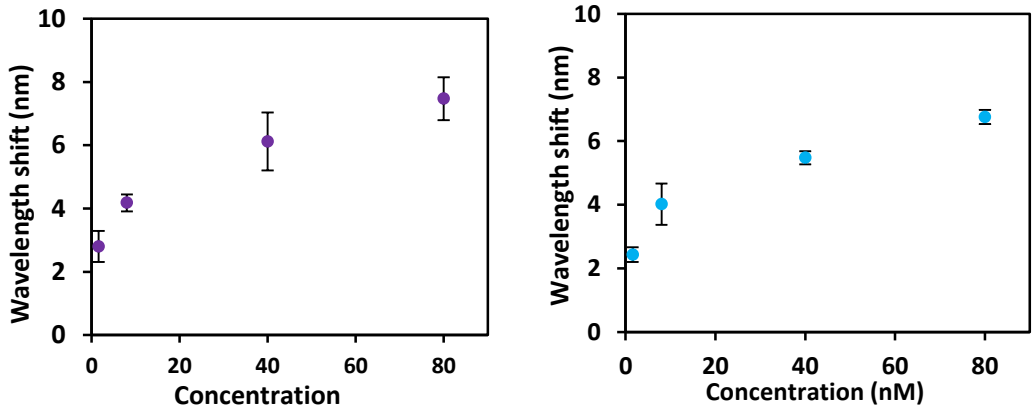

Figure 5.14: (a) Peak wavelength shift of AuNP-based LSPR biosensor and (b) LPW peak wavelength shift of AuNR-based LSPR biosensor as a function of concentration of anti-human IgG after a 2h period of incubation.

The correlations between the peak wavelength shift data after 2 hours of incubation and the concentration of the antigen were plotted in Fig. 5.14. Three independent measurements from different sensor probes were carried out for the analysis of the averages and the standard deviations. As seen in Fig. 5.14, a higher concentration of the anti-human IgG could lead to a higher shift in the peak wavelength. Aslo, the AuNP-based probes used in this work demonstrated slightly better performance in

term of sensitivity compared to the one of AuNR-based probes. It is consistent with the results from RI sensitivity test.

Even using different materials, both types of sensors in this work could achieve a limit of detection (LOD) of 1.6 nM anti-human IgG. This represented the lowest concentration of antigen anti-human IgG that the system could detect from signal change in the peak wavelength. Thus, it is important to account for the fact that the detection limit of the LSPR biosensor is not only dependent on the refractive index sensitivity of nanomaterials, but also affected by the capability of the sensor to capture the target molecules effectively.

The results obtained in this work have also been compared to those reported in literature. The defection limit of the developed sensors in this experiment was comparable to that reported by Mayer group [18] and higher than the one reported by Marinakos *et al.* [40]. Moreover, this LOD was much lower than that of a solution-phase LSPR sensor [41], with AuNRs being suspended in solutions. The chip based LSPR sensor has shown a lower detection limit [40], but the sensor system requires more expensive bulky components, such as a UV-Vis spectrophotometer and a greater volume of samples needed, compared to the optical fibre based sensor system used in this work. The promising results obtained herein show that the LPSR based optical fibre sensors prepared in this work have the ability to be sensitive and label-free biosensors for studying the interaction between biomolecules.

5.4. Conclusions

In this chapter successful synthesis and preparation of AuNPs with a mean diameter of 60 nm and of AuNRs with an aspect ratio of 4.1 were reported, based on their respective optimisation results obtained. Subsequently, a simple yet fast fabrication procedure was employed in order to produce LSPR-based sensor probes using those prepared nanomaterials. High sensitivities have been achieved with a value up to 914 nm/RIU for AuNPs-based LSPR sensors and 601 nm/RIU for AuNRs. These high sensitive probes were then subjected to a series of surface modification and functionalisation for bio-applications. The final bio-sensors created have exhibited an excellent capacity for studying the kinetics of antibody-antigen interaction, with the

reported associate constant value of 0.07 s^{-1}. And 1.6 nM was shown to be the lowest detectable concentration of anti-human IgG that the developed sensor probes can measure. Compared to previously reported LSPR optical fibre sensors, which are only based on the absorbance or intensity interrogation (due to the poor wavelength sensitivity), the sensors demonstrated in this work could be interrogated, based on their wavelength shifts, due to their high wavelength sensitivities to the refractive index changes. The LSPR optical fibre sensors reported were relatively inexpensive to produce, thus potentially disposable after a single use and able to be developed further for a range of other bio-sensing applications, especially enabling the wavelength interrogation approach which has shown to be successful in this work to be more widely used.

5.5. References

1. Wang, H., D.W. Brandl, F. Le, P. Nordlander, and N.J. Halas, *Nanorice: A hybrid plasmonic nanostructure.* Nano Letters, 2006. **6**(4): p. 827-832.
2. Skrabalak, S.E., J. Chen, Y. Sun, X. Lu, L. Au, C.M. Cobley, and Y. Xia, *Gold Nanocages: Synthesis, Properties, and Applications.* Accounts of Chemical Research, 2008. **41**(12): p. 1587-1595.
3. Dondapati, S.K., T.K. Sau, C. Hrelescu, T.A. Klar, F.D. Stefani, and J. Feldmann, *Label-free Biosensing Based on Single Gold Nanostars as Plasmonic Transducers.* ACS Nano, 2010. **4**(11): p. 6318-6322.
4. Anker, J.N., W.P. Hall, O. Lyandres, N.C. Shah, J. Zhao, and R.P. Van Duyne, *Biosensing with plasmonic nanosensors.* Nat Mater, 2008. **7**(6): p. 442-453.
5. Petryayeva, E. and U.J. Krull, *Localized surface plasmon resonance: Nanostructures, bioassays and biosensing-A review.* Anal Chim Acta, 2011. **706**(1): p. 8-24.
6. Gans, R., *The shape of ultra microscopic gold particles.* Annalen Der Physik, 1912. **37**(5): p. 881-900.
7. Gans, R., *The state of ultramicroscopic silver particles.* Annalen Der Physik, 1915. **47**(10): p. 270-U14.
8. Cao, J., E.K. Galbraith, T. Sun, and K.T.V. Grattan, *Effective surface modification of gold nanorods for localized surface plasmon resonance-based biosensors.* Sensors and Actuators B: Chemical, 2012. **169**: p. 360-367.
9. Link, S., M.B. Mohamed, and M.A. El-Sayed, *Simulation of the Optical Absorption Spectra of Gold Nanorods as a Function of Their Aspect Ratio and the Effect of the Medium Dielectric Constant.* The Journal of Physical Chemistry B, 1999. **103**(16): p. 3073-3077.
10. Miller, M.M. and A.A. Lazarides, *Sensitivity of metal nanoparticle surface plasmon resonance to the dielectric environment.* Journal of Physical Chemistry B, 2005. **109**(46): p. 21556-21565.
11. Lin, T.J. and M.F. Chung, *Detection of cadmium by a fiber-optic biosensor based on localized surface plasmon resonance.* Biosens Bioelectron, 2009. **24**(5): p. 1213-1218.
12. Mitsui, K., Y. Handa, and K. Kajikawa, *Optical fiber affinity biosensor based on localized surface plasmon resonance.* Appl Phys Lett, 2004. **85**(18): p. 4231-4233.
13. Chau, L.K., Y.F. Lin, S.F. Cheng, and T.J. Lin, *Fiber-optic chemical and biochemical probes based on localized surface plasmon resonance.* Sensors and Actuators B-Chemical, 2006. **113**(1): p. 100-105.
14. Lai, N.S., C.C. Wang, H.L. Chiang, and L.K. Chau, *Detection of antinuclear antibodies by a colloidal gold modified optical fiber: comparison with ELISA.* Anal Bioanal Chem, 2007. **388**(4): p. 901-907.
15. Sai, V.V.R., T. Kundu, and S. Mukherji, *Novel U-bent fiber optic probe for localized surface plasmon resonance based biosensor.* Biosens Bioelectron, 2009. **24**(9): p. 2804-2809.
16. Huang, K.T., T.J. Lin, and M.H. Hsu, *Determination of cyclic GMP concentration using a gold nanoparticle-modified optical fiber.* Biosens Bioelectron, 2010. **26**(1): p. 11-15.
17. Grabarek, Z. and J. Gergely, *Zero-length crosslinking procedure with the use of active esters.* Anal Biochem, 1990. **185**(1): p. 131-135.
18. Mayer, K.M., S. Lee, H. Liao, B.C. Rostro, A. Fuentes, P.T. Scully, C.L. Nehl, and J.H. Hafner, *A Label-Free Immunoassay Based Upon Localized Surface Plasmon Resonance of Gold Nanorods.* ACS Nano, 2008. **2**(4): p. 687-692.

19. Yu, C. and J. Irudayaraj, *Multiplex Biosensor Using Gold Nanorods.* Analytical Chemistry, 2006. **79**(2): p. 572-579.
20. Cao, J., E.K. Galbraith, T. Sun, and K.T.V. Grattan, *Cross-Comparison of Surface Plasmon Resonance-Based Optical Fiber Sensors With Different Coating Structures.* IEEE Sensors Journal, 2012. **12**(7): p. 2355-2361.
21. Tu, M.H., T. Sun, and K.T.V. Grattan, *Optimization of gold-nanoparticle-based optical fibre surface plasmon resonance (SPR)-based sensors.* Sensors and Actuators B: Chemical, 2012. **164**(1): p. 43-53.
22. Turkevich, J., P.C. Stevenson, and J. Hillier, *A study of the nucleation and growth processes in the synthesis of colloidal gold.* Discussions of the Faraday Society, 1951. **11**: p. 55.
23. Nikoobakht, B. and M.A. El-Sayed, *Preparation and growth mechanism of gold nanorods (NRs) using seed-mediated growth method.* Chemistry of Materials, 2003. **15**(10): p. 1957-1962.
24. Zhang, Q., C. Xue, Y. Yuan, J. Lee, D. Sun, and J. Xiong, *Fiber Surface Modification Technology for Fiber-Optic Localized Surface Plasmon Resonance Biosensors.* Sensors, 2012. **12**(3): p. 2729-2741.
25. Balachander, N. and C.N. Sukenik, *Monolayer transformation by nucleophilic substitution: Applications to the creation of new monolayer assemblies.* Langmuir, 1990. **6**(11): p. 1621-1627.
26. Grabar, K.C., R.G. Freeman, M.B. Hommer, and M.J. Natan, *Preparation and Characterization of Au Colloid Monolayers.* Analytical Chemistry, 1995. **67**(4): p. 735-743.
27. Daniel, M.-C. and D. Astruc, *Gold Nanoparticles: Assembly, Supramolecular Chemistry, Quantum-Size-Related Properties, and Applications toward Biology, Catalysis, and Nanotechnology.* Chemical Reviews, 2003. **104**(1): p. 293-346.
28. Grabarek, Z. and J. Gergely, *Zero-length Crosslinking Procedure With The Use Of Active Esters.* Analytical Biochemistry, 1990. **185**(1): p. 131-135.
29. Staros, J.V., R.W. Wright, and D.M. Swingle, *Enhancement by N-hydroxysulfosuccinimide of water-soluble carbodiimide-mediated coupling reactions.* Analytical Biochemistry, 1986. **156**(1): p. 220-222.
30. Becker, R., B. Liedberg, and P.-O. Kall, *CTAB promoted synthesis of Au nanorods - Temperature effects and stability considerations.* J Colloid Interface Sci, 2010. **343**(1): p. 25-30.
31. Gou, L.F. and C.J. Murphy, *Fine-tuning the shape of gold nanorods.* Chemistry of Materials, 2005. **17**(14): p. 3668-3672.
32. Jiang, X.C. and M.P. Pileni, *Gold nanorods: Influence of various parameters as seeds, solvent, surfactant on shape control.* Colloids and Surfaces a-Physicochemical and Engineering Aspects, 2007. **295**(1-3): p. 228-232.
33. Busbee, B.D., S.O. Obare, and C.J. Murphy, *An improved synthesis of high-aspect-ratio gold nanorods.* Advanced Materials, 2003. **15**(5): p. 414-+.
34. Kang, S.K., S. Chah, C.Y. Yun, and J. Yi, *Aspect ratio controlled synthesis of gold nanorods.* Korean Journal of Chemical Engineering, 2003. **20**(6): p. 1145-1148.
35. Chen, H., X. Kou, Z. Yang, W. Ni, and J. Wang, *Shape- and Size-Dependent Refractive Index Sensitivity of Gold Nanoparticles.* Langmuir, 2008. **24**(10): p. 5233-5237.
36. Li, Q.L., T. Burgi, and H. Chen, *Preparation of gold nanorods of high quality and high aspect ratio.* Journal of Wuhan University of Technology-Materials Science Edition, 2010. **25**(1): p. 104-107.
37. Chau, L., Y. Lin, S. Cheng, and T. Lin, *Fiber-optic chemical and biochemical probes based on localized surface plasmon resonance.* Sensors and Actuators B: Chemical, 2006. **113**(1): p. 100-105.

38. Sadana, A. and D. Sii, *Binding kinetics of antigen by immobilized antibody: influence of reaction order and external diffusional limitations.* Biosensors and Bioelectronics, 1992. **7**(8): p. 559-568.
39. Sadana, A., *Antigen-Antibody Binding Kinetics for Biosensors: The Fractal Dimension and the Binding Rate Coefficient.* Biotechnology Progress, 1995. **11**(1): p. 50-57.
40. Marinakos, S.M., S. Chen, and A. Chilkoti, *Plasmonic detection of a model analyte in serum by a gold nanorod sensor.* Anal Chem, 2007. **79**(14): p. 5278-83.
41. Yu, C., L. Varghese, and J. Irudayaraj, *Surface modification of cetyltrimethylammonium bromide-capped gold nanorods to make molecular probes.* Langmuir, 2007. **23**(17): p. 9114-9.

Gold-silver alloy nanoparticles LSPR sensor

6.1. Introduction

As discussed extensively in Chapter 3, gold and silver nanoparticles have been well known for decades for their unique characteristics and the surface plasmon resonance (SPR) effect using such particles has been widely recognised and exploited for a broad spectrum of sensor applications ranging from catalysis [1, 2] and medical analysis [3, 4] to chemical and biological measurements [2, 5, 6]. The combination of two or more metal nanoparticles, rather than using a single metal, has been of significant interest recently, resulting in a body of research literature in this area. In the case of gold and silver, even though their combination in a nanoparticle alloy had been first synthesised and was investigated in 1976 [7], significant developments in the field have only occurred in the last decade [8] with an aim to maximise their use.

Hybrid and bimetallic nanoparticles between gold and silver can be generated in several differential forms and the two most important structures reported are core-shell structure [9-21] and alloy formation [7, 8, 17, 22-33]. The latter inherits the advantages of both gold nanoparticles with a high plasmonic effect and silver nanoparticles with a sharp plasmonic absorption peak. In addition, it is possible to tune the plasmonic absorption by varying the alloy content ratio which enables the alloy nanoparticles to be made specifically to meet some special needs. Therefore this chapter is focused on the development of a set of novel LSPR sensors based on alloys of gold and silver nanoparticles, with an aim to enhance the sensor performance compared to those coated with particles made of a single metal as discussed in Chapters 4 and 5.

As discussed in Chapter 3, the morphology of nanostructures, which relates specifically to their size and shape, plays a very important role in contributing to the plasmonic effects caused by the nanoparticles. There have been a number of synthesis methods reported to create gold and silver alloys with different morphologies, ranging from mono-dispersed nanospherical alloys [6, 24, 34] to nanocubes [35], nanoframes [36], nanocages [37] and nanorice [38], configured as bimetallic structures of gold and silver. However, the more complex the structure, the harder it is to achieve a good dispersion ('monodispersity') of the particles. Unlike single metal nanoparticles, bimetallic alloy particles are usually created, under most circumstances, using a chemical technique, due to their complicated structures and the required controllability of the synthesis process. Therefore it might be the best to consider first the synthesis of spherical bimetallic alloy particles. Among the several commonly known methods, co-reduction [8] is recognised as the simplest and easiest method for achieving the Au-Ag alloy particles required. The limitation of this method, however, lies in both the difficulty in controlling the morphology and the possible formation of a silver halide, making the synthesis process less predictable than desired [2]. Annealing the core-shell particles could be considered as an effective approach to overcome the above limitation [9, 17]. In some reports, it has been suggested that a digestive ripening technique could also be used for creating small (around 5nm in diameter) alloy nanoparticles, but this is not suitable for the larger particles required, for example, bigger than 11 nm in diameter [26, 31]. Another approach is to use a replacement reaction, but the particles synthesised are typically small and usually have diameters of less than 10nm [16, 26, 30, 39, 40].

It has also been reported recently that the step-wise method could be used to create alloy particles of larger size and better shape [26, 41]. Zhang *et al.* [2] have reported results obtained from the creation of larger size monodispersed gold-silver alloy particles (over 20nm in diameter). In their work, a silver precursor and a reductant were mixed together, brought to boil and allowed to remain under the same condition for some time. After that, some gold solution was added following which a reaction took place, accompanied by heating and vigorous stirring. This simple

method overcomes a number of difficulties highlighted previously in producing a monodispersed large nanoalloy.

Despite the fact that nanoalloys of gold and silver particles have been developed intensively, there has been limited report in literature considering them as promising materials for the construction of LSPR-based sensors for various sensing applications. Several theoretical calculations have been made, for example by Kyeong-Seok Lee *et al.* [33], and Sharma *et al.* [42, 43], but the results reported are not readily comparable. One possible explanation is that the plasmonic sensing effect involves a number of factors including diameter, shape and alloy content, but only a limited set of factors could be taken into account for ease of theoretical calculations under each circumstance. Thus this chapter is focused on the experimental exploration, with an aim to develop a new yet feasible approach for the creation of a sufficiently sensitive optical fibre based refractive index (RI) sensor using such alloy particles. This is achieved by modification of a section of an unclad optical fibre, followed by the subsequent coating of nanoalloys of gold and silver synthesised on the fibre surface. As a result the surface-plasmon resonance effect between the alloy particles and the optical fibre can thus be employed for refractive index measurement.

6.2. Experimental setup

6.2.1. Chemical and Apparatus

The following chemicals used were purchased from Sigma-Alrich: 3-aminopropyl trimethoxysilane (APTMS) 97%, gold chloride hydrate ($HAuCl_4.3H_2O$), silver nitrate ($AgNO_3$) and sodium citrate tribasic dehydrate ($Na_3C_6H_5O_7$). CH_3OH (Analytical Reagent Grade) and H_2SO_4 95% (Laboratory Reagent Grade) were purchased from Fisher Scientific. De-ionized water and H_2O_2 37% solution were purchased from ACROS.

The optical fibre was purchased from Thorlab, of type BFH37-600; the light source was a halogen light source, type HL-2000-FHSA obtained from Mikropack and the spectrometer used was Maya type 2000PRO, obtained from Ocean Optics.

6.2.2. Synthesis of alloy nanoparticles

Successful synthesis of large monodispersed alloy nanoparticles of gold and silver has been reported recently by Zhang *et al.* [24] and a similar approach is used in this work. Briefly this can be described as follows: initially, solutions of 2mM HAuCl4 and 2mM AgNO3 are prepared, as well as a 35mM sodium citrate solution which acted as both a reducing agent and a surfactant. Different alloy content ratios can thus be controlled by changing the molar ratio of the gold and silver solutions. The size of the alloy particles can be modified by varying the ratio and molarity of the total metals (gold and silver) and the molarity of the reducing agent ($Na_3C_6H_5O_7$). In this work, several different gold-silver alloy nanoparticles solutions were prepared and labelled and the details are shown in Table 6.1.

Table 6.1: Solution Code and Characteristics

Solution Characteristics / **Molar ratio of metal : sodium citrate for alloy size control**	25% Ag, 75% Au	75% Ag, 25% Au
1:7	**A25-1**	**A75-1**
1:3	**A25-2**	**A75-2**
1:1.5	**A25-3**	**A75-3**

1:0.9	**A25-4**	**A75-4**
1:0.45	**A25-5**	**A75-5**

Two groups of samples, with ten different gold-silver alloy nanoparticles, were synthesised. The A25 group, represented by alloy particles with 25% Ag and 75% Au (in their molar ratio), with solutions being coded A25-1 to A25-5 (with the second number representing the particle size, the higher number is the bigger size) and A75, represented by alloy particles with 75% Ag and 25% Au in the group with solution being coded A75-1 to A75-5 (again with the second number representing the particle size).

At first, to synthesise the A75-1 Alloy (as described in Table 6.1, an alloy with 75% Ag and 25% Au), 1.875 mL of prepared silver solution was mixed with 1mL of 35mM sodium citrate solution in a round bottom flask equipped with a condenser and a stir bar. 50 mL of deionized water was then added before the solution was heated to boiling and maintained under the boiling condition for 30 min. This was followed by the addition of 0.625 mL $HAuCl_4$ solution, applying vigorous stirring. The reacting solution gradually became darkened and was left being heated, and stirred, for 30 min. After that, the heat source was removed but stirring is maintained for another 30 min. The resultant solution of A75-1 has a yellowish colour and was then transferred to and kept in a refrigerator (at 4 ^oC) until it was required for use.

Similarly, alloy A25-1 was synthesised using the same method, but exchanging the amounts of the gold and silver solutions used from those indicated above. In this particular case, 0.625 mL of $AgNO_3$ has been used first, being followed by 1.875 mL of $HAuCl_4$ solution. The colour of the final solution thus obtained is cardinal red.

To achieve different particle sizes of the A75 and A25 groups, the amount of sodium citrate was varied and, as a result, 10 solutions of different particle sizes and gold/silver content were created and thus made ready for sensor fabrication, using the process described below.

6.2.3. Sensor preparation process

As shown in Fig. 6.1, 600 µm diameter optical fibres were chosen for use in this work with a length of approximately 20 cm. These larger core fibres offer a larger surface area for coating and ease of coupling of light from the source used. Both ends of the fibre were polished with different polishing papers (from Thorlabs, using types 5 µm, 3 µm, 1 µm and 0.3 µm, respectively). Finally, one end of the fibre was stripped off its cladding, leaving the sensing area (the fibre core) of 20 mm length and ready for the application of the coating.

The unclad part of the fibre (the fibre core) is required to undergo a series of cleaning and surface modifications prior to the coating being applied and for it to act as a sensor. The same coating procedure was given in previous chapters. In summary, the fibre was initially cleaned by using Piranha solution (70% H_2SO_4, 30% H_2O_2) for 30 min, then washed several times by using distilled water followed by oven curing at 120^{o}C for 1 h. Following that the fibre was coated with a thin layer of APTMS for over 4 hrs before being washed carefully again using methanol and finally treated in the oven overnight at 80 ^{o}C. Subsequently, a dip-coating method was used for the formation of a thin layer of the alloy nanoparticles on the surface of the unclad fibre. This layer was designed to perform as the sensing material, responding to the surrounding reflective index change through the localised surface plasmon resonance (LSPR) effect between the alloy particles and the dielectric fibre, when the fibre was illuminated by light from the light source described earlier.

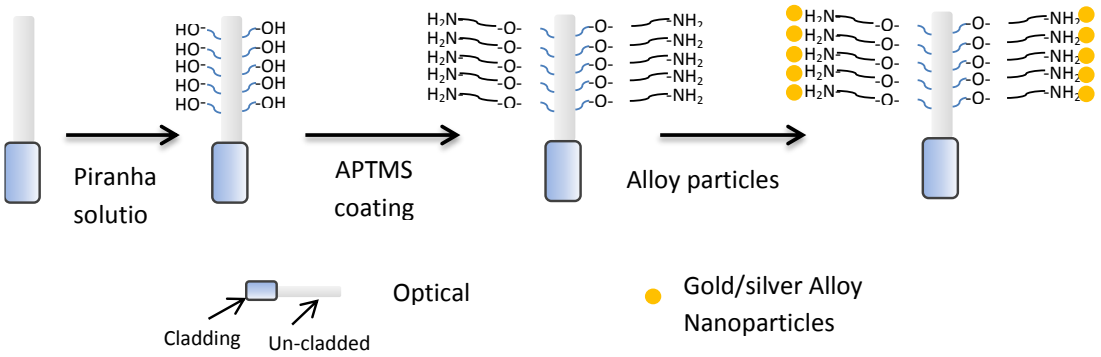

Figure 6.1: Illustration of the preparation of the fibre optic sensor

6.2.4. Sensor system setup for solution refractive index measurement

The sensor system configuration used in this work was also described in Chapter 4 and is shown schematically in Fig. 6.2. In this work, instead of using gold nanoparticles, the gold/silver alloy nanoparticles prepared as described above were used for the fabrication of LSPR sensors and their performance in response to the variation of the external refractive index (RI) was investigated.

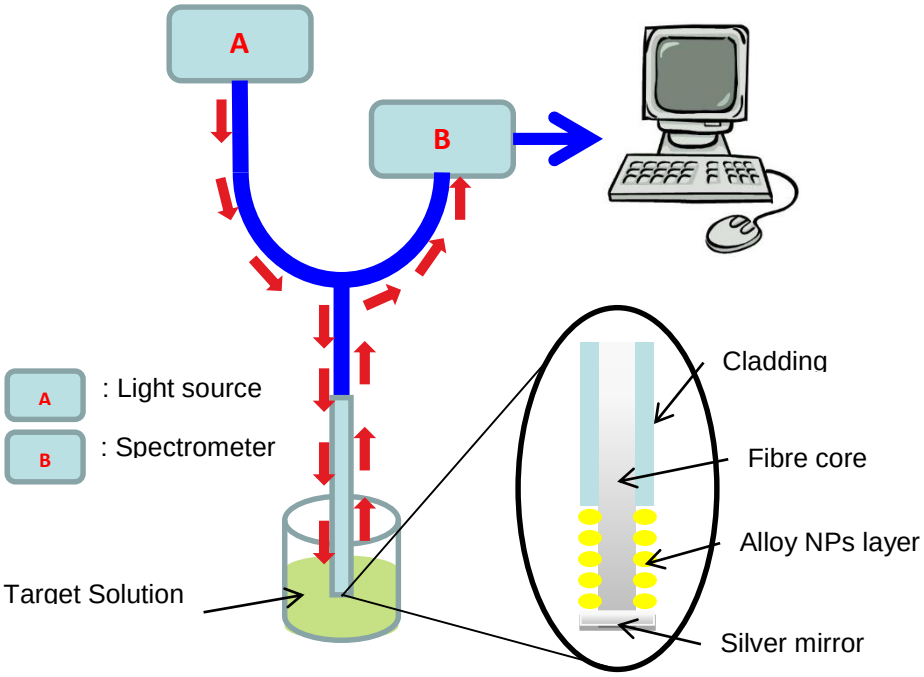

Figure 6.2: Schematic diagram of an experimental setup used in this work

6.3. Results and Discussions

6.3.1. Gold-silver alloy characteristics

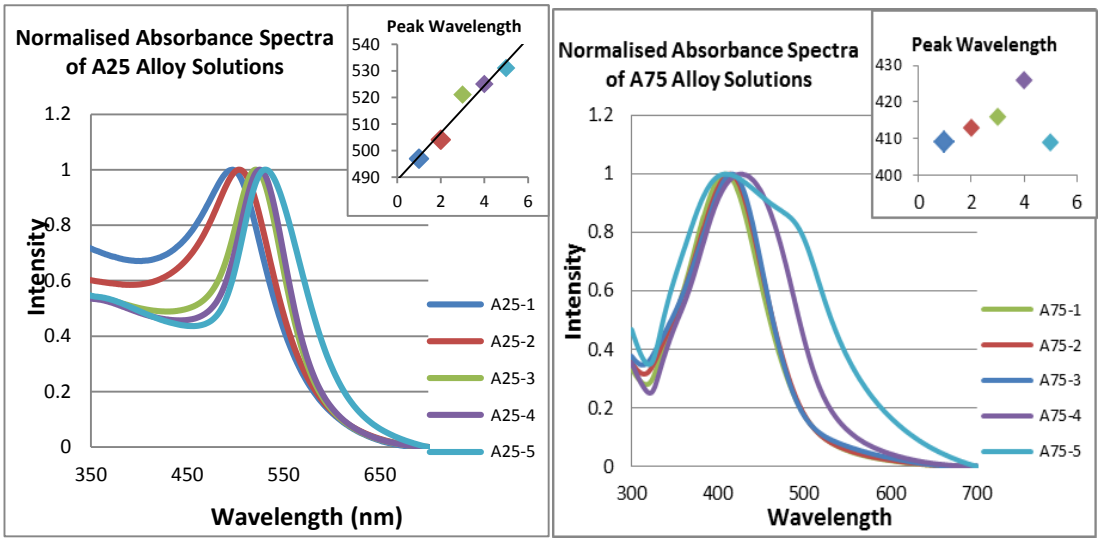

Figure 6.3: Normalised Absorbance Spectra of the Alloy Solutions prepared (Left: A25 Alloy Solutions, Right: A75 Alloy Solutions)

Figure 6.3 shows the UV-Vis absorbance spectra obtained from both A25 and A75 alloy solutions, with their corresponding absorbance peak wavelengths being scattered within the range from around 440nm to 500nm. This observation further confirmed the successful synthesis of A75-1 and A25-1 alloy solutions. The only abnormal condition is A75-5, showing a broadened spectrum containing two distinctive peaks as illustrated in Fig. 6.4. This indicates that in this case, the alloy could not be formed and that what seems to have occurred is a mixture of gold and silver nanoparticles. With a smaller amount of sodium citrate being introduced in the solution, a greater red-shift of the absorbance peak was observed, indicating that a larger size of alloy particles has been achieved.

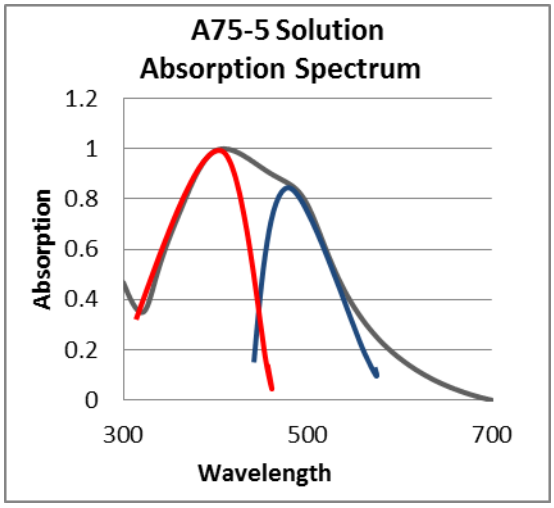

Figure 6.4: A75-5 Absorption Spectrum – spectrum to the left illustrates the absorption peak of silver nanoparticles while that to the right the absorption peak of the gold nanoparticles.

Figure 6.5 further confirmed the conclusion made based on the results shown in Fig. 6.3, through a cross-comparison made by the measurement of the peak wavelength in the absorbance spectra of gold nanoparticle solution, silver nanoparticle solution and 2 alloy nanoparticle solutions (A25-1 and A75-1), with the same amount of metallic precursor used for the synthesis. Silver nanoparticle solution had its peak absorbance wavelength at around 420nm, and the one of gold nanoparticle solution was at around 520nm. Alloy nanoparticle solutions have their own distinct peaks in between those values, with the trend shown in Fig. 6.5b.

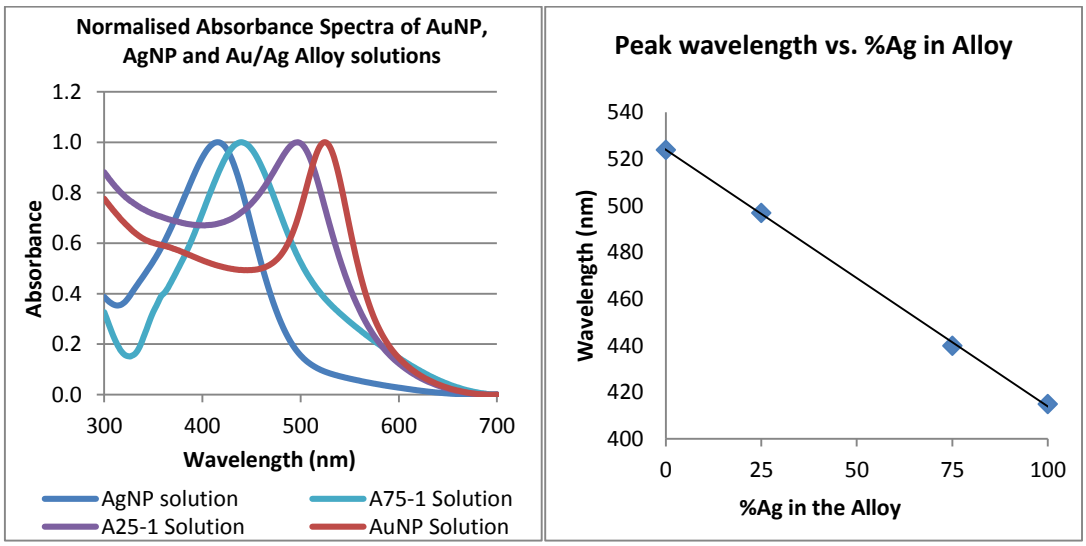

Figure 6.5: Normalised Absorbance Spectral comparison of AuNP, AgNP and alloy nanoparticle solutions. (a) Normalised absorbance spectra of of AuNP, AgNP and Au/Ag Alloy solutions and (b) Plot of the peak wavelength and the amount of Ag in the Alloy.

The morphology of the alloy particles synthesised above has been investigated using an electron microscope and a series of TEM images obtained (using a JEM-1010 Electron Microscope at 80kV) is presented in Fig. 6.6. The images show that the alloy particles are well dispersed (showing monodispersity) and in most cases spherical-like particles are observed. The average diameter of the alloy particles in each solution is calculated by monitoring > 100 particles in each TEM image and calculating the average in each case. Results obtained show that the A25 group has particles with average diameters of 13.7 ± 3.8nm, 15.0 ± 4.8nm, 17.2 ± 3.7nm, 24.2 ± 3.7nm and 34.1 ± 6.4nm, respectively for samples A25-1, A25-2, A25-3, A25-4 and A25-5, while for A75, it is 12.9 ± 3.1nm, 13.8 ± 4.3nm, 19.3 ± 5.2nm, 33.7 ± 6.2nm and 17.1 ± 4.2nm respectively for the A75-1, A75-2, A75-3, A75-4 and A75-5 samples. It is noticeable that, for the A75-5 sample, the diameter of the particles is smaller than would have been expected, given the consistent results obtained from the other alloys and the reduced amount of reducing agent being used for the solution. This evidence, combined with the spectral data shown in Fig. 6.4, points to a conclusion that the expected alloy particles were not formed, but a mixture that is largely of separated gold and silver particles.

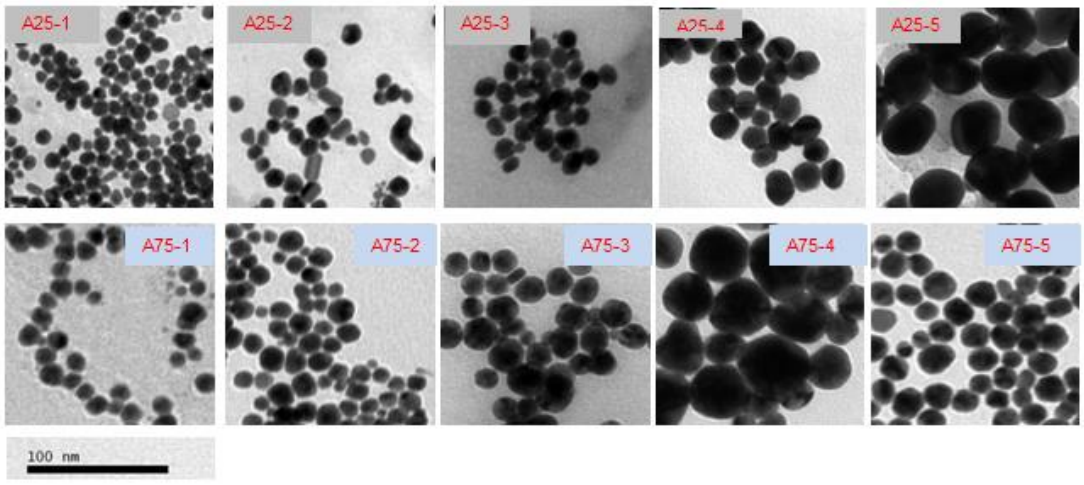

Figure 6.6: TEM Images of Alloy nanoparticles (codes for the type of alloys have been included in the images)

By considering the effect of the amount of sodium citrate on creating different particle sizes, a clear relationship between the molar ratio of the reductant to metal used and the calculated average diameter of the alloys has been established. A similar effect is seen for both A25 and A75 types. Sodium citrate, in this work, acts

not only as a reductant but also a surfactant, preventing small particles from aggregating. The lesser the amount of sodium citrate used, the larger the alloy size created, in this way similar to the results seen for gold nanoparticles which were characterised in Chapter 4. It seems clear that at first, when the sodium citrate is overly abundant (the molar ratio is 7), small particles with diameters around 13nm in both the A25 and the A75 alloy group are created. By lowering the ratio to 3, the size of the alloy particles increases from an average diameter of 13.7nm to 15.0nm. In this situation, the amount of sodium citrate is sufficient to reduce all the gold and silver salts to nanoparticles, and the remaining amount of sodium citrate, acting as surfactant and being less than that in the previous case, leads to the formation of slightly larger nanoparticles. By continuing to reduce the total amount of sodium citrate, the amount of surfactant is proportionally reduced, thus making the diameters of synthesised alloys bigger and bigger, reaching the highest at an average of 34.1nm. Going for further reduction of the amount of sodium citrate, it would not be sufficient both to reduce all the metal salts and to achieve a sufficient surface-covering of the newly created nanoparticles. In those cases, alloys with non-uniform shapes and sizes would appear as the result of the synthesis process not being well controlled. The only exception in this experiment is the result seen for the A75-5 case. The evidence from a close investigation of the UV-Vis spectra is that A75-5 is likely a simple mixture, rather than an alloy of gold and silver nanoparticles. Therefore, the diameter of particles under such circumstances would be quite small and the data obtained do not fit the pattern established with the other alloys (this is shown as the isolated square in Fig. 6.7). It is also observed that the morphology of the largest alloy particles show them somewhat deviated from being spherical. This agrees with what is reported in the literature [2, 26], that it is indeed difficult to control the size and shape of alloy nanoparticles as they continue to grow larger.

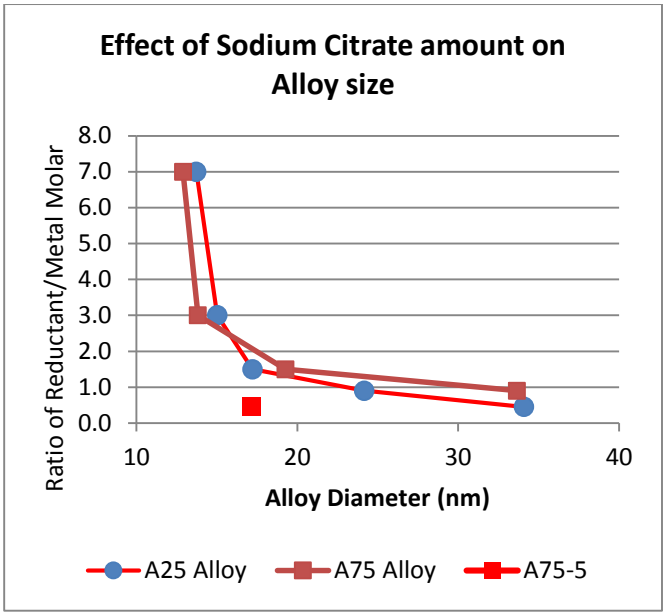

Figure 6.7: Effect of the amount of Sodium Citrate on the Alloy size

The correlation between the absorption peak and the diameter of particles is shown in Fig. 6.8, where the greater absorption peak wavelength of the alloy particles corresponds well to situations where the particles sizes are larger. Again A75-5 has shown to be an exception (because the particles are not the expected alloy and thus have different properties), this being reflected clearly in the change of both the peak wavelength and the diameter. If the data for this suspect A75-5 case are ignored (the lower dot on the right hand side of Fig. 6.8), the overall picture is similar for both the A25 and the A75 alloy groups within the experimental error.

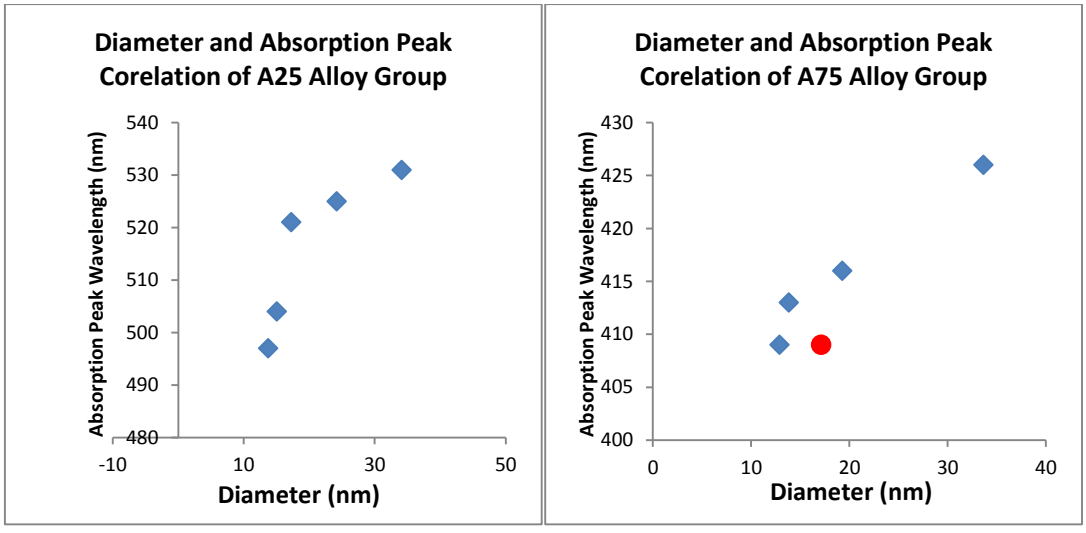

Figure 6.8: Diameter and Absorption Peak Correlation in the cases of the A25 Alloy (left) and the A75 Alloy (right) (data for the A75-5 case, where the alloy did not form, are shown as a circle)

6.3.2. Sensor performance

LSPR sensors created by coating optical fibres with gold-silver alloy nanoparticles discussed above were subsequently used for Refractive Index (RI) measurement. To do so, the sensitivity of each sensor was calculated using the method reported previously in chapter 4. A set of solutions with known RIs was made by using different solvents. Table 6.2 shows a list of solvents used and their corresponding RIs of the solutions made.

Table 6.2: Solvents used for the calibration and their refractive index values

Solvent	*Refractive Index*
Distilled Water	1.333
Acetonitrile	1.344
Acetone	1.359
Petroleum Ether	1.365
n-Hexane	1.375
n-Propyl alcohol	1.385
Tetrahydrofuran	1.407

The absorption peak wavelength observed from the sensor when evaluated in each solvent was thus recorded, with its sensitivity being calculated using equation 6.1:

$$S = \frac{d\lambda_{max}}{dn} \qquad \text{(Eq. 6.1)}$$

Two probes of each alloy type were prepared, fabricated and tested to ensure that the results were representative. As verified by both the theoretical analysis [32, 33] and the experimental data, the particle size plays a vital role in contributing to the sensitivity of the probe. The calculated sensitivities to RI of different alloy particle-coated optical fibre sensors are cross-compared and the results obtained are presented in Fig 6.9, confirming the general trend that the larger the particle's size for the alloy-coated sensor, the greater the sensitivity. The particle sizes for A25-1 and A25-2 (and also for the A75-1 and A75-2 cases) are the same within experimental error and thus only one histogram is displayed. A25-2 and A75-2, because of their similarities in particle size to A25-1 and A75-1 respectively (within the experimental error shown) have thus been excluded from further individual investigation of their sensing performance and are subsumed into the data labelled A25-1 and A75-1. Subsequently, for A25 group, explicit data are given for A25-1, A25-3, A25-4 and A25-

5, and in the other A75 group, the same situation applies for the A75-1, A75-3, A75-4 grouping. A75-5 has not been considered to be an alloy based on the discussions made earlier and hence the sensitivity is not included in Fig. 6.9 for cross-comparison.

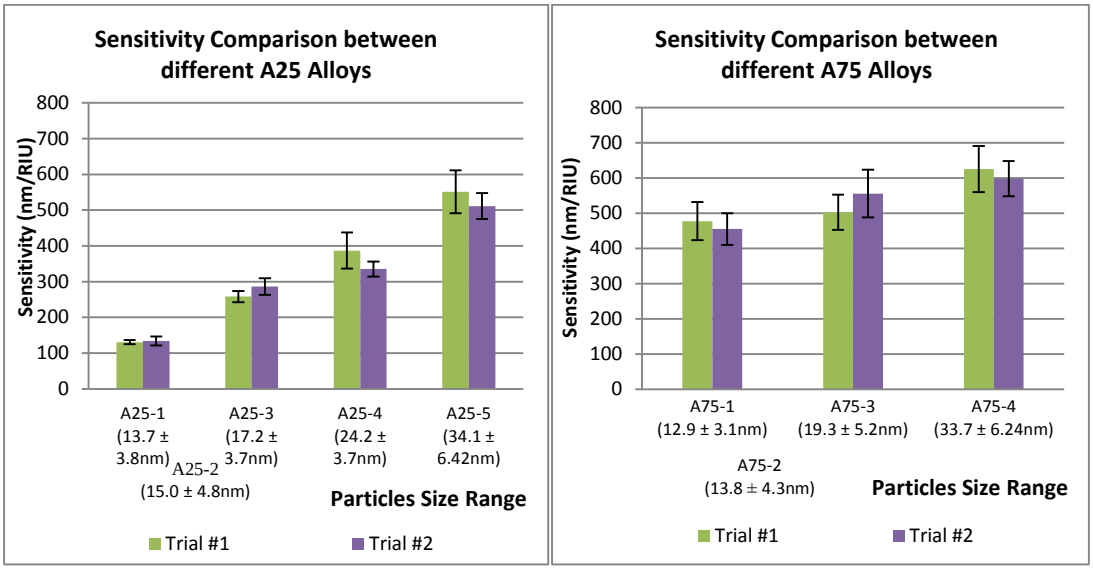

Figure 6.9: Sensitivity comparison of different Alloy coated fibres (left: A25, right: A75)

As a result, it can be seen that A25-5 shows the highest sensitivity (of 531nm/RIU) among the A25 group; as can be seen, it is approximately four times of that of the A25-1 sample. On the other hand, for the A75 group, (and excluding the A75-5 data), a smaller increase in the sensitivity with the increase of alloy particle size is observed. Fig 6.9 summarises the results obtained, confirming the trend in the sensitivity increase with the increase of the diameter of the alloys. For smaller particle sized (from 10-20nm diameter) alloys, A75 alloy-coated sensors (by comparison to A25 alloy-coated sensors) demonstrate a much higher sensitivity to RI change. However, when the size is greater, the A25 group of coated sensors demonstrates a rapidly increasing sensitivity, approaching that seen for those coated with the A75 group of nanoparticles. In summary, with an average particle size diameter of 33.7 ± 6.2nm, the fibre sensors coated with nanoparticles alloy of 75% Silver and 25% Gold exhibit the best sensing capability (i.e. the A75 group). The special case of A75-5 (shown as a circle in Fig. 6.10) is also included for completeness but it is clear from the graph that the actual non-alloy smaller particles obtained do not perform as well in the sensor as would the larger alloy particles (that were expected from such a synthesis), as was seen for the A25 cases.

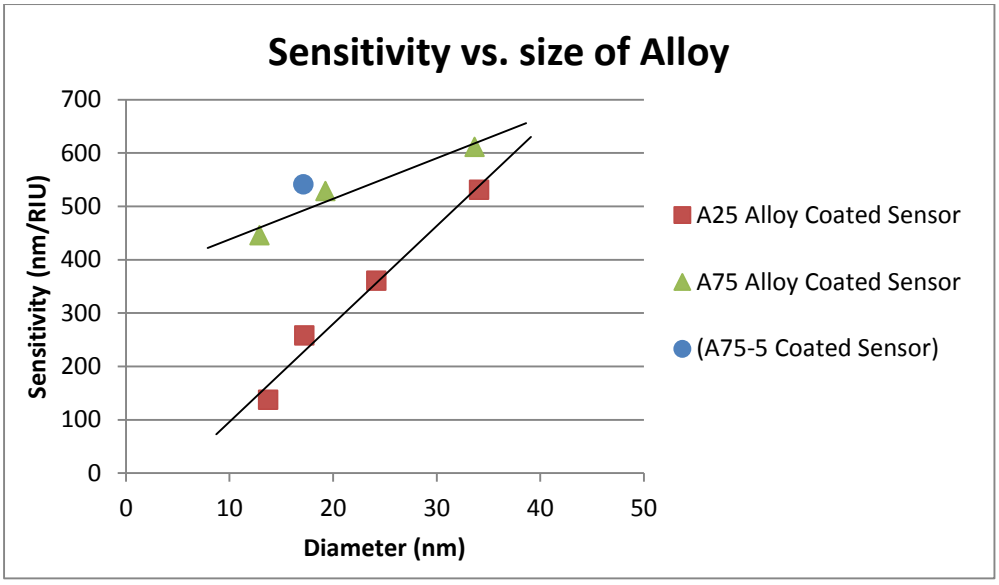

Figure 6.10: Correlation between the sensitivity of the alloy-coated sensors and the alloy size

From literature, advanced techniques for refractive index measurement using photonic crystal fibres (PCFs) have been predicted theoretically to have a very high sensitivity at 70,000 nm/RIU [44], with several experimental reports to date. For example, Long-Period Gratings using PCFs could achieve a sensitivity of 1500 nm/RIU experimentally [45]; a modified Fabry-Perot interferometer-based technique has reported a sensitivity as high as 1731 nm/RIU [46] or using PCFs with four-wave mixing could enhance the sensitivity up to 8800 nm/RIU [47]. The highest sensitivity reported to date is also achieved by using a method involving PCFs, with a sensitivity up to 30,000 nm/RIU [48], but limited to liquid samples with a refractive index higher than that of the waveguide material (i.e. 1.45). With regarding to sensitivity of refractive index measurement, this work is meant to provide a simple and affordable preparation technique using optical fibre. The main purpose, as discussed in this work, is to employ a gold-silver alloy monolayer as an effective sensing platform for further analysis. This flexibility, however, cannot be achieved by using photonic crystal fibres (PCFs) techniques. For example, through the modification of the alloy layer for immobilisation of an antibody, a biosensor would be easily created and implemented for specific antigen identification. In addition to this, the developed probes, compared to PCF sensors, are easy to clean, easy to recycle and affordable for mass production and disposal. It should also be noted that, sensitivity

improvement is achievable by using alloys of larger sizes and different shapes, as well as using different fibre structures, such as tapered fibres or side-polished fibres.

The data obtained clearly show the trends with particle size and alloy type and this allows for the tailoring of the sensor design to achieve the sensitivity required. This can be done either by using different synthesis approaches to produce alloy particles with appropriate sizes, or through the control of the content of the gold and silver in the alloy, to ensure the creation of a sensor with the required sensitivity yet with an optimum sensor design.

6.4. Conclusions

A systematic investigation into the potential of using bimetallic nanoparticle alloys of gold and silver for the creation of enhanced SPR-based optical fibre sensors has been undertaken and discussed in detail in this chapter. The sensitivity of the sensors created can readily be tailored through the design process. In this chapter the sensors designed and fabricated through optimization have shown both a high and reproducible sensitivity to refractive index (RI) change. Based on the experimental results obtained, the detailed characteristics and capabilities of the novel RI sensors created can be summarised as follows:

- The size of the alloy particles can be modified reproducibly by altering the amount of sodium citrate in a simple one-step preparation of gold-silver nanoalloys, confirming the success of the fabrication of monodispersed nano-spherical alloy particles with different sizes, both for the gold-rich (A25) and the silver-rich alloys (A75).

- In a way similar to single metal nanoparticles, the increase in diameter of spherical alloy nanoparticles is shown to enhance the sensitivity of the alloy particle-coated SPR sensors.

- The alloy content also influences the sensitivity of the alloy particle-coated SPR sensors. The silver-rich alloy particles (A75) produce a comparatively more sensitive device in term of RI sensing, with (in both the cases of the A25 and A75 groups) the highest sensitivity being demonstrated with the larger particle size.

In conclusion, refractive index sensors based on surface plasmon resonance (SPR) using gold-silver alloy nanoparticles coated on optical fibre have shown considerable promise and high sensitivity which can be tailored for different applications, for example in the bio-sensing area.

6.5. References

1. Zhang, H., J. Okuni, and N. Toshima, *One-pot synthesis of Ag-Au bimetallic nanoparticles with Au shell and their high catalytic activity for aerobic glucose oxidation.* J Colloid Interface Sci, 2011. **354**(1): p. 131-8.
2. Zhang, Q., J. Xie, Y. Yu, and J.Y. Lee, *Monodispersity control in the synthesis of monometallic and bimetallic quasi-spherical gold and silver nanoparticles.* Nanoscale, 2010. **2**(10): p. 1962-75.
3. Nambiar, S. and J.T. Yeow, *Conductive polymer-based sensors for biomedical applications.* Biosens Bioelectron, 2011. **26**(5): p. 1825-32.
4. Wu, D. and X. Liu, *Optimization of the bimetallic gold and silver alloy nanoshell for biomedical applications in vivo.* Applied Physics Letters, 2010. **97**(6).
5. Wang, J., *Electrochemical biosensing based on noble metal nanoparticles.* Microchimica Acta, 2012. **177**(3-4): p. 245-270.
6. Wang, J., D. Song, L. Wang, H. Zhang, H. Zhang, and Y. Sun, *Design and performances of immunoassay based on SPR biosensor with Au/Ag alloy nanocomposites.* Sensors and Actuators B: Chemical, 2011. **157**(2): p. 547-553.
7. Papavassiliou, G.C., *Surface-plasmons In Small Au-Ag Alloy Particles.* Journal of Physics F-Metal Physics, 1976. **6**(4): p. L103-L105.
8. Link, S., Z.L. Wang, and M.A. El-Sayed, *Alloy formation of gold-silver nanoparticles and the dependence of the plasmon absorption on their composition.* Journal of Physical Chemistry B, 1999. **103**(18): p. 3529-3533.
9. Alam, M.J., M. Tsuji, M. Matsunaga, and D. Yamaguchi, *Shape changes in Au-Ag bimetallic systems involving polygonal Au nanocrystals to spherical Au/Ag alloy and excentered Au core Ag/Au alloy shell particles under oil-bath heating.* CrystEngComm, 2011. **13**(8): p. 2984-2993.
10. Zhang, Q., J. Xie, J.Y. Lee, J. Zhang, and C. Boothroyd, *Synthesis of Ag@AgAu metal core/alloy shell bimetallic nanoparticles with tunable shell compositions by a galvanic replacement reaction.* Small, 2008. **4**(8): p. 1067-1071.
11. Yang, Y., J. Shi, G. Kawamura, and M. Nogami, *Preparation of Au–Ag, Ag–Au core–shell bimetallic nanoparticles for surface-enhanced Raman scattering.* Scripta Materialia, 2008. **58**(10): p. 862-865.
12. Steinbrück, A., A. Csáki, G. Festag, and W. Fritzsche, *Preparation and Optical Characterization of Core–Shell Bimetal Nanoparticles.* Plasmonics, 2006. **1**(1): p. 79-85.
13. Khlebtsov, B.N. and N.G. Khlebtsov, *Plasmon resonance of gold nanoshells: Sensitivity to the local dielectric enviromment - art. no. 616402*, in *Saratov Fall Meeting 2005: Coherent Optics of Ordered and Random Media VI*, D.A.K.N.G. Zimnyakov, Editor. 2006. p. 16402-16402.
14. Kalele, S., S.W. Gosavi, J. Urban, and S.K. Kulkarni, *Nanoshell particles: synthesis, properties and applications.* Current Science, 2006. **91**(8): p. 1038-1052.
15. Cui, Y., B. Ren, J.-L. Yao, R.-A. Gu, and Z.-Q. Tian, *Synthesis of AgcoreAushell Bimetallic Nanoparticles for Immunoassay Based on Surface-Enhanced Raman Spectroscopy.* The Journal of Physical Chemistry B, 2006. **110**(9): p. 4002-4006.
16. Yang, J., J.Y. Lee, and H.-P. Too, *Core−Shell Ag−Au Nanoparticles from Replacement Reaction in Organic Medium.* The Journal of Physical Chemistry B, 2005. **109**(41): p. 19208-19212.
17. Hubenthal, F., T. Ziegler, C. Hendrich, M. Alschinger, and F. Träger, *Tuning the surface plasmon resonance by preparation of gold-core/silver-shell and alloy nanoparticles.*

The European Physical Journal D - Atomic, Molecular, Optical and Plasma Physics, 2005. **34**(1): p. 165-168.

18. Tam, F., C. Moran, and N. Halas, *Geometrical Parameters Controlling Sensitivity of Nanoshell Plasmon Resonances to Changes in Dielectric Environment.* The Journal of Physical Chemistry B, 2004. **108**(45): p. 17290-17294.
19. Grady, N.K., N.J. Halas, and P. Nordlander, *Influence of dielectric function properties on the optical response of plasmon resonant metallic nanoparticles.* Chemical Physics Letters, 2004. **399**(1-3): p. 167-171.
20. Lu, L.H., H.S. Wang, Y.H. Zhou, S.Q. Xi, H.J. Zhang, H.B.W. Jiawen, and B. Zhao, *Seed-mediated growth of large, monodisperse core-shell gold-silver nanoparticles with Ag-like optical properties.* Chemical Communications, 2002(2): p. 144-145.
21. Cao, R. Jin, and C.A. Mirkin, *DNA-Modified Core−Shell Ag/Au Nanoparticles.* J Am Chem Soc, 2001. **123**(32): p. 7961-7962.
22. Wu, H.X., P. Wang, H.L. He, and Y.D. Jin, *Controlled synthesis of porous Ag/Au bimetallic hollow nanoshells with tunable plasmonic and catalytic properties.* Nano Research, 2012. **5**(2): p. 135-144.
23. Stefanie, D., K. Christian, S. Andreas, R. Gunnar, and E. Bernd, *Near- and off-resonant optical limiting properties of gold–silver alloy nanoparticles for intense nanosecond laser pulses.* Journal of Optics, 2012. **14**(7): p. 075203.
24. Zhang, W., L. Huang, J. Zhu, Y. Liu, and J. Wang, *Synthesis of monodisperse Ag–Au alloy nanoparticles with large size by a facile fabrication process.* Materials Chemistry and Physics, 2011. **131**(1-2): p. 136-141.
25. Doria, G., M. Larguinho, J.T. Dias, E. Pereira, R. Franco, and P.V. Baptista, *Gold–silver-alloy nanoprobes for one-pot multiplex DNA detection.* Nanotechnology, 2010. **21**(25): p. 255101.
26. Zhang, Q., J. Xie, J. Liang, and J.Y. Lee, *Synthesis of Monodisperse Ag-Au Alloy Nanoparticles with Independently Tunable Morphology, Composition, Size, and Surface Chemistry and Their 3-D Superlattices.* Advanced Functional Materials, 2009. **19**(9): p. 1387-1398.
27. Wilcoxon, J., *Optical Absorption Properties of Dispersed Gold and Silver Alloy Nanoparticles†.* The Journal of Physical Chemistry B, 2008. **113**(9): p. 2647-2656.
28. Sharma, A.K. and G.J. Mohr, *On the performance of surface plasmon resonance based fibre optic sensor with different bimetallic nanoparticle alloy combinations.* Journal of Physics D: Applied Physics, 2008. **41**(5): p. 055106.
29. Ibanez, F.J. and F.P. Zamborini, *Chemiresistive sensing of volatile organic compounds with films of surfactant-stabilized gold and gold-silver alloy nanoparticles.* Acs Nano, 2008. **2**(8): p. 1543-1552.
30. Zhang, Q., J.Y. Lee, J. Yang, C. Boothroyd, and J. Zhang, *Size and composition tunable Ag-Au alloy nanoparticles by replacement reactions.* Nanotechnology, 2007. **18**(24).
31. Smetana, A.B., K.J. Klabunde, C.M. Sorensen, A.A. Ponce, and B. Mwale, *Low-Temperature Metallic Alloying of Copper and Silver Nanoparticles with Gold Nanoparticles through Digestive Ripening.* The Journal of Physical Chemistry B, 2006. **110**(5): p. 2155-2158.
32. Sharma, A.K. and B.D. Gupta, *Fibre-optic sensor based on surface plasmon resonance with Ag–Au alloy nanoparticle films.* Nanotechnology, 2006. **17**(1): p. 124-131.
33. Lee, K.-S. and M.A. El-Sayed, *Gold and silver nanoparticles in sensing and imaging: Sensitivity of plasmon response to size, shape, and metal composition.* Journal of Physical Chemistry B, 2006. **110**(39): p. 19220-19225.
34. Cortie, M.B. and A.M. McDonagh, *Synthesis and optical properties of hybrid and alloy plasmonic nanoparticles.* Chem Rev, 2011. **111**(6): p. 3713-35.

35. Ma, Y., W. Li, E.C. Cho, Z. Li, T. Yu, J. Zeng, Z. Xie, and Y. Xia, *Au@Ag Core−Shell Nanocubes with Finely Tuned and Well-Controlled Sizes, Shell Thicknesses, and Optical Properties.* Acs Nano, 2010. **4**(11): p. 6725-6734.
36. Mahmoud, M.A. and M.A. El-Sayed, *Gold Nanoframes: Very High Surface Plasmon Fields and Excellent Near-Infrared Sensors.* Journal of American Chemical Society, 2010. **132**(36): p. 12704-12710.
37. Panfilova, E., A. Shirokov, B. Khlebtsov, L. Matora, and N. Khlebtsov, *Multiplexed dot immunoassay using Ag nanocubes, Au/Ag alloy nanoparticles, and Au/Ag nanocages.* Nano Research, 2012. **5**(2): p. 124-134.
38. Wang, H., D.W. Brandl, F. Le, P. Nordlander, and N.J. Halas, *Nanorice: A hybrid plasmonic nanostructure.* Nano Letters, 2006. **6**(4): p. 827-832.
39. Zhao, H., H. Fu, T. Zhao, L. Wang, and T. Tan, *Fabrication of small-sized silver NPs/graphene sheets for high-quality surface-enhanced Raman scattering.* J Colloid Interface Sci, 2012. **375**(1): p. 30-4.
40. Petri, M.V., R.A. Ando, and P.H.C. Camargo, *Tailoring the structure, composition, optical properties and catalytic activity of Ag–Au nanoparticles by the galvanic replacement reaction.* Chemical Physics Letters, 2012. **531**: p. 188-192.
41. dos Santos, M.M., M.J. Queiroz, and P.V. Baptista, *Enhancement of antibiotic effect via gold: silver-alloy nanoparticles.* Journal of Nanoparticle Research, 2012. **14**(5).
42. Sharma, A.K. and G.J. Mohr, *On the Application of Different Bimetallic Alloy Nanoparticle Combinations in Fiber Optic Surface Plasmon Resonance Salinity Sensor and Its Performance Optimization Against Thermal Effects.* Journal of Nanoscience and Nanotechnology, 2010. **10**(5): p. 3145-3154.
43. Sharma, A.K., H.S. Pattanaik, and G.J. Mohr, *On the temperature sensing capability of a fibre optic SPR mechanism based on bimetallic alloy nanoparticles.* Journal of Physics D: Applied Physics, 2009. **42**(4): p. 045104.
44. Wu, Y., G.E. Town, and O. Bang, *Refractive Index Sensing in an All-Solid Twin-Core Photonic Bandgap Fiber.* Sensors Journal, IEEE, 2010. **10**(7): p. 1192-1199.
45. Jain, P.K. and M.A. El-Sayed, *Noble Metal Nanoparticle Pairs: Effect of Medium for Enhanced Nanosensing.* Nano Letters, 2008. **8**(12): p. 4347-4352.
46. Yuan, W., F. Wang, A. Savenko, D.H. Petersen, and O. Bang, *Note: Optical fiber milled by focused ion beam and its application for Fabry-Perot refractive index sensor.* Review of Scientific Instruments, 2011. **82**(7): p. 076103-3.
47. Frosz, M.H., A. Stefani, and O. Bang, *Highly sensitive and simple method for refractive index sensing of liquids in microstructured optical fibers using four-wave mixing.* Opt. Express, 2011. **19**(11): p. 10471-10484.
48. Wu, D.K.C., B.T. Kuhlmey, and B.J. Eggleton, *Ultrasensitive photonic crystal fiber refractive index sensor.* Opt. Lett., 2009. **34**(3): p. 322-324.

LSPR optical fibre sensors based on hollow gold nanostructures

7.1. Introduction

As discussed extensively in Chapter 3, noble metal nanoparticles, especially gold, have shown a strong plasmonic effect at the boundary with a dielectric material and therefore they have been used widely to create localised surface plasmon resonance (LSPR)-based sensors, in which they are immobilised on the surface of an optical fibre. This approach has been used in monitoring the refractive index variation in the medium surrounding the probe or for biological sensing when the nanoparticles are functionalised, for example, with antibodies [1]. The previous research undertaken and discussed respectively in Chapters 4, 5 and 6, has enabled both a detailed investigation and a cross-comparison of the sensitivities of optical fibre sensing probes coated with several different solid structures, including gold nanospheres, gold nanorods and gold-silver alloy nanoparticles. This chapter aims to take such work further and thus to explore ways to enhance the sensitivity of a LSPR sensor by varying the nanostructures from solid to hollow, as theoretically the latter exhibits a stronger plasmonic effect due to the enhanced coupling between the exterior and interior surface fields [2]. In this chapter, the synthesis and fabrication of hollow gold particles will be discussed in detail and the LSPR sensor developed and based on this type of hollow nanostructures has been evaluated, its performance optimised and the results cross-compared with those based on solid nanostructures.

Sun *et al.* [3] first introduced the technique of synthesising gold nanoboxes in a controllable manner in 2002 through sacrificing silver nanostructure templates in a galvanic reaction with a gold precursor. Further reports by the group have included the enhancement of the homogeneity and stability of the products in addition to the creation of other hollow/porous particles such as gold nanocages (AuNCs), nanoframes, porous nanorods, etc. [4-18]. In their reports, the detailed mechanism

of reduction, Galvanic replacement and the de-alloying process in the synthesis was proposed and discussed [13, 14, 19, 20]. Since then, the properties of gold nanocages and their applications in various areas have been explored widely, for example, for cancer imaging and therapy [21, 22], photo-acoustic imaging [23] with a particular focus on biomedical applications [4], but limited research has been reported for sensor development.

Mahmoud *et al.* in 2010 [24] reported the potential of using hollow gold nanoframes for refractive index sensing. In their work, they examined various gold nanoframe structures with different wall length and width, and used a DDA (discrete dipole approximation) calculation to simulate their extinction spectra. Based the theoretical analysis, the highest sensitivity reported was 729 nm/RIU with gold nanoframes of 50 nm wall length and 9 nm wall width, or with an aspect ratio of 5.5. It was also reported that the aspect ratio plays an important role in determining the sensitivity of a LSPR sensor based on gold nanoframes. However, even with the same aspect ratio, there is no direct correlation shown between the device sensitivity and the size of the nanoframes, i.e. the sensitivity demonstrated by bigger frames (e.g. 90 nm wall length and 21.6 nm wall width) is not necessarily to be higher than that of the probes with smaller frames.

In light of the above, this work aims to explore the sensing capacity of hollow gold nanocages by immobilising them on a multimode optical fibre to create a LSPR sensor for refractive index measurement. The sensitivity of the sensor thus created was then determined, based on the experimental data obtained and the result cross-compared with that of those reported and from devices created using different materials and structures, synthesised using different methods.

7.2. Experimental setup

7.2.1. Chemicals and Apparatus

The following chemicals used were purchased from Sigma-Alrich: Polyvinylpyrrolidone (PVP, M_W ~55000), 3-aminopropyl trimethoxysilane (APTMS) 97%, gold chloride hydrates ($HAuCl_4.3H_2O$), silver nitrate ($AgNO_3$), Silver trifluoroacetate (CF_3COOAg), Sodium Sulfide (Na_2S) and Dextrose. Ethylene Glycol (EG), CH_3OH (Analytical Reagent Grade) and H_2SO_4 95% (Laboratory Reagent Grade) were purchased from Fisher Scientific. De-ionized water and H_2O_2 37% solution were purchased from ACROS.

The optical fibre was purchased from Thorlab, of type BFH37-600, with core diameter of 600 µm; the light source was a halogen light source, type HL-2000-FHSA obtained from Mikropack and the spectrometer used was Maya type 2000PRO, obtained from Ocean Optics.

7.2.2. Synthesis of Hollow Gold Nanocages

Gold nanocages were prepared by a 2-step method reported by Xia *et al.* [3, 10, 15, 19]. Firstly, a template silver nanocube (AgNCs) was synthesised by polyol reduction of silver trifluoroacetate under the protective polymer PVP [25]. In a typical preparation, 5 mL of EG was boiled in a 25 mL round bottom flask and stirred at 150 ^oC for 1 hour. Then 70 µL of Na_2S solution (3mM in EG) was quickly added. 2 min later, 0.5 mL HCl (3mM in EG) was injected into the reaction flask and this was immediately followed by adding 1.5 mL PVP (20 mg/mL in EG). After 2 min, 0.5 mL solution of CF_3COOAg (282mM in EG) was added. Throughout the reaction, a stable stirring speed was maintained at 450 rpm. The reaction stopped after 60 min, resulting in a silky white coloured solution. The acquired solution was then cleaned with acetone and deionised water several times with centrifugation to wash out the excess PVP and EG. Finally, the silver nanocubes obtained were stored in 4 mL of deionised water and kept in the dark for further use.

Secondly, silver nanocube template was used to prepare hollow gold nanocages via galvanic reaction with $HAuCl_4$ [10]. In a typical synthesis, 5 mL of PVP solution in deionised water (1 mg/mL) was prepared and brought to mild boiling in a 25 mL round bottom flask, equipped with a condenser and a stir bar. 200 µL of as-prepared silver nanocubes was added into the flask. After 10 min, 1.25 mL $HAuCl_4$ (200 mM in deionised water) was introduced into the flask by a syringe pump (KDScientific, KDS100) at the rate of 0.5 mL/min. The reaction was completed after 10 min and then left to cool down slowly to room temperature. During the reaction period, the liquid was stirred vigorously. Afterwards, the final solution was washed with acetone and deionised water several times by centrifugation, and the final product was redispersed in deionised water for further use.

7.2.3. Sensor probe preparation and system setup

Figure 7.1: Photograph of a sensing probe created, with its size comparing with a 5 pence coin.

The fibre probes are treated with a series of cleaning, silanisation and curing steps using the same sensor fabrication protocol reported in previous chapters. In a typical preparation, two ends of a 20 cm optical fibre of 600 µm diameter was firstly polished using different polishing papers (from Thorlabs, using types 5 µm, 3 µm, 1 µm and 0.3 µm, respectively). Following that, one end was stripped of its jacket and then decladded. To facilitate the next step sensor fabrication, the fibre was further treated with Piranha solution (70% H_2SO_4, 30% H_2O_2) for 30 min, and then washed several times by using distilled water before being oven-cured at 120 ^oC for 1 hour. The fibre then was silanised with a solution of 10% APTMS in methanol over 4 hours, sonicated thoroughly 3 times with methanol and finally treated in an oven, overnight at 80 ^oC. The probes thus prepared were then dip-coated with the 'as-prepared' solutions of gold nanocages for 6 hours. Subsequently, they were coated with a silver mirror and dried under a gentle draught of nitrogen gas, to form the reflective probes required. They were then stored in a dark box until they were required for

evaluation. Figure 7.1 shows a photograph of a prepared LSPR probe, coated with gold nanocages and used in this work.

The sensor system configuration that was employed has previously been described in detail in previous chapters and is shown again schematically in Fig. 7.2. In summary, the sensing area was illuminated by using light from a broadband light source, a halogen lamp, via a 1x2 fibre coupler. The silver mirror coated on the end surface of the fibre enabled the modulated light due to the interaction between the LSPR probe and the solution in the fibre to be reflected back and via the 1x2 coupler used to the mini-spectrometer for analysis. That spectrometer was connected to a computer so that the reflected absorbance spectra could be recorded in real-time, when the probe was submerged in solutions with known yet different refractive indices for calibration.

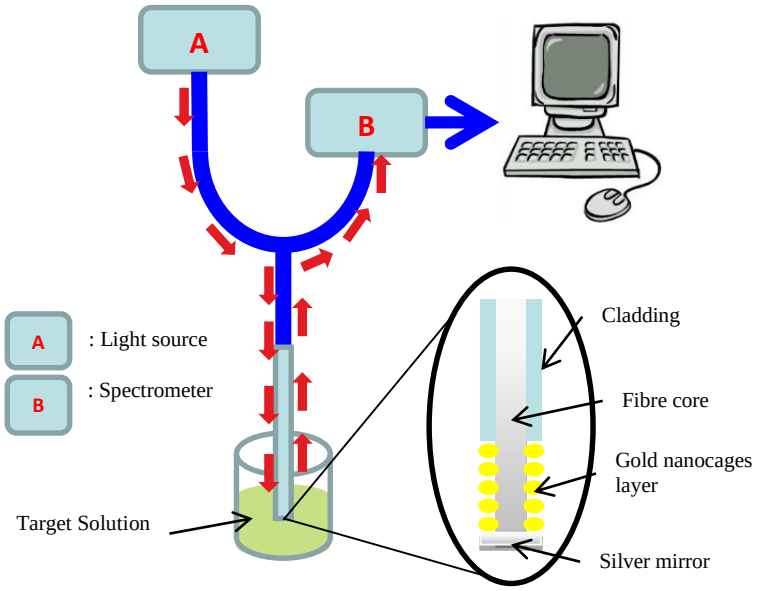

Figure 7.2: Schematic illustration of a LSPR sensor system

7.2.4. Characterisation of silver and gold nanoparticles solution

TEM images have been taken by JEM-1010 Electron Microscope at 80kV and UV-Vis spectra have been acquired by a Perkin Elmer spectrometer Lambda 25.

7.3. Results and discussions

7.3.1. Silver nanocubes and gold nanocages synthesis

As described above, a two-step method reported by Xia *et al.* [3, 10, 15, 19] is used in this work for the synthesis of gold nanocages which involves two main processes: firstly, forming silver nanocubes and secondly, creating gold hollow structures.

a) Synthesis of silver nanocubes

Silver nanocubes have been reported to be synthesised using several different methods, including water-based reduction from metal salts by HTAB [26], seed-mediated synthesis [17] and polyol reduction [3, 27]. Among those, polyol reduction provides the most reliable results in term of monodispersity, yield and stability. $AgNO_3$ as precursor, PVP as surfactant, HCl and Na_2S as catalyst are the main components in this recipe. All solutions were prepared in Ethylene Glycol (EG), and essentially, minimum amount of H_2O should be included in the synthesis.

The process requires a strict control of reaction parameters, such as temperatures, stirring rate, stir bar's size as well as reaction time [10]. A slight modification of those parameters could result in a completely different morphology of silver cubes. At 150 ^oC, Ag^+ would be reduced by EG, forming silver seed. PVP presented in the solution has higher affinity toward <fcc> face, therefore, the binding would be more favourable towards this face. In growing process, more Ag would be deposited onto these remaining two faces, hence creating nanocube structure [27]. It is also important that the ratio of PVP/$AgNO_3$ has to be lower than 1.5, and the final concentration of $AgNO_3$ must also be high (from 0.125M to 0.25M) [3]. Based on the seed's morphology (i.e. cubooctahedron, decahedral or quasi-spherical), different types of nanostructures could be synthesised, including nanocube, nanorods or nanosphere. More detailed discussion of this nucleation and growth steps for shape control could be found in literature [27].

In reality, it is important but really hard to control the reaction in order to create the desired shape and size of nanostructures. Even following exactly the same protocol, step-by-step, as that proposed by Skarabalak *et al.* [10], the first several attempts by

the author failed. The synthesised particles were shown either spherical or a mixture of different shapes including rods, spheres, cubes, as shown in Fig. 7.3. This is due to the lack of control in both the initial prepared PVP/$AgNO_3$ and its ratio when the reaction occurs. Given the fact that PVP was already in the reaction flask, the ratio of PVP/$AgNO_3$ is required to be kept high.

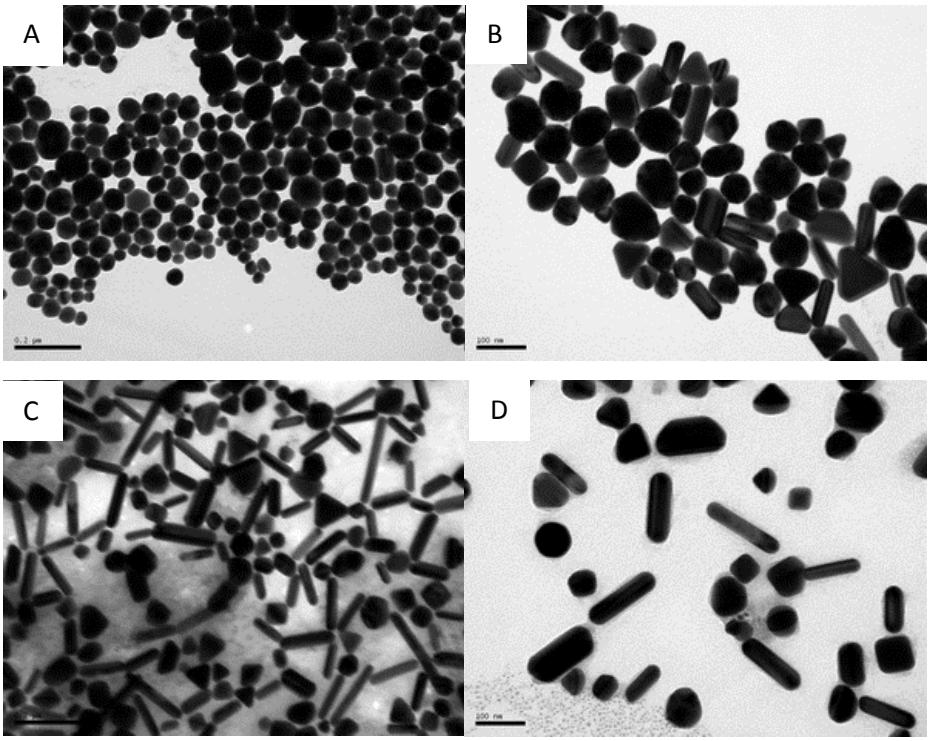

Figure 7.3: Some unsuccessfully synthesised silver nanocubes
A) nanospheres, B,C,D) Mixtures of spheres, rods, cubes, triangles.

In 2010, Zhang et al [17, 25] proposed a new method to achieve a better control of the size and shape of silver nanocubes. By using CF_3COOAg instead of $AgNO_3$, the reaction rate was reported to be slower, hence making it easier to control over nuclei and growth mechanisms. It was also reported that both the concentration and presence of NaSH and HCl are critical in the formation of the cubes as the absence of any of those could lead to other morphology of silver particles. Longer reaction time (approximately 90 min) has helped a proper reaction control, as this has made regular checking and comparison of absorbance spectra of the product being possible during the reaction period. As expected, a quality batch of silver nanocubes with monodispersity (as seen in TEM image in Fig. 7.4) has been successfully synthesised using this approach.

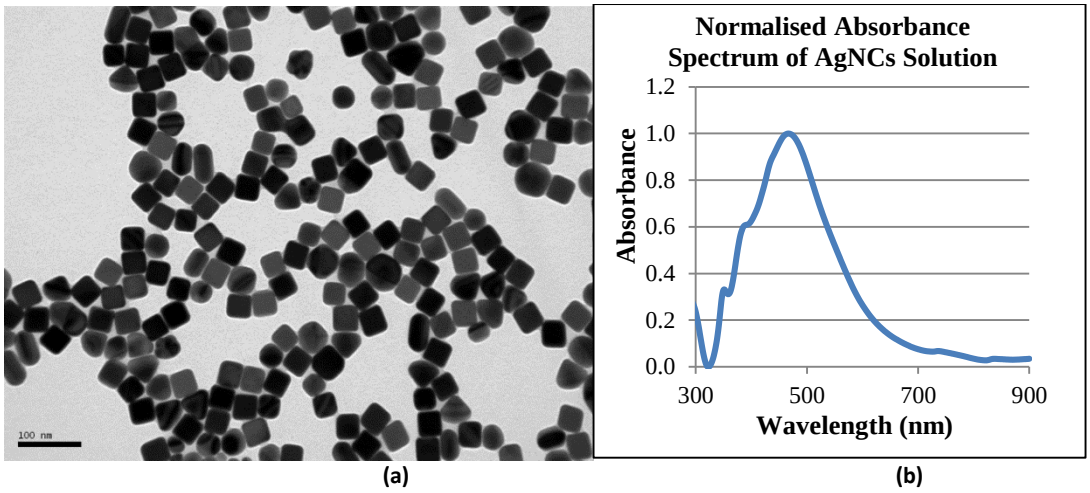

Figure 7.4: (a) TEM image and (b) absorbance spectrum of AgNCs prepared with CF_3COOAg

The absorbance spectrum of the silver nanocubes was characterised by three distinctive peaks at wavelengths of 351 nm, 400 nm and 467 nm (Fig. 7.4b) respectively. As predicted by theory, these three peaks were resulted from out-of-plane quadrupole, in-plane quadrupole and in-plane dipole plasmon resonance modes respectively [27]. The morphology of silver nanoparticles was also characterised by transmission electron microscopy (TEM). In this work, an analysis and subsequent statistical calculation undertaken using over 100 particles from the TEM images confirmed the mean length of the silver nanocubes produced to be 37.3 ± 5.1 nm. It is also important to note that further enlargement of the cubes was made possible either by increasing the reaction time [25], or by using seed-growth method [17]. The solution of AgNCs when left in storage was shown to be stable for several months after synthesis.

b) Gold nanocages formation

The silver nanocubes were used as a sacrificial template in titration with $HAuCl_4$ to create the hollow gold nanocages [14] where, via a galvanic reaction, the gold atoms gradually induced pores in the facets of the silver nanocube and thus created hollow gold/silver alloy particles. Subsequently, gold atoms are deposited continually on the wall of the cube, resulting in a gold nanocage with a hollow cube shape. By increasing the amount of $HAuCl_4$, the main absorption peak was continuously red-shifted, this varying from a peak wavelength of 497 nm (AuNC1), to 594 nm (AuNC2) and then to

737 nm (AuNC3), as shown in Fig. 7.5. This indicates the continous development of the hollow nature of the nanocages, as illustrated in Fig. 7.6, increasing from AuNC1 to AuNC3, with the increasing amount of $HAuCl_4$ used. However, there is a limit in that a further increase of the amount of $HAuCl_4$ used leads to the destruction of the cubes, resulting in groups of small particles, as seen in the image of AuNC4 (shown in Fig. 7.6D). When this happened to the cubes, the corresponding absorbance peak was found to be dramatically blue-shifted, back to a wavelength of 524 nm and close to the position where the absorbance peak of gold nanoparticles occurs (at a wavelength of around 520 nm).

Due to the nature of the galvanic replacement reaction used to form cavities on the silver nanocubes, the final solutions of gold nanocages, when analysed, showed that there were some irregular shapes formed other than the cages themselves. This could occur (forming the irregular shapes) by the replacement reaction having taken place on the sharp corners or on the edges, rather than on the faces of the silver nanocubes. This could be the reason why the absorbance spectra of the synthesised gold nanocages were quite broad. The water absorbance peak was seen at around a wavelength of 970 nm in the absorbance spectra of all the solutions.

It was noted that the size of the gold nanocages formed was usually larger than that of their precursor silver nanocubes. This observation has not been explored further in this thesis but more details about the alloying and dealloying mechanisms can be found in literature e.g. by Yugang Sun and Younan Xia [19].

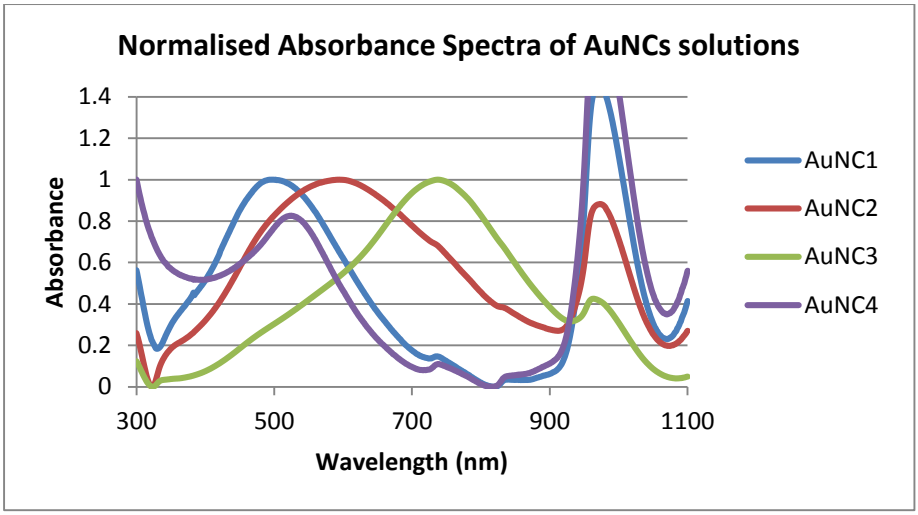

Figure 7.5: Normalised absorbance spectra of different AuNCs solutions

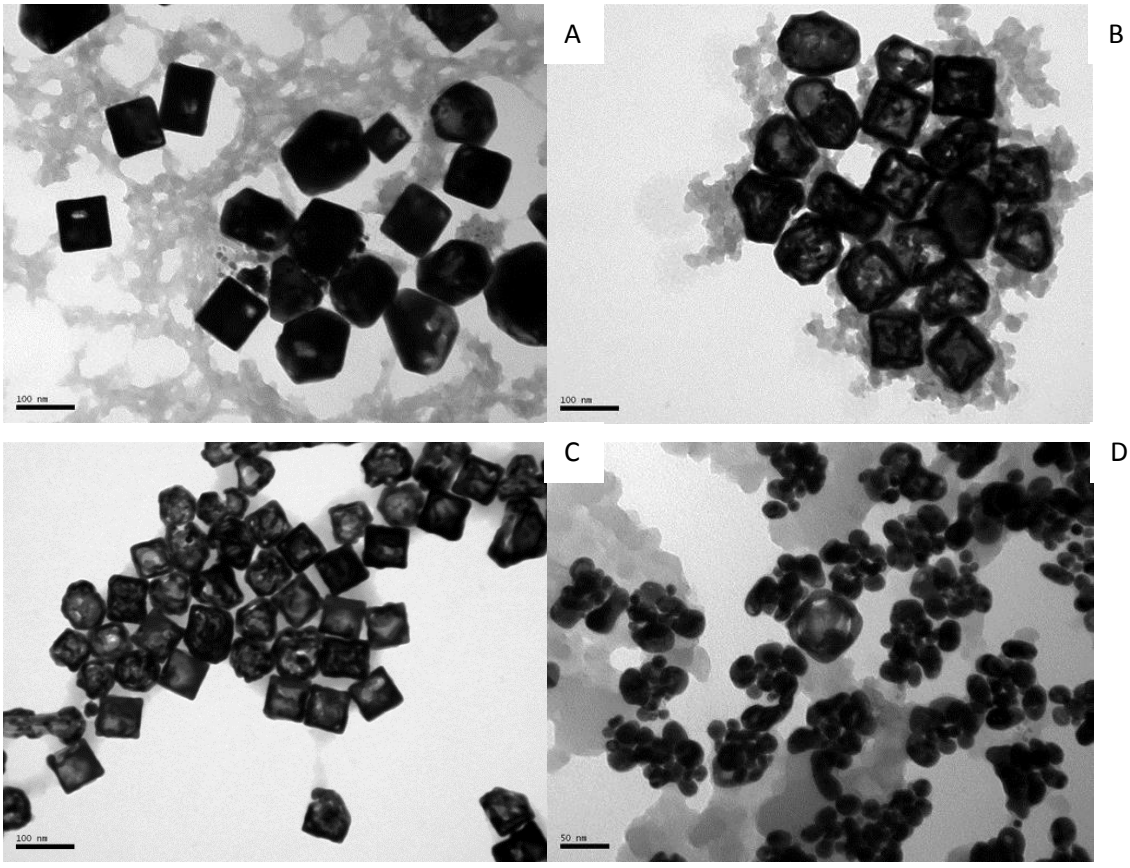

Figure 7.6: TEM Images of different AuNCs by different amount of $HAuCl_4$

A) AuNC1 – 0.75 mL – B) AuNC2 – 1.0 mL – C) AuNC3 1.5 mL – D) AuNC4 – 3 mL

7.3.2. Experimental tests and results

The AuNCs formed, as discussed above (AuNC1 – AuNC4), were subsequently coated onto four pre-treated optical fibre samples to create four types of LSPR sensor probes (labelled as Probes 1 – 4), prior to their intensive tests being carried out on their use for refractive index measurement. With each type of AuNCs, three probes were prepared using the same procedure to enable the evaluation of the reproducibility of the sensors produced (labelled as Trials 1, 2 and 3). In the experiments carried out, eight different solvents (with different yet known values of refractive index from 1.333 to 1.404) were used in the measurements carried out. The sensitivity values of the devices created were calculated (and specified in units of wavelength shift per refractive index unit), as shown in Equation 7.1, with the calculation undertaken using Origin software.

$$S = \frac{d\lambda_{max}}{dn} \qquad \text{(Eq. 7.1)}$$

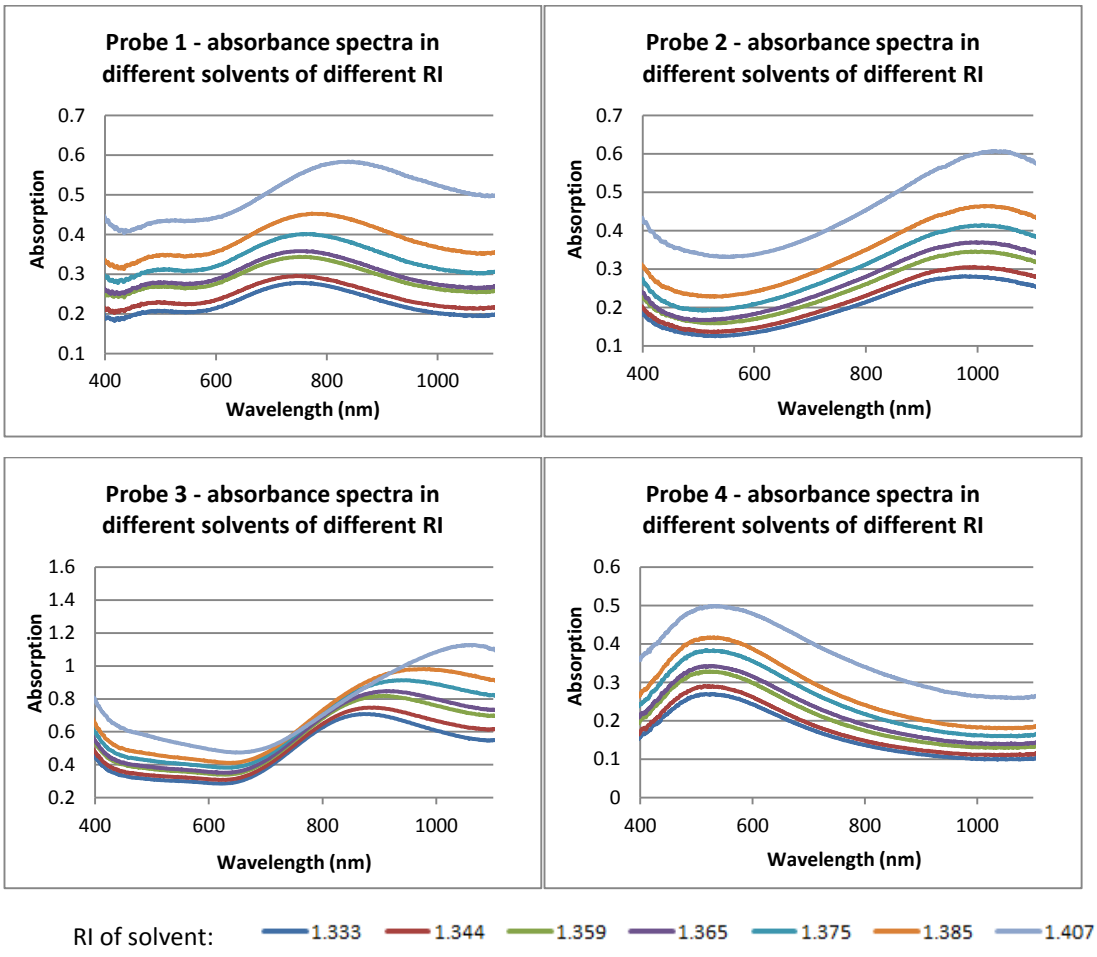

Figure 7.7: Evaluation of the performance of the probes created – measurement of a series of absorbance spectra in different solvents, each representing different values of RI (colour coded and indicated above)

Illustrations of representative absorbance spectra from 4 different probes (Probes 1 to 4) evaluated using different solvents (representing RI values from 1.333 to 1.407) are shown in Fig. 7.7. From the data, the sensitivities of these four probes, coated with different AuNC samples, are presented in Fig. 7.8 and it is useful to note that a high level of precision has been achieved throughout the whole course of the experiment. An analysis of the data has shown that the highest sensitivity was obtained from AuNC3 coated sensor (Probe 3), with a mean value of 1933 ± 108.2 nm/RIU. The values of sensitivity determined for samples of AuNC1 (Probe 1), AuNC2 (Probe 2) and AuNC4 (Probe 4), each coated to create appropriate optical fibre sensors, is 783.9 ± 12.0 nm/RIU, 980.4 ± 77.0 nm/RIU and 415.5 ± 16.5 nm/RIU, respectively. The data reported show that the sensitivity changes with the change in morphology of the particles (as can be seen from the images inset in Fig. 7.8). With the increase of the degree of hollowness of the structures, the sensitivity of the sensors created has shown a significant increase from 784 nm/RIU to 1933 nm/RIU. However when the nanocages were deconstructed (as in the case where AuNC4 was used), the coupling effect between the exterior and the interior plasmonic fields ceased to exist and this, as a consequence, was seen to lead to a dramatic drop in the sensitivity of the probe formed using this material (Probe 4).

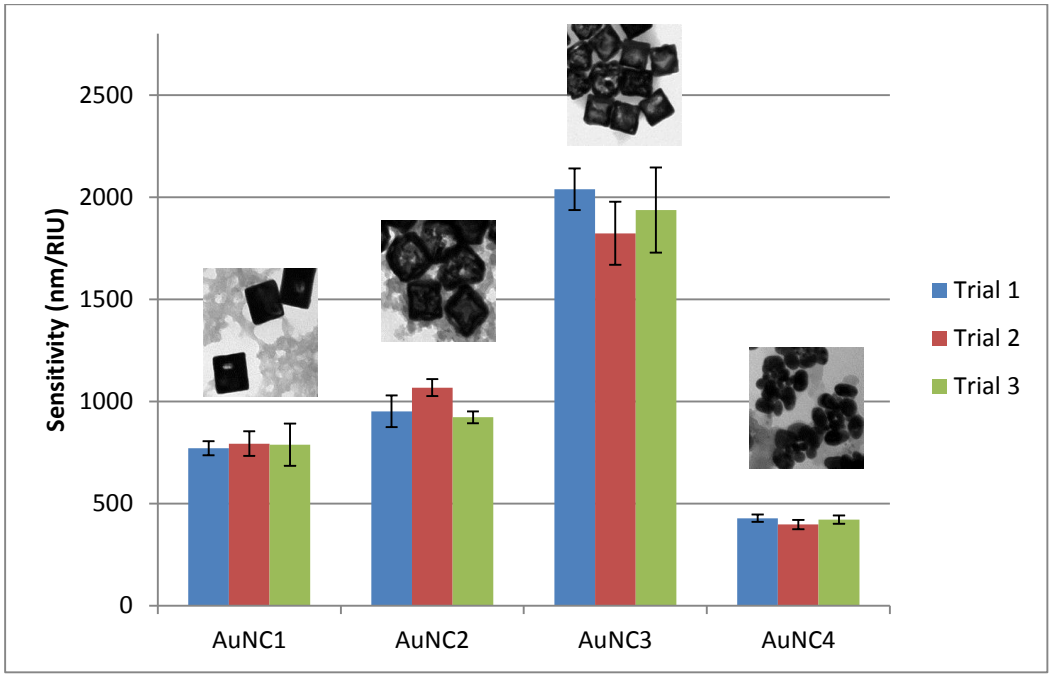

Figure 7.8: Sensitivity comparison between probes

It is important to consider the results from these sensors, in light of both previous work by the authors and other published data. Thus compared to those LSPR sensors reported earlier either by the authors or by the other researchers, the LSPR sensors based on hollow particles have demonstrated better performance and sensitivity. For example, the sensitivity has been shown to be approximately 4.5 times greater than that based on gold nanoparticles of similar size (40nm) (comparing to a sensitivity figure of 418 nm/RIU for 40 nm AuNPs to 1933 nm/RIU for the AuNC3 coated probe) [28]. Further, considering the reported sensitivity to RI of the LSPR sensors based on gold nanorods, the use of gold-silver alloy particles has not yet achieved a comparable sensitivity to that from AuNCs either. Even the low sensitivity demonstrated by Probe 4 (at 415 nm/RIU) is in fact approximately 50% more sensitive than that of 20 nm AuNP-coated sensors (at 266 nm/RIU). This enhanced sensitivity can be explained by consideration of the underpinning theory through the inter-particle interaction based on the work reported by Jain *et al.* [29] for gold nanospherical particles. A smaller interparticle distance would greatly enhance the plasmonic coupling effect, which therefore would produce a higher value of sensitivity. In the case of AuNC4, the cage structure was deconstructed with small parts still being held together by the surfactant. Therefore, the plasmonic coupling effect could still occur and this would result in a higher sensitivity, in comparison to using similar solid nanospherical particles.

A graphical summary of the experimental results obtained in this work, together with those reported in the literature [28, 30-32], is shown in Fig. 7.9, in which the sensitivity values of the probes were plotted against the plasmonic peak of the nano-materials in their original solutions. The data for the gold nanorods have been adapted from the experiments reported by Cao *et al.* [30, 33] and discussed in Chapter 5. Particles of the same type were grouped together and the sensitivity variation trend of each group can be clearly observed and cross-compared to that of the other groups. Within each group, it was noticed that the increase of the red-shift of the absorbance peak of the material was related to the increase of the sensitivity of its corresponding sensor, although the magnitude of increase was different for different types of materials. Mayer *et al.* [34] have stated that the position of the

plasmonic peak, the sensitivity, and the materials size and type all play important roles and have demonstrated a more complicated correlation of the effects of these different parameters.

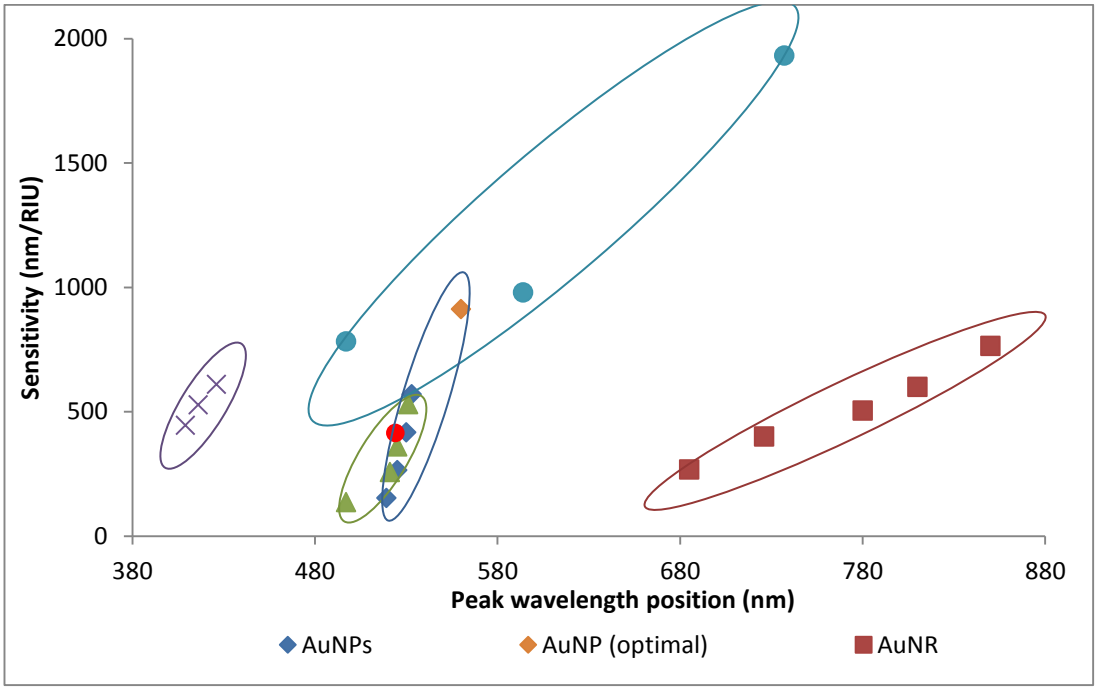

Figure 7.9: Plot of sensitivity vs. plasmonic peak of different gold nanostructures.
AuNPs: Gold nanospherical particles; AuNRs: Gold nanorods; AuNCs: Gold nanocages particles;
A25, A75 Alloy: Gold/silver alloy nanospherical particles with 25% and 75% Ag content, respectively.

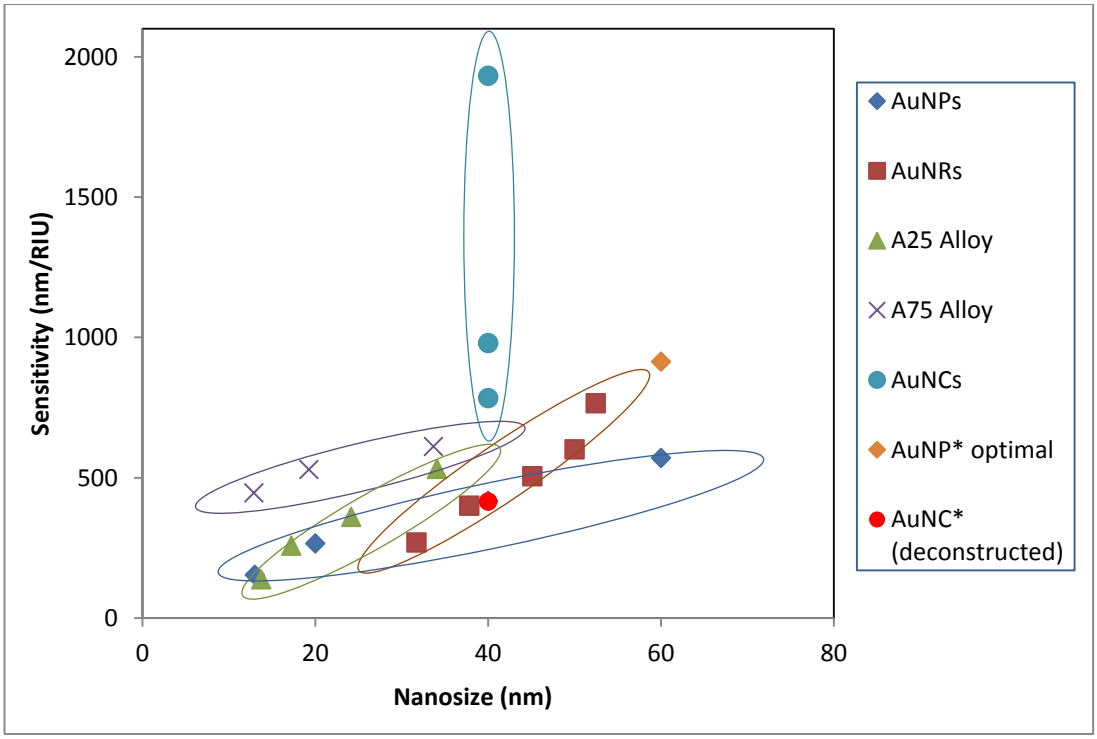

Figure 7.10: Plot of sensitivity vs. size of different gold nanostructures

A comprehensive summary of the corresponding sensitivities of the sensor probes created, as a function of the particle size used, is shown in Fig. 7.10. In this illustration, all the AuNCs samples used are illustrated in the figure on the basis of their size being the same size of the original cube (40 nm). The size of the nanorods was represented by the length of the rods, just for the ease of comparison.

Mahmoud *et al.* [24] has summarised the sensitivity of the different types of gold nanoparticles considered, based on the published data, showing a sensitivity of 44 nm/RIU with gold nanospheres, 150-285 nm/RIU with gold nanorods, 408 nm/RIU with hollow gold nanocages and 620 nm/RIU with gold nanoframes [24]. Compared to those data published in the literature and listed below in Table 7.1, the LSPR sensors based on AuNCs reported in this work have shown a superior performance, showing a higher value of sensitivity, this being in the range of ***783 - 1933 nm/RIU***.

Table 7.1: Sensitivity comparison of some results in literature

Nanostructure	Sensitivity	Ref.
Gold colloidal nanoparticles	*071 nm/RIU*	*[35]*
Gold nano rods	*650 nm/RIU*	*[36]*
Hollow gold nano shell	*408 nm/RIU*	*[35]*
Arrays of gold nanodisk	*167 nm/RIU* *327 nm/RIU*	*[37]*
Gold nanodisk trimers	*170 nm/RIU* *374 nm/RIU*	*[38]*
Gold nanorings	*880 nm/RIU*	*[39]*
Gold nanoring trimers	*345 nm/RIU*	*[38]*
Nanocubes	*165 nm/RIU*	*[40]*
Nanocrescents	*879 nm/RIU*	*[41]*
Nanostars	*218 nm/RIU*	*[42]*
Nanocross	*710 nm/RIU*	*[43]*
Nanobar	*1,000 nm/RIU*	
Double nanopillars with nanogap	*642 nm/RIU* *1,056 nm/RIU*	*[44]*
Nanopillar arrays	*675 nm/RIU*	*[45]*
This thesis' experiments		
Gold nanospheres	***154 - 914 nm/RIU***	***[28]***
13nm diameter	***154 nm/RIU***	
20nm diameter	***266 nm/RIU***	
40nm diameter	***418 nm/RIU***	
60nm diameter	***914 nm/RIU***	
Gold nanorods	***601 nm/RIU***	***[31, 33]***
Gold/silver nanoalloys	***131- 625 nm/RIU***	***[32]***

A25 alloy, 13nm diameter	***131 nm/RIU***
A25 alloy, 17nm diameter	***258 nm/RIU***
A25 alloy, 24nm diameter	***361 nm/RIU***
A25 alloy, 34nm diameter	***531 nm/RIU***
A75 alloy, 13nm diameter	***477 nm/RIU***
A75 alloy, 19nm diameter	***502 nm/RIU***
A75 alloy, 33nm diameter	***625 nm/RIU***
Gold nanocages	
AuNC1	***783 nm/RIU***
AuNC2	***980 nm/RIU***
AuNC3	***1933 nm/RIU***

7.4. Conclusions

In this Chapter, an intensive study of the potential of hollow nanostructures in gold has been carried out with extensive data reported, together with a cross-comparison to the previous work of the authors and literature data. Initially the required gold hollow nanostructures were successfully synthesised with controllable shapes and hollowness for a planned series of experiments using optical fibre sensor probes. They have been coated subsequently onto optical fibres to create LSPR sensors which were used for a series of refractive index measurements. An important result of the work done was the observation of a much higher sensitivity of these optical fibre probes, compared to the other types of LSPR sensors reported, having demonstrated values of sensitivity of up to 1933 nm/RIU. The key advantage of using the techniques reported is that the sensitivity value of the sensor thus created is controllable, showing an increase with the hollowness by changing systematically the aspect ratio, i.e. increasing the length of the cage wall and decreasing its width. A highly effective sensing system thus has been discussed based on these structures and demonstrated for RI measurement. However, the approach described in this work can be expanded for bio-sensing as the metal layer could be further functionalised for specific bio-agent recognition. The high sensitivity of the probes demonstrated in this work (compared to literature values) could also enable the sensor to be used in a direct sensing manner, without using the sample preparation and concentration step. Thus with a relatively short time needed for fabrication (a total time of preparation of less than 12 hours was used), the probes developed are easy to prepare. Further, they are reusable as they can conveniently be cleaned for such reuse through several normal washing cycles with water and solvent. Moreover, multimode optical fibres can be configured and are relatively cost-effective, allowing for volume production and relatively easy disposal of used probes.

Future research is needed to enhance further the sensing capacity, possibly by increasing the size or the hollowness of the cage. It is also noted that the sensitivity could be enhanced by immobilizing the gold nanocages onto optical fibre substrates of different configurations (e.g. tapered fibre or side-polished fibre).

7.5. References

1. Oldenburg, S.J., R.D. Averitt, S.L. Westcott, and N.J. Halas, *Nanoengineering of optical resonances.* Chemical Physics Letters, 1998. **288**(2–4): p. 243-247.
2. Mahmoud, M.A., B. Snyder, and M.A. El-Sayed, *Surface Plasmon Fields and Coupling in the Hollow Gold Nanoparticles and Surface-Enhanced Raman Spectroscopy. Theory and Experiment†.* The Journal of Physical Chemistry C, 2010. **114**(16): p. 7436-7443.
3. Sun, Y. and Y. Xia, *Shape-Controlled Synthesis of Gold and Silver Nanoparticles.* Science, 2002. **298**(5601): p. 2176-2179.
4. Chen, J., B. Wiley, Z.Y. Li, D. Campbell, F. Saeki, H. Cang, L. Au, J. Lee, X. Li, and Y. Xia, *Gold Nanocages: Engineering Their Structure for Biomedical Applications.* Advanced Materials, 2005. **17**(18): p. 2255-2261.
5. Liang, H.-P., L.-J. Wan, C.-L. Bai, and L. Jiang, *Gold Hollow Nanospheres: Tunable Surface Plasmon Resonance Controlled by Interior-Cavity Sizes.* The Journal of Physical Chemistry B, 2005. **109**(16): p. 7795-7800.
6. Chen, J., J.M. McLellan, A. Siekkinen, Y. Xiong, Z.-Y. Li, and Y. Xia, *Facile Synthesis of Gold−Silver Nanocages with Controllable Pores on the Surface.* J Am Chem Soc, 2006. **128**(46): p. 14776-14777.
7. Hu, M., J. Chen, Z.-Y. Li, L. Au, G.V. Hartland, X. Li, M. Marquez, and Y. Xia, *Gold nanostructures: engineering their plasmonic properties for biomedical applications.* Chemical Society Reviews, 2006. **35**(11): p. 1084-1094.
8. Schwartzberg, A.M., T.Y. Olson, C.E. Talley, and J.Z. Zhang, *Synthesis, Characterization, and Tunable Optical Properties of Hollow Gold Nanospheres.* The Journal of Physical Chemistry B, 2006. **110**(40): p. 19935-19944.
9. Lu, X., L. Au, J. McLellan, Z.-Y. Li, M. Marquez, and Y. Xia, *Fabrication of Cubic Nanocages and Nanoframes by Dealloying Au/Ag Alloy Nanoboxes with an Aqueous Etchant Based on Fe(NO3)3 or NH4OH.* Nano Letters, 2007. **7**(6): p. 1764-1769.
10. Skrabalak, S.E., L. Au, X. Li, and Y. Xia, *Facile synthesis of Ag nanocubes and Au nanocages.* Nat Protoc, 2007. **2**(9): p. 2182-90.
11. Wiley, B.J., Y. Chen, J.M. McLellan, Y. Xiong, Z.-Y. Li, D. Ginger, and Y. Xia, *Synthesis and optical properties of silver nanobars and nanorice.* Nano Letters, 2007. **7**(4): p. 1032-1036.
12. Au, L., Y. Chen, F. Zhou, P. Camargo, B. Lim, Z.-Y. Li, D. Ginger, and Y. Xia, *Synthesis and optical properties of cubic gold nanoframes.* Nano Research, 2008. **1**(6): p. 441-449.
13. Rycenga, M., J.M. McLellan, and Y. Xia, *Controlling the Assembly of Silver Nanocubes through Selective Functionalization of Their Faces.* Advanced Materials, 2008. **20**(12): p. 2416-2420.
14. Skrabalak, S.E., J. Chen, Y. Sun, X. Lu, L. Au, C.M. Cobley, and Y. Xia, *Gold Nanocages: Synthesis, Properties, and Applications.* Accounts of Chemical Research, 2008. **41**(12): p. 1587-1595.
15. Lu, X., M. Rycenga, S.E. Skrabalak, B. Wiley, and Y. Xia, *Chemical Synthesis of Novel Plasmonic Nanoparticles.* Annual Review of Physical Chemistry, 2009. **60**(1): p. 167-192.
16. Yang, Z., H. Chu, Z. Jin, W. Zhou, and Y. Li, *Preparation and properties of CdS/Au composite nanorods and hollow Au tubes.* Chinese Science Bulletin, 2010. **55**(10): p. 921-926.

17. Zhang, Q., W. Li, C. Moran, J. Zeng, J. Chen, L.-P. Wen, and Y. Xia, *Seed-Mediated Synthesis of Ag Nanocubes with Controllable Edge Lengths in the Range of 30–200 nm and Comparison of Their Optical Properties.* Journal of American Chemical Society, 2010. **132**(32): p. 11372-11378.
18. Rycenga, M., C.M. Cobley, J. Zeng, W. Li, C.H. Moran, Q. Zhang, D. Qin, and Y. Xia, *Controlling the Synthesis and Assembly of Silver Nanostructures for Plasmonic Applications.* Chemical Reviews, 2011. **111**(6): p. 3669-3712.
19. Sun, Y. and Y. Xia, *Alloying and Dealloying Processes Involved in the Preparation of Metal Nanoshells through a Galvanic Replacement Reaction.* Nano Letters, 2003. **3**(11): p. 1569-1572.
20. Sun, Y. and Y. Xia, *Mechanistic Study on the Replacement Reaction between Silver Nanostructures and Chloroauric Acid in Aqueous Medium.* J Am Chem Soc, 2004. **126**(12): p. 3892-3901.
21. Au, L., J. Chen, L.V. Wang, and Y. Xia, *Gold Nanocages for Cancer Imaging and Therapy Cancer Nanotechnology*, S.R. Grobmyer and B.M. Moudgil, Editors. 2010, Humana Press. p. 83-99.
22. Chen, J., M. Yang, Q. Zhang, E.C. Cho, C.M. Cobley, C. Kim, C. Glaus, L.V. Wang, M.J. Welch, and Y. Xia, *Gold Nanocages: A Novel Class of Multifunctional Nanomaterials for Theranostic Applications.* Advanced Functional Materials, 2010. **20**(21): p. 3684-3694.
23. Li, W., P.K. Brown, L.V. Wang, and Y. Xia, *Gold nanocages as contrast agents for photoacoustic imaging.* Contrast Media & Molecular Imaging, 2011. **6**(5): p. 370-377.
24. Mahmoud, M.A. and M.A. El-Sayed, *Gold Nanoframes: Very High Surface Plasmon Fields and Excellent Near-Infrared Sensors.* Journal of American Chemical Society, 2010. **132**(36): p. 12704-12710.
25. Zhang, Q., W. Li, L.-P. Wen, J. Chen, and Y. Xia, *Facile Synthesis of Ag Nanocubes of 30 to 70 nm in Edge Length with CF3COOAg as a Precursor.* Chemistry – A European Journal, 2010. **16**(33): p. 10234-10239.
26. Yu, D. and V.W.-W. Yam, *Controlled Synthesis of Monodisperse Silver Nanocubes in Water.* J Am Chem Soc, 2004. **126**(41): p. 13200-13201.
27. Wiley, B., Y. Sun, B. Mayers, and Y. Xia, *Shape-Controlled Synthesis of Metal Nanostructures: The Case of Silver.* Chemistry – A European Journal, 2005. **11**(2): p. 454-463.
28. Tu, M.H., T. Sun, and K.T.V. Grattan, *Optimization of gold-nanoparticle-based optical fibre surface plasmon resonance (SPR)-based sensors.* Sensors and Actuators B: Chemical, 2012. **164**(1): p. 43-53.
29. Jain, P.K. and M.A. El-Sayed, *Noble Metal Nanoparticle Pairs: Effect of Medium for Enhanced Nanosensing.* Nano Letters, 2008. **8**(12): p. 4347-4352.
30. Cao, J., E.K. Galbraith, T. Sun, and K.T.V. Grattan, *Effective surface modification of gold nanorods for localized surface plasmon resonance-based biosensors.* Sensors and Actuators B: Chemical, 2012. **169**: p. 360-367.
31. Cao, J., M.H. Tu, T. Sun, and K.T.V. Grattan, *Wavelength-based localized surface plasmon resonance optical fiber biosensor.* Sensors and Actuators B: Chemical, 2013. **181**(0): p. 611-619.
32. Tu, H., T. Sun, and K.T.V. Grattan, *SPR-Based Optical Fiber Sensors Using Gold/Silver Alloy Particles as the Active Sensing Material.* Sensors Journal, IEEE, 2013. **13**(6): p. 2192-2199.
33. Cao, J., E.K. Galbraith, T. Sun, and K.T.V. Grattan, *Cross-Comparison of Surface Plasmon Resonance-Based Optical Fiber Sensors With Different Coating Structures.* IEEE Sensors Journal, 2012. **12**(7): p. 2355-2361.

34. Mayer, K.M. and J.H. Hafner, *Localized Surface Plasmon Resonance Sensors.* Chemical Reviews, 2011. **111**(6): p. 3828-3857.
35. Sun, Y.G. and Y.N. Xia, *Increased sensitivity of surface plasmon resonance of gold nanoshells compared to that of gold solid colloids in response to environmental changes.* Analytical Chemistry, 2002. **74**(20): p. 5297-5305.
36. Lee, K.-S. and M.A. El-Sayed, *Gold and silver nanoparticles in sensing and imaging: Sensitivity of plasmon response to size, shape, and metal composition.* Journal of Physical Chemistry B, 2006. **110**(39): p. 19220-19225.
37. Lee, S.-W., K.-S. Lee, J. Ahn, J.-J. Lee, M.-G. Kim, and Y.-B. Shin, *Highly Sensitive Biosensing Using Arrays of Plasmonic Au Nanodisks Realized by Nanoimprint Lithography.* ACS Nano, 2011. **5**(2): p. 897-904.
38. Lin, V.K., S.L. Teo, R. Marty, A. Arbouet, C. Girard, E. Alarcon-Llado, S.H. Liu, M.Y. Han, S. Tripathy, and A. Mlayah, *Dual wavelength sensing based on interacting gold nanodisk trimers.* Nanotechnology, 2010. **21**(30).
39. Larsson, E.M., J. Alegret, M. Kall, and D.S. Sutherland, *Sensing characteristics of NIR localized surface plasmon resonances in gold nanorings for application as ultrasensitive biosensors.* Nano Letters, 2007. **7**(5): p. 1256-1263.
40. Galush, W.J., S.A. Shelby, M.J. Mulvihill, A. Tao, P. Yang, and J.T. Groves, *A Nanocube Plasmonic Sensor for Molecular Binding on Membrane Surfaces.* Nano Letters, 2009. **9**(5): p. 2077-2082.
41. Bukasov, R., T.A. Ali, P. Nordlander, and J.S. Shumaker-Parry, *Probing the Plasmonic Near-Field of Gold Nanocrescent Antennas.* ACS Nano, 2010. **4**(11): p. 6639-6650.
42. Dondapati, S.K., T.K. Sau, C. Hrelescu, T.A. Klar, F.D. Stefani, and J. Feldmann, *Label-free Biosensing Based on Single Gold Nanostars as Plasmonic Transducers.* ACS Nano, 2010. **4**(11): p. 6318-6322.
43. Verellen, N., P. Van Dorpe, C. Huang, K. Lodewijks, G.A.E. Vandenbosch, L. Lagae, and V.V. Moshchalkov, *Plasmon Line Shaping Using Nanocrosses for High Sensitivity Localized Surface Plasmon Resonance Sensing.* Nano Letters, 2011. **11**(2): p. 391-397.
44. Kubo, W. and S. Fujikawa, *Au Double Nanopillars with Nanogap for Plasmonic Sensor.* Nano Letters, 2011. **11**(1): p. 8-15.
45. Cetin, A.E., A.A. Yanik, C. Yilmaz, S. Somu, A. Busnaina, and H. Altug, *Monopole antenna arrays for optical trapping, spectroscopy, and sensing.* Applied Physics Letters, 2011. **98**(11).

Conclusions and Future Work

8.1. Conclusions

In this chapter, major conclusions, significances, implications and suggestions, based on the detailed work discussed in previous chapters, would be made with discussions. This will also echo the major aims and objectives set out in Chapter 1.

The primary objective of the work discussed in this thesis is to examine the sensing capacity of metallic nanostructures in an optical fibre sensor system through various experimental designs, evaluations, implementation and optimisations. The optical fibre system was chosen to be a reflective type with the sensing area being decladded, allowing for the coating of metallic nanostructures before further surface modification and functionalisation for the creation of bio-sensors. Chapter 4 has focused on the design of AuNP-based LSPR sensor design and optimisation for refractive index sensing through a systematic evaluation various parameters in order to establish an optimal procedure for maximising the sensitivity of the sensor system. More discussions and comparisons have been made in terms of the use of other novel types of nanostructures. Coupled with theoretical studies published in literature, some conclusions are withdrawn with insights and implications, which could be summed up as:

- The sensitivity of LSPR-based sensing system investigated in this thesis has shown a clear correlation with the characteristics of the coating metallic materials. For example, the LSPR sensor coated with a larger size of gold nanospherical particles leads to a higher sensitivity of the sensor when it is subjected to the refractive index change in the surrounding medium. This experimental result shows a good agreement with the theoretical studies of plasmonic effect on nanoparticles.

- Some experimental parameters related to the coating process were analysed and their direct effect on the sensitivity of the sensors created were systematically evaluated and optimised. The nature of coating process involves electrostatic interactions, covalent bonding and silanisation process; therefore external conditions such as pH, temperature and coating time could affect the quality of the sensing probe created to some extent. As discussed in Chapter 4, pH variation, in this particular experiment, from 3 to 5 expressed statistically no effect on the sensitivity of the probe. Coating time and temperature, on the other hand, could induce influences on the sensitivity. AuNPs with different sizes required different time to reach coating saturation and coating AuNPs with bigger sizes is often related to longer coating time. Similarly, higher temperature creates a higher thermodynamic system with a higher kinetic energy, which could make a significant impact on the coating process. 25 ^{o}C was experimentally proven to be the optimal temperature for ensuring both the high sensitivity and a large dynamic working range.

- Stability and repeatability of the sensor system were tested and proven to be consistent over at least ten-day period. These tests demonstrate the potential of LSPR-based sensors for future development of inexpensive, versatile and reliable sensing probes for chemical and biological applications, with possibilities of mass-production, disposability and multifunctionality.

- Cross-comparison of gold nanospheres and gold nanorods was made and their respective biosensing potential has also been demonstrated in chapter 5. The high sensitivity of the sensor can either be achieved by using relatively big nanospherical particles or by gold nanorods with a high aspect ratio. In this demonstration, LOD of the sensor was reported to be as low as 1.6 nM, which was comparable to other reports in literature.

- Following the successful optimisation of AuNP-based sensors discussed in Chapter 4 and their subsequent cross-comparison with AuNR-based sensors discussed in Chapter 5, a variety of gold/silver nanoalloys were investigated in Chapter 6 as an alternative choice of materials using a similar fabrication

process and experimental evaluation system. Alloy nanoparticles, which possess the benefit of chemical stability from gold and excellent plasmonic properties from silver, have shown to be beneficial for the sensor sensitivity enhancement. Small alloy nanoparticles were proven to achieve a higher sensitivity than that of gold nanoparticles of a similar size. More importantly, the sensitivity of the sensor was not only dependent on the diameter of the nanoparticles but also on the content of the alloy. The correlation between sensitivity, particle size and particle content is complicated.

- Novel classes of nanostructures, such as hollow nanocages particles, were also synthesised and used in fabrication of LSPR sensors with the details being discussed in Chapter 7. With the exceptional plasmonic effect caused by the coupling between the interior and exterior plasmonic fields in the hollow structure, gold nanocages were experimentally prepared and used for the construction of LSPR-based sensors, which have demonstrated an excellent sensing capacity. The plasmonic effect, which directly contributes to the sensitivity of the probe, was proven experimentally to be dependent on the hollowness or the wall thickness of the structures. The sensitivity of the system from hollow nanocages particles as discussed in Chapter 7 shows at least 3 times higher a sensitivity than that of solid ones with a similar size. This result indicated the importance of hollow structures and suggested that more advanced sensing capacity could also be explored by using larger particles with an increased hollowness.

In summary, a sensing system for refractive index measurement based on optical fibres based on localised plasmon resonance and various metallic nanostructures has been successfully investigated and fabricated. The experimental results in this work brought some important insights into and implications for further development of practical sensors.

8.2. Future work

In this thesis, a series of nanomaterials was rationally chosen for evaluation of their capacity in the fabrication of compact optical fibre sensor probes for refractive index sensing purpose. Despite the success achieved, there is still a wide scope for further research and this is discussed in detail below.

- Practical sensing purposes could be explored in various chemical and biological sensing schemes. The nanomaterials layer deposited on the fibre has shown to be an excellent platform for chemical or biological reagents, due to the metal's localised plasmonic effect. The applications could be unlimited, as long as a proper measurands-capturing mechanism is employed to achieve high selectivity and stability. As reviewed in Chapter 3, from pH, temperature to gas sensing or bacteria or DNA sensing, applications could bear no limitation in both measurands and sensing mechanisms.

- Basic research of nanomaterials and nanostructures could also be continued. For example, various alloys of different materials and contents could be examined based on theoretical studies and practical deployment (e.g. environmental stability or cost-effectiveness). Nanomaterials with hollow structure possess powerful potential in sensing area. Research in chapter 7 just shows a start but many possibilities can be explored. For example, the sensing potential of other types of hollow structures, such as nanotriangles, nanostars, nanorice, nanocresents have not yet been evaluated but their corresponding solid structures have shown a much stronger plasmonic effect than the plasmonic property of gold. Further investigation into this area could yield surprising and fascinating results and could offer an effective method for raising sensitivity of LSPR-based sensor systems.

- The controllability of the fabrication process is required but it has not yet been explored. The advance in nanomaterial research has pointed out that not only materials themselves, but also the structure of these materials at nano level could possess extreme effects such as the creation of negative

index materials or metamaterials [1]. Plasmonic metalmaterials based on gold nanorods were reported to have exceptional sensing capacity, much higher than that of freely assembled gold nanorods [2]. However, the fabrication of this type of structures requires expensive instruments. An alternative inexpensive fabrication technique based on chemical interactions has not yet been discovered. Proper control, growth and fabrication of nanostructure like gold nanorods on substrates could be made possible through an appropriate selection of surfactant, encapsulated agents, solvents and other physical parameters such as temperature, pressure, etc. In addition to that, self-assembly monolayer should also be regulated via physical interactions and/or chemical process such as polymerisation or covalent bonding.

- Moreover, optical fibre itself can also be tailored for further sensitivity enhancement. Different structures such as U-bent fibre, tapered fibre or fibre tips can increase sensing performance compared to that of standard fibres. Other types of fibres such as long period grating (LPG), Fibre-Bragg Grating (FBG) or photonic crystal fibre (PCF) could also contribute to the sensitivity improvement. It is also important to consider the miniaturisation by integrating all components into one portable system with replaceable and/or disposable sensing probes. This possibility encourages commercialisation for future development.

8.3. References

1. Smith, D.R., W.J. Padilla, D.C. Vier, S.C. Nemat-Nasser, and S. Schultz, *Composite medium with simultaneously negative permeability and permittivity.* Physical Review Letters, 2000. **84**(18): p. 4184-4187.
2. Kabashin, A.V., P. Evans, S. Pastkovsky, W. Hendren, G.A. Wurtz, R. Atkinson, R. Pollard, V.A. Podolskiy, and A.V. Zayats, *Plasmonic nanorod metamaterials for biosensing.* Nature Materials, 2009. **8**(11): p. 867-871.

List of publications

Journal papers:

- **M.H. Tu**, T. Sun, K.T.V. Grattan, LSPR optical fibre sensors based on hollow gold nanostructures, Sensors and Actuators B: Chemical, Volume 191, February 2014, Pages 37-44, ISSN 0925-4005.
- Jie Cao, **Minh Hieu Tu,** Tong Sun, Kenneth T.V. Grattan, Wavelength-based localized surface plasmon resonance optical fiber biosensor, Sensors and Actuators B: Chemical, Volume 181, May 2013, Pages 611-619, ISSN 0925-4005.
- **Tu, H.**; Sun, T.; Grattan, K.T., "SPR-Based Optical Fiber Sensors Using Gold–Silver Alloy Particles as the Active Sensing Material," Sensors Journal, IEEE, vol.13, no.6, pp.2192-2199, June 2013.
- **M.H. Tu**, T. Sun, K.T.V. Grattan, Optimization of gold-nanoparticle-based optical fibre surface plasmon resonance (SPR)-based sensors, Sensors and Actuators B: Chemical, Volume 164, Issue 1, 31 March 2012, Pages 43-53, ISSN 0925-4005.

Conferences:

1. Poster Presentation in 3rd International Bio-Sensing Technology Conference (BITE-2013). Time and location: May 12-15, 2013 in Sitges, Spain.

   Title: Gold-silver alloy particles as sensing material for SPR-based optical fibre sensor.

   Author: **M.H Tu**, T. Sun, K.T.V. Grattan.

2. Poster Presentation in International Conference on Specialty Glass & Optical Fiber: Materials, Technology & Devices (ICGF-2011). Time and location: August 4-6, 2011 in Kolkata, India.

   Title: Optimisation of Gold-nanoparticle-based Optical fibre Surface Plasmon Resonance (SPR) Sensors.

   Author: **M.H Tu**, T. Sun, K.T.V. Grattan.